Application of electronic and physical techniques to the study of short range atmospheric dispersion and related topics

Jones, Christopher D.

Application of Electronic and Physical Techniques to the study of Short Range Atmospheric Dispersion and Related Topics.

Volume I.

A Thesis submitted for the Degree of Doctor of Science

of the University of Durham

by

Christopher D Jones

PhD, FIMA, C. Math.,FRMetSoc.

1995.

Statement of Copyright.

Declaration.

It is stated here that the material contained in this thesis has not been previously submitted for a degree in this or any other university. In the case of publications having joint or multiple authorship, the particular contribution of the candidate is indicated in the extended summary statement that follows later.

C D Jones

Application of Electronic and Physical Techniques to the Study of Short Range Atmospheric Dispersion and Related Topics.

C D Jones DSc. 1995.

Abstract.

Novel instrumental techniques have been conceived, developed and in one case, patented, which were employed to investigate various aspects of atmospheric dispersion and related topics. The first technique made use of unipolarly ionised air as the tracer 'material', and the results obtained formed the earliest direct experimental evidence of significant concentration fluctuations in vapour/particulate clouds dispersing in the lower atmosphere. Fluctuations are important because they are critical in determining the physiological response associated with exposures to toxic substances and those of importance in malodour nuisance. Later developments in technique included precision control of the unipolar ion current released; these were sufficiently novel to secure a patent. Subsequent innovations involved the development and substantial modification of an existing gas detection method to render its performance fully acceptable for pollution monitoring. This advance led to the invention of the UVIC® detector, described in Volume II, and generated the numerous patent applications referenced therein.

Several papers discuss the nature and implications of the information obtained using the experimental methods developed. Examples are the open terrain atmospheric dispersion experiments and analyses, the work on insect pheromones and that on dispersion around an isolated building. From these papers, notably the first, the full impact of concentration fluctuations on the assessment of risks associated with exposure to toxic substances began to emerge.

Two papers are included on the investigation of electric field effects arising from factory chimney plumes. Prior to publication, the existence of this phenomenon was not recognised. Papers on the use of electrically charged aerosols for improving deposition efficiency in crop spraying and on the examination of the effects of electrical charging on the behaviour of mildew spores, demonstrate the application of electrical techniques to novel areas of research. It is shown that the method may also have utility for wind tunnel investigations.

Application of Electronic and Physical Techniques to the Study of Short Range Atmospheric Dispersion and Related Topics.

C D Jones DSc. 1995.

Preface.

In the following paragraphs explanatory technical detail is presented in smaller type.

This thesis comprises two volumes: the first consists of a series of Journal papers demonstrating the development of novel instrumentation and its application to the study of various phenomena, both natural and man-made, occurring in the lower atmosphere; the second contains commercially sensitive material and gives an account of the initial concept, subsequent development, evaluation and ultimate commercial exploitation of a novel gas detection device. In view of the status of the material in Volume II, it is described only in outline in this preface.

Volume I details the original concept and development of the Ionised Air Tracer Technique (IATT) and its subsequent application in a number of atmospheric dispersion investigations involving a considerable variety of meteorological and terrain types. In addition a number of other papers are included which exemplify the underlying philosophy of applying electrical/physical based measurement techniques and theories to the study of various atmospheric phenomena. The papers are presented in chronological order of publication in order to facilitate cross-referencing.

The first paper, by Jones and Hutchinson, refines and extends the candidate's PhD research and, in particular, provides some rationalisation of ideas regarding the behaviour of fluctuating plumes and their effect on the ground level electric field. This early work demonstrated, unequivocally, the presence of substantial spatial and temporal variations of material concentration downwind of a small source and, although this was a self-evident feature of turbulent dispersion in the atmosphere, it was one that had largely been ignored for a variety of reasons.

Whilst the existence of such fluctuations can be readily adduced from common experience, eg the observation of a bonfire smoke plume, instrumentation **suitable for field use** and capable of responding to these rapid changes (0.01s or less) of concentration did not exist at that time (1974). As a result, all calculations relating to the quantification of hazard due to exposure to toxic

materials or that presented by the presence of a flammable gas/vapour had, of necessity, to be expressed in relation to the long term mean concentration as defined by the effective time resolution of the then available detectors - generally in the region of 3 - 15min. In certain cases this is perfectly acceptable, as in the assessment of a radiological hazard where it is known that the effects are related linearly to the product of the exposure time and concentration, ie the dosage. However, in the case of toxic damage, this is not generally so and it has been found useful to define a hazard weighting function (W) of the form:

$$W = [\int [\chi(t)]^n.dt] / [\int \chi(t).dt] \quad \text{.....(1)}$$

where $\chi(t)$ is the concentration at time t, n an index dependent on the material being considered (in most cases n is considerably greater than unity) and the integrals are taken over the time period of concern. Note that in (1) above the denominator is just the product of the time averaged concentration and exposure time, whilst the numerator reflects the degree of disproportionality in damage resulting from the effects of the high concentrations. In practice it is found that the toxic damage levels often observed imply very substantial degrees of non-linearity in behaviour and, for example in the case of chlorine, an accepted value for n is 2.7.

The ramifications of equation (1) are particularly significant in situations where clouds of toxic material are undergoing atmospheric dispersion and therefore contain substantial spatial heterogeneities. Consider a hypothetical situation and suppose a quantity Q of material to be released instantaneously into the atmosphere and that after a time t the cloud volume is V(t). If it is further assumed that the material comprising the cloud were distributed uniformly within its boundary then clearly the average concentration is simply

$$\chi_{av} = Q / V(t) \quad \text{.....(2)}$$

and W assumes a value of unity irrespective of n. Suppose next that the cloud possesses internal structure such that it is partitioned into two 'phases' occupying volumes $V_1(t)$ and $V_2(t)$ in which all the material comprising the cloud ie Q resides in the first. Assuming that the cloud material is mixed uniformly in this volume then the average concentration within it must be

$$\chi_{av1} = \chi_{av} [V(t) / V_1(t)] \quad \text{.....(3)}$$

by mass conservation. In reality this concept encapsulates precisely what occurs in nature because atmospheric turbulence acts in such a way as to expose progressively increasing areas of cloud material to the effects of molecular diffusion by the action of eddy energy transfer through a series of decreasing length scales. It is only this latter process that can reduce the local concentration gradients, and this results ultimately in a uniformly mixed cloud. Now consider the effect of this modified cloud structure on the value of W as calculated in Equation (1). In the case in point, it emerges, after some algebra, that

$$W = \{[(\chi_{av} V(t)) / V_1(t)]^n T_1\} / \{\chi_{av} T\} \quad \text{.....(4).}$$

where T and T_1 are the times of exposure relevant to the continuous and partitioned cloud respectively. If it is now assumed that the cloud is advected steadily past a fixed observation point then it is plausible to assert that

$$T / T_1 = V(t) / V_1 (t) \quad \text{.....(5)}$$

ie there is an implied, but not rigorously demonstrable, connection between the partition volume ratio and the observed intermittency (I) at a point in space experiencing effects due to the cloud. If the intermittency is defined as the fraction of the time that the concentration is zero (or for all practical purposes zero) then

$$I = 1 - [\, V_1 (t) / V(t) \,] \quad \text{.....(6).}$$

The importance of equation (6) lies in the fact that the value of I can be determined experimentally with fast response sensors whereas the partition volume ratio for the whole cloud can only be deduced indirectly. Hence it is possible in principle at least, provided statistically stationary conditions obtain (in this context the wind vector), to estimate this ratio. Combining equations (4), (5) and (6), one can then estimate the effect of this intermittency on the toxic hazard as

$$W = [\chi_{av}^{n-1}]. [1 / (1 - I)]^{n-1} \quad \text{.....(7)}$$

a similar result being obtained in a slightly different way by Griffiths and Harper (1985)[1] and extended by Griffiths (1991)[2]. Typically one encounters intermittency values in the region of 0.7 - 0.9 (see, for example, the papers containing results of dispersion experiments in this thesis but, in particular, that entitled "On the Structure of Instantaneous Plumes in the Atmosphere") in situations of relevance to hazard estimation, eg in the vicinity of a pipe failure in a chemical plant. Clearly, for any particular toxic substance n will remain constant, and thus the behaviour of equation (7) may be explored with respect to a variation in intermittency. Consider the ratio of the values of W for two values of intermittency I_1 and I_2; denoting this by β one can write

$$\beta = [(1 - I_2) / (1 - I_1)]^{n-1} \quad \text{.....(8).}$$

Consider the value of β for the case of I_1 set to 0.8, a typically observed value and $I_2 = 0$, which corresponds to a non-partitioned cloud ie with the material distributed evenly throughout its volume. Equation (8) then becomes

$$\beta = 5.0^{n-1}$$

As indicated above, if one were considering the effects of exposure to chlorine, with an n value of 2.7, $\beta = 15.4$ which is clearly a very significant factor in this context.

The above analysis, though based on simple arguments, nevertheless demonstrates unequivocally the importance of concentration fluctuations in the context of atmospheric dispersion. It has formed the basis of the justification for conducting much of the experimental work reported in the publications in this thesis.

The recognition of the true importance of concentration fluctuations in defining toxic and other hazards, coupled with the arrival of a very promising experimental technique capable of providing information on the fine structure of dispersing clouds that had been so conspicuously lacking in the past provided the incentive to conduct the extensive series of field and other investigations detailed below.

During the period 1975 -1977 the fast response ion collector was developed from its original rather crude form, as described in the candidate's PhD thesis, into a useful scientific instrument of sufficient robustness to be deployed in a variety of field experiments. The first of these experiments is reported in Jones (paper 5) together with a more detailed examination of the effects of ionic self-repulsion (which render the tracer non-passive). Typical ion concentration traces are also shown and a number of qualitative inferences drawn concerning plume and puff structure. This work is extended in the paper by Murlis and Jones (paper 8). (In this the candidate was responsible for the data gathering and analysis, with the co-author interpreting the results obtained in the context of insect behaviour.) In particular, in this paper, the time distribution of concentration 'events' ie both the **bursts** and the **gaps** is examined for the first time.

Concurrent with the above work a major series of field experiments, also utilising the IATT system, was carried out in Norway with the objective of obtaining as much quantitative data as possible on the concentration fluctuations present in both dispersing plumes and puffs. An important element in this programme, compared with those previous, was the recognition that large quantities of data needed to be obtained and analysed in order to build up a statistical, rather than the hitherto more deterministically based, picture of the dispersion process. Attempts were made to fit the data to the log-normal distributio;, however, these were only partially successful. On the experimental

side two special features may be noted: i. multiple unipolar ion sources were used for the first time as a means of simulating a release occurring from a spatially extended source and, ii., a tightly packed sensor array was employed to obtain information on the concentration cross-correlation behaviour. These developments are reported by Storebø et al. (paper 10).

Paper 11 presents a more philosophical and penetrating examination of various aspects of short range atmospheric dispersion and is, in some respects, a review of the subject. By that time considerable improvements had been made in experimental technique in terms of portability and data-logging arrangements, thus enabling investigations to be carried out on a more opportunistic basis. It had also became clear to the author that the best method of advancing research in this subject would involve combining the statistical analysis techniques already applied to earlier experimental data with an explicit recognition of the underlying physical processes that were causing the concentration fluctuations. In particular, it was evident that the statistical stationarity of the turbulent wind field in which experiments were conducted had a significant effect on the value and quality of the results. The first systematic attempt to examine this problem is contained in the paper by Jones and Murlis (1979)[3] (not included in this thesis) and is given further attention in the current paper. In addition the paper also addresses three important practical aspects of the work. First, the effect of low-pass filtering on the perceived statistics is examined; this is important for many applications such as detector design and the assessment of hazards where the 'receptor' response, eg the human lung, may differ from that of the sensor used to acquire the original data. Second, an attempt was made to derive values for the instantaneous plume radius as function of downwind distance with a correction **included** for the effects of electrostatic repulsion. Finally, the observed peak concentrations were corrected for reduction caused by these same effects, and then examined to establish whether they could possibly have been the result of advection, without any significant dilution, of pure 'source material' to the sensor involved. This last was a significant hypothesis to test in that there was then and, still continues to be, considerable discussion and disagreement about the crucial role of molecular diffusion in effecting cloud dilution.

The next paper (12), by Jones and Griffiths, is concerned with atmospheric dispersion in the vicinity of a small building, in contrast with the earlier investigations which had been conducted in relatively flat and unobstructed terrain. It was felt, by that time (1982/83), that the IATT had reached a sufficiently mature stage that its use could be seriously contemplated in environments that had hitherto been regarded as 'difficult'. This is particularly the case when conducting experiments close to an effectively earthed object, ie a building, and considerable attention was given to an examination of the combined effects of electrostatic repulsion and image effects on the passivity of the tracer. Even so much valuable information was obtained on the transient features of building wakes - the first time this had been achieved at field scale employing a tracer technique and, more specifically, extremely useful data on the motion of 'parcels' of marked fluid (ie ion puffs) in the building vicinity was acquired. These

results were also applied to form the design basis for a subsequent series of more sophisticated experiments involving the use of a passive, ie electrically neutral, tracer technique described in Vol II.

In the intervening period (1984/89) a number of substantial advances in experimental technique were made by progressive refinements in the technology employed. Whilst most of these were essentially routine, a notable improvement in performance was obtained by developing a Controlled Output Ion Generator so as to provide a very closely defined (nominally $\pm 3\%$) release rate of unipolarly ionised air. The device featured a number of technical innovations and was granted a Certificate of Patent in 1992[4].

The final paper (15) on the topic of short range atmospheric dispersion is concerned with a series of experiments conducted in southern New Mexico, USA. Interest was focussed on the behaviour of plumes in stable (ie nighttime) and unstable (daytime) conditions and, specifically, how the atmospheric stability affected the concentration fluctuation statistics. The use of the IATT was contemplated with considerable caution in this work because a prerequisite for the meteorological conditions sought was that wind speeds should be no greater than $2ms^{-1}$.

It is evident that, for a given release rate of unipolar ions, say i Amps, the charge per unit length of the plume (λ Coulombs/m), will be

$$\lambda = i / u \quad \text{.....(10)}$$

where u is the wind speed in ms^{-1}. For the idealised case of a long straight plume it easy to show that the electric field vector E, directed radially towards (or away depending on the polarity of the ions) the plume axis, is given by the expression

$$E = i / 2\pi r\epsilon_0 u \quad \text{.....(11)}$$

where r is the radial distance from the plume axis, and it has now been assumed additionally that the plume approximates to a line charge. Equation (11) shows clearly the potentially adverse effect of low wind speed on the passivity of the IATT, since the velocity vector v of an ion in an electric field is given by the well known relation

$$v = \mu E \quad \text{.....(12).}$$

where μ is the ionic mobility. Consequently an extraneous radial velocity of magnitude proportional to 1 / u is imposed on the ion, but the effect is exacerbated because, in addition, the ion requires more time (again proportional to 1 / u) to reach a given distance downwind. As a

result the effect on passivity is proportional to $1 / u^2$ and is thus highly significant at low wind speeds. Further and more detailed analysis is contained in several of the papers in this thesis but, specifically, in that by Chatwin et al (paper 14).

The paper contains a careful evaluation of the data quality in terms of statistical stationarity and, whilst the results were found to be generally encouraging in this respect, certain deficiencies still remained. Central moments were evaluated for a range of averaging and sampling times, and then examined in some detail. It is interesting to note that some of the data obtained in daytime unstable (ie convective) conditions display quasi-periodic behaviour apparently associated with the structure of the atmospheric boundary layer. Visual examination of the time series obtained also showed marked differences between the stable and unstable data, the intermittency being much higher in the latter case. In addition to the above analysis, a more rigorous approach was applied to the treatment of instrument, ie electronic, noise. The approach adopted in the past had generally been one of applying a threshold sufficiently large to ensure its effective removal. However, it should be pointed out that, for most purposes, the sensor employed, ie the ion collector, was a relatively noise-free instrument. Typical noise levels are in the region of 5pA RMS, whereas signals could be up to several hundred times larger than this. Nonetheless even these noise levels become important when the data are employed to derive Probability Density Function (PDF) estimates from which, ultimately, dispersion models may be formulated. Subsequent developments, especially the UVIC® detector, which has noise levels effectively two orders of magnitude less than the ion collector, have largely eliminated difficulties in this area.

The initial field studies using the IATT were supplemented by two wind tunnel investigations into the behaviour of unipolar ion plumes and puffs. Here the motivation was to quantify, experimentally and in a controlled environment, the effects of ionic self-repulsion and, if possible, obtain an indirect estimate of the mobility. The first series of experiments, detailed in paper(4), was conducted in a low turbulence wind tunnel using the same ion generator and collector system that had been employed in the earlier series of field experiments. Ion concentration profiles were obtained at two distances downstream of the generator at a range of air speeds. Using the data it proved possible to confirm the expected axisymmetric nature of the ion plume, and to deduce the total ion current output by carrying out a (numerical) spatial integration, in a cross-stream plane, of the concentration profiles.

The results of the wind tunnel investigation described above encouraged the candidate to explore the possibilities for adapting the IATT for use as a tracer for wind tunnel studies in its own right. However, notwithstanding any other difficulties, the physical dimensions alone of the field system would have precluded its use in the wind tunnel. Accordingly, scaled-down versions of the instrumentation were designed, fabricated and evaluated in a variety of flow regimes. Results were generally very satisfactory. In particular it proved possible to conduct studies of flow and dispersion in the **Lagrangian** framework (difficult with conventional systems) by releasing short (0.01s) puffs of ionised air. This was

achieved by applying appropriately sequenced EHT voltage waveforms to the ion generator central electrode. This work is described in paper (6).

As indicated above, the aspirated coaxial tube ion sensor (collector) had been improved steadily since first deployed in this role in 1973. However, the need for a fan/pump to provide the necessary suction seemed an unnecessary encumbrance when, in field experiments, the motion of the air itself (ie the wind) could possibly provide the required aspiration directly. In view of this a novel ion detector was developed, based on the Langmuir probe concept used in plasma physics research, and tested in both the wind tunnel and the field. The results of an initial field test are described in paper (13) and, whilst encouraging in general terms, highlighted certain difficulties regarding the quantification of the collection efficiency/cross-section of the new sensor as a function of ambient wind speed. This rendered it very difficult to relate the ion flux, the physical quantity actually measured by the new probe, to the required parameter ie the instantaneous ion concentration. Despite the promising performance of the new probe it was clear that it would be necessary to monitor the wind speed, at a sampling rate carefully matched to its own frequency response and in physical juxtaposition, if a determination of the instantaneous ion concentration were to be obtained. Whilst technically feasible the approach was regarded as too complex to be economically justifiable.

Papers (2) and (3) deal with a phenomenon first observed by the candidate, but not then reported, during his PhD studies. It was noticed, at Lanehead (the University's field station in the Northern Pennines) that on some occasions with Easterly winds, the fairweather electric field displayed unusually large fluctuations which could not be ascribed to any particular cause. However, it became evident later, following consultations, that a local cement works plume (using electrostatic precipitators to remove particulates) at Eastgate, Co. Durham, some 13 km East, may have been responsible. A subsequent investigation, conceived by the candidate, involved conducting a detailed electric field survey at distances of up to 9km from the plant. This confirmed the existence of a highly electrically charged plume with local ground level fields occasionally exceeding $10kVm^{-1}$. Further investigations also indicated that electric field levels were sufficient to initiate corona discharge; this could have significant implications for plant safety in processes where flammable materials are involved.

The remaining two papers (7) and (9) are concerned with agricultural applications of electrical measurements and associated theory. The first reports a series of innovative experiments designed to quantify the benefits of employing electrically charged aerosol sprays to treat plant pathogens. Conventional crop spraying systems suffer from two major problems: i. substantial spray loss due to wind drift, and ii. the need to disseminate excessive quantities of aerosol to compensate for the poor efficiency of impaction on the 'target-area'. Often the target-area is on the underside of leaves, a relatively sheltered environment, where pests etc tend to accumulate. Early work by the co-author, Dr Hopkinson, indicated clearly that electrical charging of the aerosol droplets dramatically

improved spray performance, but it was far from clear how best to optimise the spray design in terms of, inter alia, droplet size and charge. The candidate designed and carried out a series of selected experimental measurements on the charged spray so as provide basic data on the total charge, electric field distribution etc. Simultaneously a simple model of the relevant charged droplet parameters was formulated on the basis of certain physically plausible assumptions. Following careful validation checks, the model was used to determine droplet trajectories for a selected range of operating conditions eg level of applied high voltage and spray height above crop canopy. This then enabled a rational approach to the optimal design of the spray system to be devised.

The research described in Paper (9) is concerned with the effect of possible electrical charging on the behaviour of Barley Mildew Spores. At the time of this investigation, there was some weak evidence for anomalous behaviour of such spores, and one of the hypotheses advanced to explain this involved the assumption of a certain degree of electrical charging being present. In an attempt to resolve these points a short series of intensive field investigations was conducted in which the candidate played a leading role in the design of equipment, its operation in the field and subsequent analysis and interpretation of data.

As indicated above, Volume II of this thesis contains detailed reference to and description of commercially sensitive material and therefore it is not possible to include certain information in this synopsis. The research reported therein is concerned with the initial recognition, and subsequent investigation, of various major design flaws in a number of proprietary UV (Ultra-Violet) photo-ionisation detectors. Reference has been made earlier to the difficulties experienced with the IATT when its use was contemplated in light wind environments and those involving partially enclosed flows eg in building wakes. In an attempt to circumvent these difficulties considerable efforts were made to identify alternative **fast response** tracer-detector technologies which did not require the use of an electrically charged 'material' for their functioning. Many possibilities were explored, including oxygen deficiency, flame photometry, radioactive tracers, mass spectrometry, optical extinction, photo-ionisation and various solid state devices. Following detailed consideration of all the above techniques, it was concluded that UV Photo-Ionisation Detectors (PIDs) offered the most promise for field applications. In broad terms the capabilities of the commercially available instruments were as follows:

1. Response times in the range 1 - 3 seconds,
2. Minimum detectable concentration $\approx$0.1ppm and
3. Calibratable range 0 - $\approx$2000ppm

and, although far from ideal, were sufficient to justify their inclusion in field research programmes. Several groups of workers [see for example Higson, (1993)[5]; Higson et al, (1994)[6] and Mylne and Mason, (1991)[7]] developed the method over a period of several years generating a substantial quantity of useful

data and results. In most experiments propylene, which is about 1½ times heavier than air, was used as the tracer; however, the density of this vapour can pose difficulties with non-passive behaviour in experiments in very light winds or at long range when high release rates are required.

As experience began to accrue with these devices, it became clear that they were deficient in many respects, but most notably with regard to:

1. Lack of sensitivity,
2. Baseline instability and noise,
3. Poor speed of response and
4. Rapid fouling of the UV lamp window, leading to the need for frequent cleaning and recalibration.

A detailed consideration of these limitations suggested that, whilst the overall operating concept of the PID system was perfectly satisfactory, the particular configuration employed was very far from optimal, especially for a field instrument. In an effort to devise remedial measures, the principal innovation destined to establish an instrument obviating **all** of the deficiencies noted above was made by the candidate in 1991. This was achieved by combining the best features of the ion sensor, developed for the IATT system, with a source of 10.6eV UV radiation. The new instrument, although clearly similar in concept to its commercial counterparts, was configured and operated in a manner quite distinct from conventional PID practice. The instrument was initially referred to as a UVIC (**U**ltra-**V**iolet **I**on **C**ollector), but following IPR protection and the registration of a trademark it became known as the UVIC® detector. Initial field evaluation of a prototype UVIC® detector took place in July 1991 with immediately encouraging results, the critical performance parameters investigated being listed below:

1. Sensitivity (based on propylene) 10ppb and
2. Response time - in the region of 0.01s.

Subsequently it emerged that the novel geometrical configuration had also virtually eliminated lamp fouling, and thereby removed the need for frequent recalibration. Moreover the superior electronic performance of the ion collector, on which the UVIC® detector was based, reduced baseline drift to insignificant levels.

The performance gains offered by the new instrument were so substantial, particularly in the research context, that the existing proprietary photo-ionisation detectors were replaced as rapidly as possible with the new UVIC® detector system. This led to an immense improvement in data quality, with much greater reliability and ease of calibration under field conditions. In addition, the essentially unique capability of the instrument to respond both very rapidly and with extreme sensitivity to a wide variety of organic and inorganic compounds

aroused considerable national and international interest in both the research and industrial sectors. As an example the UVIC® detector played a pivotal role in the EU sponsored **FLADIS** programme (**F**lashing **L**iquid **A**mmonia **DIS**persion).

The technical advantage of the UVIC® detector in relation to its competitive products was fully sufficient to justify commercial exploitation. Accordingly a company (EnviroSystems Ltd., Stockport, Cheshire, UK) was incorporated in October 1992 to develop, manufacture and sell a commercial version of the instrument.

On the research side the most recent development, also conceived and developed by the candidate, involves the UVIC® detector system being deployed in combination and co-location with an FID (Flame Ionisation Detector). The use of such an arrangement relates to the solution of an important problem in turbulence and dispersion, namely the specification of the concentration field produced downwind of a **number** of pollutant sources. In this situation a major difficulty arises, because whilst the time-averaged mean concentrations produced by each source (using the principle of linear superposition) must be **linearly additive**, this does not apply to the higher order statistics and other parameters such as the PDF. Consider the concentration variance arising from a pair of spatially separated sources. It is easy to show that

$$\mathrm{Var}(\mathbf{1}+\mathbf{2}) = \mathrm{Var}(\mathbf{1}) + \mathrm{Var}(\mathbf{2}) + 2 \times \mathrm{Covar}(\mathbf{1},\mathbf{2}) \quad \text{.....(13),}$$

where the numbers 1 and 2 refer to the first and second sources respectively. As discussed at the beginning of this preface this is of very little significance where the long term averaged concentration is the main factor in determining the hazard; however, if the presence of fluctuations in concentration materially affects the overall outcome arising from an exposure to the hazardous substance, then attention must also be paid to the complicating effects produced by multiple and spatially separated sources. The development of models of multiple source dispersion, based on a **realistic physical description** of the atmospheric turbulence etc, clearly requires an appropriate theoretical framework on which to establish the mathematical procedures and, ultimately, the algorithms necessary for incorporation into computer programmes. Whilst much is known regarding the detailed structure of turbulent flows, see for example Tennekes and Lumley (1972)[8], there is still a need for experimental data to provide the basis for our understanding of the physics of the dispersion process. The difficulties associated with conducting field experiments of this type have resulted in there being virtually no experimental data reported in the literature which are addressed specifically towards this problem except the paper by Sawford, Frost and Allen (1985)[9]. However the data obtained, whilst representing a considerable advance at that time, were relatively poorly resolved in the temporal sense and much of the **joint fine structure** of the concentration field would have almost certainly been missed. Clearly this would have had a concomitant effect on the statistics derived.

The experimental technique recently introduced by the candidate makes use of the fact that the UVIC® detector responds strongly to ammonia but is insensitive to propane, whilst for the FID, the converse applies. This combination of instruments offers the researcher, for the first time, a means of **identifying, separately and simultaneously**, the contributions to the **total concentration** arising from **each** of (two) tracer sources. This exciting development is currently being exploited and detailed information on the progressive loss of correlation occurring as initially co-located sources are moved apart has already been obtained.

Volume II, in addition to the above, also includes the following:

1. Design criteria for UVIC® detectors,
2. Calibration methodologies,
3. The development of a physico-mathematical model of the UVIC® detector,
4. An overview of the commercial and research applications and
5. An assessment of the future possibilities.

References.

1. Griffiths, R. F. and Harper, A. S. 1985.
   A speculation on the importance of concentration fluctuations in the estimation of toxic response to irritant gases.
   J. Haz. Mat. **11**, 369-372.

2. Griffiths, R. F. 1991.
   The use of probit expressions in the assessment of acute population impact of toxic releases.
   J. Loss Prev. Proc. Ind. **4**, 49-57.

3. Jones, C. D. and Murlis, S. J. 1979.
   Stationarity of the concentration intermittency in short range atmospheric dispersion.
   Proceedings of the 10th International Technical Meeting (NATO/CCMS) on Air Pollution Modelling. Rome.

4. Jones, C. D., Elias, J. E. and Taylor, D. M. 1992.
   Controlled Output Ion Generator.
   UK Patent GB 2239740 B.

5. Higson, H. L. 1993.
   Atmospheric dispersion around an isolated building.
   PhD Thesis. University of Manchester, Faculty of Technology.

6. Higson, H. L., Griffiths, R. F., Jones, C. D. and Hall, D. J. 1994.
   Concentration measurements around an isolated building: a comparison between wind tunnel and field data.
   Atmos. Environ. **28**, 1827-1836.

7. Mylne, K.R. and Mason, P. J. 1991.
   Concentration fluctuation measurements in a dispersing plume at a range of up to 1000m.
   Q. J. Roy. Met. Soc. **117**, 177-206.

8. Tennekes, H. and Lumley, J. L. 1972.
   A First Course in Turbulence.
   MIT Press, Cambridge.

9. Sawford, B. L., Frost, A. C. and Allen, T. C. 1985.
   Atmospheric boundary layer measurements on concentration statistics from isolated and multiple sources.
   Bound. Lay. Met. **31**, 249-268.

Jones C. D. and Hutchinson W. C. A. (1976).

Plumes of electric space charge in the lower atmosphere.

J. Atmos. and Terr. Phys. **38**, 485 - 494.

Journal of Atmospheric and Terrestrial Physics, Vol. 38, pp. 485 to 494. Pergamon Press, 1976. Printed in Northern Ireland

Plumes of electric space charge in the lower atmosphere

C. D. JONES* and W. C. A. HUTCHINSON
Physics Department, University of Durham, England

(*Received* 14 *July* 1975)

Abstract—Artificially produced ions are released from a point source a few m above ground surface. It is shown experimentally and theoretically that they form a plume rather similar to a smoke plume. Measurements of vertical electric field and space charge concentration downwind yield information about the ion plume, and its behaviour is related to local meteorological conditions. Results with a bidirectional vane suggest that ions can be used successfully as a tracer in short range atmospheric diffusion studies.

1. INTRODUCTION

Since the dispersal of gases and suspended particulate matter from point sources in the atmosphere is of so great general interest it seemed worthwhile to consider whether the techniques of atmospheric electricity could be employed to study the behaviour of plumes.

Existing methods of investigating atmospheric diffusion fall into three categories, (a) Optical outline, (b) Lagrangian, and (c) Concentration (or dosage) using some form of tracer material. (The dosage is the integral of concentration with respect to time; it corresponds to the time average of concentrations at a point.) Under (a), a smoke plume may be photographed. The method is useful but has its limitations. It is not easy to define the plume's optical boundary which depends on the ambient light level. Nor does the method yield information about the distribution of material within the boundary. The properties of plumes and puffs are discussed by FRENKIEL and KATZ (1956). In Lagrangian-type measurements of category (b) the paths taken by individual parcels of air may be followed with neutrally weighted balloons or similar devices, as described by EDINGER (1952) and GIFFORD (1955). Method (c) has been most commonly used. Material with characteristic properties is released, usually at a controlled rate, and its concentration is monitored at various points downwind of the source. Many types of gaseous and particulate tracer have been employed, especially sulphur dioxide and fluorescent particles. Dosage, rather than concentration, is usually measured, though this has the disadvantage that instantaneous concentration levels downwind of a source are not known. In this third category (c) falls the atmospheric electric method we describe, and it does not suffer from the disadvantages just mentioned.

The naturally occurring positive and negative ions in the lower atmosphere (see, for example, CHALMERS, 1967) are constantly being produced by agents such as cosmic rays and radioactivity and dissipated by various processes of combination and recombination. The so-called small ions have mobilities between 1×10^{-4} and 2×10^{-4} $m^2V^{-1}s^{-1}$. If a small ion of either sign becomes attached to an Aitken nucleus the product is a large ion. This has a much lower mobility, some 1/500 times that of a small ion. Concentrations of ions of both signs vary within wide limits according to locality and conditions. The overall excess of positive over negative ion concentration is the electric space charge density. This again depends on place and conditions, but at land stations its magnitude is typically of the order of 10 pCm^{-3}. If a quantity of space charge is suddenly introduced into a volume of a few m^3, say, of the atmosphere its exponential decay has a time constant, 5 min or longer, which is inversely proportional to the conductivity of the surrounding air. The ions move in the Earth's electric field, which is vertical near the surface. Its value is somewhere near 100 Vm^{-1} in clean air in fair weather, usually increasing rapidly with atmospheric pollution. In fair weather the small ions will thus have a resulting speed of several mms^{-1} whereas large ions will hardly respond at all to the electric field, so that the motion of ions of both kinds will be essentially that of the air itself. Moreover, the space charge will have an associated electric field which in favourable conditions can be detected as an addition to the natural ambient field. This provides the basis of a useful technique

* Now at Chemical Defence Establishment, Porton Down, Salisbury.

for investigating ion plumes and clouds. (In the experiments described below it was not necessary to distinguish between positive and negative fields. All field values shown in the figures are consequently magnitudes only).

Previously CRAMER *et al.* (1954) had considered the feasibility of using a charged smoke for investigating turbulent diffusion, and LARGE and PIERCE (1957) indicated that their artificially produced point discharge ions might be employed to study air motions and turbulence; and BENT and HUTCHINSON (1966) and OGDEN and HUTCHINSON (1970) observed fluctuations apparently occurring naturally in space charge density and related them to atmospheric turbulence. We have now made an exploratory study of the nature of space charge plumes and have compared their behaviour with that of uncharged plumes. It is possible, though tedious, to follow the conventional concentration or dosage method of investigation by using special collectors for obtaining ion or space charge density. Measuring the associated electric field, however, is much easier and it offers a unique tool for probing diffuse plumes. The field at a nearby point depends on both the total charge present and also its distribution within. Hence this electric field measurement yields information about the plume treated as a whole, no analogous method being available for uncharged tracers.

2. THEORETICAL

It is to be expected that for a charged plume the turbulent diffusion and electrostatically induced motion will interact in a complex way, but we will begin by considering the two effects separately. First, apart from effects due to the charges themselves, the plume will be progressively diluted as it becomes mixed with the surrounding air. The turbulence process, depending on local conditions including thermal stability in the lowest layers of the air, will be the same as for any other plume material. We assume that for the surrounding air the decay time constant of electrical dissipation mentioned in Section 1 is long enough to take space charge as being conserved; special treatment would be necessary in the case of measurements made at points more than a few minutes downwind of the source.

The theoretical results for Fickian diffusion of material from a raised continuous point source have been applied with some success to turbulent diffusion in the atmosphere; solutions of the equation of diffusion are discussed by SUTTON (1953). Hence an approximate estimate of the mean electric field at any point under an ion plume could be obtained by applying this approach to the atmospheric diffusion of ions. For our purposes the strength of an ion source is represented by the corresponding electric current i. At a point (x, y, z) downwind the mean electric space charge density $\bar{\rho}$ is then given by

$$\bar{\rho}(x, y, z) = \frac{i}{4\pi Kx} \exp\left[-\frac{\bar{u}y^2}{4Kx}\right] \times \left[\exp\left(-\frac{\bar{u}(z-h)^2}{4Kx}\right) + \exp\left(-\frac{\bar{u}(z+h)^2}{4Kx}\right)\right] \quad (1)$$

where K is the coefficient of eddy diffusivity, and $\bar{u}$ is the mean wind speed defining the x direction in a coordinate system with origin in the surface; the y and z axes are respectively across wind and vertical, and the source is at height h above the origin. The surface is regarded as reflecting, to produce an image source whose effect is taken into account in equation (1). This is not to be confused with the electrical image of the charge mentioned below. It is assumed that K is constant, so we must be careful to use a value of K appropriate to each occasion. From equation (1) it is possible to find the time average of the distribution of space charge downwind and hence calculate the resulting mean electric field at any point where measurements might be made.

In atmospheric electricity only the vertical component of electric field is usually important near the surface. The vertical component E_z at a point (x', y', z') due to a charged plume is given by

$$E_z(x', y', z') = \frac{1}{4\pi\varepsilon_0} \int_{\text{plume}} \frac{\bar{\rho}(x, y, z)}{R^2} \sin\alpha \, dv \quad (2)$$

where R is the distance between a plume element at (x, y, z) and the point (x', y', z'), and α is the angle of elevation of the plume element with respect to the point (x', y', z'). The integration is taken over the entire ion plume. The value of $\bar{\rho}(x, y, z)$ from equation (1) was substituted into equation (2) and the necessary numerical solution procedure employing a computer was devised. Account was taken of the effect of the electrical image of the plume since the ground is a conductor in this context. In fact the results of computer analysis indicated that, with values of K appropriate to stable and neutral meteorological conditions, the electric field due to the mean plume differed

relatively little from that of a semi-infinite line charge provided the distance downwind from the ion source was not too great. However, at distances exceeding about 100 m from the source, by which distance the plume had become well dispersed, the computed (and observed) electric field values declined rapidly.

The plume will also be subject to the electrostatic forces arising from the space charge contained in it. These are represented in Fig. 1; they are (a) outward radial forces of electrostatic repulsion, (b) downward electrical image forces, and (c) longitudinal forces of repulsion tending to increase the length of the plume. In the case of (c) let us consider the plume as a horizontal line of space charge of total length l downwind from the source. The linear space charge density σ from a source of strength i with wind speed u is i/u,and the resulting field acting on a small particle of the plume at distance x_1 from the source is easily shown to be $(1/4\pi\varepsilon_0)(\sigma/x_1)(l - 2x_1)/(l - x_1)$ where ε_0 is the electric space constant. Since for all practical purposes $l \gg x_1$ this reduces to $(1/4\pi\varepsilon_0)\sigma/x_1$. In a wind of speed as low as 2 ms^{-1} an element of the plume 10 m downwind of a 0.3 μA source will be subject to a horizontal electric field of 130 Vm^{-1}. Then even for the fastest ions of mobility 10^{-4} $m^2V^{-1}m^{-1}$ the resulting longitudinal velocity component will be only about 0.01 ms^{-1}, which is negligible compared with u. We need not consider further the longitudinal forces (c).

For radial repulsion (a) it can be shown (see Appendix) that in the absence of turbulent diffusion, i.e. in a completely steady wind of speed u, the width of the ion plume is given approximately by

$$S = \left(S_0^2 + \frac{\mu i x}{u^2 \pi \varepsilon_0}\right)^{1/2} \qquad (3)$$

where S is the radius of the plume cross-section, assumed circular, at a distance x downwind of the source, S_0 the initial radius and μ the small ion mobility. (These are the fastest ions, of mobility about 10^{-4} m^2V^{-1} s^{-1}.) An approximate idea of the magnitude of these radial forces may be obtained by substituting values appropriate to our experimental conditions in this equation. Typically x might be 50 m and u 5 ms^{-1}; and i and S_0 are fixed at 0.3 μA and 0.1 m respectively throughout this work. In such circumstances S is found to be 1.5 m, which is approximately one-third the radial dimension that the cloud would have attained in normal turbulence. Contrast this however with the situation when u is reduced to 1 ms^{-1}, the remaining quantities being unchanged. In this case S becomes 7 m, a figure comparable with, if not larger than, that arising from the crosswind turbulent spreading of the plume.

The effect of image forces (b) (see Appendix), which tend to reduce the plume's height as it moves downwind, is given by

$$H = \left(H_0^2 - \frac{\mu i x}{2u^2 \pi \varepsilon_0}\right)^{1/2} \qquad (4)$$

where H_0 is the initial height and H the value at distance x downwind. A similar analysis to that used in the discussion on radial repulsion forces indicates that provided the ion source height is in excess of about 2 m, image force effects are not significant except for wind speeds below 2 ms^{-1}.

So far the electric field and ion concentration at just a single point have been considered. Much more useful information will be available if the field is measured at several points in the neighbourhood of the plume, and in the experiments four field mills were set out on the ground for this purpose. At any point under the plume the field will change constantly in response to the varying charge distribution. However, certain distinctive features, particularly kinks and loops, often develop in plumes, and when such an entity passes over a given point distinctive electric field patterns will often be produced. In addition, if the kink passes over (or near) two measuring points in succession we would expect similar field patterns to be recorded, but with an appropriate time displacement between them. Two possible types of behaviour are illustrated in Fig. 2. Suppose a vertical kink (K) developes in a plume and then

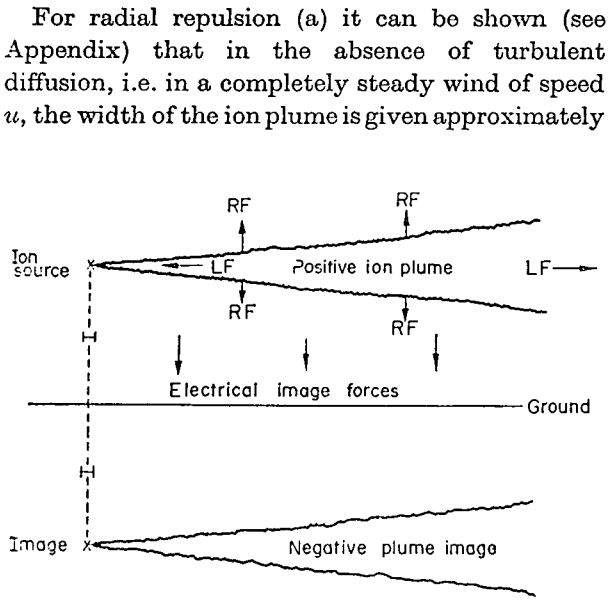

Fig. 1. Electrical forces influencing ion plumes. The positive ion source at height H produces a positive ion plume. The electrical mirror image is negative. There are also outward radial forces of electrostatic repusion (RF) and longitudinal forces of repulsion (LF).

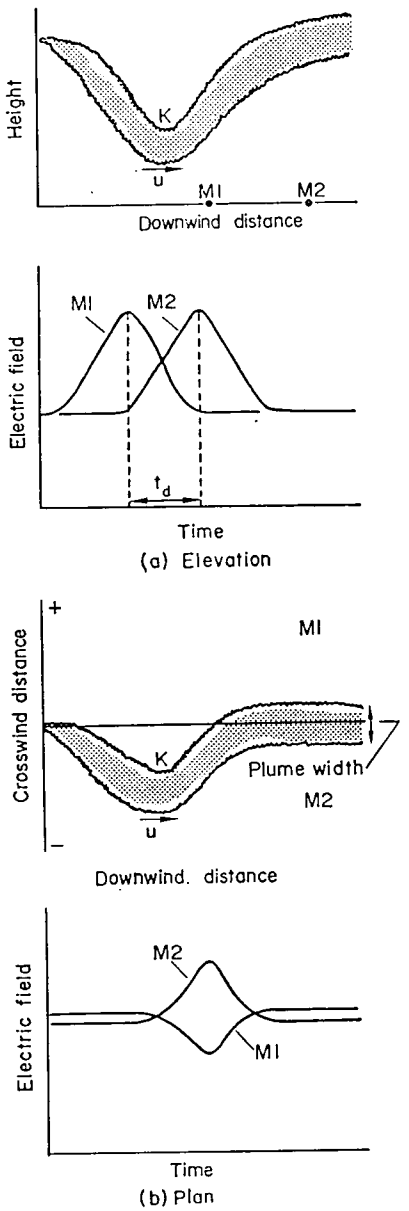

Fig. 2. Plume detail in plan and elevation and the associated electric field as measured at points downwind and crosswind (see text).

travels downwind. It is obvious that the presence of such a kink near a measuring point would result in an enhanced electric field. In the diagram $M1$ and $M2$ represent the positions of typical electric field recording stations and the graph indicates the trend of the field variations anticipated. The field maxima will be displaced in time an amount t_d depending on the separation of $M1$ and $M2$ and the mean wind speed u. Hence a cross-correlation analysis of the records would possess maximum value at a lag number corresponding to the delay time t_d. A second possibility is that a horizontal kink develops and travels downwind. Suppose now that the measuring stations $M1$ and $M2$ are deployed cross-wind as illustrated; in this case a little thought will show that the variations recorded by $M1$ and $M2$ will be in antiphase if the projection of the kink onto the ground passes between them and hence a negative cross-correlation would result. Thus examination of the cross-correlation between pairs of electric field sensors placed both cross-wind and along wind should provide useful information regarding the nature of the charge distributions responsible for the field variations.

In the later experiments a bidirectional vane was used to estimate the approximate plume configuration as a function of time. Then a simple model was used to facilitate computation of the resultant electric field variation. This bivane model was based largely on the results of some observations due to DAVIDSON and HALITSKY (1958), who found that, if smoke plumes were photographed on cine film and the processed film then projected in reverse, those portions of the plume which were identifiable appeared to travel back toward the source in virtually straight lines. Conversely therefore, the instantaneous plume configuration could be predicted from a knowledge of the wind vector at the source. The results obtained with this technique, which were most encouraging, are discussed in Section 5.

3. EXPERIMENTAL

Experimental requirements fell into four basic categories, viz:

(1) an ion generator,
(2) ion detectors (ion collectors and field mills),
(3) meteorological instrumentation, and
(4) a data collection system.

The operation of the ion generator was straightforward, ionization being produced by point discharge within a co-axial electrode system. The asymmetric electric field distribution resulted in the space between the electrodes being filled with unipolar, and relatively slow-moving, ions. These were expelled from the apparatus by a current of air along the axis, providing a constant stream of ions into the atmosphere. The ion current output was estimated from the electric field variations produced immediately downwind of the generator. The output was approximately 0.3 μA for positive ions and 0.5 μA for negative.

The ion collector was in principle similar to that of EBERT (1901), but only the small-ion collecting portion of the instrument was constructed, and solid state circuitry was used. The limiting

sensitivity of this ion collector was 10^{-9} cm^{-3}. The field mills were conventional in most respects (see MAPLESON and WHITLOCK, 1955). However, certain minor modifications were incorporated so that the machines could be fully portable and able to cope with the wide range of electric fields (up to 6 kVm^{-1}) likely to be encountered near ion plumes.

The meteorological instrumentation was required principally in order to relate the electrical measurements to the local meteorological environment. This equipment, which was supported on a portable telescopic mast of maximum height 12 m, consisted of two aspirated thermistor sensors to determine the temperature gradient, two anemometors to determine the wind shear, and a simple wind vane, later replaced by the bidirectional vane mentioned in Section 2. From these observations it was possible to determine parameters such as the Richardson number and mean wind speed which were likely to have a bearing on plume behaviour.

Magnetic tape was used for recording, and a sufficient number of channels were obtained by suitable time-division multiplexing. Appropriate decoding equipment enabled the original signals to be reconstructed in the laboratory, and that data were made acceptable to a computer.

4. DATA ANALYSIS

In work on boundary layer turbulence high speed sampling (each channel to be sampled at least every 2s) and recording are necessary if essential features of the fluctuations are not to be lost. Similarly since the electric field and ion concentration variations downwind of ion sources result directly from turbulent processes, equally rapid system response was required in these experiments. The necessity to sample rapidly inevitably resulted in the accumulation of large quantities of data and, consequently, the only reliable approach to analysis was by statistical techniques. Several computer programmes were developed in order that such analyses could proceed on a routine basis, and in later work graphical records were also constructed by the computer enabling a visual assessment of the experimental results to be made.

The statistics of the electric field variations must be fundamentally related to the ion plume behaviour which, in turn, is determined largely by the local meteorological conditions. Considerable dependence on certain other factors, in particular the height of the ion source and the positions of the field mills, was also expected. However, with a similar experimental procedure in a variety of meteorological conditions, it was hoped that comparison of the resulting electric field statistics and records would allow the important features of ion plume behaviour to be ascertained. Additionally, auto- and cross-correlation analysis could provide valuable information on the time scale of the individual records and the nature of the relationship between pairs of records respectively (see BENDAT and PIERSOL, 1966). In later work, in which a bivane was employed, it was possible, using the technique outlined previously, to predict values of the electric field fluctuations at a given point. It would then be feasible, by correlation techniques, to establish quantitatively what relationship such predicted variations bore to those actually recorded. Hence the validity of the various hypotheses leading to the formulation of the bivane data model could be critically assessed.

5. DISCUSSION

The relationship between electric field records obtained from separated field mills is likely to depend on a number of factors but in particular on whether the mills are placed in a line along or perpendicular to the wind vector. In the record of Fig. 3 the ion source was at a height of 9 m whilst field mills were placed 15 m, 30 m, 60 m, and 90 m directly downwind of the source. It can be seen that, in the 15 m record, a small electric field peak (A) occurred 11 s after recording commenced. Suppose that, whatever the actual charge distribution was that produced A, this distribution progresses downwind, presumably passing over or near the remaining mills at successively later times. The peaks B, C and D confirm this idea and, from simple kinematical principles, the velocity of the charge singularity was found to be close to that of the mean wind. Also of interest is the fact that the electric field peak attains a maximum size in the 60 m record. It was thought that the charge singularity moved gradually toward the ground, under the action of both electrostatic image forces and turbulence, as it progressed downwind. Additionally however the singularity must have been dispersed, principally by turbulence, and consequently at distances greater than 60 m the electric field diminishes.

Typical results obtained with the field mills in a line perpendicular to that of the wind vector are shown in Fig. 4, where it is clear that the relationship between the records is now quite different. For instance, note that in the mill 3 record a peak (A) occurs simultaneously with a trough (A') in the mill 2 record. A similar, but more pronounced recurrence of this phenomenon is also demonstrated

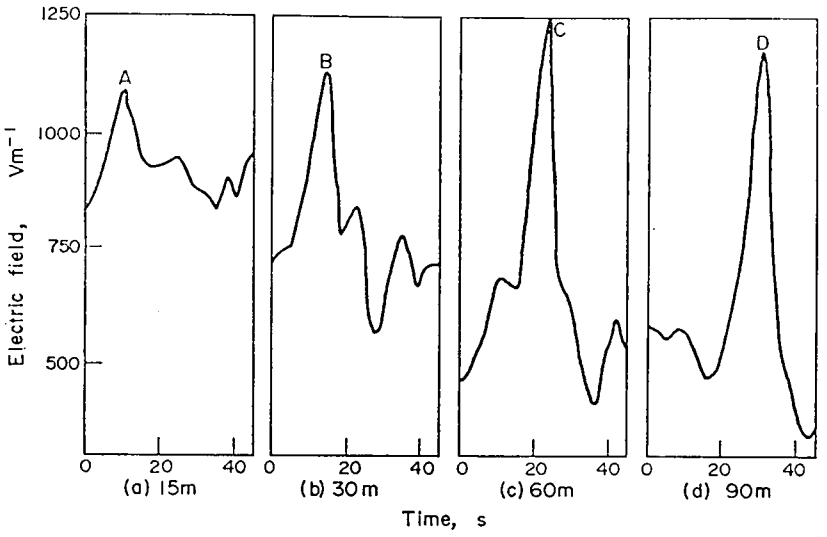

Fig. 3. Simultaneous electric field variations observed at four points on the ground 15, 30, 60 and 90 m in line downwind of an ion source 9 m high. A particular charge distribution travelling with the wind produces peaks *A*, *B*, *C* and *D* at the corresponding observing points at progressively later times. Mean wind speed = 4.4 ms^{-1}.

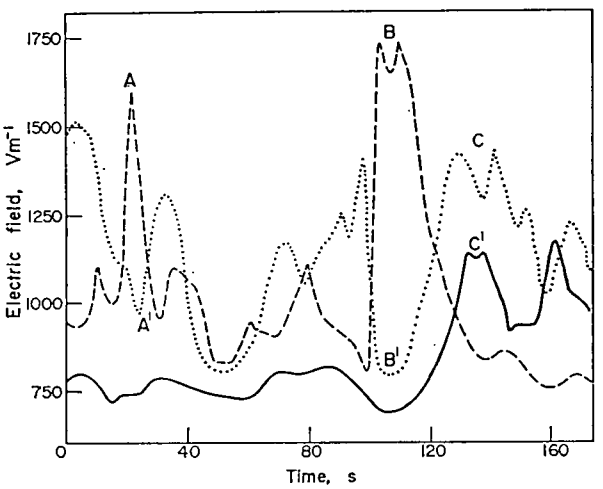

Fig. 4. Electric field variations observed with three field mills set 10 m apart on the ground in a crosswind line 20 m downwind of an ion source 4.9 m high. The central mill (no. 2, curve .....) was directly downwind of the source. Mill 3 (curve - - - - -) was to the left hand, viewed from the source, and Mill 4 (curve ———) to the right. For details of the features, see text. Mean wind speed = 2.3 ms^{-1}.

by the features *B* and *B'*. Such variations could have been produced in either or both of two ways. Firstly (see Fig. 2) a horizontal loop could have passed over mill 3 or secondly, if the plume were already nearer that mill, then the passage of a vertical loop would have produced the same effect. A different type of behaviour is evidenced by the in-phase peaks *C* and *C'*. Here a charge singularity must have been moving nearer both mills simultaneously and again there are a number of ways for this to occur. Calculations show that, in order to produce two peaks of roughly the same size, it is most likely that a charge singularity passed between mills 2 and 4 rather than to one side of them.

In statistical terms, of the parameters examined, by far the most revealing were found to be the electric field mean and standard deviation. Despite the wide scatter of the mean field values in Fig. 5 certain trends are apparent. The lines indicate the overall behaviour of the mean field

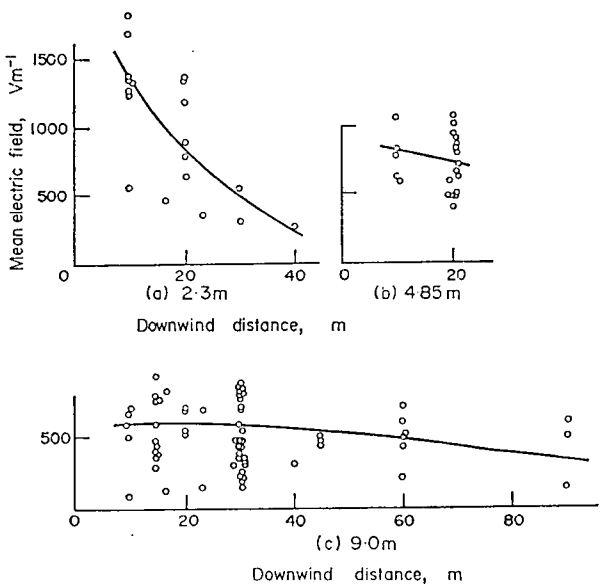

Fig. 5. Mean values (averaged over a 24 min run) of observed electric field at points downwind of an ion source (a) 2.3 m, (b) 4.85 m and (c) 9.0 m above the ground. The typical fair weather electric field upwind of the source is 120 Vm^{-1}.

(averaged over a 24 min run) for ion source heights of 2.3, 4.85 and 9.0 m as a function of the distance downwind, scatter in the values from individual runs being attributed to both random variations in plume behaviour and differing meteorological conditions. Equations (3) and (4) indicate that, for the 9 m plume, neither image nor electrostatic repulsion effects were expected to be substantial, except in very light winds. Thus, on the majority of occasions, ion plume behaviour would be dominated by turbulent processes. Consideration of the typical mean concentration downwind of the source leads one to conclude that, for a charged plume, the mean electric field values would behave largely as these observations suggest. In marked contrast to this are the results obtained with the ion source at 2.3 m. Here, with the ions much nearer the ground, image forces are markedly stronger with the result that electrical effects attributable to the plume are not discernible above about 50 m downwind. The electric field standard deviations are presented in Fig. 6 and, by consideration of these factors likely to produce electric field variations, simple explanations, analogues to those above, can be developed to account for the trends found.

Use of the cross-correlation techniques described earlier in fact provided interesting information on ion plume behaviour. As might be anticipated, it was observed that regardless of whether the field mills were placed along—or across-wind, the cross-correlation between their readings declined steadily with increasing separation. In the along-wind direction the correlogram always showed

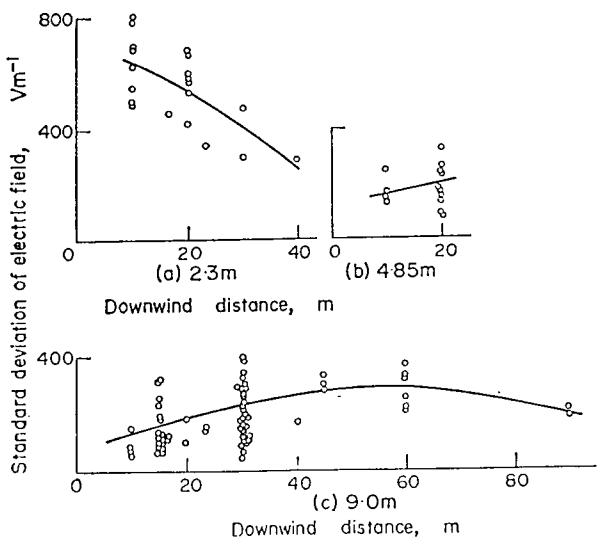

Fig. 6. Standard deviations of observed electric field corresponding to mean values presented in Fig. 5. The typical standard deviation for fair weather is 30 Vm^{-1}.

maximum cross-correlation at a point displaced from zero time lag by an amount corresponding to the transit time of the ions between the field mill pair. The actual cross-correlation fell from 0.7–0.9 at 20 m separation to 0.4–0.6 at 80 m separation, these figures being relatively insensitive to the meteorological conditions. However, in the cross-wind direction the behaviour was far less systematic, the cross-correlation often being negative at quite small angular separations (as small as 12° on one occasion) of the field mill pair.

Examination of the ion plume behaviour as a function of the atmospheric stability proved relatively inconclusive. Whilst the stability and wind structure are related the dependence is very complex, thereby rendering analysis difficult. However later results (discussed below) did show conclusively that, at least for short distances downwind ($\leq$100 m) of the ion source, the wind speed and direction variations were the principal factors controlling ion plume behaviour.

For the bivane results it is best to consider a section of typical record which serves to demonstrate that ion plume behaviour is determined largely by turbulent processes. The overall agreement between the predicted and actual values of electric field (Fig. 7) is selfevident and, apart from relatively minor exceptions, this was so in most of the other records. Nearly everywhere on this record the predicted values are somewhat less than the actual readings, although the magnitude of the variations is much the same. This discrepancy is due to the presence of the Earth's natural field, which was not taken into account in the development of the bivane data model.

As an illustration of the type of plume motions causing the field variations, two computed configurations are shown in Fig. 8, the position coordinates being obtained from the bivane observations. At time *A* part of the reconstructed plume lies almost immediately above the mill *F* and, because of the inverse square law, it is these local charges which make by far the largest contribution to the electric field. Contrast this with the situation at time *B* where the entire plume is at an angle to the source-mill line thus resulting in a low value of the electric field being predicted.

In the majority of experiments field mills were not placed further than 100 m from the source, largely for technical reasons. However, a preliminary investigation into the longer range behaviour of ion plumes was made, in which connexion some work was done with a source-mill distance of 300 m. Under such conditions the observed field variations

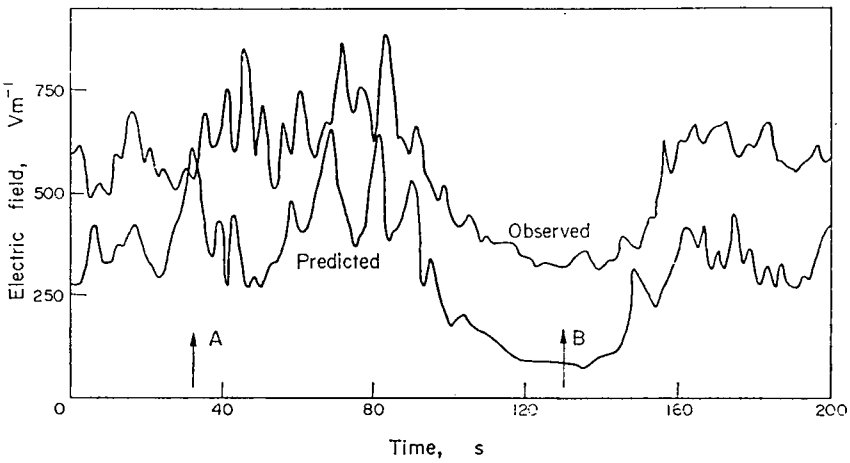

Fig. 7. Time variations of observed electric field at the surface 10 m downwind of an ion source 5 m high, together with values computed from bivane data. Mean wind speed = 3.4 ms^{-1}. The nearly constant difference of about 250 Vm^{-1} corresponds to the prevailing natural electric field upwind of the source.

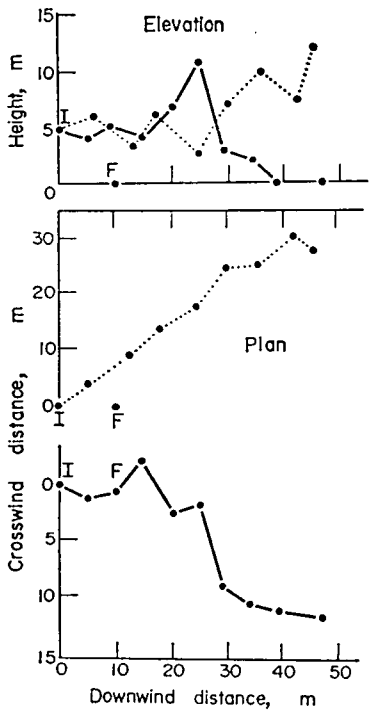

Fig. 8. Examples of computed ion plume configurations for time A (———) and time B (. . . . .) of Fig. 7. (see text.) I = ion source. F = field mill.

were much smaller, being typically between 60 and 200 Vm^{-1}. An important point was that, in these experiments, the mean wind speed was only about 1 ms^{-1}, and hence it was demonstrated that artificially produced ions were capable of being detected for at least 5 min after their generation.

Experiments with the ion collector could not be undertaken until the later stages of the project. Owing to its rather limited sensitivity the device could only be placed within about 30 m of the ion source, but despite this, the short time constant of the collector demonstrated clearly the potential ability of the technique to resolve the microstructure of diffusing clouds.

6. CONCLUSION

The experimental data have substantiated the ideas about ion plume behaviour discussed theoretically in Sections 1 and 2, that with the strength of ion source used in this work ion movement and dispersion would largely be determined by the pattern of the local air motion. However, two important exceptions were deduced theoretically and later established experimentally. Firstly, in light winds (2 ms^{-1} or less) the radial electrostatic forces between the ions comprising the plume caused a larger crosswind and vertical spreading than did the effects of turbulence. Secondly, image charge effects resulted in downward forces being exerted on the ions and this was particularly manifest when the plume was already near the ground. Hence in all but the lightest wind and except at the lowest levels ion plume behaviour is determined by the characteristics of the local turbulent field. Consequently, provided those limitations are borne in mind, there would appear little reason why such ions could not be used as a tracer in small scale diffusion experiments. The advantage of such a choice would be as follows. Ions are cheap and easy to produce and have minimal physiological effects. The detection of ions and measurement of ion concentration, either by electric field methods or by the more direct approach using ion collectors, do not require elaborate techniques. The response time of the majority of sensors to changes in

concentration is often relatively long and the alternative of an entirely electrical detection system, apart from its convenience in use, offers the attractive possibility of designing very rapid response instruments. This could be of particular value in resolving the fine structure of the concentration variations within plumes and puffs—a subject about which relatively little is known.

Since there is no unique relationship between charge distribution, distance and electric field a single field mill can only yield limited information about charge systems passing near or over it. However the use of two (or more) field mills appropriately placed has been shown capable of revealing considerably more information about plume behaviour. We would expect to obtain a much more detailed picture if we had mills capable of measuring the horizontal component of field as well, but their design presents special difficulties, and meantime the results from mills placed in the ground surface could best be supplemented with those obtained from ion collectors.

Acknowledgement—Thanks are due to the Natural Environment Research Council for the Research Studentship held by C.D.J. during the course of this work.

REFERENCES

Bendat J. S. and Piersol A. G.	1966	*Measurement and Analysis of Random Data.* Wiley, New York.
Bent R. B. and Hutchinson W. C. A.	1966	*J. atmos. terr. Phys.* **28**, 53.
Chalmers J. A.	1967	*Atmospheric Electricity.* Pergamon Press, Oxford.
Davidson B. and Halitsky J.	1958	*J. Air. Poll. Centr. Assoc.* **7**, 316.
Elbert H.	1901	*Phys. Z.* **2**, 662.
Frenkiel F. N. and Katz I.	1956	*J. Met.* **13**, 388.
Gifford F.	1955	*Monthly Weather Rev.* **23**, 292.
Large M. I. and Pierce E. T.	1957	*J. atmos. terr. Phys.* **10**, 251.
Mapleson W. W. and Whitlock W. S.	1955	*J. atm. terr. Phys.* **7**, 61.
Ogden T. L. and Hutchinson W. C. A.	1970	*J. atmos. terr. Phys.* **32**, 1131.
Sutton O. G.	1953	*Micrometeorology*, McGraw-Hill, New York.

Reference is also made to the following unpublished material:

Cramer H. E., Gill G. C. and Record F. A.	1954	*Research into atmospheric turbulence and associated diffusion of aerosols and gases near the earth's surface.* Massachusetts Institute of Technology Report under contract AF 19 (604) 145.
Edinger J. G.	1952	*A technique for measuring the detailed structure of atmospheric flow,* International Symposium on atmospheric turbulence in the boundary layer, Geophys. Res. Paper No. 19, Geophys. Res. Directorate, Cambridge, Mass., U.S.A.

APPENDIX

Forces of radial repulsion at plume surface

In a long horizontal cylinder of space charge at rest with radius S consider a volume element $\mathrm{d}V$ of length l. We will assume that only electrical forces are acting. If the radial field produced at some point on the surface is E, then by Gauss's Law

$$2\pi SlE = \frac{1}{\varepsilon_0}\int \rho \,\mathrm{d}V$$

$$= \frac{1}{\varepsilon_0}\pi S^2 l\bar{\rho}$$

where ρ and $\bar{\rho}$ are respectively the point and average values of space charge density. Assuming that space charge is conserved, let us use initial values S_0 and $\bar{\rho}_0$ when time t is zero, the space charge having been established before that. It easily follows that

$$E = \frac{1}{2\varepsilon_0}\frac{S_0^2}{S}\rho_0.$$

If the space charge is due to ions of mobility μ the resultant radial speed is μE, so that

$$\frac{\mathrm{d}S}{\mathrm{d}t} = \frac{\mu}{2\varepsilon_0}\frac{S_0^2}{S}\bar{\rho}_0$$

which on integration from 0 to t yields

$$S^2 = S_0^2 + S_0^2\frac{\mu}{\varepsilon_0}\bar{\rho}_0 t.$$

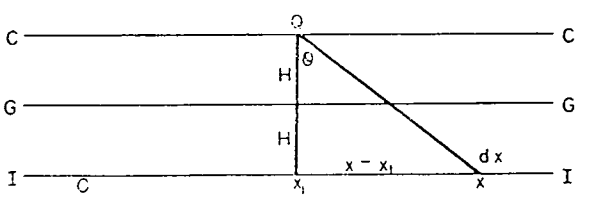

Fig. 9. Force of attraction between a line of space charge CC and its electrical image II. The ground GG may be regarded as a good conductor. (See text.)

If now a plume of space charge is being generated steadily from a point source of strength i the charge per unit length will be equal to i/u and also of course to $\pi S_0^2 \bar{\rho}_0$, where u is the wind speed which is assumed constant with no turbulence fluctuations. Let us consider a small packet of space charge which left the source at $t = 0$ and which now at time t is a distance x downwind. Then $t = x/u$, so that $\bar{\rho}_0 = i/(u\pi S_0^2)$ and the plume radius is given by

$$S = S_0^2 + \left(\frac{\mu i x}{u^2 \pi \varepsilon_0}\right)^{1/2} \tag{3}$$

Electrical image forces

For a long thin horizontal line CC of space charge (Fig. 9) at height H above the ground GG and having charge per unit length λ the image II lies a distance H below the ground. Let the origin 0 be in the image and the x-coordinate parallel to II. If we consider a small part Q of the actual charge, above coordinate point x_1 where $x_1 \gg H$, and the forces acting on Q due to an element dx of the image, with coordinate x and carrying charge $-\lambda\, dx$, we find that the total downward component of electric field at Q is

$$\frac{1}{4\pi\varepsilon_0} \int_{-\pi/2}^{\pi/2} \frac{\lambda\, dx}{(2H/\cos\theta)^2} \cos\theta$$

where θ gives the angular distance of element dx from the vertical below Q (see Fig. 9). If we replace $x - x_1$ by $2H \tan\theta$ and dx by $2H \sec^2\theta\, d\theta$ and integrate over the whole image between $-\pi/2$ and $\pi/2$ the downward field component is found to be $\lambda/4\pi\varepsilon_0 H$. For ions of mobility μ in this field the resulting downward speed $-dH/dt$ is $\mu\lambda/4\pi\varepsilon_0 H$, and integrating with initial condition that $H = H_0$ when $t = 0$ we obtain

$$H^2 = H_0^2 - \frac{\mu\lambda t}{2\pi\varepsilon_0}.$$

Extending this result to a linear plume of space charge from a source at height H_0 immediately over the origin we will obtain there a minimum value of image force since near the source θ goes to $\pi/2$ from 0 rather than from $-\pi/2$. For wind speed u a small portion of charge having left the source when $t = 0$ will be above coordinate point x where $x = ut$. Again $\lambda = i/u$, so λt becomes ix/u^2 and

$$H = \left(H_0^2 - \frac{\mu i x}{2u^2\pi\varepsilon_0}\right)^{1/2}. \tag{4}$$

Jennings S. G. and Jones C. D. (1976).

High electric fields from industrial stack plumes.

Nature. **264**, No. 5583, 236 - 7.

(Reprinted from Nature, Vol. 264, No. 5583, pp. 236–237, November 18, 1976)

High electric fields from industrial stack plumes

THE use of electrostatic precipitators on an industrial stack to remove particulate matter and aerosol particles is now quite common. The plume emanating from such an installation is likely to be highly electrically charged, and consequently associated electrical effects should be observable downwind of the stack.

Measurements were carried out from July 6 to July 10, 1976 of the vertical component of the electric field downwind of a 110-m chimney stack of a cement works at Eastgate, Co. Durham, using a series of conventional field mills[1]. Eastgate, ~33 km W of Durham City, is sited in a broad valley, 235 m above m.s.l., running E–W into the Pennine chain. The weather conditions were slightly unstable and cloudless with an easterly wind of between 3 and 4 m s^{-1} measured at 2 m above ground. Averages of readings taken over 10-min periods at 15-s intervals yield electric field values in the region of $+4{,}000$ V m^{-1} at sites within 500 m of the stack. Peak values up to $+10{,}000$ V m^{-1} were recorded within the same distance from the stack. The direction of the electric field corresponds to a negatively charged plume caused by an applied -60 kV to the corona wires of the electrostatic precipitators. The high electric field values can be compared with a typical value of the normal fair weather electric field upwind of the stack of ~ -200 V m^{-1}.

Large perturbations in the normal electric field were observable for distances up to 8 km downwind of the chimney stack. The decay in the electric field, E_P, at a position P was found to agree with the fundamental line charge equation[2], modified by an empirical dissipation factor $\exp(-x/d)$ as follows

$$E_P = \frac{\lambda}{2\pi\varepsilon_0 h}\left[1+\frac{x}{(x^2+h^2)^{1/2}}\right]\exp(-x/d) \qquad (1)$$

where λ is the electric charge per unit length, h is the height of the plume, x is the distance of the position P downwind of the stack, ε_0 is the permittivity of free space, and d is the distance at which the electric field is reduced to $1/e$ of its initial value. Experimental results indicate that d possessed values of between 1 and 2 km. The effect of turbulent diffusion in the plume was estimated from the plume observations to be sufficiently small to validate the line charge approximation up to at least 2 km downwind of the stack.

In view of the high values of the electric field, a series of experiments was performed to establish the occurrence of point discharge. Measurements of point discharge current from an insulated elevated point, 9.25 m above ground level, were made at 15-s intervals by means of a Keithley electrometer, model 640, 700 m downwind of the stack. Simultaneous measurements were made of the electric field at a distance 10 m upwind of the point. It was found that an electric field of 2.2 kV m^{-1} was necessary to initiate the point discharge. A maximum value of point discharge current of 3 μA was observed over a 20-min period. It was also found that the point discharge current, i, and the electric field, E, followed the theoretical relationship[3]

$$i = k(E-E_0) \qquad (2)$$

closely, where k is a constant, E is the value of electric field and E_0 is the onset value of electric field for the occurrence of point discharge.

In studying the dispersal of plumes by atmospheric turbulence, the electrical methods described here may provide a useful supplement to conventional concentration and dosage measurements[4,5]. The flow of negative charge away from the stack in the form of the charged plume leads to an equal positive current flow down the stack to Earth. Taking into consideration the numerous chimney stacks in operation, it is reasonable to assert that this hitherto unknown charge separation process could significantly modify estimates of the Earth's electrical current 'balance sheet'[6].

The presence of large electric fields in the vicinity of certain chimney stacks must result in significant point discharge currents occurring from sufficiently high metallic objects. If the objects concerned are poorly earthed they could acquire large electric potentials, which may well lead to electric spark production. This would not be of any practical consequence in most cases. If, however, the atmosphere downwind of the stack contained inflammable material, caused for example by an industrial leak, the occurrence of sparks could result in the ignition or detonation of the material.

The preliminary work described here will be elaborated in more detail in a subsequent publication.

We acknowledge the cooperation of Mr D. S. Reid, and Mr J. G. Wright, (Associated Portland Cement Manufacturers Ltd). This work has been carried out with the support of the Ministry of Defence and the Department of Physics, University of Durham.

S. G. JENNINGS

Department of Physics,
Science Laboratories,
South Road,
Durham DH1 3LE, UK

C. D. JONES

Chemical Defence Establishment,
Porton Down, Salisbury,
Wiltshire SP4 0JQ, UK

Received August 12; accepted September 29, 1976.

1 Mapleson, W. W., and Whitlock, W. S., *J. atmos. terr. Phys.*, 7, 61–72 (1955).
2 Davis, R., and Standring, W. G., *Proc. R. Soc.*, A191, 304–422 (1947).
3 Chalmers, J. A., *J. atmos. terr. Phys.*, 24, 339–344 (1962).
4 Pasquill, F., *Atmospheric Diffusion* (Van Nostrand, London, New York, and Toronto, 1962).
5 Jones, C. D., and Hutchinson, W. C. A., *J. atmos. terr. Phys.*, 38, 485–494 (1976).
6 Chalmers, J. A., *Atmospheric Electricity* (Pergamon, Oxford, 1967).

Jones C. D. and Jennings S. G. (1977).

Large electric fields due to industrial chimney stack plumes.

Atmos. Environ. **11**, 1197 - 1207.

Atmospheric Environment Vol. 11, pp. 1197–1207. Pergamon Press 1977. Printed in Great Britain.

LARGE ELECTRIC FIELDS DUE TO INDUSTRIAL CHIMNEY STACK PLUMES

C. D. JONES

Chemical Defence Establishment, Porton Down, Salisbury, Wiltshire, SP4 OJQ U.K.

and

S. G. JENNINGS*

Department of Physics, University of Durham, South Road, Durham DH1 3LE U.K.

(*First received* 6 *October* 1976)

Abstract—Large values of electric field due to a charged plume from an industrial chimney stack have been observed. Downwind and crosswind profiles of the electric field were measured using 4 field mills. Average values of between 5 and 6 kV m^{-1} over 10 minute periods were measured at distances within 200 m of the stack. Electric field values as large as 3.5 kV m^{-1} were present at a distance of 3 km from the stack. It was found that the electric field did not return to its normal fair-weather value until the downwind distance from the stack had exceeded 9 km.

The decrease in the average value of the electric field, E_p, under the plume gave good agreement with an equation derived from line charge theory, modified by an empirical decay factor $\exp(-R/D)$

$$E_p = -\frac{\lambda \exp(-R/D)}{2\pi\epsilon_0 h}\cdot\left[1 + \frac{R}{\sqrt{h^2 + R^2}}\right]$$

where λ is the charge per unit length, h the plume height, R the distance of the position P downwind, and D the distance at which λ is reduced by $1/e$. The experimental results yielded a value for D of about 1.5 km.

Point discharge currents as large as 3 μA were measured at a distance of 700 m from the stack. Measurements at heights ranging from 9.25 m to 3.25 m agreed with the theoretical relation

$$i = k\,(E - E_0)$$

where E is the measured value of electric field at a distance 10 m upwind from the discharge point, E_0 the critical value of electric field above which point discharge will occur and k is a constant. Values of E_0 of about 2 kV m^{-1} were found for the two highest points.

The results suggest that electric field measurements may be a valuable supplement to concentration data in atmospheric diffusion experiments using charged plumes.

INTRODUCTION

It has been known for some time that combustion processes can produce electric space charge. Muhleisen (1953) found large positive charges in diesel exhaust gases and negative charges in the effluents of chemical factories and gasworks. Chalmers (1967) suggested that if space charge could be generated artificially, then measurements of charge density downwind of an ion source might provide useful information on atmospheric diffusion. Jones and Hutchinson (1976) made measurements of the electric field and space charge concentration to investigate the behaviour of artificially produced ions released from a point source a few metres above ground. Jones (1977) showed that ion plume behaviour was mainly determined by atmospheric motion and turbulence and that artificial ions could serve as useful tracers in studying short range diffusion.

The use of electrostatic precipitators at industrial stacks to remove particulate matter is now quite common. The smoke plume from such installations is therefore likely to be highly charged and hence electrical effects should be detectable in the vicinity of the stack. Electric field measurements might therefore provide useful additional information on the behaviour of charged plumes. No previous study of chimney stack plumes using electrostatic techniques has come to the authors' attention. A preliminary description of the work has already been given by Jennings and Jones (1976).

THEORETICAL TREATMENT

2.1. *Initial Considerations*

Several groups of workers, for example, Davis and Standring (1947), Maund and Chalmers (1960) and Jones and Hutchinson (1976) have investigated the behaviour of plumes of unipolar small ions near the earth's surface. Their studies indicated that, within certain limitations, the electric field at the ground arising from such plumes could be calculated using line charge concepts. However, the effects of atmos-

* Present address: Atmospheric Sciences Laboratory, White Sands Missile Range, NM 88002, U.S.A.

pheric turbulence, electrostatic self-repulsion and image forces often significantly modify the behaviour of such plumes as shown by Jones (1977). Consequently, the line charge concept becomes invalid at large distances downwind of the ion source. In addition, recombination results in ions being continually lost from the plume.

In this work, the plumes consisted of negatively charged aerosol rather than ions and hence it is probable that they would behave differently from ion plumes. In particular, the mobility of the charge carriers and their recombination rate will be lower, as discussed by Chalmers (1967). Therefore, such a plume is likely to be electrically more persistent than a small ion plume and will respond less to image and repulsion effects.

2.2. *The Effects of Atmospheric Turbulence*

The experiments with artificial ion plumes by Jones and Hutchinson (1976) and Jones (1977) demonstrated that the effects of turbulence could be correlated with the variations in electric field whilst the mean electric field (over a period of several minutes) could be associated with the mean wind vector. This becomes invalid at long distances downwind, particularly in unstable conditions, because parts of the plume begin to approach the ground, thereby resulting in large fluctuations of the electric field. However, in the experiments described herein the effects of turbulence were of less importance for two reasons. Firstly, the conditions were near neutral rather than unstable for the majority of the work, and secondly, the aerosol plume was released at a considerably greater height than the ion plume (120 m as compared with 10 m) hence reducing surface effects. Visual observation of the plume indicated that it remained compact up to at least 1 km downwind and thus the line charge assumption is justifiable for up to 2–3 km from the stack.

2.3. *The Effects of Electrostatic Repulsion and Image Forces*

It has been deduced by Jones and Hutchinson (1976) that

$$S = \left[S_0^2 + \frac{\mu\lambda x}{u\pi\epsilon_0}\right]^{1/2} \tag{1}$$

where S_0 is the original plume radius, μ the average mobility of the charged particles, ϵ_0 the permittivity of free space, x the distance downwind, u the mean wind speed, and S the plume radius at distance x.

Whilst λ the charge per unit length can be found experimentally (see Section 4) from electric field readings close to the stack, μ was estimated from the mean size and electric charge of the particles. In the same paper, it was also shown that image forces produced a downward motion of the charged particles. An approximate analysis yields

$$h = \left[h_0^2 - \frac{\mu\lambda x}{2u\pi\epsilon_0}\right]^{1/2} \tag{2}$$

where h_0 is the initial height of the plume and h is the height at distance x downwind.

Numerical estimation of these two effects, together with that of the natural electric field, is deferred to Section 4.

2.4. *Calculation of the Electric Field in the Vicinity of a Charged Plume*

The line charge theory developed in the Appendix enables all three components of the electric field at any point in space to be calculated. In this work, only the vertical component, F_z, at ground level was measured but the more general theory is presented because it is intended to measure the electric field in the x and y directions in the near future.

For $z = 0$, equation A (18) reduces to

$$F_z = \frac{-\lambda}{2\pi\epsilon_0}\left(\frac{h}{h^2 + R^2\sin^2\phi}\right)\left(1 + \frac{R\cos\phi}{[R^2 + h^2]^{1/2}}\right). \tag{3}$$

F_z depends only on R and ϕ (the polar coordinates of the measuring point with respect to the foot of the stack and plume axis) for constant λ. Consequently we may write

$$F_z\alpha\left(\frac{h}{h^2 + R^2\sin^2\phi}\right)\left(1 + \frac{R\cos\phi}{[R^2 + h^2]^{1/2}}\right) = G(R,\phi) \tag{4}$$

which is shown plotted for R positive (downwind) and R negative in Figs. 1 and 2 respectively.

2.5. *Calculation of the Electric Field Due to a Decaying Line Charge*

As the plume moves downwind and becomes more dilute recombination processes will slowly neutralize its charge and thus λ will steadily decrease along its length. Clearly this must significantly modify the

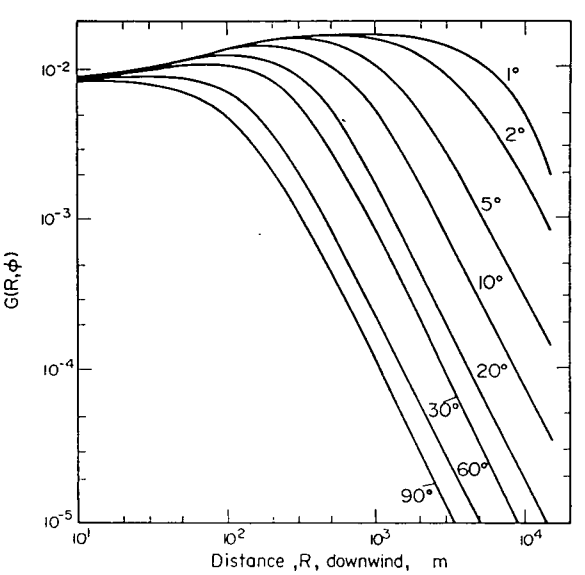

Fig. 1. Values of the function

$$G(R,\phi) = \left[\frac{h}{h^2 + R^2\sin^2\phi}\right]\left[1 + \frac{R\cos\phi}{[R^2 + h^2]^{1/2}}\right]$$

plotted for selected values of ϕ and R downwind of the stack. Stack height $h = 120$ m.

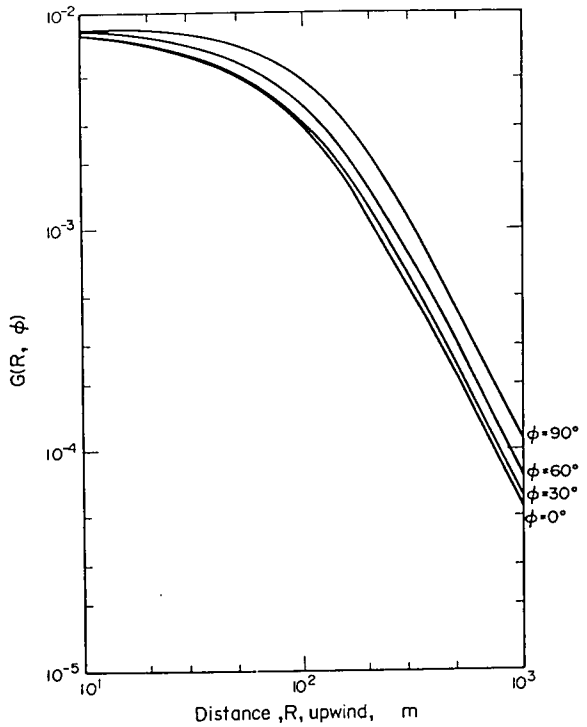

Fig. 2. Values of the function

$$G(R,\phi)=\left[\frac{h}{h^2+R^2\sin^2\phi}\right]\left[1+\frac{R\cos\phi}{[R^2+h^2]^{1/2}}\right]$$

plotted for selected values of ϕ and R upwind of the stack. Stack height $h = 120$ m.

values of electric field observed under the plume: the following analysis is an attempt to quantify this effect.

The rate of change of the concentration N of negatively charged particles, following Chalmers (1967) is given by

$$\frac{dN}{dt}=-\bar{\eta}PN \tag{5}$$

where $\bar{\eta}$ is the mean recombination coefficient between the negatively charged particles and oppositely charged ions and particles, and P is the number of positive charges per unit volume.

Since new air is continually being entrained into the plume as shown by Csanady (1973), it is reasonable to assume that P remains approximately constant. Equation (5) is then integrable and becomes

$$N=N_0\exp(-\bar{\eta}\,Pt) \tag{6}$$

where

$$N=N_0 \text{ at } t=0.$$

If the distance downwind along the plume is x, then $t = x/u$ where u is the mean wind speed. Therefore,

$$N=N_0\exp\left(\frac{-\eta Px}{u}\right). \tag{7}$$

It follows that

$$\lambda=\lambda_0\exp\left(\frac{-\eta Px}{u}\right) \tag{8}$$

which can be written as

$$\lambda=\lambda_0\exp\left(\frac{-x}{D}\right) \tag{9}$$

where D is a constant having the dimensions of length. From equation A(7) for $z = 0$ and taking into account the image charge, it follows that:

$$\delta F_z=\frac{-\lambda}{2\pi\epsilon_0}\frac{h}{[h^2+R^2\sin^2\phi]}\cos\beta\,\delta\beta. \tag{10}$$

Hence for a decaying line charge equation (10) becomes

$$\delta F_{z_{\text{decaying}}}=\frac{-\lambda_0}{2\pi\epsilon_0}\exp\left(\frac{-x}{D}\right)\frac{h}{[h^2+R^2\sin^2\phi]}\cos\beta\,\delta\beta \tag{11}$$

which is not integrable analytically.

This difficulty can be overcome as follows. Consider equation (10) for constant λ and $\phi = 0$. It is found that

$$\delta F_z=\frac{-\lambda}{2\pi\epsilon_0 h}\cos\beta\,\delta\beta \tag{12}$$

and therefore the field contribution from a line segment extending from β_1 to β_2 (see Appendix) is

$$F_z(\beta_1,\beta_2)=\frac{-\lambda}{2\pi\epsilon_0 h}\{\sin\beta_2-\sin\beta_1\}. \tag{13}$$

If equation (13) is rewritten in terms of x, the result

$$F_z(x_1,x_2)=\frac{+\lambda}{2\pi\epsilon_0 h}\left[\frac{R-x_2}{\{h^2+(R-x_2)^2\}^{1/2}}-\frac{R-x_1}{\{h^2+(R-x_1)^2\}^{1/2}}\right] \tag{14}$$

is obtainable, see Fig. A1 (Appendix). NB: the sign preceding λ has been changed to take account of the fact that β increases in an anticlockwise sense whereas x increases in a clockwise sense. This field contribution is compared with the field due to the entire plume, that is $F_z(0,\infty)$. Now,

$$F_z(0,\infty)=+\frac{\lambda}{2\pi\epsilon_0 h}\left\{-1-\frac{R}{[h^2+R^2]^{1/2}}\right\}. \tag{15}$$

Therefore,

$$\frac{F_z(x_1,x_2)}{F_z(0,\infty)}=\frac{\dfrac{R-x_2}{[h^2+(R-x_2)^2]^{1/2}}-\dfrac{R-x_1}{[h^2+(R-x_1)^2]^{1/2}}}{\left[-1-\dfrac{R}{[h^2+R^2]^{1/2}}\right]}. \tag{16}$$

Equation (16) enables one to estimate the fractional contribution due to a segment extending from x_1 to x_2 of an infinite line charge. Let R be equal to nh where h is the stack height, $x_1 = (n-1)h$ and $x_2 = (n+1)h$.

Equation (16) gives,

$$\frac{F_z(x_1,x_2)}{F_z(0,\infty)}=\frac{-2/\sqrt{2}}{-\left[1+\dfrac{n}{(1+n^2)^{1/2}}\right]} \tag{17}$$

and providing n exceeds about 3, the denominator of equation (17) can be approximated to -2. Hence the ratio of equation (17) tends to $1/\sqrt{2} \approx 71\%$. Similar calculations for intervals of $2h$ and $3h$ yield ratios of 89 and 95% respectively. Since the rate of charge decay is slow (as confirmed by the experimental results discussed in section 4), the exponential func-

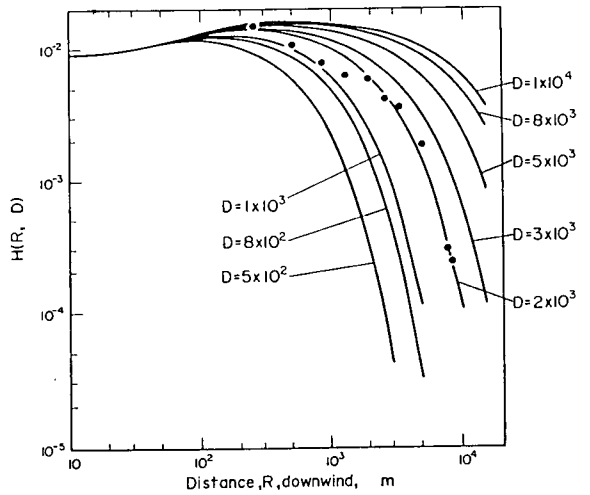

Fig. 3. Values of the function

$$H(R, D) = 1/h \exp(-R/D)\left\{1 + \frac{R}{(h^2 + R^2)^{1/2}}\right\}$$

for selected values of D and R. ● represents the maximum normalized values of electric field measured downwind of the plume.

tion in equation (11) may, with good approximation, be taken outside the integral when evaluating $F_{z_{decaying}}$ for ϕ equal to zero. This will also hold for small values of ϕ, but when this angle becomes large it is apparent on geometrical grounds that a much longer section of plume will contribute significantly to the electric field.

Therefore, an approximate expression for the electric field directly beneath a decaying line charge can be written as,

$$F_{z_{decaying}} = -\frac{\lambda_0 \exp(-R/D)}{2\pi\epsilon_0 h}\left\{1 + \frac{R}{(h^2 + R^2)^{1/2}}\right\} \quad (18)$$

where the decay constant D must exceed $3h$. Values of the function

$$H(R, D) = \frac{1}{h}\exp(-R/D)\left\{1 + \frac{R}{(h^2 + R^2)^{1/2}}\right\} \quad (19)$$

are shown in Fig. 3.

3. EXPERIMENTAL APPARATUS AND PROCEDURE

3.1. *Experimental Procedure*

Measurements of the vertical component of the electric field at ground level were carried out both upwind and downwind of the stack. The electric field was measured using field mills placed at four locations. Simultaneous readings were made manually at 15 s intervals by means of a prearranged starting time through the use of synchronized stop watches. In general, recordings were carried out for periods of ten minutes, after which the instruments were moved to new locations. Using this procedure it was possible to take electric field measurements over a considerable area in the vicinity of the stack in a few hours. The field mill locations were ascertained by reference to a detailed ordnance survey map and where conditions permitted, by also siting the stack with a prismatic compass. Since the stack height was known, it was possible to use angle of elevation measurements to provide an alternative estimate of the range of the stack. Care was taken to place the field mills on flat ground away from trees and fences, which could have shielded the electric field. The average wind speed (over a ten minute period) was measured as often as possible during the work. Atmospheric stability was gauged, with reference to the guidelines set by Pasquill (1974), from wind speed measurements (at 2 m), state of sky and time of day.

3.2 *The Field Mills*

The basic design and principles of the field mill have been described by Mapleson and Whitlock (1955). The performance of the field mills was improved by incorporating a F.E.T. input stage having an input resistance in excess of 10^9 Ω. This high resistance, when shunted with a large input capacitor, enabled the output signal to be independent of the rotor speed—a useful feature with battery-powered equipment. Six ranges were provided on the mills enabling fields from 100 V m^{-1} to 10 kV m^{-1} to be measured to an accuracy of better than 5%. Calibration of all four mills was checked before and after the work (using a parallel plate electrode system to which accurately known voltages could be applied). One of the field mills was provided with sign discrimination, this being achieved by the use of a photocell actuated phase-sensitive detector. The discriminating mill was particularly useful at locations where there were likely to be ambiguities in sign—for example at long distances downwind or crosswind.

3.3 *Point Discharge Measurements*

A metal discharge point, polished at its uppermost end was insulated from ground and supported by a mast which was varied in height from 9.25 m down to 3.25 m. The lower end of the metal point was connected by means of a low noise cable via a sensitive (Keithley Model 640) electrometer to a good earth. The equipment was located 700 m downwind of the chimney stack. Measurements of the point discharge current were made at 15 second intervals in synchronism with vertical electric field measurements at upwind and downwind locations at distances of 10 m from the mast. In addition, periodic measurements of the wind speed at a height of 2 m were recorded.

4. EXPERIMENTAL RESULTS AND DISCUSSION

An electric field profile obtained at groups of four positions is shown in Fig. 4—the values being averaged over 10 minute intervals. It can be seen that the electric field varies from about 5 kV m^{-1} at a distance of 270 m from the chimney stack down to 1 kV m^{-1} at 2 km from the stack. Mean upwind values of the fair-weather field varied from −240 V m^{-1} to −140 V m^{-1} during the measurement period.

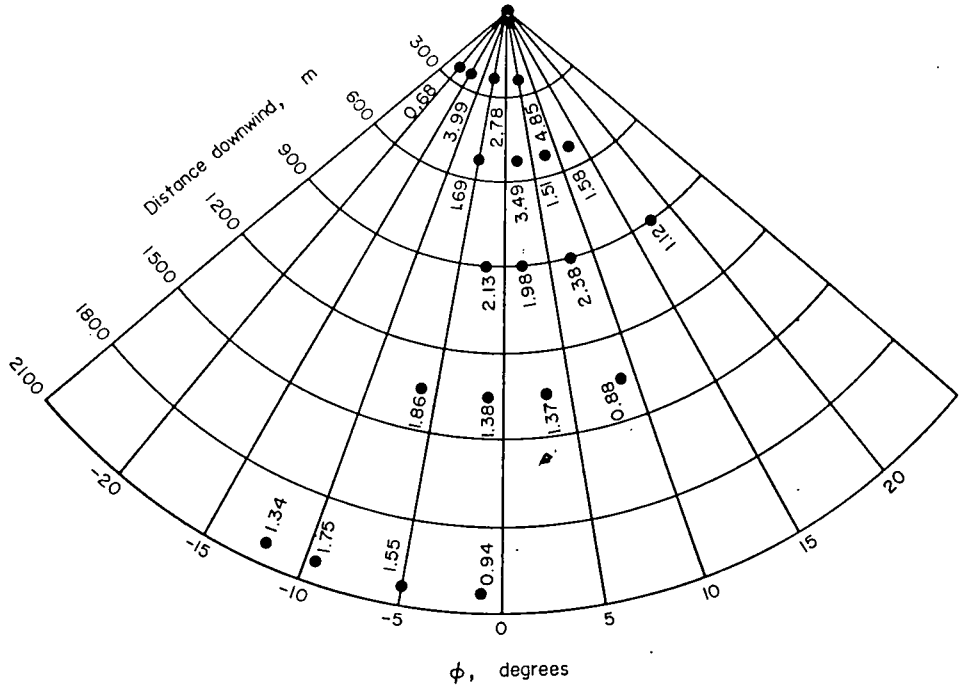

Fig. 4. Measured profiles of the mean electric field downwind of the stack. The electric field value at each site has units of kV m^{-1}.

The mean wind speed measured at 2 m was 3.1 m sec^{-1}, the predominant direction being Easterly.

Although the direction of the wind varied throughout the measurements, the overhead plume position was assumed to correspond to the location of the maximum averaged electric field value in the crosswind array. The variation of the maximum normalized value of electric field with distance downwind is shown in Fig. 3. The measurements show reasonably good agreement with the theoretical relation (19). It can be seen that the results suggest a value for the decay constant D of between 1 and 2 km. Measurements at greater distances downwind suggested that upwind values, that is values of the natural electric field, were only regained at distances in excess of about 9 km.

A typical variation in the electric field values over a ten minute period at four crosswind sites at a distance 490 m from the stack is shown in Fig. 5. Correlation coefficients of 0.68, 0.75 and 0.52 were computed for the three paired sites at distances of 63 m, 67 m and 57 m apart. A comparison between the predicted values of electric field at various angles ϕ to the maximum plume position according to equation (3), with the observed values is shown in Table 1 for a range of downwind distances. On average, the line charge relation underestimates the decrease in electric field by about 25% for distances up to 500 m down-

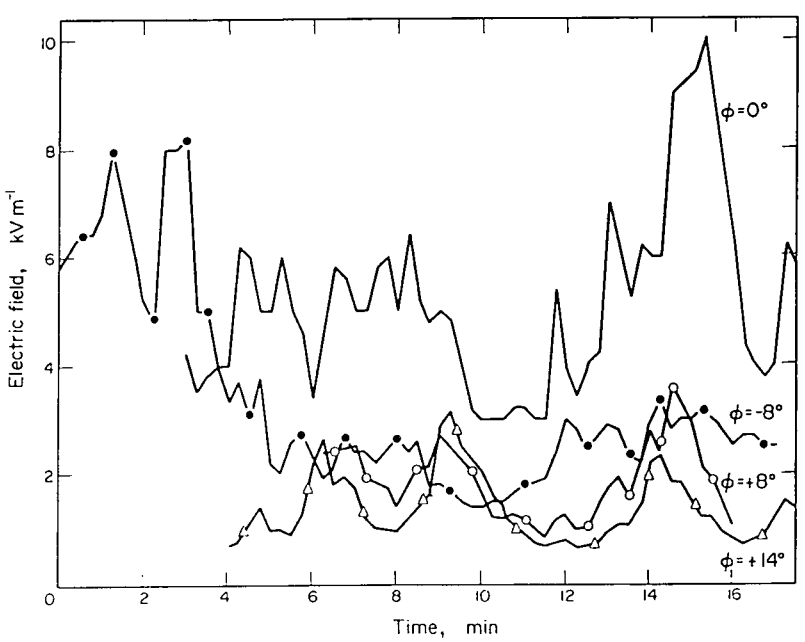

Fig. 5. Variation in electric field values at four crosswind positions defined by the ϕ values, 490 m from the stack.

Table 1. A comparison of experimental values of electric field at selected crosswind positions with the predicted values according to equation (3)

Date	R(m)	ϕ (degrees)	Normalized value of F_z (equation 3)	Normalised measured value
6 July 1976	160 m	0	1	1
(evening)	160 m	−3.6	0.99	0.87
	160 m	+3.6	0.99	0.88
	160 m	7.2	0.97	0.74
	160 m	+7.2	0.97	0.79
	280 m	0	1	1
	280 m	−5	0.96	0.66
	280 m	−9	0.88	0.39
	280 m	−11	0.83	0.81
	280 m	−20	0.59	0.65
6 July	500 m	0	1	1
	500 m	−8	0.75	0.49
	500 m	+8	0.75	0.36
	500 m	+14	0.49	0.28
7 July	273 m	0	1	1
	273 m	−9	0.88	0.57
	273 m	−18	0.65	0.82
	273 m	−24.5	0.51	0.14
	518 m	0	1	1
	518 m	−7	0.78	0.48
	518 m	+5	0.87	0.43
	518 m	+10	0.64	0.45
	900 m	0 1	1	
	900 m	−9.5	0.39	0.90
	900 m	−5.5	0.66	0.83
	900 m	+10	0.37	0.47
	1350 m	0	1	1
		+5	0.51	0.74
		+9.5	0.22	0.74
		+15	0.10	0.47
	2040 m	0	1	1
		+4.5	0.36	0.89
		−2.5	0.65	0.77
		+8.5	0.14	0.54

wind, and overestimated the decrease by about a factor of 2 at greater distances downwind. However, in conditions of reduced turbulence, for evening measurements, reasonably good agreement between theory and experiment was achieved.

Two sets of simultaneous measurements were carried out of the electric field at (A) distances 160 m, 447 m, 856 m and 1303 m downwind and (B) at 1303 m, 1648 m, 2057 m and 2790 m. The field mills were approximately along a straight line for these two sets of measurements. A cross-correlation analysis was carried out on the measurements and the results are shown in Table 2.

It can be seen that there is a greater cross-correlation between the field values at the sites for distances from the stack less than 1300 m (experiment A) than in the experiment B case. This probably is a consequence of the plume being more diffuse at the greater distances downwind. A cross-correlation analysis at various time lags in units of 15 seconds was also carried out. With the exception of one set of results which predicts a mean wind speed of 9 m sec^{-1} aloft, the cross-correlation analysis for the 6 paired electric field sites in experiments A and B give results consistent with an average wind speed of 3.2 m sec^{-1} measured at 2 m above ground. This gives a value of 5.1 m sec^{-1} at a height of 120 m above ground, using the wind profile relation of

$$\frac{U_1}{U_2} = \frac{\ln Z_1 - \ln Z_0}{\ln Z_2 - \ln Z_0} \tag{20}$$

where Z_0, the roughness length was taken to be 0.3 cm, and U_1 is the wind speed at height Z_1 and U_2 that at Z_2.

The calculated wind speed lies within the limits of the averaged value of wind speed derived from the cross-correlation analysis.

Electric field variations for experiment B are shown in Fig. 6(i). In Fig. 6(ii), these variations are shown displaced along the time axis by an amount corresponding to the lag-number for maximum correlation.

The mean value of electric field taken over a twenty minute period, 160 m directly downwind of the stack in stable conditions was found to be 4.92 kV m^{-1}. From this, the charge per unit length, λ, was calculated to be 1.82×10^{-5} C m^{-1} using equation (3). The charge per unit time, i, flowing out of the stack is given by

$$i = \lambda u \tag{21}$$

where u is the wind speed at the plume height. Using equation (20) u was estimated as 5 m sec^{-1}. Therefore i is 9.1×10^{-5} amperes.

A particle size distribution recently measured, from a sample at the exit of the electrostatic precipitators, by Wright (1976) is given in Table 3. These data yield an average particle radius of 7.5 μm. A mass concentration of 2.5×10^{-4} Kg m^{-3} at the stack exit was deduced from data supplied by the Eastgate management. Using this, an average particle number concentration of 5.1×10^{7} m^{-3} was derived. The volume flow rate through the stack was given as 130 m^3 sec^{-1}. Therefore the number of particles released per second, N_c, is about 6.6×10^{9}.

The particle charge q is given by

$$q = i/N_c \tag{22}$$

from which q is estimated to be 1.37×10^{-14} coulomb. This is equivalent to 1.2×10^{5} electronic units of charge and corresponds reasonably well with calculations based on field charging theory developed by White (1951).

Using a mobility of 1.3×10^{-5} m^2 sec^{-1} V^{-1} for the mean particle size of 7.5 μm, and the value of λ of 1.82×10^{-5} C m^{-1} equation (1) predicts an increase in plume radius of 40 m due to electrostatic repulsion at 1 km downwind of the stack. On the other hand, the predicted reduction in plume height due to image forces according to equation (2) is negligible (3%) at a similar distance downwind.

[In light winds (i.e. $\ll 5$ m s^{-1}) the effects of both electrostatic repulsion and image forces (see equations (1) and (2)) could be considerably larger than noted

Table 2. Cross-correlation values C_{xy} between adjacent sites x and y downwind of the stack for two experimental runs A and B

Experiment	Position	Distance Downwind from Stack (m)	Cross-Correlation Coefficient C_{XY}	Lag Number l 0	1	2	3	4	5	6	7	8	9	10
	1	160	C_{12}	0.532	0.546	0.619	0.729	0.886	0.889	0.807				
	2	447	C_{23}	0.265	0.396	0.642	0.782	0.672	0.43	0.195				
A	3	856	C_{34}	0.229	−0.279	−0.345	−0.132	0.188	0.414	0.509	0.383	0.151		
	4	1303												
	1	1303	C_{12}	0.080	0.058	0.156	0.324	0.363	0.734	0.800	0.607	0.412		
B	2	1648	C_{23}	−0.606	−0.018	0.098	0.267	0.617	0.646	0.590	0.476			
	3	2057	C_{34}	0.090	0.070	0.247	0.415	0.517	0.471	0.552	0.574	0.623	0.642	0.532
	4	2790												

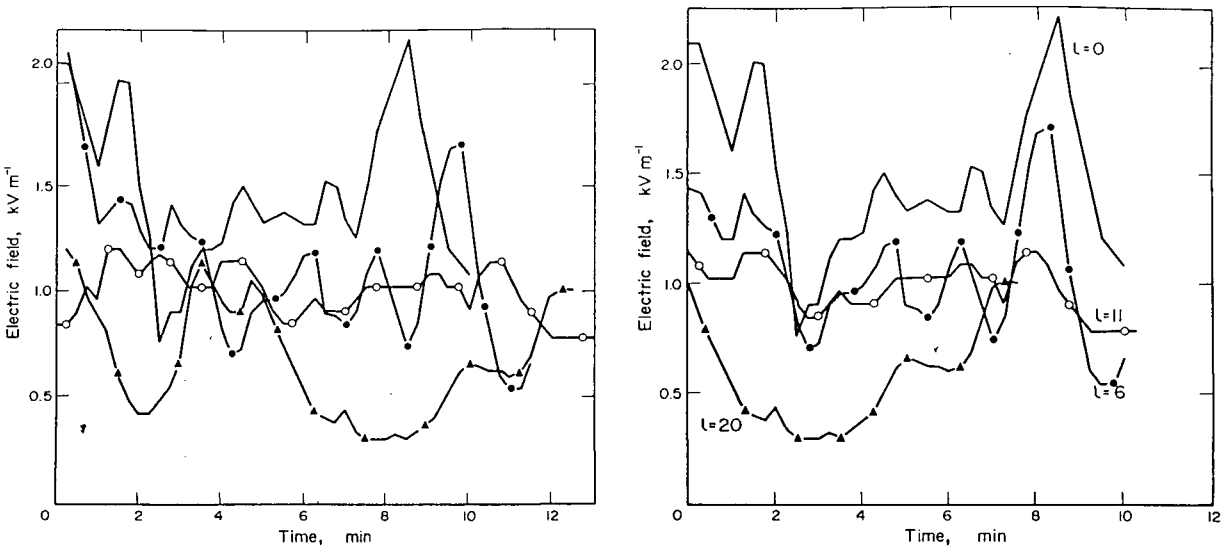

Fig. 6. (i) The variation in electric field at four sites downwind of the stack: 1300 m ——; 1650 m -●-●-●-; 2057 m -O-O-O-; 2790 m -▲-▲-▲-.

Fig. 6. (ii) Electric field variations for the same sites as in Fig. 6 (i). The electric field values are displaced along the time axis by lag number l (unit of 15 seconds) for maximum correction between the sites.

Table 3. A particle size distribution of a sample measured at the exit of the electrostatic precipitators at Eastgate

Projected Area Diameter (Micrometres)	Percentage of Particles Smaller than Stated Value (%)
64	89.5
32	69.5
16	52.5
8	34.5
4	18.0
2	8.0

Particle Density = 2.8×10^3 Kg m^{-3}.

above. Also in fine weather conditions (as obtained in this work) the atmospheric electric field is about $-100\ \mathrm{Vm}^{-1}$ and hence the plume velocity due to this would have been about $2 \times 10^{-3}\ \mathrm{m\,s}^{-1}$ upward—which is negligible. However, in disturbed weather, where the natural electric field can attain values exceeding $10\ \mathrm{kV\,m}^{-1}$, the effect on the plume trajectory may be substantial]

Measurements at 15 s intervals of both point discharge current and electric field were made continuously over a twenty minute period for a point height of 9.25 m. The variation of the point discharge current follows closely the variation of the electric field in the upwind position as shown in Fig. 7. Similar patterns were also observed over a ten minute period for point heights of 7.75 m, 6.25 m and 4.75 m, and for a point height of 3.25 m over a shorter period. Note that relatively large values of point discharge current, up to a maximum of 3 microamperes were recorded.

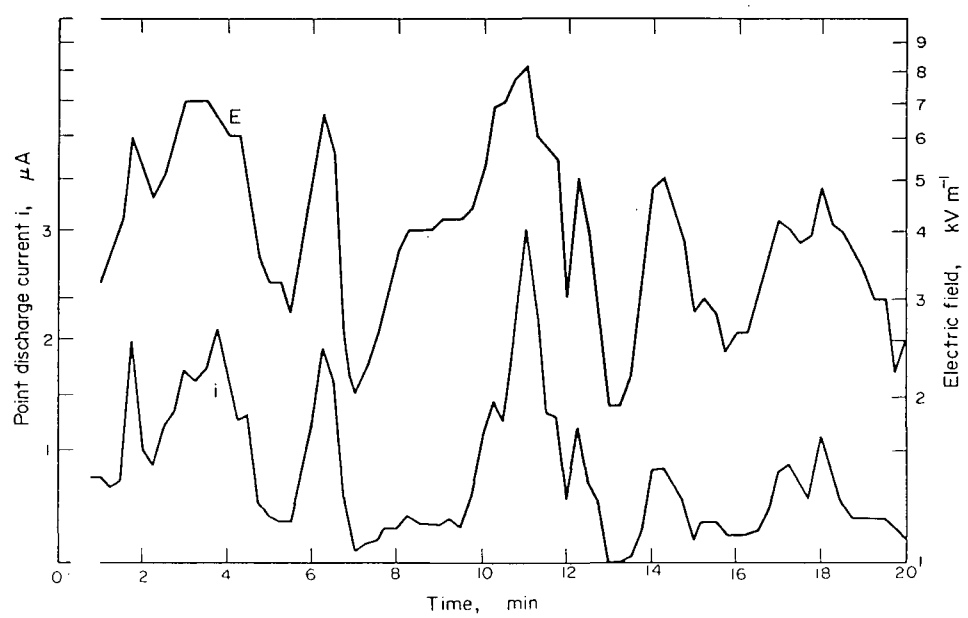

Fig. 7. Simultaneous measurement of point discharge current i and electric field E 10 m upwind of the point.

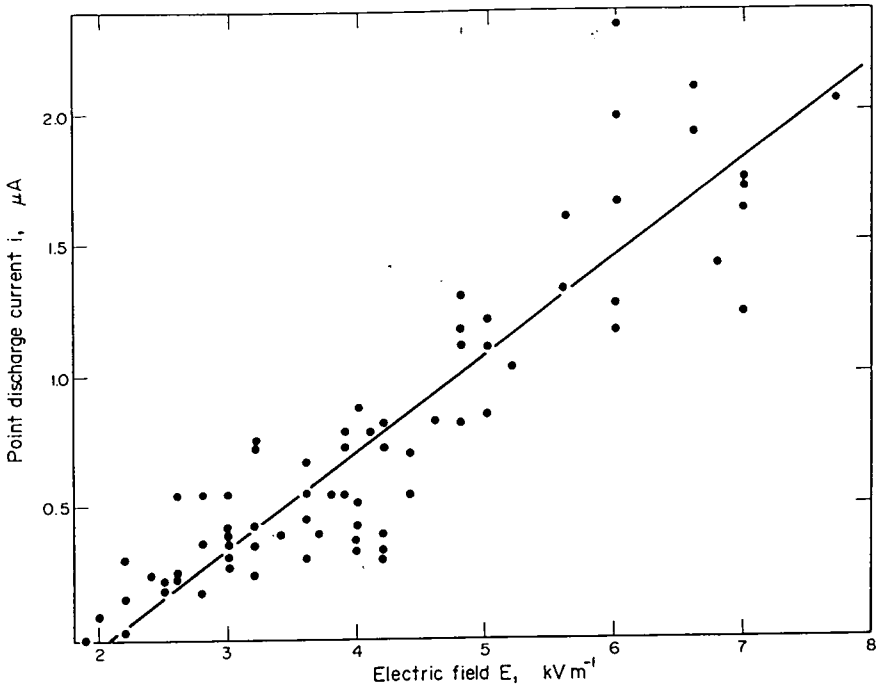

Fig. 8. The measured relation between point discharge current i and the upwind electric field E. The line of best fit is given by $i = 0.374\ (E - 2.08)$.

The individual values of point discharge current i in microamperes are plotted against the corresponding values of upwind electric field E, for the highest point. This is shown in Fig. 8. Similar results were also obtained for the other points. Lines of best fit using the least squares method yielded the following equations for the four point heights

(a) height 9.25 m $\quad i = 0.374\ (E - 2.08)$

(b) height 7.75 m $\quad i = 0.281\ (E - 2.02)$

(c) height 6.25 m $\quad i = 0.172\ (E - 2.37)$ (23)

(d) height 4.75 m $\quad i = 0.105\ (E - 2.58)$

where i is measured in microamperes, and E is in kV m^{-1}.

The form of the relation between i and E shows good agreement with the theoretical expression derived by Chalmers (1962):

$$i = 2\pi\ \epsilon_0\ u\ (E - E_0) \qquad (24)$$

where u is the wind speed, and E_0 is the value of the field below which no point discharge occurs. It is not possible to make a direct comparison of the experimental values with relation (24) as continuous measurements of wind speed could not be made during the experiments.

The presence of high values of electric field will cause significant point discharge to occur from sufficiently elevated metallic objects as evidenced from the described experiments. This could lead to electric spark production if the metal objects are poorly earthed. If the atmosphere in the vicinity of such metallic objects is inflammable, the occurrence of sparks could result in ignition. This hitherto unreported effect could present a considerable hazard and warrants further study.

5. CONCLUSIONS

1. The large electric fields observed (up to 10 kVm^{-1}) reflect the considerable plume charging arising from its passage through the electrostatic precipitators and suggest that, even with the relatively low mobility of the aerosol particles, significant electrostatic repulsion and trajectory modification could occur in light wind conditions. Electrical image forces might thus cause higher ground level concentrations than might have been expected from estimates based purely on diffusion theory.

2. Measurements of the electric field due to charged plumes could supplement conventional concentration measurement techniques described by several workers including Pasquill (1974), to study the basic features of plume diffusion. As pointed out by Moore (1973) there are various properties of plume behaviour such as plume rise and visibility which depend on the instantaneous values of material concentration within the plume rather than the normally measured time-averaged concentration. The field mill technique used in this work has the advantage of rapid response. This may be of particular significance in the investigation of concentration variations within charged plumes.

3. Significant point discharge currents were measured at 700 m from the stack. Hence, spark production could occur in the vicinity of charged plumes, and in unfavourable conditions may lead to the ignition of inflammable material.

Acknowledgements—The authors wish to acknowledge the cooperation of Mr. D. S. Reid, General Works Manager

of the Associated Portland Cement Manufacturers Ltd. (Weardale Works), and that of Mr. J. G. Wright, Northern Area Technical Services, the Associated Portland Cement Manufacturers Ltd.

They also wish to acknowledge Dr. W. C. A. Hutchinson, Department of Physics, University of Durham for the suggestion to undertake point discharge current measurements.

This work was supported, in part, by the Procurement Executive Ministry of Defence.

REFERENCES

Chalmers, J. A. (1962) The relation of point-discharge current to potential difference and wind-speed. *J. Atmos. Terr. Phys.* **24,** 339–344.

Chalmers, J. A. (1967) *Atmospheric Electricity*, 2nd Edition. Pergamon Press (Oxford).

Csanady, G. T. (1973) *Turbulent Diffusion in the Environment.* D. Reidel

Davis, R. and Standring, W. G. (1947) Discharge currents associated with kite balloons. *Proc. Roy. Soc.* **A. 191,** 304–322.

Jennings, S. G. and Jones, C. D. (1976) High electric fields due to industrial stack plumes. *Nature* **264,** 236.

Jones, C. D. (1977) Concentration variations at short distances downwind of continuous and quasi-instantaneous point sources. *Pestic. Sci.* **8,** 84.

Jones, C. D. and Hutchinson, W. C. A. (1976) Plumes of electric space charge in the lower atmosphere. *J. Atmos. Terr. Physics* **38,** 485–494.

Mapleson, W. W. and Whitlock, W. S. (1955) Apparatus for accurate and continuous measurement of the earth's electric field. *J. Atmos. Terr. Phys.* **7,** 61–72.

Maund, J. E. and Chalmers, J. A. (1960) Point-discharge currents from natural and artificial points. *Quart. J. Roy. Met. Soc.* **86,** 85–90.

Moore, D. J. (1973) Predicting the concentration of effluent material within a plume emitted from a tall chimney. Faraday Symposia of the Chemical Society, No. 7 Fogs and Smokes, 222–228.

Muhleisen, R. (1953) Die luftelektrischen Elemente in Grosstadbereich *Z. Geophys.* **29,** 142–60.

Pasquill, F. (1974) *Atmospheric Diffusion*, 2nd Edition, Ellis Horwood, Chichester.

White, H. J. (1951) Particle charging in electrostatic precipitation, *Trans. Am. Inst. Elec. Eng.* **70,** 1186–91.

Wright, J. G. (1976) Private communication.

APPENDIX. DERIVATION OF EXPRESSIONS FOR THE x, y AND z COMPONENTS OF THE ELECTRIC FIELD DUE TO A LINE CHARGE SEGMENT

1. *General solution for the field components*

Let the point A, at which the field is required, be defined by the cylindrical polar coordinates (R, Φ, z), the pole being at the base of the stack OS. Consider an element of charge $\delta l(FE)$ shown in Fig. A.1. If the line charge is λ coulomb per metre, then the electric field due to the element is

$$\delta E = \frac{-\lambda \delta l}{4\pi\epsilon_0 r^2}. \qquad \text{A(1)}$$

The negative sign indicates that the field is directed away from the charge and along EA. If the angles GAE and GAC are denoted by θ and α respectively, then the x, y and z components of the field can be written:

$$\delta E_x = \frac{\lambda \delta l}{4\pi\epsilon_0 r^2} \cos\theta \sin\alpha \qquad \text{A(2)}$$

$$\delta E_y = \frac{\lambda \delta l}{4\pi\epsilon_0 r^2} \cos\theta \cos\alpha \qquad \text{A(3)}$$

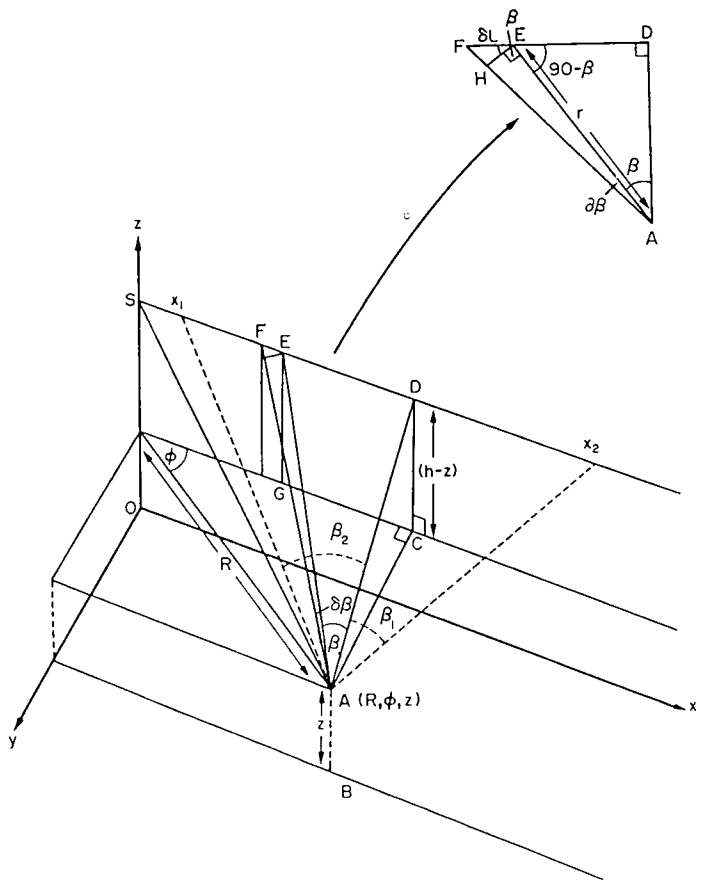

Fig. A.1. The coordinate position and associated parameters of a point A with reference to a line charge originating at a point S, height h above ground.

$$\delta E_z = -\frac{\lambda \delta l}{4\pi\epsilon_0 r^2}\sin\theta \qquad \text{A(4)}$$

from which it can be deduced that:

$$\delta E_x = \frac{\lambda}{4\pi\epsilon_0}[(h-z)^2 + R^2\sin^2\phi]^{-1/2}\cdot\sin\beta\,\delta\beta \qquad \text{A(5)}$$

$$\delta E_y = \frac{\lambda}{4\pi\epsilon_0}\frac{R\sin\phi}{[(h-z)^2 + R^2\sin^2\phi]}\cos\beta\,\delta\beta \qquad \text{A(6)}$$

and

$$\delta E_z = \frac{-\lambda}{4\pi\epsilon_0}\frac{(h-z)}{[(h-z)^2 + R^2\sin^2\phi]}\cos\beta\,\delta\beta. \qquad \text{A(7)}$$

Integration of expressions A(5), A(6) and A(7) gives:

$$E_x = \frac{\lambda}{4\pi\epsilon_0}[(h-z)^2 + R^2\sin^2\phi]^{-1/2}\cdot[-\cos\beta]_{\beta_1}^{\beta_2} \qquad \text{A(8)}$$

$$E_y = \frac{\lambda}{4\pi\epsilon_0}\frac{R\sin\phi}{[(h-z)^2 + R^2\sin^2\phi]}\cdot[\sin\beta]_{\beta_2}^{\beta_1} \qquad \text{A(9)}$$

and

$$E_z = -\frac{\lambda}{4\pi\epsilon_0}\cdot\frac{(h-z)}{[(h-z)^2 + R^2\sin^2\phi]}\cdot[\sin\beta]_{\beta_1}^{\beta_2}. \qquad \text{A(10)}$$

The line charge is situated at a height h above ground. The effect of the ground, which is assumed to be an infinite flat conducting sheet, can be included by using the concept of image charges. The image charge resides a distance h below ground. Denoting the field components due to this image charge by E_x^1, E_y^1 and E_z^1 it follows that,

$$E_x^1 = -\frac{\lambda}{4\pi\epsilon_0}\cdot[(h+z)^2 + R^2\sin^2\phi]^{-1/2}\cdot[-\cos\beta^1]_{\beta_1^1}^{\beta_2^1} \qquad \text{A(11)}$$

$$E_y^1 = -\frac{\lambda}{4\pi\epsilon_0}\cdot\frac{R\sin\phi}{[(h+z)^2 + R^2\sin^2\phi]}\cdot[\sin\beta^1]_{\beta_1^1}^{\beta_2^1} \qquad \text{A(12)}$$

and

$$E_z^1 = -\frac{\lambda}{4\pi\epsilon_0}\cdot\frac{+(h+z)}{[(h+z)^2 + R^2\sin^2\phi]}\cdot[\sin\beta^1]_{\beta_1^1}^{\beta_2^1}. \qquad \text{A(13)}$$

Therefore the total electric field components F_x, F_y and F_z are given by,

$$\left.\begin{aligned} F_x &= E_x + E_x^1 \\ F_y &= E_y + E_y^1 \\ F_z &= E_z + E_z^1 \end{aligned}\right\}. \qquad \text{A(14)}$$

2. Expressions for a line charge originating at S and extending to infinity in the positive X direction

In this case, the lower limits of integration (β_1 and β_1^1) are both equal to $-\pi/2$, assuming β increases in an anti-clockwise direction. Using Fig. A1 the following relations can be derived:

$$\begin{aligned} F_x = \frac{\lambda}{4\pi\epsilon_0}\Bigg[&\left\{\frac{1}{[(h-z)^2 + R^2\sin^2\phi]}\right\}^{1/2} \\ &-\left\{\frac{[(h-z)^2 + R^2\sin^2\phi]}{[R^2 + (h-z)^2]}\right\}^{1/2} \\ &-\left\{\frac{1}{[(h+z)^2 + R^2\sin^2\phi]}\right\}^{1/2} \\ &-\left\{\frac{[(h+z)^2 + R^2\sin^2\phi]}{[R^2 + (h+z)^2]}\right\}^{1/2}\Bigg] \end{aligned} \qquad \text{A(15)}$$

$$\therefore\quad F_x = \frac{\lambda}{4\pi\epsilon_0}\cdot\left[\frac{1}{\{R^2 + (h+z)^2\}^{1/2}} - \frac{1}{\{R^2 + (h-z)^2\}^{1/2}}\right] \qquad \text{A(16)}$$

$$\begin{aligned} F_y = \frac{\lambda}{4\pi\epsilon_0}\Bigg(&\left[\frac{R\sin\phi}{\{(h-z)^2 + R^2\sin^2\phi\}}\right] \\ &\times\left[\frac{R\cos\phi}{\{R^2 + (h-z)^2\}^{1/2}} + 1\right] \\ &-\left[\frac{R\sin\phi}{\{(h+z)^2 + R^2\sin^2\phi\}}\right] \\ &\times\left[\frac{R\cos\phi}{\{R^2 + (h+z)^2\}^{1/2}} + 1\right]\Bigg) \end{aligned} \qquad \text{A(17)}$$

and

$$\begin{aligned} F_z = \frac{-\lambda}{4\pi\epsilon_0}\Bigg(&\left[\frac{(h-z)}{\{(h-z)^2 + R^2\sin^2\phi\}}\right] \\ &\times\left[\frac{R\cos\phi}{\{R^2 + (h-z)^2\}^{1/2}} + 1\right] \\ &+\left[\frac{(h+z)}{\{(h+z)^2 + R^2\sin^2\phi\}}\right] \\ &\times\left[\frac{R\cos\phi}{\{R^2 + (h+z)^2\}^{1/2}} + 1\right]\Bigg). \end{aligned} \qquad \text{A(18)}$$

Jones C. D. (1977).

Ionised air as a wind tunnel tracer.

J. Phys E: Scientific Instruments. **10**, 1287 - 1291.

Ionised air as a wind tunnel tracer

C D Jones
Chemical Defence Establishment, Porton Down, Salisbury, Wilts SP4 0JQ, UK

Received 7 March 1977, in final form 1 July 1977

Abstract The results of some space charge concentration and electric field measurements made downstream of a source of positive ions in a low-turbulence wind tunnel are described. The plume expansion due to electrostatic effects is compared with the predictions of a simple theory. It is shown that the experimental technique, previously used for full-scale diffusion experiments in the open air, could probably be adapted for wind tunnel work.

1 Introduction

Recently Jones and Hutchinson (1976) and Jones (1977) have successfully used unipolarly ionised air as a tracer in short-range (i.e. less than 100 m downwind) atmospheric diffusion experiments and the technique was shown to possess several advantages over more conventional methods which generally employ chemical tracers. In their outdoor experiments a continuous stream of positively ionised air was produced by application of a stabilised high voltage (20 kV) to a coaxial electrode system through which air was blown. The cylindrical outer electrode was of 0·06 m radius, the inner being a wire of 5 μm radius: the resultant radially asymmetric field distribution ensured that, with a positive high voltage on the wire, only positive ions would be produced by the apparatus (because all negative ions and electrons would be rapidly discharged at the central wire). The ion concentration downwind of the ion generator was measured by drawing the ionised air into a coaxial electrode arrangement (outer electrode radius 0·02 m) across which a bias voltage of 900 V was maintained. The ion currents, typically in the range 10^{-11}–10^{-8} A, were measured with a solid state electrometer (Keithley, model 602).

A particular advantage of the method, as compared with chemical techniques, is that it permits concentration measurements to be made at very high resolution; the response time of the ion collector employed in this work was about 10 ms and even this figure could be considerably bettered if required. However, a serious difficulty in practice is that the ions will only 'trace' air motions accurately provided that they are not subjected to strong electric fields. Whilst this will generally be the case when the ion plume is well downwind of the release point (and hence dilute), nearer the ion generator considerable self-repulsion effects can occur. An attempt has been made to quantify these effects theoretically by Jones and Hutchinson (1976), but experimental validation is difficult in the atmosphere because of the highly irregular, turbulent and uncontrollable nature of the flows experienced therein. Hence the purpose of the present investigation was to determine under controlled conditions the ion concentration distribution in the ion plume at short distances downstream and, from the data accrued, to ascertain firstly the numerical magnitude of the repulsion effect, and secondly whether a scaled-down version of the ion tracer technique might be of use in a wind tunnel environment.

2 Theoretical

2.1 Plume current

In a wind tunnel (unlike in the atmosphere) it is reasonable to assume that the plume axis is straight; thus the system can be very conveniently described in terms of cylindrical polar coordinates (d, r, θ). Here d is the distance downstream from the ion generator, r the radial distance from the plume axis and θ the angle made by the radius vector to an arbitrary, fixed radial vector. Generally the space charge concentration ρ will depend on d, r and θ; thus the charge crossing a small area δs (perpendicular to the axis) can be written in the form

$$u\rho(d, r, \theta)\, r\delta\theta\delta r$$

where $\delta s = r\delta\theta\delta r$ and u is the air speed. The total current i crossing the perpendicular plane at a distance d downstream is therefore

$$i(d) = u\int_0^R \int_0^{2\pi} \rho(d, r, \theta)\, r\, \mathrm{d}\theta\, \mathrm{d}r \qquad (1)$$

where R is the maximum plume radius and u has been assumed independent of r and θ. (Note that i will only be independent of d if recombination and wall losses are negligible – see §3.2.2).

For an axisymmetric plume, equation (1) reduces to

$$i(d) = 2\pi u\int_0^R \rho(d, r)\, r\, \mathrm{d}r. \qquad (2)$$

2.2 Plume expansion caused by self-repulsion effects

At the surface of (and also within) an ion plume the radial electric field causes it to expand at a rate dependent upon the magnitude of the field and upon the mobility μ of the ionic species involved. Provided that the expansion rate is not so large that the plume shape is far from cylindrical it has been shown by Jones and Hutchinson (1976) that, if R_0 is the initial radius of the plume (i.e. at the source) and R its radius at a distance d downstream,

$$R = \left(R_0^2 + \frac{\mu i d}{u^2 \pi \epsilon_0}\right)^{1/2} \qquad (3)$$

where ϵ_0 is the permittivity of free space.

It should be stressed that, in the derivation of equation (3), the effects of turbulent motions upon the plume expansion have been ignored – however, this is compatible with the very low level of turbulence present in the wind tunnel that was used in the experimental work.

A further point is that whereas equation (3) was originally derived for an ion plume in the open air and well away from any boundaries, it can be deduced (from Gauss's theorem) that the result will also apply to an ion plume in a conducting tube, provided that the radius of the tube is small compared with its length.

2.3 Calculation of the electric field produced by the ion plume

It should be stressed that the electric field measurements were not intended to be anything more than subsidiary in this work. In fact their role was essentially corroborative, indicating that the values of plume current deduced from the ion concentration observations bore some relation to those calculated from electric field data. The electric field can be estimated by noting that the plume radius increases as $\sqrt{d}$ (approximately) and hence the plume can be regarded as near-cylindrical over short sections of its length. In addition, if field measurements are made at a point sufficiently far downstream of the ion generator that the plume length subtends an angle approaching 180° at the observation point (Jones and Jennings 1977), one may apply Gauss's theorem to estimate the field. For such a plume in a conducting cylinder, the electric field E is given by

$$E=\lambda/2\pi r\epsilon_0$$

where λ is the charge per unit length (C m^{-1}) and r is the perpendicular distance from the plume axis ($r>R$). Further, since

$$\lambda=i/u$$

we have

$$E=i/2\pi r\epsilon_0 u. \tag{4}$$

Alternatively one might consider the electric field E', due to an identical charge distribution distant r from an infinite, flat, conducting sheet, as being equally realistic. This is given by (Jennings and Jones 1976) the relation

$$E'=i/\pi r\epsilon_0 u. \tag{5}$$

Hence, for example, if the floor of the wind tunnel had a significantly higher conductivity than the walls and ceiling (which was probably true) the electric field would tend to a value nearer E'. Note that E is only half E', so an accurate estimate of the plume current is not really possible in these experiments.

3 Results and discussion

3.1 Initial notes

The wind tunnel used in this work was of rectangular cross section (width 1·37 m, height 1·22 m) and was of the closed-circuit type. The working section was 3 m in length. The air speed, which was measured using a built-in differential pressure manometer system, could be accurately set between 1 and 60 m s^{-1}. Turbulence levels (previously determined to be about 0·15% or less) were intentionally kept to a minimum so that plume expansion would be dominated by electrostatic effects. The ion generator, described in §1, was streamlined using a parabolic nose-cone; however, at low air speeds the jet of ionised air emerging from the generator (at 7 m s^{-1}) unavoidably introduced a certain amount of small-scale turbulence into the air stream. The walls of the wind tunnel working section (one of which was largely of Perspex) were treated with antistatic fluid to aid dissipation of any collected charges.

3.2 Ion concentration measurements (figure 1)

3.2.1 The spatial distribution of mean concentration Provided that ion concentration measurements were not taken within a few centimetres of the plume boundary the values observed were generally steady to within a few per cent of their average. Readings of concentration were taken over the entire tunnel cross section, 2 m downstream of the ion generator at 0·1 m spatial intervals (both vertical and horizontal) for selected air speeds up to 15 m s^{-1}. A less extensive survey was also conducted in a plane 1 m downstream of the generator.

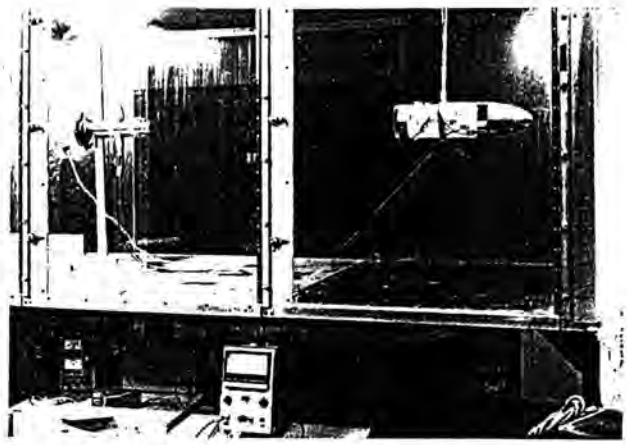

Figure 1 Photograph showing the ion collector (left) and the ion generator (right).

The results obtained, particularly at 2 m downstream, showed that the plume possessed a high degree of axisymmetry which enabled the average profiles (presented in figure 2) to be constructed without loss of accuracy. (The corresponding 1 m profiles are shown in figure 3 but less reliance can be placed on the data from which they are derived.)

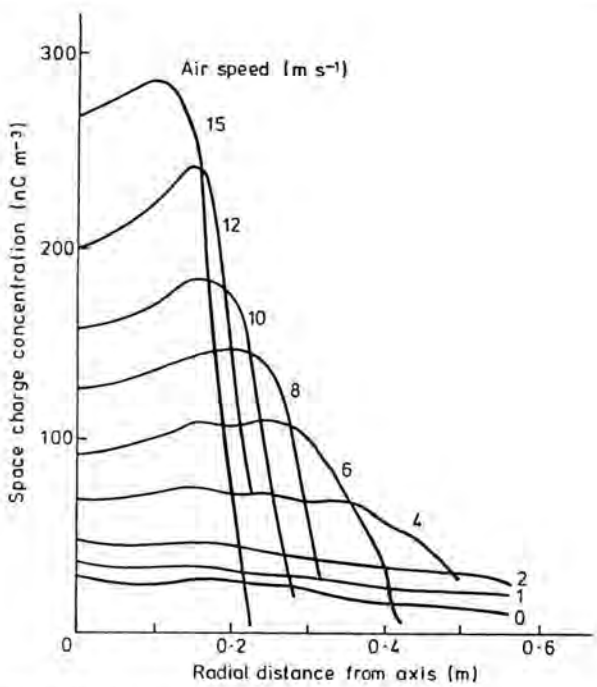

Figure 2 Radial concentration profiles at 2 m downstream.

3.2.2 Estimation of the plume current Reference to equation (2) suggests that $i(d)$ could be readily determined from the profiles by numerical integration. The results obtained are given in table 1.

A somewhat unexpected feature of these results is the variation of plume current with air velocity. This can, however, be explained as follows. The action of this type of ion generator utilises the fact that the positive ions, created in the corona region within 2–3 mm of the central wire, take several milliseconds to reach the outer electrode and be discharged. Hence a stream of positively ionised air can be readily produced by simply blowing air through the electrode system. However if

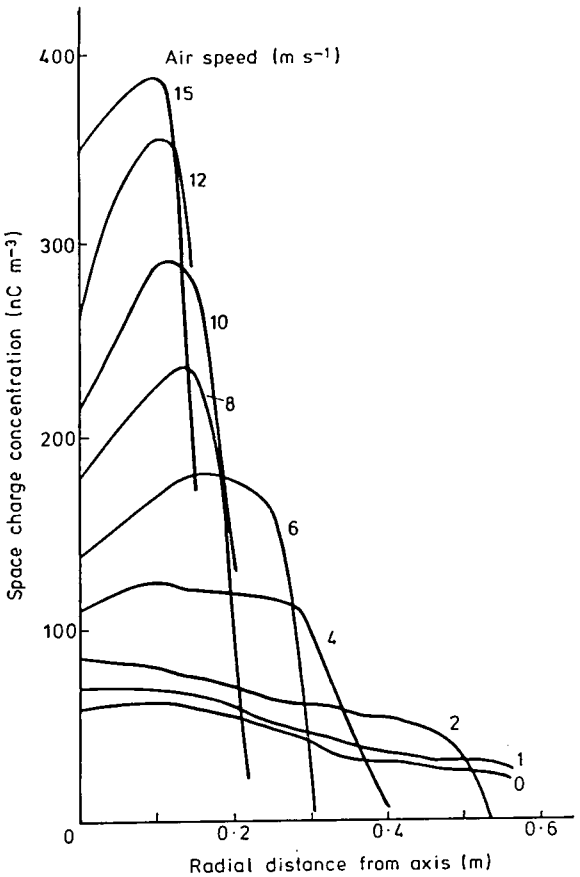

Figure 3 Radial concentration profiles at 1 m downstream.

Table 1 Values of plume current at 2 m downstream.

Air speed (m s^{-1})	Plume current (μA)
4	0·20
6	0·25
8	0·29
10	0·35
12	0·36
15	0·40

maximum ion output is to be obtained it is necessary to mount the electrodes right at the end of their supporting tube in order to minimise wall losses. Consequently, in low or zero air velocities in the wind tunnel, local space charges may reduce ion production (by repulsion) whilst, at higher air speeds, interaction of the tunnel stream with the air flow over the electrodes (by wake and boundary layer effects) could augment ion production.

The effects of ionic recombination must also be considered. Charge neutralisation by combination with negative ions or electrons clearly cannot occur in a unipolar plume, but combination with 'large' atmospheric particles (Chalmers 1967) might reduce their mobility to such an extent that collection with the system employed would be very inefficient. However, much experience with the ion generator and collector in the open air suggests that, as a substantial fraction of the small ions released can be observed even at 100 m downwind, this type of combination process will not deplete the small ion concentration significantly in the experiments reported here.

3.2.3 Plume expansion and ionic mobility The values of i in table 1 can be used in a number of ways. Perhaps the most interesting possibility is to use the data, in conjunction with the radial concentration profiles given in figure 2 and equation (3), to estimate the ionic mobility. Table 2 lists the results obtained.

Table 2 Plume data at 2 m downstream.

Air speed (m s^{-1})	Plume radius (from figure 2) (m)	Mobility (estimated from equation (3)) (10^{-4} m^2 V^{-1} s^{-1})
4	0·45	2·21
6	0·37	2·67
8	0·29	2·47
10	0·25	2·37
12	0·21	2·25
15	0·18	2·25
Mean mobility $= 2{\cdot}37 \times 10^{-4}$		

Accepted values (Chalmers 1967) of atmospheric small ion mobility are in the range $1\text{–}2 \times 10^{-4}$ m^2 V^{-1} s^{-1}, but somewhat higher values would be expected for the ions here because they were being observed only a few tenths of a second after their creation (Ungethum 1974). The mean mobility value derived may be used to calculate (again with equation (3)) the plume dimensions at 1 m downstream, and the results compared with those observed (table 3).

Table 3 Observed and calculated plume radii at 1 m downstream.

Air speed (m s^{-1})	Observed radius (m)	Calculated radius (m)
4	0·32	0·33
6	0·28	0·25
8	0·21	0·21
10	0·19	0·18
12	0·15	0·16
15	0·13	0·14

The fact that reasonably good agreement is obtained suggests that the value of mobility deduced is approximately correct. It is interesting to note that, if the value of mobility deduced for an air speed of 6 m s^{-1} at 2 m downstream is used to calculate the plume radius at 1 m downstream, the result 0·27 m is obtained. It is possible that this may not be entirely fortuitous but could well indicate that flow interactions are occurring between the tunnel air stream and the emergent ionised air stream – which is at about 7 m s^{-1}.

3.2.4 Ion concentration fluctuations Well within the ion plume the concentration variations were small in magnitude and a typical record, taken at 2 m downstream, 0·2 m off the plume axis and at an air speed of 6 m s^{-1}, is given in figure 4. Any variations that did occur were thought to arise from:

(i) The effect of the turbulence in the ionised air stream emerging from the ion generator;

(ii) Wake effects due to the presence of the ion generator in the wind tunnel air stream.

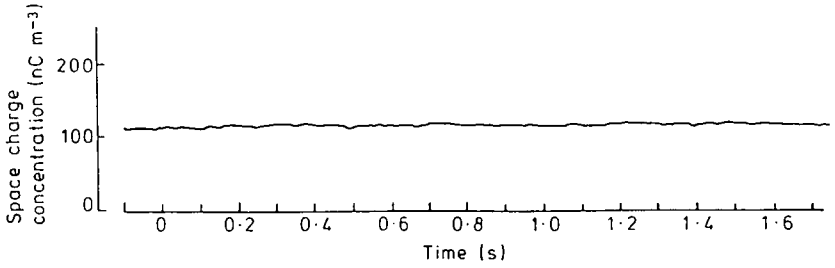

Figure 4 Space charge concentration record at 2 m downstream, 0·2 m off-axis of ion generator (air speed 6 m s^{-1}).

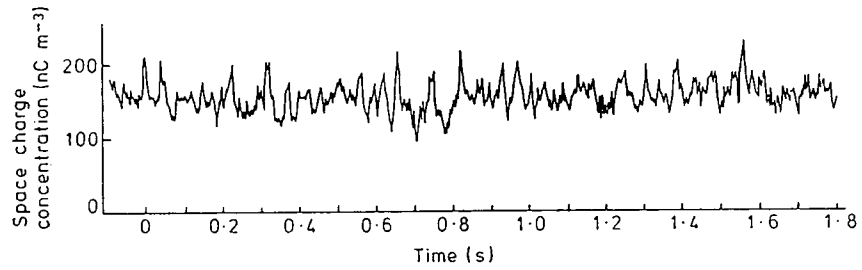

Figure 5 Space charge concentration record at 2 m downstream, 0·2 m off-axis of ion generator (air speed 12 m s^{-1}).

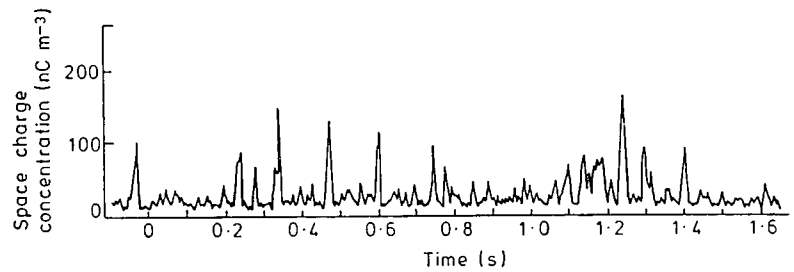

Figure 6 Space charge concentration record at 2 m downstream, 0·2 m off-axis of ion generator (air speed 15 m s^{-1}).

Figure 5 shows the concentration observed at the same point but at a higher air speed (12 m s^{-1}) such that the ion collector was just within the plume boundary. At still higher speeds (15 m s^{-1}) (figure 6) the ion collector recorded a low background concentration against which frequent, short-lived bursts (about 10 m s^{-1}) of high concentration can be discerned. These latter are doubtless a result of small-scale, transverse, turbulent motions and entrainment processes occurring at the plume boundary.

Similar effects were also observed at different distances from the plume axis although of course at different air stream velocities.

3.3 *Electric field measurements*

These measurements were made with a field mill (similar to that described by Mapleson and Whitlock 1955) set into the floor of the wind tunnel. Observations were made directly beneath the plume axis at a point 2·2 m downstream of the ion generator and were confined to high air speeds (at which it was known from the ion concentration measurements that the plume must have conformed quite closely to a cylindrical charge configuration). The electric fields observed are given in table 4. In the 10 m s^{-1} run the observed field lay between the values (1·03 and 2·06 kV m^{-1}) predicted by equations (4) and (5) respectively for the value of plume current given in table 1. Note that the observed electric field at 20 m s^{-1} was less than half that at 10 m s^{-1}, which does not accord with the previously deduced trend of i increasing with u. No explanation of this, apart from the obvious one that the trend is not maintained at speeds greater than 15 m s^{-1}, can be advanced at this stage.

Table 4 Electric field data.

Air speed (m s^{-1})	Observed field (kV m^{-1})
10	1·43
20	0·62

Charge retention on the wind tunnel walls did not appear to be a problem as the electric field decayed immediately the ion generator was switched off; furthermore, all charges were completely dissipated before passing around the wind tunnel circuit. In addition no significant extraneous fields were observed from the high-voltage wiring to the ion generator, which could have introduced errors in these measurements.

4 Applications and conclusions

From the foregoing it would appear that the ionised air tracer technique, previously applied in full-scale atmospheric diffusion experiments, might have some potential for wind tunnel diffusion studies. However, before its application can be seriously contemplated, it is evident that a very considerable scaling-down of the present system will be required. In principle this should not be difficult because the ion concentrations observed in the tunnel were some 10^3 times larger than those which have been successfully detected in the open air. Scaling down the system would also confer the important

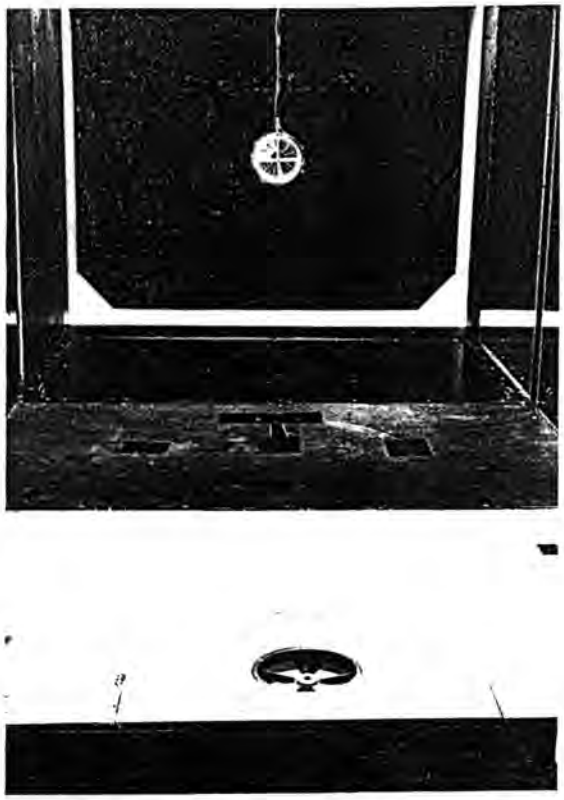

Figure 7 Photograph showing field mill in the lower foreground with the ion generator above.

advantage of reducing mutual repulsion effects to virtually negligible proportions, as is shown in the following example. Consider an ion generator of 10^{-10} A output having an outlet radius of 5 mm operating in an air stream of 10 m s^{-1}. Use of equation (3) shows that in the absence of turbulent (and molecular) diffusion the plume will have increased its radial dimension to only 6·5 mm at 2 m downstream. Compared with the effects of turbulent diffusion this is virtually insignificant (in the majority of cases) and thus ion concentration measurements could provide a relatively cheap and extremely high-resolution means of observing the concentration structure of plumes. At such low concentrations the ions could probably be piped quite successfully and released through a scale model of, for example, a factory chimney. The ion concentration in such a plume would be in the region of 20 nC m^{-3} – readily detectable with a simple ion collector. For example, with a collector of 2 mm radius sampling isokinetically, the observed current would be about 2 pA (easily measurable with an electrometer). In addition the temperature of the emergent ionised air stream could be varied to model buoyancy or slumping, such alterations having very little effect upon the operation of the ion generator and collector.

One conceivable disadvantage of the technique arises from the fact that objects near the ion plume will develop induced charges which will cause the plume to be attracted towards them. However an examination of the probable magnitude of this effect suggests that it will be insignificant (in the example cited above) except where there are very sharply curved objects such as corners and points. The slight rounding-off of corners on scale models needed to eliminate the effect would almost certainly not detract from the fluid mechanical reality of the system being investigated.

The results of some experiments using scaled-down versions of the ion generator and collector will, it is hoped, be reported in a future publication.

Acknowledgment

The author is indebted to Dr J K Harvey, Department of Aeronautics, Imperial College, London, for the use of the wind tunnel and for many helpful suggestions concerning this work.

References

Chalmers J A 1967 *Atmospheric Electricity* (Oxford: Pergamon) chap. 4

Jennings S G and Jones C D 1976 *Nature* **264** 236

Jones C D 1977 *Pesticide Sci.* **8** 84

Jones C D and Hutchinson W C A 1976 *J. Atmos. Terr. Phys.* **38** 485

Jones C D and Jennings S G 1977 *Atmos. Environ.* in the press

Mapleson W W and Whitlock W S 1955 *J. Atmos. Terr. Phys.* **7** 61

Ungethum E 1974 *J. Aerosol Sci.* **5** 25

Jones C. D. (1977).

Ion concentration variations at short distances downwind of continuous and quasi-instantaneous point sources.

Pestic. Sci. **8**, 84 - 95.

Pestic. Sci. 1977, 8, 84–95

Ion Concentration Variations at Short Distances Downwind of Continuous and Quasi-instantaneous Point Sources[a]

Christopher D. Jones

Chemical Defence Establishment, Porton Down, Salisbury, Wilts.

(*Manuscript received 4 February 1976*)

An improved experimental technique is described which enables the fine structure of the ion concentration variations downwind of both continuous and instantaneous point sources to be examined. The method, which involves the use of ionised air, permits resolution of features within diffusing clouds of the order of centimetres since the detector response time is about ten milliseconds. The success of the method can be attributed to the fact that the measurements are entirely electrical in nature, thereby eliminating certain defects inherent in most other sensing techniques. However, the method does possess disadvantages and these are critically examined. Experimental results are presented which show clearly the presence of considerable fine structure hitherto suspected, but not quantitatively observed, in diffusing plumes, i.e. from continuous sources, and puffs, i.e. from instantaneous sources. The implications of these data are considered briefly.

1. Introduction

Scientific examination of activities such as crop-spraying necessitates detailed understanding of the small-scale transport and diffusion processes occurring in the lower atmosphere. Near the surface, atmospheric motion is usually turbulent[1] and, moreover, this turbulence is spatially inhomogeneous and temporally non-stationary.[2] Prediction of both the trajectories of and the concentration distributions within individual clouds is therefore extremely difficult if not inherently impossible; however, in many cases,[3–5] the assumption of Gaussian profiles of dosage and concentration has proved of value, even though the justification for it is weak. The deficiencies of Gaussian profiles are most evident in the investigation of instantaneous concentration distributions and have long been recognised,[6] though relatively little work has been undertaken in this field because of the very considerable theoretical and experimental difficulties encountered. Consideration of the frequency spectrum of the velocity variations present in atmospheric turbulence[7] suggests that, at least as far as 100 m downwind from a source, fine structure having a scale of the order of tens of centimetres will exist in diffusing clouds. Therefore, in any experiments to investigate these phenomena stringent requirements will be placed on detector response-time if adequate resolution of the structure is to be obtained. Thus, although Gosline[8], using nitric oxide as a tracer with a detector response time of 10 s, and Ramsdell and Hinds,[9] using krypton with a response time of 38 s, employed fast response instruments by normal standards, the more rapid variations in concentration would probably have been missed. Despite this limitation, subsequent analysis[10] showed that the time distribution of the concentration variations experienced at a given point was approximately logarithmic-normal, provided zero readings of concentration were discounted. If this type of analysis is to have maximum applicability in practical situations then examination of the entire spectrum of the concentration variations would be highly desirable. In this paper an experimental technique[11,12] for investigating the fine structure of diffusing clouds is presented and some preliminary observations are discussed.

[a] Presented at a meeting *Droplets in air. Part I; The generation and behaviour of airborne dispersions* on 7 October 1975, organised jointly by the Physicochemical and Biophysical Panel (Pesticide Group) and the Colloid and Surface Chemistry Group, Society of Chemical Industry, and the Society of Cosmetic Chemists of Great Britain.

2. Theory and limitations of the ion tracer technique

2.1. Initial remarks

Unipolar ions are capable of persisting in the lower atmosphere for several minutes[13] before they are neutralised by recombination. Because in short-range atmospheric diffusion investigations travel times are only a few tens of seconds, such ions might be a suitable tracer to use in this work.[14,15] However, the charge on the cloud will affect it in two ways as compared with an uncharged cloud.[12] Firstly, the cloud will expand because of the outward electrostatic forces and secondly, due to the proximity of the ground, electrostatic image forces will induce downward motion.[a] If these effects are substantial compared with those of turbulent diffusion, then the use of ions in the application envisaged would be precluded.

2.2. The electrostatic repulsion force and comparison of its effects with those of turbulent diffusion

Assuming that the expansion is due entirely to electrostatic forces, for an ion plume (i.e. from a continuous source) of initial radius r_0, the radius[b] r_{plume} at a distance x downwind is given approximately[12] by

$$r_{\text{plume}} = \left[r_0^2 + \frac{\mu i x}{u^2 \pi \epsilon_0} \right]^{1/2} \tag{1}$$

where μ is the small-ion mobility, i the ion generator output current, u the wind velocity and ϵ_0 the permittivity of free space.

The relation

$$r_{\text{puff}} = \left[r_0^3 + \frac{3\mu i \Delta\tau x}{4u\pi\epsilon_0} \right]^{1/3} \tag{2}$$

where $\Delta\tau$ is the short time interval over which the ions are released, has been derived for an ion puff,[11] i.e. that from an instantaneous source.

The next step is to incorporate the effects of turbulent diffusion into equations (1) and (2). In many cases the turbulent spreading of puffs and plumes can be approximately estimated from empirical formulae involving power laws of x. In neutral conditions a representative puff radius r' is given by[16]

$$r' = 0.13x^{0.92} + r_0' \tag{3}$$

where r_0' is the initial radius. This relation is particularly useful in that it can also be used to estimate the *instantaneous* transverse radius of a plume. However, further simplification is required prior to developing the analysis and this is achieved by approximating r' to a linear function of x. In the region of interest equation (3) can be adequately described by

$$r' = Kx + r_0', \text{ where } K = 0.1. \tag{4}$$

Consider the situation at x where the radius is R. If the total expansion rate, for a charged system is $\mathrm{d}R/\mathrm{d}x$ then

$$\frac{\mathrm{d}R}{\mathrm{d}x} = \left(\frac{\partial R}{\partial x}\right)_{\text{electrostatic}} + \left(\frac{\partial R}{\partial x}\right)_{\text{turbulent}}, \tag{5}$$

[a] The additional motion arising from the Earth's natural electric field will not be significant in fair weather and is therefore ignored.

[b] The longitudinal expansion rate can be shown to be small in most conditions and is therefore not considered here.[12]

where the expression for $(\partial R/\partial x)_{\text{electrostatic}}$ will depend on whether a plume or puff is being treated. For the ion plume, equations (1), (4) and (5) give

$$\frac{dR_{\text{plume}}}{dx} = \frac{\mu i}{2R_{\text{plume}}u^2\pi\epsilon_0} + K$$

which is better written

$$\frac{dR_{\text{plume}}}{dx} = \frac{L}{R_{\text{plume}}} + K. \tag{6}$$

Integration of equation (6) gives

$$x = \frac{R_{\text{plume}} - R_{0\,\text{plume}}}{K} - \frac{L}{K^2}\ln\left[\frac{L + KR_{\text{plume}}}{L + KR_{0\,\text{plume}}}\right] \tag{7}$$

where $R_{0\,\text{plume}}$ is the original radius of the ion plume, i.e. at $x=0$. Similarly, for the ion puff the result

$$x = \frac{R_{\text{puff}} - R_{0\,\text{puff}}}{K} - \sqrt{\frac{M}{K^3}}\left[\tan^{-1}\left(\sqrt{\frac{K}{M}}\cdot R_{\text{puff}}\right) - \tan^{-1}\left(\sqrt{\frac{K}{M}}\cdot R_{0\,\text{puff}}\right)\right] \tag{8}$$

where

$$M = \frac{\mu i \Delta\tau}{4u\pi\epsilon_0}$$

is obtained.

Inspection of equations (7) and (8) reveals that the first term on the right hand side expresses the effects of turbulent diffusion alone whilst the second term, containing L and K or M and K, relates the interaction between turbulent and electrostatic effects. Hence the applicability of the ion tracer technique can be assessed by evaluating equations (4) (describing the uncharged plume and puff) (7) (the charged plume) and (8) (the charged puff) over appropriate ranges of distance downwind and wind speed. Values of the other parameters were set as follows:

$$i = +0.15\ \mu\text{A};^a\ \Delta\tau = 2\ \text{s};\ \mu = 1\times10^{-4}\ \text{m}^2/\text{V s};\ R_{0\,\text{plume}} = 0.5\ \text{m};^b\ R_{0\,\text{puff}} = 0.5\ \text{m}^b,$$

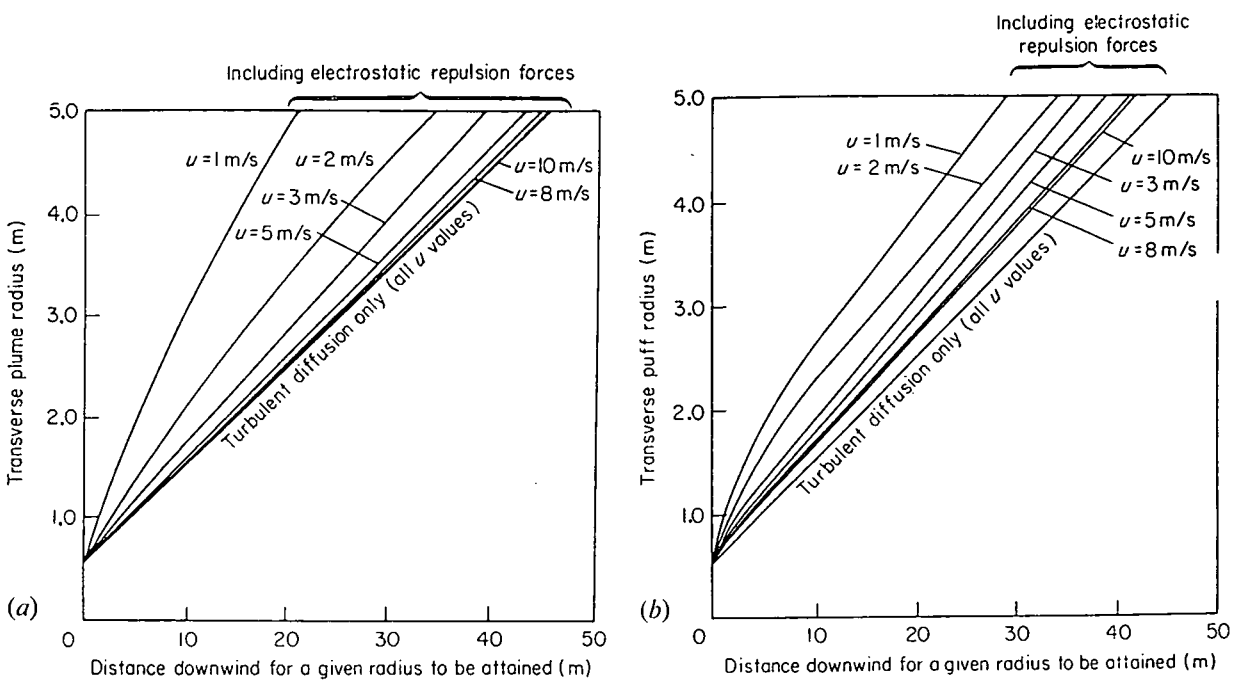

Figure 1. (a) The effect of electrostatic repulsion forces on ion plumes. (b) The effect of electrostatic repulsion forces on ion puffs.

[a] See Section 3.2.
[b] Determined by experiment.

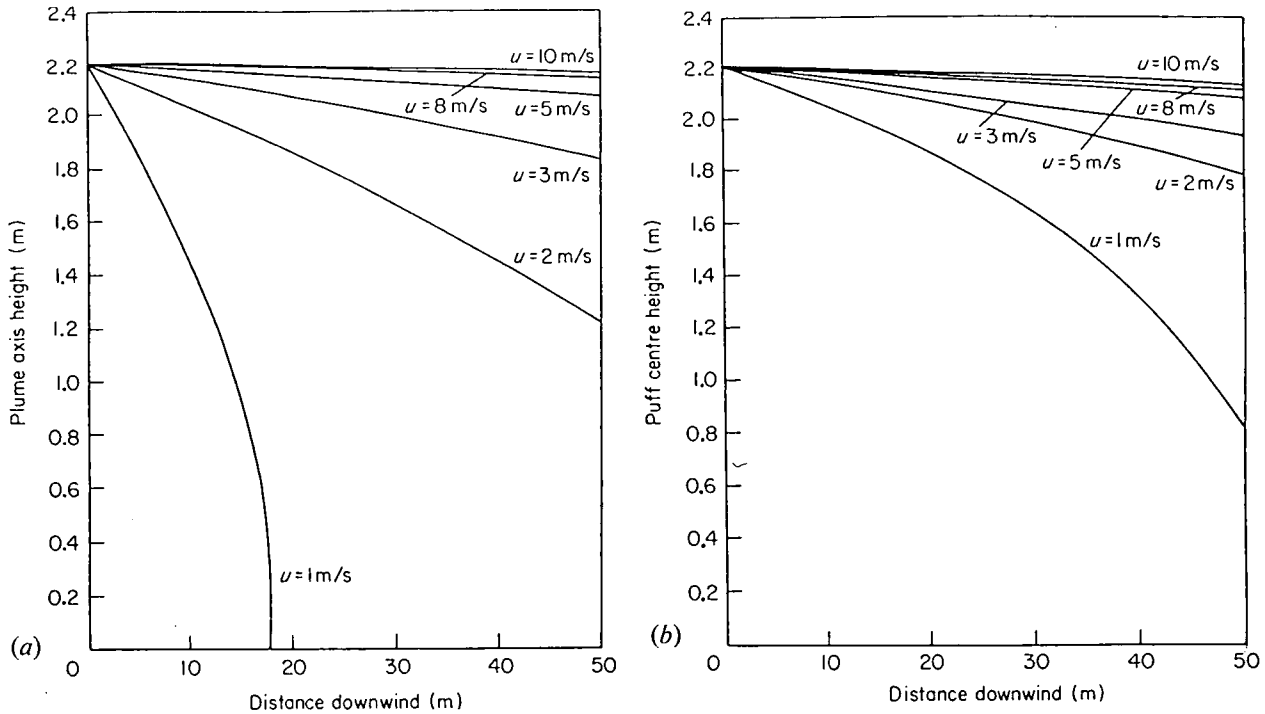

Figure 2. (a) The effect of electrostatic image forces on ion plumes. (b) The effect of electrostatic image forces on ion puffs.

thereby enabling the results presented in graphical form in Figures 1(a) and 1(b) to be calculated. These figures show that firstly, in light winds, the ion puff is more severely affected by the electrostatic repulsion forces than the ion plume and, secondly in strong winds, the repulsion effect is much smaller for both the plume and puff.

These are important limitations to the ion tracer technique and, with the ion generator system used in the work reported here, it is evident that the behaviour of the ion plumes and puffs produced will depend markedly on electrostatic effects in addition to those of turbulent diffusion unless the wind speed exceeds about 3 m/s.

2.3. The effects of electrostatic image forces

For an ion plume, if h_0 be the height of release of the ions, then the height h of the plume axis a distance x downwind is given[12] approximately by the expression

$$h = \left[h_0^2 - \frac{\mu i x}{2u^2 \pi \epsilon_0} \right]^{1/2} \tag{9}$$

and, for an ion puff,[11] the result

$$h = \left[h_0^3 - \frac{3\mu i \Delta \tau x}{16 u \pi \epsilon_0} \right]^{1/3} \tag{10}$$

is obtained. Inspection of Figures 2(a) and (b), which are based on equations (9) and (10) with appropriate values[a] inserted, indicates that, as with electrostatic repulsion, image effects should not be troublesome unless the wind speed is less than about 3 m/s.

[a] In this work h_0 was 2.2 m.

3. Experimental

3.1. Introductory

Basically the experimental arrangements differed little from those of any other diffusion investigation, consisting of a source of tracer material (ions] and appropriately deployed detectors (ion collectors and electric field mills)[11,13] of that material. In addition an anemometer and wind vane, placed near the ion generator, were employed to monitor the local wind variations. The outputs of all these sensing devices (which were analogue voltages directly proportional to the parameters being measured) were recorded on an eight channel instrumentation tape recorder. A brief outline of the special equipment used in this work now follows.

3.2. The ion generator (Figure 3)

Ions were produced by the application of a very high voltage (about 20 kV) to a coaxial electrode system. The outer electrode (o) consisted of a short cylindrical section of stainless steel mounted in a "Perspex" tube (radius 60 mm). The inner electrode (w) was a gold plated tungsten wire (radius 5 μm) to which the high voltage was connected. Within a few millimetres of this wire the electric field was sufficient for ionisation to occur and, depending on the polarity of the high voltage, either positive or negative ions would be repelled outward. This outer region would thus be filled with relatively slow moving ions and, if air were blown along the axis of the electrodes, some of these ions could be expelled into the atmosphere. It has been shown[11] that, for all the ions to be removed from the generator, the air velocity (v) must exceed a critical value given by

$$v=\frac{2\mu VL}{(b^2-a^2)\ln(b/a)} \tag{11}$$

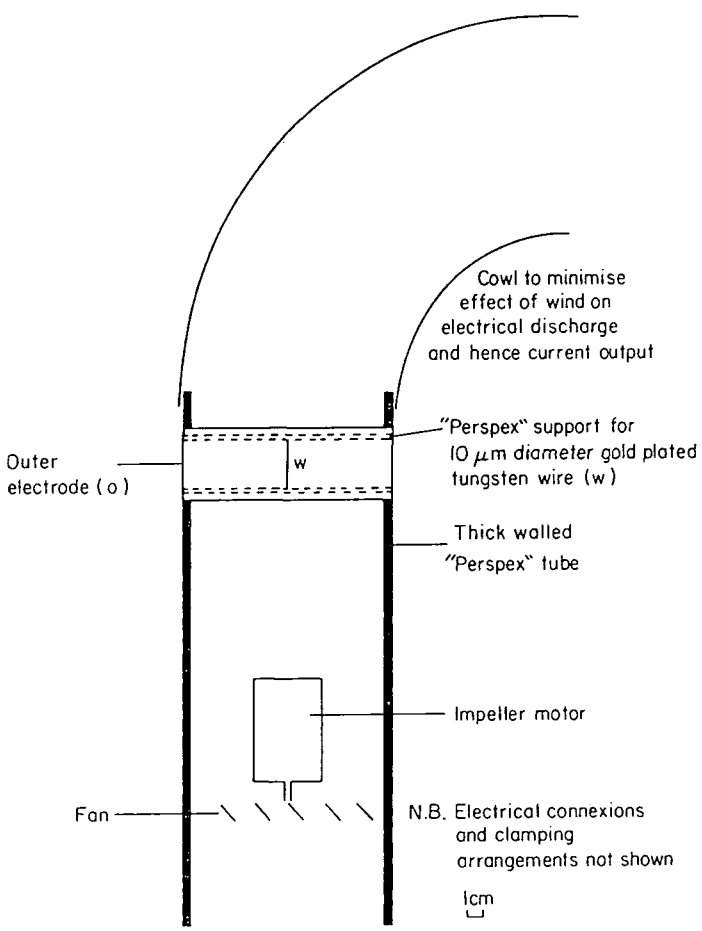

Figure 3. The ion generator.

in which a is the inner electrode radius, b is the outer electrode radius, L is the length of the electrode system and V the applied voltage.

Substitution of appropriate values in the above shows that the critical velocity is about 4 m/s—a figure easily realisable in practice.

The output of the ion generator was determined by collecting the emergent ions using an additional coaxial electrode system. This system, designed to fit directly on to the ion generator outlet cowl, was an appropriately scaled-up version of the ion collector described in the next section. Provided that the bias voltage was sufficient (3 kV minimum), all the ions could be collected and the current observed would be an accurate indication of the ion generator output. Positive ions were used throughout this project and, for these ions, the output was found to be $+0.15\ \mu A \pm 10\%$.

In the field the ion generator could be operated in two ways. Either it was run continuously, hence creating an ion plume, or alternatively, ions could be released in short bursts—thus producing a series of very short plume segments approximately equivalent to ion puffs. This latter mode of operation was achieved by arranging for the ions to be *removed* from the ion generator outlet when they were not required. This technique, which involved applying suitably timed 3 kV pulses to the additional coaxial electrodes referred to earlier, was found far more satisfactory than attempting to control the output directly, i.e. by switching the 20 kV supply to the generator itself. Ions were released in 2 s bursts at intervals of between 10 and 30 s depending on the type of experiment being conducted.

3.3. The ion collector (Figure 4)

In operation air was drawn into this device at a mean velocity of 15 m/s using an aspirator fan, a high potential (+600 V) being applied to the outer electrode OO′ whilst the central electrode CC′ was connected to earth through the electrometer (Keithley Model 602). Incoming positive ions were thus repelled towards the central electrode, the bias voltage being sufficient to ensure that all the small ions entering the device were collected.[13]

The response time of the ion collector was essentially determined by two factors. Firstly the geometry of the collector and the mean air speed within it fix the transit time of ions along the axis of the electrodes and hence place an inherent limit on the resolution. Transit times in these collectors were ~0.013 s; which implies a far more rapid response than most previous concentration monitors of any type. A second, and equally important, factor is that the electrometer used to amplify the ion collector signal must be designed and operated so that the input capacitance of the connecting cables and remaining equipment does not degrade the high frequency response. In practice this was overcome by the use of negative feedback techniques and, once correct electrical

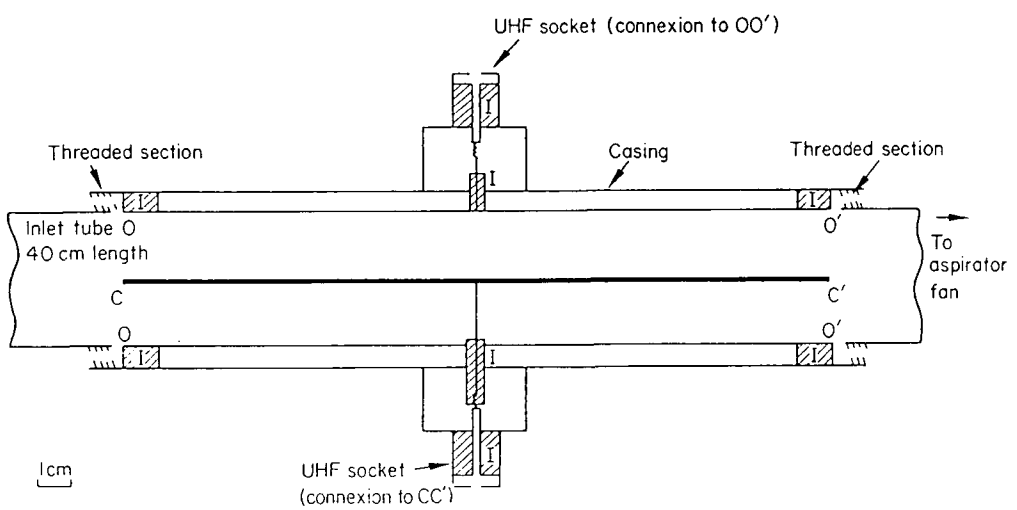

Figure 4. The ion collector. Material: brass, internal surfaces polished and nickel plated; I, PTFE insulators; CC′, central electrode; OO′, outer electrode.

conditions were established, electrometer limitations did not inhibit the inherently rapid ion collector response.

Because any turbulence in the air flow within the collector might produce associated irregular transverse motion of ions, it was mandatory, before ascribing *observed current* variations to *actual ion concentration* variations, to examine the collected ion current under conditions of constant ambient ion concentration. Experiments indicated that the ion current was constant to within $\pm 3\%$ in these conditions: this was regarded as satisfactory.

The ion concentration ρ is given by

$$\rho = I/Q \text{ C/m}^3 \tag{12}$$

where I is the observed current (in amperes) and Q is the volume flow rate through the collector (in m^3/s). In these collectors Q was $0.019\ m^3/s \pm 10\%$.

4. Results and discussion

4.1. General

Experimental work was conducted over an area of short grass within 100 m of large buildings, fences and trees, thus, compared with an unobstructed site, the airflow would have been rather disturbed. However, as the object of this work was to assess the ion tracer technique rather than undertake a definitive investigation into short-range diffusion the site was satisfactory. In all the experiments ions were released at a height of 2.2 m. Careful observation of the windvane attached to the ion generator support enabled the ion collectors and field mills to be appropriately sited at distances of up to 50 m downwind of the ion generator.

4.2. Results obtained with a single ion collector

4.2.1 With a continuous ion source

A typical ion concentration and electric field record, taken 30 m downwind of the ion generator in moderate winds (3–5 m/s), is illustrated in Figure 5. Very rapid changes in concentration are evident: note the very narrow but large peak at about 50 s into the record. In addition, even though the ion collector was placed at a bearing with respect to the ion generator corresponding to the *mean* wind direction, for a considerable fraction of the record little or no ions were detected. This effect has been referred to as "intermittency" by Csanady[10] and has two distinct, but related, explanations. Firstly, the collector could have been within the plume boundary throughout the record and thus the zero-concentration periods arose from "holes" in the plume. Secondly, and this is the more likely explanation, the plume itself could have meandered both horizontally and vertically in response to the larger elements of turbulence and thus the ion collector could have been outside the entire plume at times. In practice both effects could occur together.

During the remaining periods, i.e. in which ions were detected, it is evident that the concentration variations are both large and rapid—the concentration varying from near zero to several times its mean value in as little as 0.1 s. Hence, in winds of a few metres per second this implies that the spatial scale of the variations is considerably less than 1 m, which emphatically does not accord

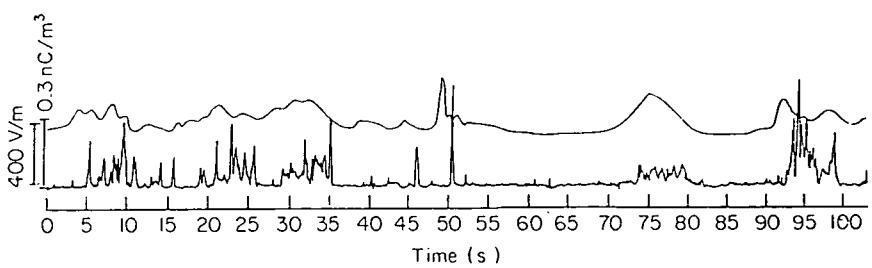

Figure 5. Ion concentration and electric field variations downwind of a continuous point source of positive ions. Ion source height, 2.2 m; output, 0.15 μA; ion collector, 30 m downwind at 1.5 m height; field mill, 25 m downwind on ground; meteorological conditions, slightly unstable, 22.8.75.

with the much-used concept of a "Gaussian plume". The observed concentration variations are the result of a variety of contorting and entraining processes, caused by turbulent eddies having scales ranging from a few millimetres to tens of metres, acting on the plume. Consequently Fick's diffusion theory, with its implicit assumption of molecular scale processes, is inappropriate.

Two factors should be borne in mind when examining the electric field record in Figure 5: note the magnitude only is shown. Firstly, the observed field is the algebraic sum of the field due to the ion plume and the Earth's fine weather field.[13] In all the experiments this latter field lay between -100 and -300 V/m and, since positive ions were used, the electric field *below* the plume would

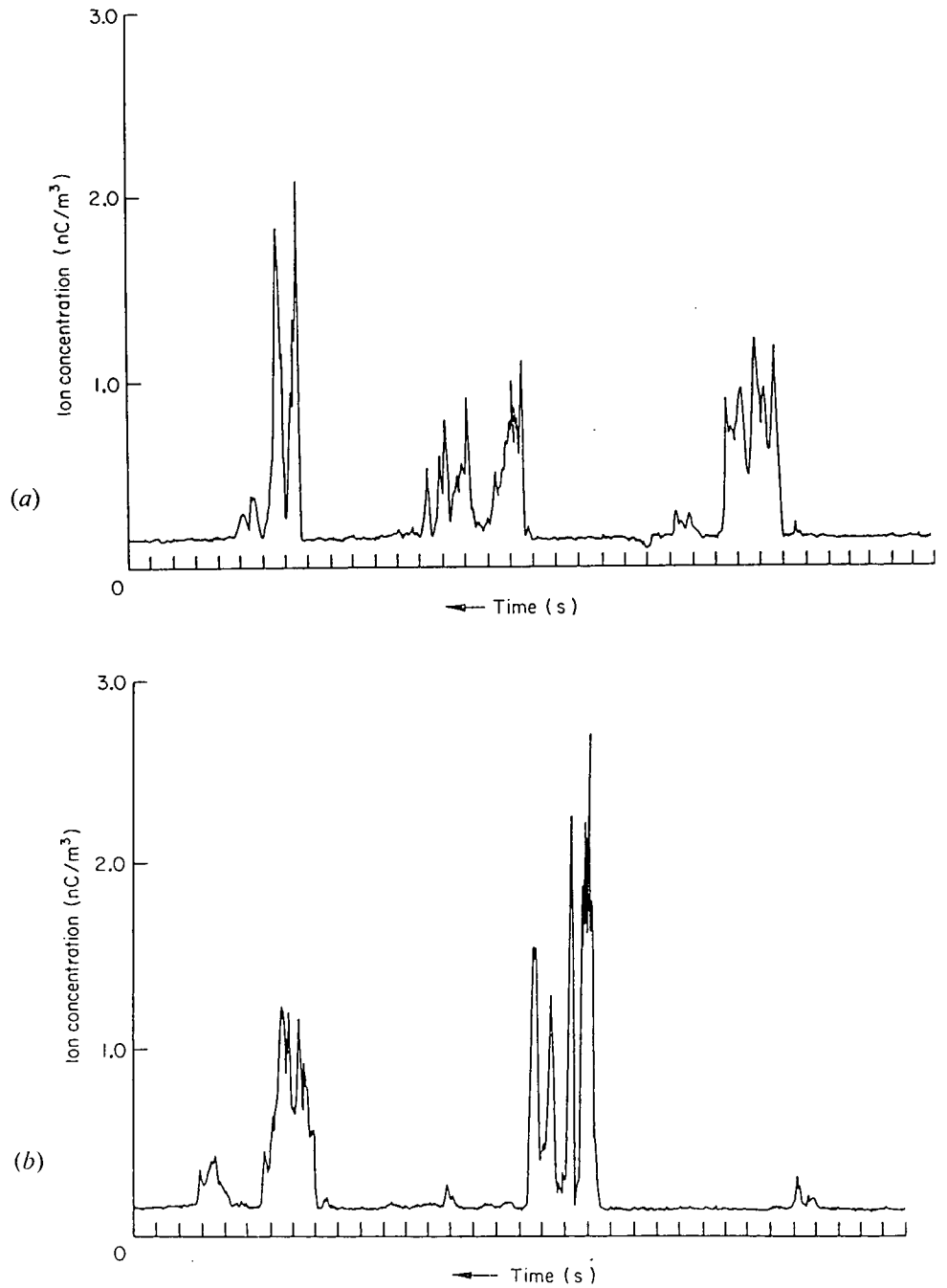

Figure 6. (a) and (b). Ion concentration variations 10 m downwind of a pulsed source. 1 division on horizontal axis represents 1 second.

have been negative. Hence observed values should be adjusted by having an amount corresponding to the prevailing ambient field subtracted from them (about 300 V/m in the figure). Secondly the field mill responds to the plume in its entirety rather than to discrete parts of it as does the ion collector. Hence the field changes are much slower than the ion concentration variations.[12]

4.2.2. With a pulsed ion source

In this experiment [Figure 6(a) and 6(b)] the ion collector was sited 10 m downwind of the ion generator, which produced a 2 s burst of ions every 10 s. The winds were light, being no more than 2–3 m/s, and the meteorological conditions were unstable. The periodic nature of the concentration fluctuations is evident, as would be expected, but note two additional features. Firstly, ions were detected over intervals considerably longer than 2 s thus implying considerable longitudinal distortion of the puff even at 10 m downwind. Secondly, there is a tendency for the ion concentration to be higher at the puff edges than in the central region[a] although the concentration variations are so large and rapid that this assertion could be difficult to substantiate quantitatively. Both effects could have arisen as a result of turbulent processes (e.g. eddies contorting the puff) or electrostatic forces (i.e. longitudinal repulsion and image phenomena).

4.3. Results obtained with a pair of ion collectors

Figures 7–9 show a sequence of ion concentration records obtained in similar conditions with pairs of ion collectors 30 m downwind of the ion generator and separated by vertical distances of 0.05, 0.5 and 1.5 m respectively. The excellent agreement between the records in Figure 7 conclusively demonstrates that any effects due to turbulence within the collectors or the lack of isokinetic sampling are minimal. Relatively small differences can be observed between the records, but whether these are real, which is possible even at 0.05 m separation, or artefacts caused by the ion collectors is not known.

Results obtained with a single ion collector revealed the presence of considerable *longitudinal* fine structure in the concentration variations, hence, assuming the eddy energy spectrum[2] were approximately isotropic at these scales, it is reasonable to expect the transverse concentration structure to

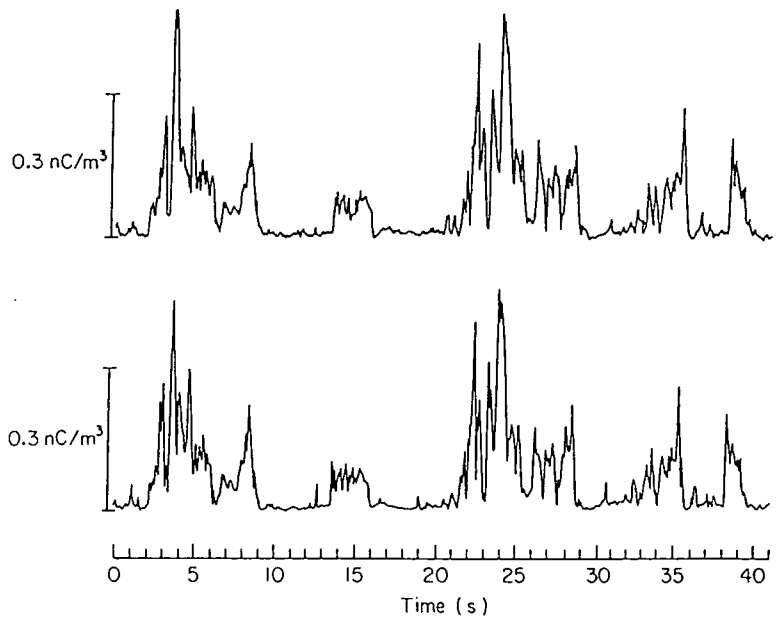

Figure 7. Simultaneous ion concentration measurements at vertically separated points. Upper trace, 1.5 m; lower, 1.45 m; ion collectors, 30 m downwind of a continuous point source of ~0.15 μA at 2.2 m height; wind speed, 2–5 m/s; slightly unstable conditions, 22.8.75.

[a] Other records have also exhibited this tendency.

be similar. Figures 8 and 9 substantiate this assertion—the correlation between the pairs of records declining rapidly with increased separation. Indications, purely visual, are that the scale of the concentration variations is similar in both directions and of the order of tens of centimetres. (Application of auto- and cross-correlation techniques to a larger sample of ion concentration data should enable these scales to be precisely quantified.)

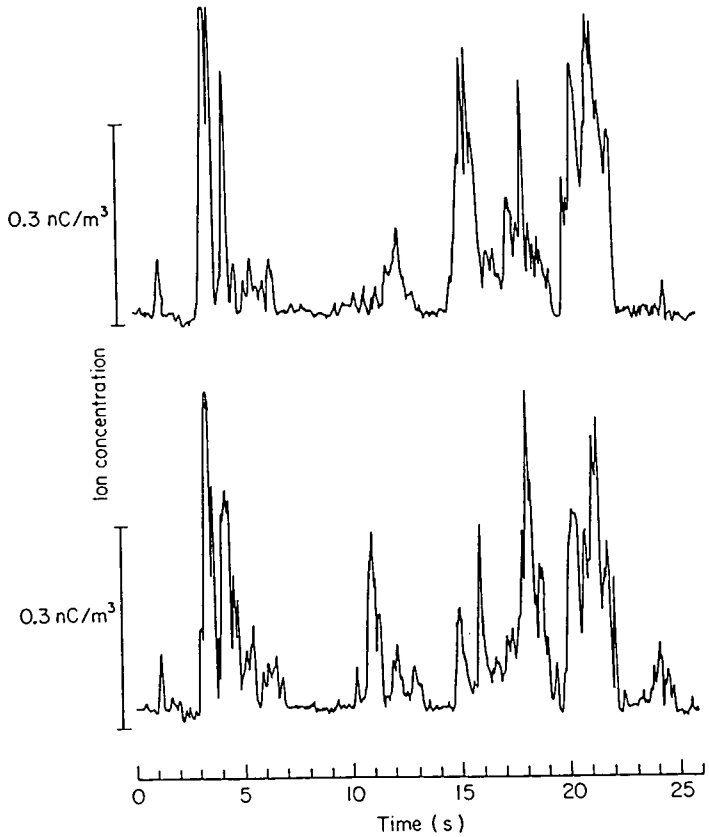

Figure 8. Simultaneous ion concentration measurements at vertically separated points. Upper trace, 1.5 m; lower, 1.0 m; ion collectors, 30 m downwind of a continuous point source of +0.15 μA at 2.2 m height; wind speed, ~ 2–5 m/s; slightly unstable conditions, 22.8.75.

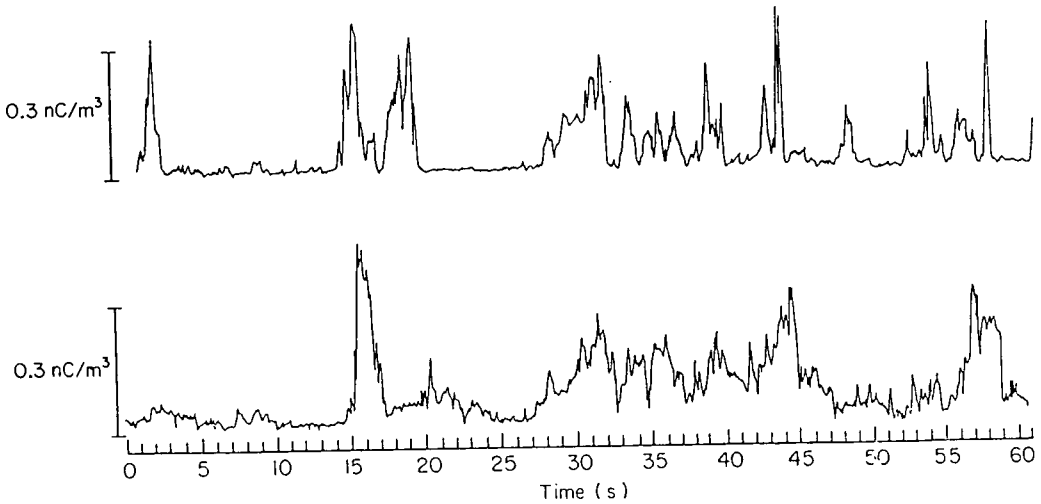

Figure 9. Simultaneous ion concentration measurements at vertically separated points. Upper trace, 1.75 m; lower 0.25 m; ion collectors, 30 m downwind of a continuous point source of +0.15 μA at 2.2 m height; wind speed, ~2–5 m/s; slightly unstable conditions, 22.8.75.

5. Conclusions

The results indicate that an essential feature in short range diffusion is the existence of very sharply defined boundaries in both plumes and puffs. Concentration gradients are substantial even well inside the plume or puff, reflecting that the overall spatial variability of concentration is large.[a] However, it is reasonable to expect the statistics of the the concentration variations to depend upon factors such as distance from the plume axis or puff centroid, release height, distance downwind, turbulence statistics, terrain type etc. Thus for a sequence of investigations carried out in quasi-stationary conditions, the data obtained could be grouped into suitable statistical ensembles, e.g. on the basis of ion collector–puff centroid distance, prior to analysis.

The existence of instantaneous values of concentration considerably in excess of the average, even for a small fraction of the time, is important particularly in cases where the response to a diffusing species may be non-linear or exhibit threshold effects. In situations where dosage rather than concentration is of concern the ion-tracer technique is also convenient because dosage data can be obtained directly by measuring the electric charge collected over the given period.

Acknowledgement

Appendix

Symbol	Unit	Definition
a	m	Radius of central rod of ion collector
b	m	Radius of inner cylinder of ion collector.
h_0	m	Height of ion plume or puff above ground at release.
h	m	Height of ion plume or puff above ground at a distance x downwind
i	A	Current output of ion generator
I	A	Ion collector current
L	m	Length of electrode of ion collector
Q	m^3/s	Ion collector air flow rate
r_0'	m	Puff radius at release } Used when discussing turbulent diffusion effects
r'	m	Puff radius at a distance x downwind } Used when discussing turbulent diffusion effects
r_0	m	Plume or puff radius at release } Used for discussing electrostatic repulsion effects
r_{plume}	m	Plume radius at a distance x downwind } Used for discussing electrostatic repulsion effects
r_{puff}	m	Puff radius at a distance x downwind } Used for discussing electrostatic repulsion effects
R_{0plume}	m	Plume radius at release } Used when discussing the *joint* effects of turbulent diffusion and electrostatic repulsion
R_{0puff}	m	Puff radius at release } Used when discussing the *joint* effects of turbulent diffusion and electrostatic repulsion
R_{plume}	m	Plume radius at a distance x downwind } Used when discussing the *joint* effects of turbulent diffusion and electrostatic repulsion
R_{puff}	m	Puff radius at a distance x downwind } Used when discussing the *joint* effects of turbulent diffusion and electrostatic repulsion
u	m/s	Mean wind speed
v	m/s	Critical air velocity in ion generator
V	V	Voltage applied to ion collector electrodes
x	m	Distance downwind from ion generator
$\Delta\tau$	s	Time for which ion generator is producing ions when operating in pulsed mode
ϵ_0	F/m	Permittivity of free space
μ	$m^2/V\,s$	Ionic mobility
ρ	C/m^3	Ion concentration

[a] In uncharged plumes and puffs concentration variability might be even larger due to the absence of electrostatic repulsion effects.

References

1. Lumley, J. L.; Panofsky, H. A. *The Structure of Atmospheric Turbulence*. Wiley-Interscience, London, 1964, p. 99.
2. Lumley, J. L.; Tennekes, H. *A First Course in Turbulence*. MIT Press, London, 1972, p. 197, p. 262.
3. Schmidt, W. *Sber. Akad. Wiss. Wien*. 1918, **127**, 1942.
4. Roberts, O. F. T. *Proc. R. Soc. A*. 1923, **104**, 640.
5. Sutton, O. G. *Micrometeorology*. McGraw-Hill, London, 1953, p. 105.
6. Pasquill, F. *Atmospheric Diffusion*. Ellis Horwood, Chichester, 1974, 2nd edn., p. 106.
7. Smith, F. B.; Hay, J. S. *Q. Jl. R. Met. Soc*. 1961, **87**, 82.
8. Gosline, C. A. *Chem. Engng Prog*. 1952, **48**, 165.
9. Ramsdell, J. W.; Hinds, W. T. *Atmosph. Envir*. 1971, **5**, 483.
10. Csanady, G. T. *Turbulent Diffusion in the Environment*. D. Reidel, 1973, p. 222.
11. Jones, C. D. Ph.D. Thesis 1974, University of Durham.
12. Jones, C. D.; Hutchinson, W. C. A. *J. atmosph. terr. Phys*. 1976, **38**, 485.
13. Chalmers, J. A. *Atmospheric Electricity*. Pergamon Press, London, 1967, 2nd Edn., p. 119, p. 143, p. 93, p. 122.
14. Large, M. I.; Pierce, E. T. *J. atmosph. terr. Phys*. 1957, **10**, 251.
15. Ogden, T. L. Ph.D. Thesis 1967, University of Durham.
16. Jones, C. D. Uniform Concentration Models of Diffusing Puffs suitable for use in Evaporation Studies. 1975. Unpublished MOD Report.
17. Bleaney, B. I.; Bleaney, B. *Electricity and Magnetism*, Clarendon Press, Oxford, 1965, 2nd Edn., p. 48.

Jones C. D. and Gulliford N. T. (1979).

Developments in the use of ionised air as a wind tunnel tracer.

J. Phys. E: Scientific Instruments. **12**, 321 - 327.

J. Phys. E: Sci. Instrum., Vol. 12, 1979. Printed in Great Britain

Developments in the use of ionised air as a wind tunnel tracer

C D Jones and N T Gulliford†
Chemical Defence Establishment, Porton Down, Salisbury, Wiltshire, UK

Received 2 May 1978, in final form 1 December 1978

Abstract This paper describes a series of experiments performed in turbulent and quasi-laminar wind tunnel flows to further assess unipolarly ionised air as a tracer for examining the microstructure of diffusing plumes and puffs. The experimental techniques have been improved which, together with spectral and qualitative correlation analysis, have facilitated a more penetrating examination of ion plume/puff behaviour. Some new insights into the electrostatic aspects of ionised air dispersion have also been gained.

1 Introduction

Recently Jones (1977) reported that unipolarly ionised air has potential as a tracer for examining the microstructure of plumes and puffs diffusing in turbulent wind tunnel flows. However, in those experiments the equipment had been specifically developed for atmospheric work where source-to-detector distances are generally much greater than in wind tunnels. In addition, because of the requirement for very high sensitivity, the detectors had *relatively* coarse temporal and spatial resolution and were bulky. Considering the wide use of wind tunnels, particularly for atmospheric dispersion modelling, it was felt worthwhile to reduce the size of the ion generator and collectors and then conduct a further series of experiments to appraise more realistically the technique for the type of application envisaged.

As stated in the previous paper electrostatic effects interfere with the passivity of any electrically charged tracer and must be considered carefully for a balanced evaluation of the technique. Consequently, although the experiments were conducted to assess the feasibility of the technique for studying turbulent diffusion, part of this paper is concerned with electrostatic rather than fluid mechanical considerations.

2 Theoretical

2.1 *Tracer passivity considerations*

2.1.1 *General note* It is impossible for any electrically charged tracer to be strictly passive because there must be repulsion between the ions or ionised particles, and they will thus possess non-zero velocities relative to the host fluid. (Only unipolar systems are being considered, hence the exclusion of attractive forces.) However, if the space charge concentration (equivalent to the ion concentration, expressed in charge units, for a unipolar system) can be reduced to a level at which repulsion becomes insignificant when compared with other dispersive processes, principally turbulence, then the requirement for passivity should be satisfied. A criterion is therefore needed for determining whether the use of ionised air as a tracer is feasible and, if so, the design requirements of the ion generator. Development of this idea rests upon whether the rate of plume/puff expansion under the experimental conditions envisaged can be estimated. The anticipated radius can then be compared with that which would have been obtained in a low-turbulence flow (from theory) and the contribution arising from interfering electrical effects assessed.

Such a treatment is deficient in at least one important respect: it does not consider the effects of electrostatic repulsion on the evolution of the concentration fluctuations so characteristic of plumes/puffs diffusing under the action of turbulence. However, electric field and mobility considerations suggest that the effect of repulsion *between* small volumes containing high charge concentrations will be minor in relation to the overall radial expansion.

2.1.2 *Plumes* It has been shown by Jones and Hutchinson (1976) that, in the absence of turbulence or any other mechanical dispersive agency, the radius of a plume of ions of mobility μ at a distance d downstream from their source is

$$R \approx \left(\frac{\mu i d}{u^2 \pi \epsilon_0}\right)^{1/2} \tag{1}$$

where i is the current output of the ion generator, u the airstream velocity, and ϵ_0 the permittivity of free space. Rearrangement yields

$$i = \frac{\pi \epsilon_0}{\mu} \frac{u^2 R^2}{d} \tag{2}$$

thus enabling the ion generator current output to be determined in order to achieve a given value of R in wind tunnel conditions specified by u and d. (For positively ionised air $\mu = 2{\cdot}4 \times 10^{-4}$ m^2 V^{-1} s^{-1}.)

2.1.3 *Puffs* The situation here is rather more complex because the theory deduced by Jones (1974) is only applicable to spherical puffs, where the electric field is radial. If this assumption can be justified the puff radius R is given by

$$R \approx \left(\frac{3\mu i q d}{4u\pi\epsilon_0}\right)^{1/3} \tag{3}$$

where q is the total charge in the puff. From equation (3) it is then simple to deduce that

$$q = \frac{4\pi\epsilon_0}{3\mu} \frac{u}{d} R^3 \tag{4}$$

which can be used to determine the puff charge required to comply with a given passivity criterion.

Production of spherical puffs demands that the time interval over which ionised air is released be very short, typically a few milliseconds. If this is not possible, then one may treat the puff as a plume segment and *approximately* estimate the radial expansion using equation (1). The longitudinal expansion can be determined by noting that the electric field strength E at the end faces (and on the axis) of a cylindrical space charge cloud of length L and radius R is

† Present address: Physics Department, University of Bath, Claverton Down, Bath, Avon, UK.

0022-3735/79/040321+07 $01.00

$$E=\frac{q}{2\pi R^2 L\epsilon_0}[(L^2+R^2)^{1/2}-(L+R)] \qquad \dagger(5)$$

from which the instantaneous expansion velocity v can be found using

$$v=\mu E. \qquad (6)$$

2.2 *Space charge concentration in non-dispersive conditions*

2.2.1 *Plumes* Consider an ion generator of output current i in an airstream of velocity u. If the plume radius at a distance d downstream is R, then

$$i=\pi R^2 u\rho \qquad (7)$$

where ρ is the space charge concentration. From equations (1) and (7)

$$\rho=\frac{\epsilon_0}{\mu}\frac{u}{d} \qquad (8)$$

which, for positively ionised air, becomes

$$\rho=37{\cdot}4\,\frac{u}{d}\,(\text{nC m}^{-3}). \qquad (9)$$

2.2.2 *Puffs* Assuming the puff is spherical and of uniform concentration,

$$q=\tfrac{4}{3}\pi R^3\rho$$

from which the relation

$$\rho=\frac{\epsilon_0}{\mu}\frac{u}{d}$$

can be obtained using equation (3). This is identical to the expression already obtained for a plume and, although only proven for two idealised cases, these results suggest that the space charge concentration, irrespective of source strength or whether it is released continuously or not, tends to a value dependent only on the time elapsed (d/u) since its creation and the mobility of the charge carriers.

2.3 *Measurement of plume current and puff charge*

Whilst the determination of plume current has already been considered by Jones (1977) the analogous measurement in puffs, i.e. of total charge q, has not been treated and is described here. Mathematically q is the volume integral of the space charge concentration taken over the entire puff. Hence

$$q=\int_{d}^{d+l}\int_{0}^{R}\int_{0}^{2\pi}\rho(d,r,\theta)r\,\mathrm{d}\theta\,\mathrm{d}r\,\mathrm{d}d \qquad (10)$$

in which the coordinate system is identical to that used in the previous discussion on plume current and the puff extends from d to $d+l$ in the longitudinal direction (as defined by the tip of the r, θ vector). Experiments have revealed, as was true for plumes, that the charge distribution is axisymmetric, and thus equation (10) can be reduced to

$$q=2\pi\int_{d}^{d+l}\int_{0}^{R}\rho(d,r)r\,\mathrm{d}r\,\mathrm{d}d. \qquad (11)$$

In practice observations are made at fixed points in space – the puff being advected past the ion collector by the air flow. Consequently, equation (10) would be more relevant if the longitudinal spatial integral could be transformed into a time integral. If the puff takes a time $\tau(=l/u)$ to traverse the collector, then

$$q=2\pi u\int_{0}^{\tau}\int_{0}^{R}\rho(d,r)r\,\mathrm{d}r\,\mathrm{d}t \qquad (12)$$

where the integration is started at the instant the puff arrives at the detector.

† Equation (5) is obtained by writing down the potential due to an annular element of charge and then integrating over the entire cylinder. The electric field may then be obtained by differentiation with respect to the appropriate coordinate vector.

3 Experimental

3.1 *General*

The experimental arrangements were similar to those before: hence comments are superficial with the exception of those concerning items which are either novel or have been extensively modified.

The wind tunnel had a smaller working section (0·9 m × 0·9 m by 3 m in length) than that employed previously and was of the open-circuit type, drawing in outside air through a 6 mm honeycomb mesh followed by a contracting section of 4:1 area ratio. Turbulence, when required, was produced by placing a matrix of wood laths, arranged in squares of side 0·075 m, a short distance upstream of the ion generator.

3.2 *The ion generator* (figures 1 and 2)

It was clear that the generator used previously was too large both physically and in ion output for satisfactory operation in

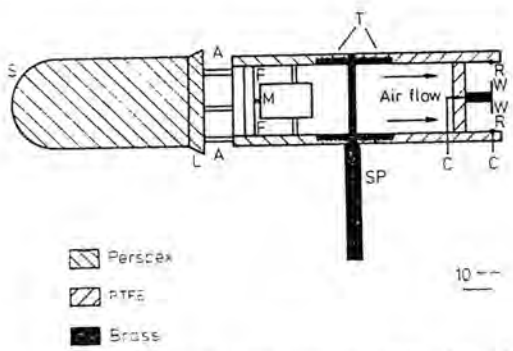

Figure 1 The ion generator: sectional drawing (electrical connections not shown). S, streamlining; L, lip; A, air intake; F, fan; M, fan motor; SP, support pillar; T, threaded section; R, ring (outer electrode); W, diametral wire (inner electrode); C, contact point.

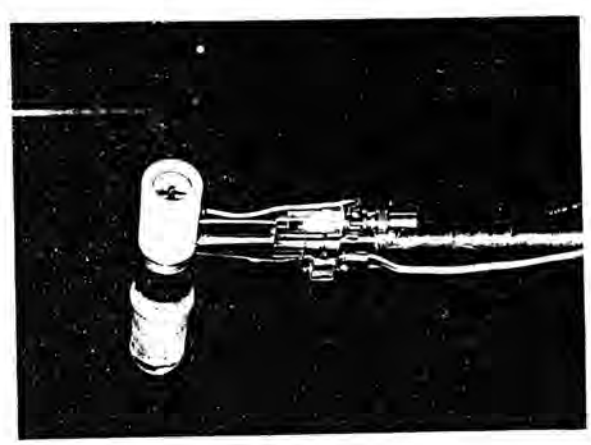

Figure 2 Photograph of the ion generator.

small-scale experiments. Hence considerable effort was devoted to miniaturisation, and in the current series of experiments, the generator was 0·17 m long by 0·03 m in diameter, and had a current output in the region of 10 nA (compared with 250 nA previously). An attempt was also made to reduce the effect of changes of wind tunnel air velocity on the ion generator output, a small lip L being incorporated just in front of the air intake to counteract suction effects at the exit of the device. It was discovered empirically that mounting the fine wire W diametrically, instead of axially as before, considerably increased the output of ions thereby enabling the device to be operated at lower voltages than the earlier designs.

Any interference to the wind tunnel air flow caused by the generator itself is clearly undesirable. The velocity of the emergent ionised airstream from the device is 2·8 m s^{-1}; hence at tunnel air speeds less than this the major disturbing influence would be the ionised jet whilst at higher speeds wake effects will predominate. Isokinetic release of ions would minimise jet effects but was not possible with the present system; however, the low jet velocity and small radius (cf the plume widths observed, §4) suggest that little additional dispersion was caused by its presence. At higher tunnel air speeds the Reynolds number of the flow around the generator was about 10^4 and thus the resultant wake must have been turbulent and hence dispersive. Consequently minimising drag, by incorporation of streamlining, was essential to reduce the wake intensity as much as possible. The results obtained in conditions of low wind tunnel turbulence (§4.1) indicate that the additional dispersion caused by the above mechanisms, though evident, was not sufficiently obtrusive to invalidate any of the conclusions drawn.

3.3 *The ion collector* (figures 3 and 4)

The inlet diameter of the collector was reduced to 0·012 m and this figure is indicative of the spatial resolution likely to have been obtained in the experiments. Experimental and theoretical estimates of the temporal response suggest that the detector has a capability in excess of 1 kHz. The ion collector(s) was operated with its axis perpendicular to the airstream being sampled to avoid ram effects and hence any disturbance to the flow within the device. Wake effects with collectors operated in the same plane downstream (as was the case in the majority of experiments) are immaterial, but in the Lagrangian velocity measurements (§4.3) the disturbance from the upstream collector must inevitably have modified the concentration distribution observed by that downstream. The volume rate of air flow through the collectors was so small that the possibility of any deleterious effects arising from this can be discounted.

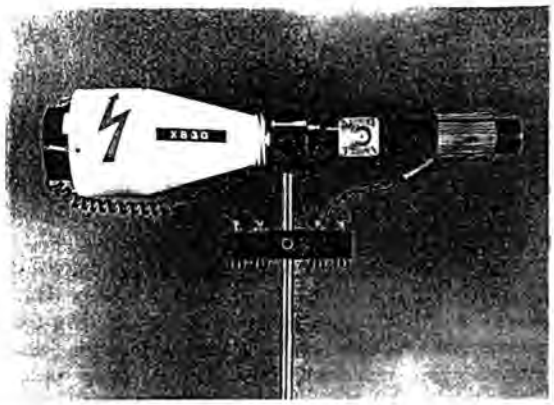

Fig. 4 Photograph of the ion collector.

Limitations to the sensitivity, particularly at high frequencies, can often be attributed to vibrations from the fan motor causing piezoelectric and displacement currents in the device. A considerable improvement in performance has been obtained by mounting the fan motor in vibration-absorbing material and maintaining the central electrode C under tension so as to reduce the amplitude of any oscillations. Operation of ion collectors in the open air, and even in closed-circuit wind tunnels, for extended periods can lead to failure due to the insulation being compromised by deposition of dust particles, etc. Whilst the problem itself has not been solved the present device has been designed so that electrode removal for cleaning is a simple and rapid operation. Use of collectors in humid atmospheres is difficult because any moisture on the insulators will rapidly cause failure. In the current design this has been overcome by maintaining the electrode at some 30°C above ambient by means of a small electrical heater. The modified collectors will now operate continuously in saturated air without any significant deterioration in performance.

3.4 *Electrometers and other special equipment*

As the electrometers used to measure the ion currents were proprietary items, a detailed description is not warranted here. Keithley model 602s were employed throughout the work, except in the determination of the high-frequency limit of

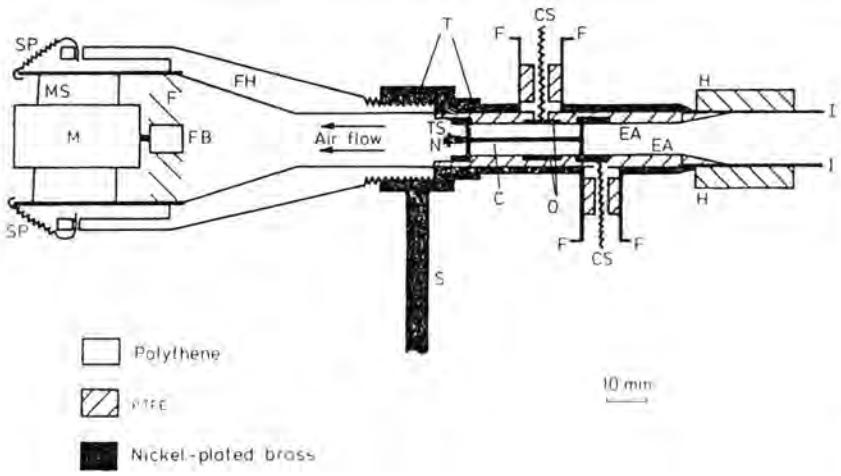

Figure 3 The ion collector: sectional drawing. SP, motor retaining spring; MS, motor support; M, fan (F) motor; FB, fan boss; FH, fan motor housing; T, threaded section; S, support pillar; TS, N, central electrode (C) tensioning spring and retaining nut; O, outer electrode; F, BNC socket mounting flange; CS, contact spring; EA, PTFE electrode assembly carrier; H, heater (12 W); I, inlet tube.

operation of the ion collector, for which a model 427 was used.

Measurements (which were intended only to be comparative) of the contributions to the total space charge concentration fluctuations from various frequency bands were conducted in the following manner. The electrometer output, a low-impedance analogue voltage signal directly proportional to the instantaneous value of the space charge concentration, was taken through a bandpass filter (Barr and Stroud type EF3) set to the frequency of interest, the bandwidth being 10 Hz (except for the lowest band where, in order to remove the DC component, a 1–10 Hz passband was employed). The filter output was then rectified and averaged with a long-time-constant resistance–capacitance network, the voltage output of the system thus bearing a direct relationship to the mean modulus of the amplitude of the fluctuations occurring in the passband.

Previous experimental work had shown that the most reliable way to produce puffs of ionised air was by pulsing the high-voltage supply to the ion generator. For the wind tunnel experiments envisaged, it would be necessary to generate a regular series of puffs of 10 ms duration at 1 s intervals, and, whilst semiconductor devices are available which are capable of handling 3 kV at the power levels required, it was felt that a more electrically robust switching system would be preferable. A high-voltage pentode valve (EL360) was found suitable and proved very reliable.

4 Results and discussion

4.1 *Measurements on ionised air plumes in low-turbulence conditions*

4.1.1 *Radial space charge concentration profiles* Once it had been established that the charge distribution was axisymmetric it was then only necessary to sample at seven or eight points along a radius to obtain a concentration profile from which the plume current could be found (§2.3). The profiles obtained with various air speeds and applied voltages are shown in figure 5, the corresponding current outputs being listed in table 1.

The data in table 1 may be substituted into equation (1), together with a value for the ionic mobility (§2.1.2), and theoretical estimates of the plume radii obtained. The fact that satisfactory agreement between the observed and predicted radii is found supports the contention that the turbulence level was sufficiently low for electrostatic repulsion to be the dominant plume dispersion mechanism.

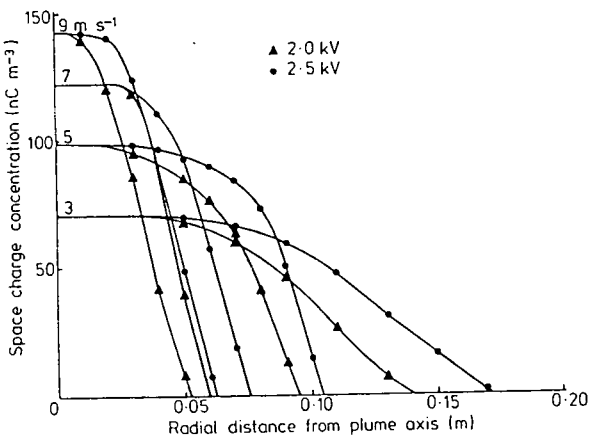

Figure 5 Radial space charge concentration profile obtained in various conditions of wind tunnel air speed and high voltage applied to ion generator (at 2 m downstream) in low-turbulence conditions.

Table 1 Ion generator current output for various conditions of wind tunnel air speed and applied high voltage.

Air speed (m s^{-1})	Ion generator output (nA)		
	at 2·0 kV	at 2·5 kV	at 3·0 kV
3	7·2	11·4	—
5	7·7	11·9	29·4†
7	5·6	9·3	—
9	5·0	7·8	—

† Single observation made for comparison purposes, see §4.3.

4.1.2 *Space charge concentrations observed and their relationship with wind tunnel air speed and distance downstream from the ion generator* Comparison between the theoretical values (from equation (9)) and those observed are given in table 2. Any discrepancies between theoretical and observed values are thought to arise from (i) approximations in the repulsion theory (Jones and Hutchinson 1976) and (ii) effects of the turbulent wake from the ion generator (which may have caused additional dispersion particularly at higher air velocities).

Table 2 Theoretical and observed values of space charge concentration at 2 m downstream on the plume axis in low-turbulence conditions.

Air speed (m s^{-1})	Theoretical value (nC m^{-3})	Observed value (nC m^{-3})
3	56	70
5	94	98
7	131	122
9	168	142

A criticism that has been levelled against the use of ionised air as a tracer is that it may not necessarily be conservative. This is because, if for example there were any negative ions present in a predominantly positive ion plume, then recombination would occur and the plume current would decrease downstream. Measurements with reverse-biased ion collectors had already shown that the fraction of ions of the opposite polarity present in the plume was very small (about 1%) but, as a further check, determinations of plume current were made at different distances downstream of the generator. The results obtained confirmed that ion loss due to recombination was negligible. This investigation also revealed that the concentration along the plume axis fell off inversely with distance from the ion generator – as predicted by equation (9).

4.1.3 *Space charge concentration fluctuations* In theory, in a non-turbulent flow, the space charge concentration (at a given distance downstream) *within* the ion plume should be constant and then fall very rapidly to zero at the boundaries. In practice a small amount of turbulence will be present in the wind tunnel airstream and wake/jet effects from the ion generator

will introduce further velocity fluctuations. Consequently the space charge concentration, even on the plume axis, is subject to small fluctuations, typically a few per cent of the mean. The magnitude of the fluctuations increases radially from the plume axis until a maximum is reached near the plume edge, after which the value decreases rapidly to zero. Figure 6 illustrates this and also shows how the energy in the fluctuations is distributed in terms of frequency.

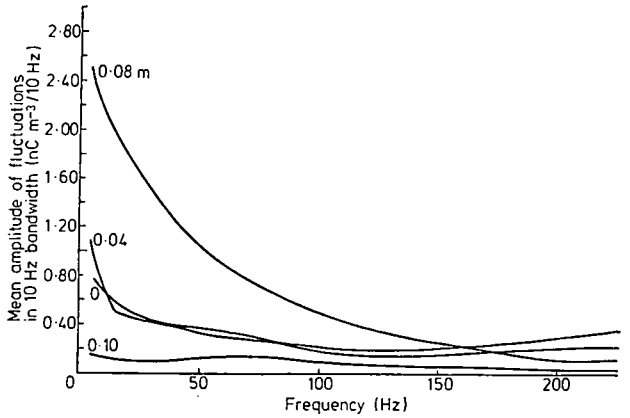

Figure 6 Space charge concentration fluctuation amplitude as a function of frequency in low-turbulence conditions (at 2 m downstream) with an air speed of 5 m s^{-1} and 2·5 kV applied to the ion generator. Numbers on curves indicate distances from plume axis, i.e. radial positions.

4.2 *Measurements on ionised air plumes in turbulent flow conditions*

4.2.1 *Opening note* The intention was, having established the characteristics of plume behaviour in a low-turbulence airstream, to compare the results with those obtained in turbulent conditions. It was found that the turbulence produced by the grid decayed only slowly downstream and, except at very low air speeds (below 3 m s^{-1}), considerable velocity fluctuations could be observed in the plane of the ion collector (2 m downstream).

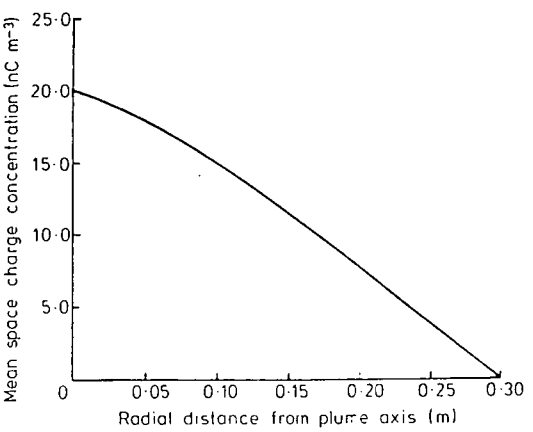

Figure 7 Mean space charge concentration profile obtained in turbulent flow conditions (2 m downstream, ion generator voltage 2·5 kV). For further details see text.

4.2.2 *Typical radial space charge concentration profile* Figure 7 shows a *mean* concentration profile obtained at an air speed of 5 m s^{-1} (prior to emplacement of the grid) at 2 m downstream from the ion generator and should be compared with the corresponding measurement for low-turbulence conditions (figure 5). The most obvious difference is that the plume radius is much larger in the turbulent flow regime, and this, together with the reduced concentration levels observed near the plume axis, reflects the diffusive effect of the velocity fluctuations present.

4.2.3 *Space charge concentration fluctuations in turbulent flow conditions* The variation, as a function of frequency, of fluctuation intensity in typical turbulent flow conditions at different radial distances from the plume axis is shown in figure 8. (The conditions in which these data were obtained were identical with those in the mean profile experiment described above.) Comparison of figures 6 and 8 reveals that the intensity is significantly increased in the turbulent case, except at the highest frequencies. Even at the plume axis the fluctuations are several times greater, the ratio between values in turbulent and low-turbulence conditions becoming progressively larger as the distance from the axis increases. The fluctuation level attains a maximum at about 0·1 m – the region where the most active turbulent mixing might be expected to occur. It is possible that some of the low-frequency energy, i.e. at about 15 Hz or less, may be associated with vortices arising from the grid rather than true turbulence.

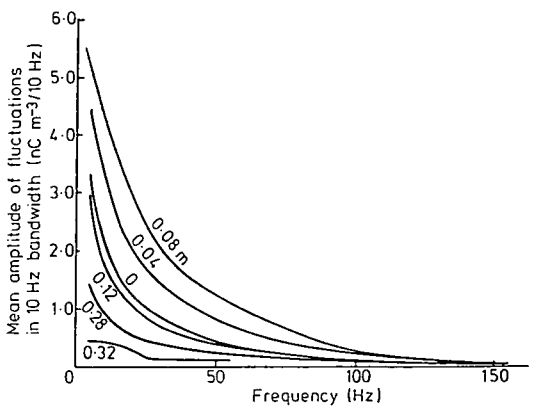

Figure 8 Space charge concentration fluctuation amplitude as a function of frequency in turbulent flow conditions (2 m downstream, ion generator voltage 2·5 kV). For further details see text. Numbers on curves indicate radial positions.

The data suggest that much could be learnt about the relationship between turbulence and turbulent diffusion if more elaborate experiments involving velocity measurements, using for example hot-wire techniques, were undertaken in conjunction with concentration fluctuation observations.

4.2.4 *Simultaneous measurements, at separated points, of space charge concentration in turbulent flow conditions* Experiments were carried out at various distances downstream, usually not more than 3 m, the lateral distance between collectors being in the range 0·05–0·3 m. The results obtained will be illustrated by reference to a typical experiment, in which measurements were made 2 m downstream at an air speed of 5 m s^{-1}

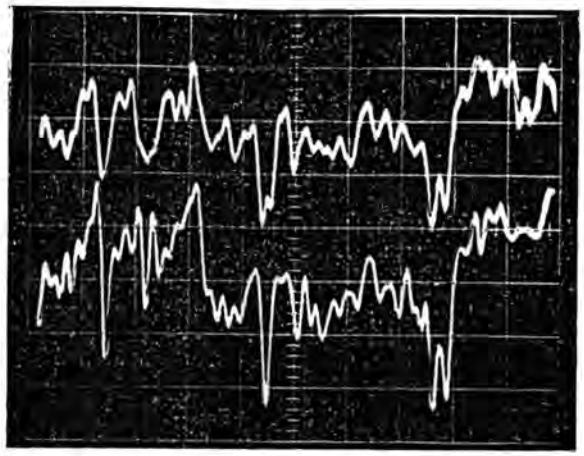

Figure 9 Space charge concentration fluctuations in turbulent flow at 2 m downstream of the ion generator at two points 0·025 m on either side of the plume axis. Vertical axis (increasing downwards) 8·3 nC m^{-3}/large division; horizontal axis 0·2 s/division. Zero of upper trace is at top; that of lower trace is two divisions down. See text for further details.

(prior to insertion of the turbulence grid) with 2·5 kV applied to the ion generator. Figure 9 shows part of a record obtained from two collectors set horizontally 0·025 m on either side of the ion plume axis. It can be seen that the correlation between the concentration variations is generally good. This is particularly so at the lower frequencies where the spatial dimensions of the entities responsible for the fluctuations are larger and thus capable of influencing both collectors simultaneously. Increasing the separation between the collectors to 0·15 m results in a considerable loss in correlation, particularly in the higher-frequency (i.e. smaller-scale) components (figure 10). This trend is even more apparent in figure 11, where the collectors were 0·3 m apart, the records now appearing to be virtually uncorrelated.

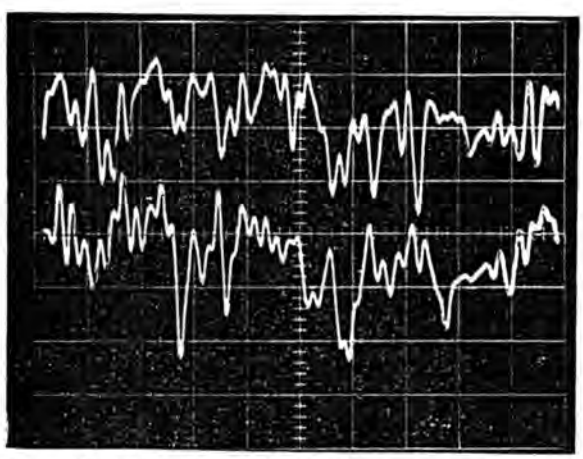

Figure 10 Space charge concentration fluctuations in turbulent flow 2 m downstream of the ion generator at two points 0·075 m on either side of the plume axis (otherwise, as figure 9).

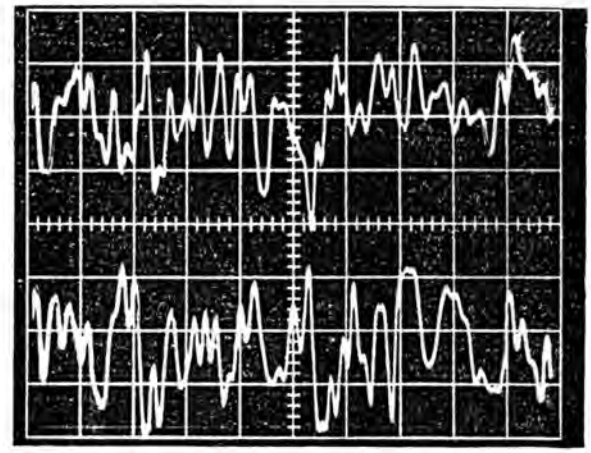

Figure 11 Space charge concentration fluctuations in turbulent flow 2 m downstream of the ion generator at two points 0·15 m on either side of the plume axis. (Otherwise, as figure 9, except that zero of lower trace is four divisions down.)

4.3 *Measurements on ionised air puffs*

All experiments were carried out at wind tunnel air speeds of 5 m s^{-1} with 3 kV applied to the generator. The pulse length was 10 ms so that, in the absence of any electrostatic repulsion, the puff length on leaving the generator would have been 0·05 m. The total charge in the puff was obtained by the method outlined in §2.3, the value found being 0·13 nC. Since the ion generator was switched on for 10 ms, the equivalent current output when operating in this (pulsed) mode was 13 nA, which is considerably less than the 29·4 nA observed for continuous operation in otherwise identical conditions. The reason for this is not clear but the effect is not due to voltage losses in the pulser circuitry. One possibility might be that the ion generation process undergoes a transient phase, perhaps as surface conditioning of the electrodes occurs, immediately after the high voltage is applied and thus the system has no chance to settle down when operating in the pulsed mode.

Table 3 Puff length and radius as functions of distance downstream from the ion generator.

Distance downstream (m)	Puff length (m)	Puff radius (m)
0·5	0·12	0·05
1·0	0·15	0·06
1·5	0·20	0·06
2·0	0·25	0·07
2·5	0·30	0·07
3·0	0·33	0·07
3·5	0·37	0·07
4·0	0·40	0·07

The puff length (determined from the duration of the corresponding ion collector current pulse) was virtually independent of the radial position of the collector. Hence the puff appeared to be cylindrical rather than spherical. The

variation of puff length with distance downstream is perplexing because the puff was quasi-spherical up to 1·5 m downstream, after which considerable elongation occurred, until at 4 m the puff was nearly three times as long as its diameter. Use of the expansion equations for spherical/cylindrical space charges reveals that the radial growth is predicted well, so evidently it is the rapid increase in puff length which is the recalcitrant element. Consideration of the cylindrical space charge field equation indicates that electrostatic repulsion effects could not have been responsible for the elongation. One explanation might be that some mechanical process occurred, possibly arising from the wake/jet caused by the ion generator. However, this does not seem likely because a mean velocity profile measurement revealed no discernible departure from 5 m s^{-1} across the width of the puff.

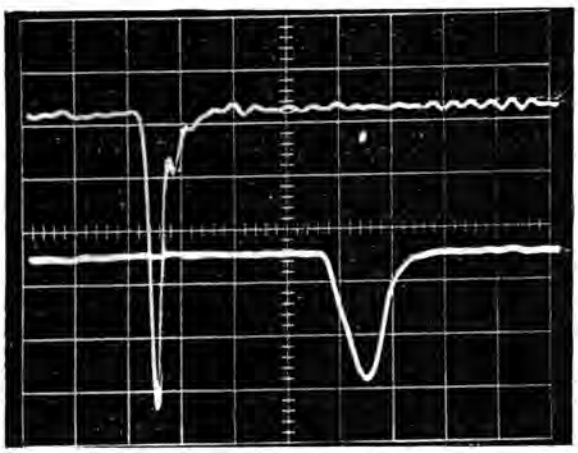

Figure 12 Space charge concentration variations observed on longitudinally separated ion collectors due to an ionised air puff. Upper trace is from collector 0·5 m downstream, lower trace from collector 1·5 m downstream. Vertical scale 16·6 nC m^{-3}/division. Air speed 5 m s^{-1}, low-turbulence conditions. Horizontal scale (oscilloscope was triggered at puff release) 50 ms/division.

An interesting possibility with ionised air puffs is that of making Lagrangian velocity measurements using longitudinally separated collectors. In fact, Brain *et al* (1975) employed a similar technique using a bipolar ion source to measure gas flow velocities in pipes. The type of result obtained in a wind tunnel with the present technique is shown in figure 12. It should be noted that the time taken for the puff to travel from the collector at 0·5 m downstream to that at 1·5 m is close to 200 ms, thus confirming that the tunnel air speed was 5 m s^{-1}.

5 Conclusions and suggestions

The present series of experiments, conducted with miniaturised equipment, has reinforced the view that unipolarly ionised air is a suitable tracer for studying small-scale turbulent diffusion and offers unique advantages over conventional techniques where very high temporal resolution of concentration fluctuations is required. In particular, the use of spectral analysis to examine the space charge concentration fluctuations was found particularly instructive and further work should be done with more complex data-processing arrangements preferably in a wider range of wind tunnel conditions. Quantitative correlation analysis would also, most likely, prove productive.

It would be desirable if electrostatic repulsion effects could be further reduced. This would require the generator output current to be 1 nA or less and raises the possibility of using a radioactive source to produce the ions. Since positive *and* negative ions will result, one polarity will need to be removed, possibly by blowing the ionised air through an appropriately biased coaxial electrode system. It may alternatively be feasible to miniaturise the existing generator design, but so far all attempts to produce a stable source of unipolarly ionised air of less than 1 nA have been unsuccessful. Miniaturisation of the generator would also confer the important advantage of reduced wake effects and hence improve the quantitative precision of the results obtained.

Acknowledgment

The authors wish to acknowledge Mr E V Bryant for constructing the ion generator and collectors used in this work.

References

Brain T J S, Reid J and MacDonald C 1975 *Proc. Conf. on Fluid Measurement in the Mid-1970s, National Engineering Laboratory, East Kilbride, Glasgow, 8–10 April*

Jones C D 1974 A study of turbulent diffusion in the lower atmosphere using artificially produced electric space charge *PhD Thesis* University of Durham

Jones C D 1977 Ionised air as a wind tunnel tracer *J. Phys. E: Sci. Instrum.* **10** 1287

Jones C D and Hutchinson W C A 1976 Plumes of electric space charge in the lower atmosphere *J. Atmos. Terr. Phys.* **38** 485

Jones C. D. and Hopkinson P. R. (1979).

Electrical theory and measurements on an experimental charged crop-spraying system.

Pestic. Sci. **10**, 91 - 103.

Pestic. Sci. 1979, **10**, 91–103

Electrical Theory and Measurements on an Experimental Charged Crop-spraying System

Christopher D. Jones and Peter R. Hopkinson[a]

Chemical Defence Establishment, Porton Down, Salisbury, Wiltshire, and
[a]Department of Electronic and Electrical Engineering, University of Sheffield, Mappin Street, Sheffield

(*Manuscript received 12 June 1978*)

A series of electric-field measurements taken in the vicinity of spinning disc atomisers maintained at a high potential is described. Information on the space charge density, droplet mobility and droplet trajectories is deduced from a theory which is developed in the paper. Direct evidence of improved performance in strong winds compared with uncharged sprays was obtained.

1. Introduction

The concept of using electrically charged droplets and dusts to improve deposition and thus raise the efficiency of agricultural and other spraying systems is not new.[1] This paper describes some results which have been obtained with spinning disc atomisers used in field conditions. In addition to the plant deposition measurements, which will form the subject of a separate paper, electric field measurements were made in the vicinity of the spray in various experimental conditions. It was hoped, from the latter and other observations, that information on the space charge density, droplet mobility and possible droplet trajectories could be derived theoretically. Using those results it might then be possible to assess the effects of crosswinds and other perturbing influences on the spray performance and hence optimise the system for a given set of criteria.

2. Theory

2.1. Initial comments

In the experimental work described later in section 4, electric field measurements were made at ground level. Measurements were repeated for a range of negative extra-high tension (EHT) voltages applied to an atomising disc in spraying and non-spraying conditions, the latter in order to ascertain the effect of the charged metal disc alone on the electric field. Observations were made both with the disc stationary and with it moving forward at normal spraying speed. Some measurements were also made with a two-disc system which indicated that the loss of spray in strong winds was small.

A detailed theoretical analysis of the spray electrodynamics would be very complex not only because of the large number of unknowns involved but also because of the intractable nature of the differential equations which would be obtained. Consequently, if progress is to be made, a number of simplifying assumptions are necessary regarding the spray dynamics. Two interrelated theoretical models have been developed for the spray system: the first being used to calculate the space charge density from which the droplet mobility is deduced, the second the determination of charged droplet trajectories.

2.2. Calculation of the mean space charge density in the spray

Visual observation of the stationary charged spray operating in light wind conditions (< 1 m s^{-1}) indicated that the aerosol produced an approximately cylindrical cloud below it (Figure 1). In

0031-613X/79/0400-0091 $02.00

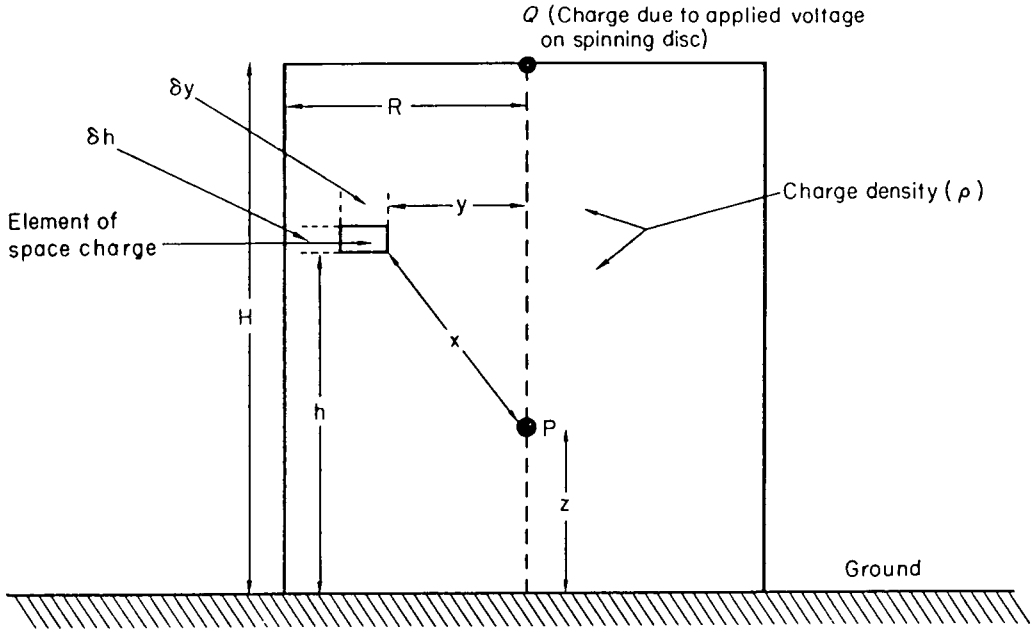

Figure 1. The cylindrical space charge approximation. H, Maximum height of space charge; R, its outer radius; z, height of a point P along the axis.

this case it is possible to show (Appendix 1) that the electric field, E_{cyl}, at any point P on the axis of a cylindrical space charge of uniform density ρ is given by the expression

$$E_{cyl}=\frac{\rho}{2\epsilon_0}\left[\sqrt{(H-z)^2+R^2}+\sqrt{(H+z)^2+R^2}+2z-2\sqrt{z^2+R^2}-|H-z|-(H+z)\right] \quad (1)$$

where H is the maximum height of the space charge, R its outer radius; z is the height of the point, P, along the axis; ϵ_0 is the permittivity of free space. In addition to this field, however, there is a contribution which arises from the potential applied to the disc itself. If the disc has a capacitance to earth of C and the applied EHT voltage is V then the charge 'Q' on the disc is given by

$$Q=CV \quad (2)$$

hence the electric field due to the disc alone (E_{disc}) is given approximately by

$$E_{disc}=\frac{CV}{4\pi\epsilon_0}\left[\frac{1}{(H-z)^2}-\frac{1}{(H+z)^2}\right] \quad (3)$$

assuming it behaves as a point charge. Thus the total electric field (E_{tot}) at any point along the axis of cylinder is given by

$$E_{tot}=E_{cyl}+E_{disc} \quad (4)$$

A calculated electric field profile for typical spraying conditions is shown in Figure 2.

For the special case of $z=0$, i.e. at ground level, equations (1) and (3) reduce to

$$E_{cyl}=\rho[\sqrt{(H^2+R^2)}-(H+R)]/\epsilon_0 \quad (5)$$

and

$$E_{disc}=-CV/(2\pi\epsilon_0 H^2) \quad (6)$$

respectively. From equations (4), (5) and (6), it is then possible to write

$$\rho=\epsilon_0[E_{tot}+CV/(2\pi\epsilon_0 H^2)]/[\sqrt{(H^2+R^2)}-(H+R)] \quad (7)$$

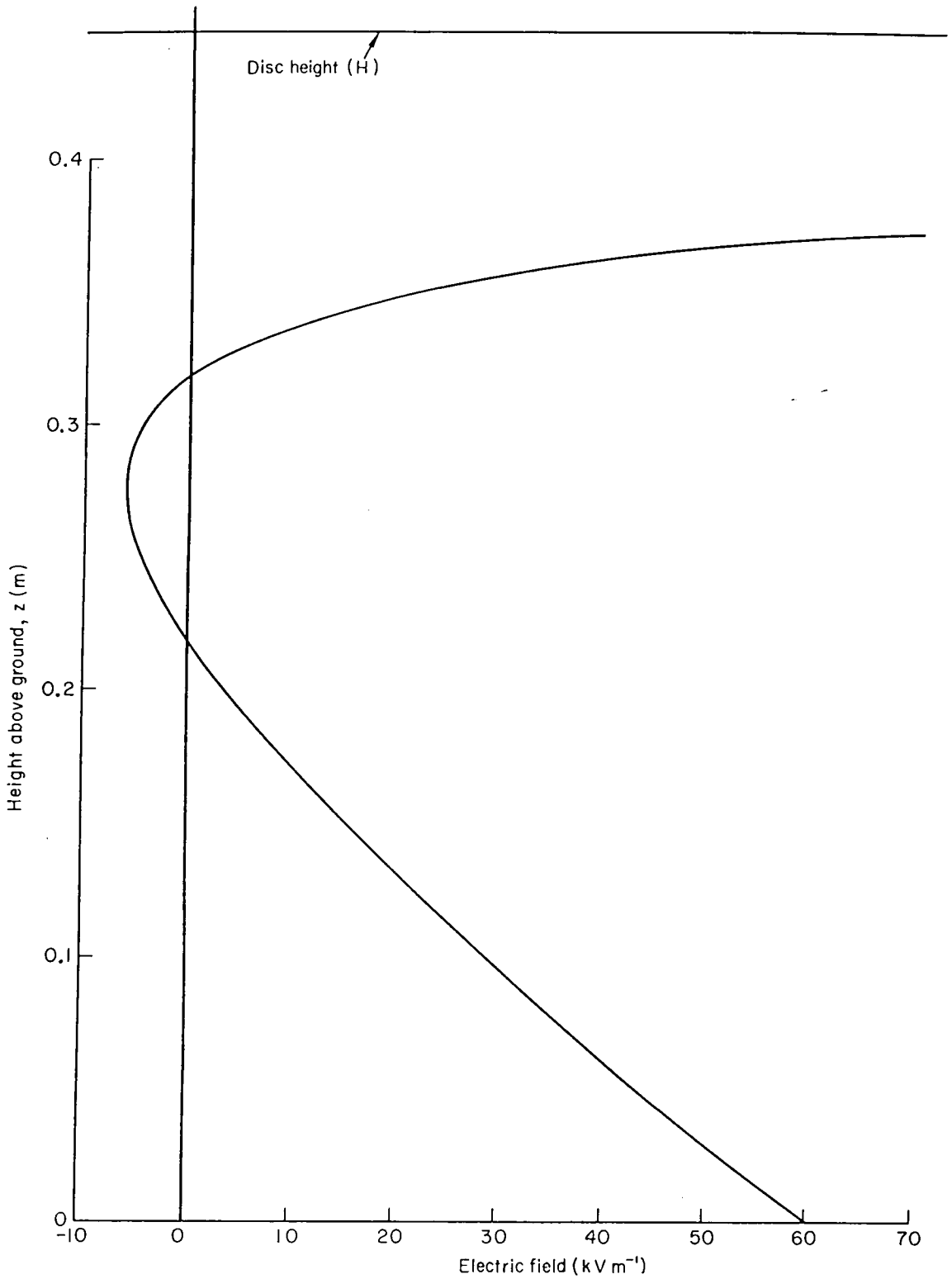

Figure 2. Theoretical variation of the electric field along the axis of the cylindrical space charge cloud for an applied voltage of −40 kV.

2.3. Estimation of the average mobility of the charged droplets

It would, in principle, be feasible to determine the droplet mobility experimentally but that has not been attempted here. Consequently a numerical value of this parameter, which is required for the trajectory calculation (section 2.4), had to be estimated indirectly. It has been shown[2] that the

mobility (μ) can be calculated from the relation

$$\mu = \frac{q}{6\pi\eta d} \tag{8}$$

where q is the droplet charge, d the droplet radius and η the viscosity of the medium through which the droplets move.

The average droplet radius, $\bar{d}$, can be found by a standard technique[3,4] and thus presents little difficulty. It is then possible to determine the average droplet charge ($\bar{q}$) in the following manner. From the spray flow rate (F) and $\bar{d}$, the number of droplets released per second, n, can be estimated from

$$n = 3F/(4\pi\bar{d}^3) \tag{9}$$

As the spray current (i) must equal the product $n\bar{q}$, $\bar{q}$ can be found provided i is known. Unfortunately i cannot be determined directly by observing the EHT current because corona effects mask the relatively small spray current. However, an alternative technique based on the method of Jones and Hutchinson[5] enabled a value for i to be obtained. Briefly, the method was as follows: the spray disc was raised to a height of 1.5 m above ground and the charged spray thus formed a plume as it was blown downwind; if certain assumptions are now made about the behaviour of such plumes it can be shown that

$$i = -E_{pl} h_{pl} \pi w \epsilon_0 \tag{10}$$

where h_{pl} is the plume height, E_{pl} the electric field directly beneath the plume and w is the wind speed.

2.4. Calculation of typical charged droplet trajectories

The velocity (u) of a charged droplet in an electric field (E) can be expressed by the vector equation

$$u = \mu E \tag{11}$$

where the sign of μ is the same as that of the droplet charge. The trajectory of the droplet is therefore described by the pair of simultaneous equations

$$\begin{aligned} \frac{\partial z}{\partial t} &= \mu E_z - v_s \\ \frac{\partial r}{\partial t} &= \mu E_r \end{aligned} \tag{12}$$

where E_z and E_r are the vertical and radial field components respectively and v_s is the Stokesian or settling velocity of the droplet.

Whilst it is theoretically possible to calculate E_z and E_r for any point in the vicinity of a cylindrical space charge, such an analysis is tedious, and moreover, for the present purpose, is not warranted. A simpler approach, adequate for a first treatment, is to reduce the cylindrical space charge distribution to an equivalent line charge, Figure 3. In Appendix 2 it is shown that in this case the vertical and radial field components are given by

$$E_z = \frac{\lambda}{4\pi\epsilon_0}\left[\frac{1}{\sqrt{(H-z)^2+r^2}} + \frac{1}{\sqrt{(H+z)^2+r^2}} - \frac{2}{\sqrt{z^2+r^2}}\right] - \frac{Q}{4\pi\epsilon_0}\left[+\frac{H-z}{[(H-z)^2+r^2]^{3/2}} + \frac{H+z}{[(H+z)^2+r^2]^{3/2}}\right] \tag{13}$$

and

$$E_r = \frac{\lambda}{4\pi\epsilon_0 r}\left[\frac{H-z}{\sqrt{(H-z)^2+r^2}} - \frac{H+z}{\sqrt{(H+z)^2+r^2}} + \frac{2z}{\sqrt{z^2+r^2}}\right] + \frac{Q}{4\pi\epsilon_0}\left[\frac{r}{[(H-z)^2+r^2]^{3/2}} - \frac{r}{[(H+z)^2+r^2]^{3/2}}\right] \tag{14}$$

where λ is the charge per unit length. A value for this quantity can be found once ρ has been obtained from the electric field measurements. At any instant the total charge in the aerosol cloud, Q_{tot}, must be given by

$$Q_{tot} = \pi R^2 H \rho \tag{15}$$

and, as

$$Q_{tot} = \lambda H \tag{16}$$

$$\lambda = \pi R^2 \rho \tag{17}$$

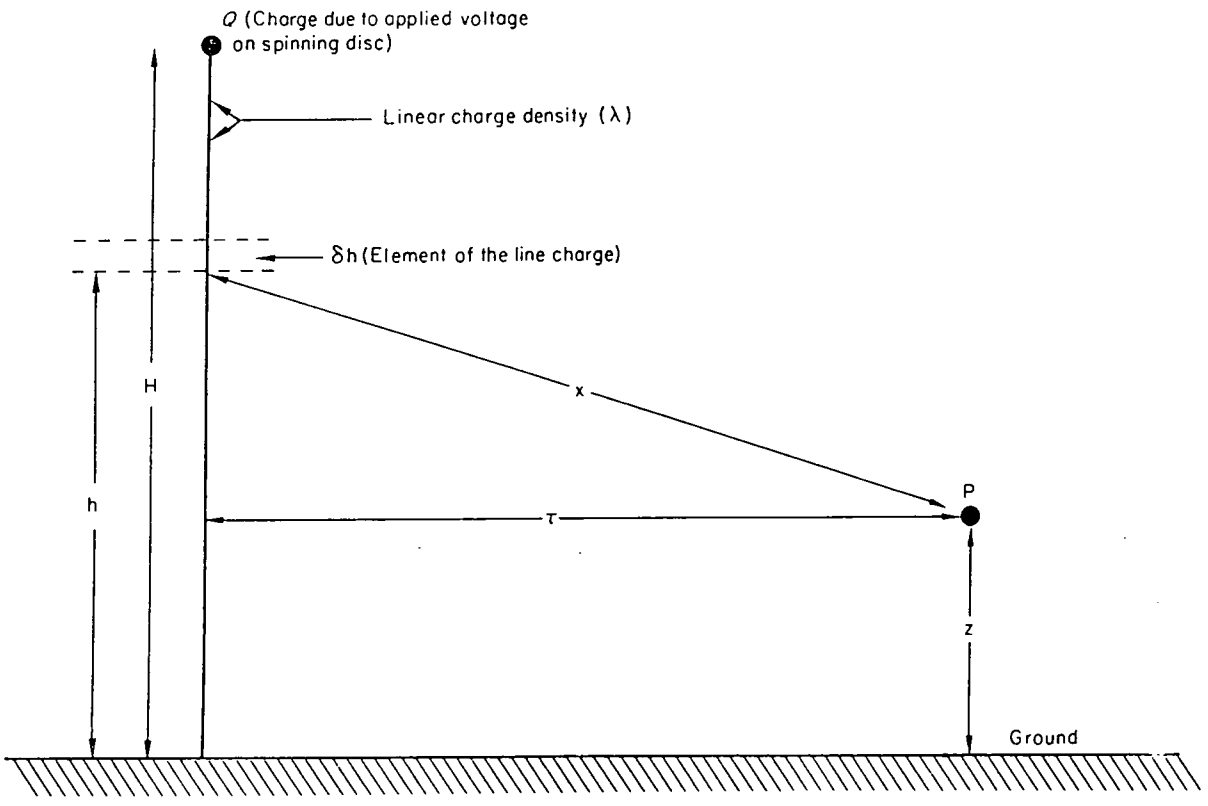

Figure 3. The linear space charge approximation. H, R and z as in Figure 1; r, distance of droplet from vertical axis of disc.

Equation 17, which gives λ in terms of ρ, applies to the case where the charged droplet is at the outer radius R of the cylindrical space charge. Clearly not all the droplets are as far out as this, thus, for a droplet distance r from the vertical axis of the disc, the effective line charge (determining E_r) must be

$$\lambda(r) = \left(\frac{r}{R}\right)^2 \lambda \qquad \text{for } r \leqslant R \tag{18}$$

Physical considerations indicate that the behaviour of E_z is best represented by retaining the charge per unit length fixed at λ irrespective of r.

Analytical solution of equation 12 is not possible with the expressions deduced above for the

field components and linear charge density because they seem to be intractable. However, some numerical solutions for typical spraying conditions have been obtained and are discussed in section 4.3.

2.5. Estimation of the fraction of spray lost in strong winds by electric-field measurements

In addition to the information on trajectories derived theoretically it was possible to assess the spray performance in strong winds in a rather more direct manner. This was done by measuring the electric field at a point several metres downwind of a stationary atomiser so that any charged aerosol passing near could be detected. In fact it was more satisfactory to perform the experiment with the two-disc systems because of the relative insensitivity of the electric field to small fluctuations in wind direction with that arrangement.

It can be shown[6] that the ground level electric field due to a plume of space charge at a point specified by the coordinates r,ϕ with respect to the release point is given by

$$E_1 = \frac{i'}{2\pi\epsilon_0 w}\left[\frac{h}{(r^2\sin^2\phi + h^2)}\left(1 + \frac{r\cos\phi}{\sqrt{r^2+h^2}}\right)\right] \tag{19}$$

where h is the plume height, w the wind speed and i' the plume current (the spray current lost). For a two-spray system where the field measurement is made at a point along the perpendicular bisector of the line joining the two sprays it can be shown that the field observed when the wind blows at angle θ to the bisector is

$$E_2 = \frac{i'}{2\pi\epsilon_0 w}\left[\frac{h}{(r^2\sin^2(\theta+\phi') + h^2)}\left(1 + \frac{r\cos(\theta+\phi')}{\sqrt{r^2+h^2}}\right) + \frac{h}{(r^2\sin^2(\theta-\phi') + h^2)}\left(1 + \frac{r\cos(\theta-\phi')}{\sqrt{r^2+h^2}}\right)\right] \tag{20}$$

Here ϕ' is the angle between the line joining either spray to the observation point and the bisector. Equation (20) is applied in section 4.4.

3. Experimental

3.1. The experimental spray system

For crop spraying, particularly the bio-assay work, three (or occasionally two) spaced spinning-disc atomisers, mounted vertically upon a boom fixed to a platform attached to the rear of a tractor, were employed. The EHT voltage was applied to an aluminium sphere which directed the incoming fluid to each atomiser. Power was derived from a conventional motor generator set. On the electric-field measurements, a one- or two-atomiser system, otherwise identical with the crop spraying arrangement referred to previously, was generally used as indicated in the text.

3.2. The field mill

This instrument has already been described in detail elsewhere.[7] Briefly, the device consisted of an insulated stator plate, usually in the shape of a Maltese cross, over which rotated a similarly shaped plate connected to earth. In the presence of an electric field the stator was successively screened from and exposed to the field and hence an alternating displacement current of magnitude directly proportional to the field was induced upon it. After suitable amplification and filtering, a signal proportional to the field was derived. If the sign of the electric field was also required then some means of determining the relative phase of the input signal was necessary, a photo-electric technique being employed in this instance.

It must be emphasised that in addition to the displacement current induced in the stator there was also an effect from the deposition of charged droplets on its surface. The latter contribution was also chopped by the rotor and was indistinguishable from the true displacement current, thereby producing errors in the electric field measurements. However, it was possible to calculate that this effect, even in the worst case, caused a 10% error only and hence its correction was regarded as unnecessary.

The mill was sited in a small hole in the ground with the stator at ground level. In this way minimum disturbance to the electric-field distribution was caused, thus improving the reliability of the observations. The output of the field mill was connected to a short-time constant chart recorder and a permanent record of the field variations was obtained. In most cases measurements were made over bare earth.

4. Results and discussion

4.1. Electric field data obtained for a stationary charged spray

Table 1 gives values of the mean electric field at ground level immediately beneath the disc for various applied EHT voltages. Considerably enhanced field values arose from the space charge due to the charged droplets. For the non-spraying condition, the electric field increased rapidly when the applied voltage exceeded about -30 kV, a consequence of the ionisation of the air in the immediate vicinity of the disc. For the capacitance of the disc with respect to earth, C, to be meaningful, it must therefore be calculated for non-ionising conditions at low voltages; hence from equation 3, $C=2.1$ pF.

Table 1. Electric field measurements directly under the stationary spray

Applied voltage to spinning disc (kV)	Electric field (kV m^{-1})	
	Spray off	Spray on
-10	$+1.8$	$+10.3$
-20	$+3.7$	$+25.1$
-30	$+8.5^a$	$+42.4$
-40	$+22.1^a$	$+59.8$
-50	$+45.0^a$	>60

[a] Ionisation occurring.

Thus, for an applied voltage of -40 kV at which the mean droplet radius had been previously determined in the laboratory,[3] the charge, Q, from equation (2), is 8.3×10^{-8} C.

Using equation (7) it can be deduced that $\rho=2.9$ μC m^{-3}, and that for the spraying parameters employed, the number of droplets produced per second, n, is 4.6×10^{7}.

In an experiment to determine the spray current i, a mean electric field of $+20$ kV m^{-1} was observed directly under the spray plume which was at a height of 1.5 m, the mean wind speed being 2 m s^{-1}. From the data obtained i was calculated to be -4.0 μA, using equation (10).

Therefore the mean charge per droplet is given by $\bar{q}=i/n=-8.7\times10^{-14}$ C.

Calculations showed that the droplet charge was approaching the maximum possible above which corona effects would automatically limit the charge. The average mobility of the charged droplets can be calculated from equation 9 which gives $\bar{\mu}=1.0\times10^{-5}$ m^2 V^{-1} s^{-1}. Figure 2 shows the theoretical variation of the electric field along the axis of the cylindrical space charge cloud using equations (1), (4) and (8) for an applied voltage of -40 kV. It shows that the electric field is reversed in the height range 0.22–0.31 m thereby implying that the field exerts an upward force on the charged droplet. The maximum upward velocity due to the field alone can be estimated from equation (11) and is approximately 0.06 m s^{-1}. This is significant because the settling velocity under gravity is of a similar magnitude. Consequently, at the height of 0.28 m where the electrostatic and gravitational forces virtually balance, the droplet will be very susceptible to the effects of, for example crosswinds. From the electric field profile it can also be deduced that the droplet velocity near the ground is in the region of 0.6 m s^{-1} which should render them considerable immunity to the effects of atmospheric turbulences at these levels.

4.2. The electric field variation under a moving charged spray

The observed variation of the electric field associated with the passage of the charged spray over the measuring point is shown in Figure 4. Despite considerable electrostatic repulsion forces, causing the spray to spread radially, very little change was observed in the electric field until the disc was within about 1 m of the field mill. The electric field then rapidly increased to a double, rather than single peak as might have been expected at first. This phenomenon is thought to have arisen in the following way. It was observed that when the spray was operating the droplets tended to form an ill-defined parabola with the disc at the apex; hence the space charge concentration would probably have been higher at the cloud edges rather than at its centre. Such a charge distribution could have produced an electric field profile of the type observed.

The electric field value at A on the curve at +45 kV m^{-1} (Figure 4), which corresponds to the overhead position of the disc was considerably lower than in the previous experiment. In that experiment the observed field was almost 60 kV m^{-1} (Table 1). This discrepancy is almost certain to have been caused by the field mill having an insufficiently short response time to follow the rapid electric field variations.

Measurements made on planted ground revealed that, with short crops such as sugar beet and barley in their early stages, the electric fields did not differ from the corresponding bare earth values

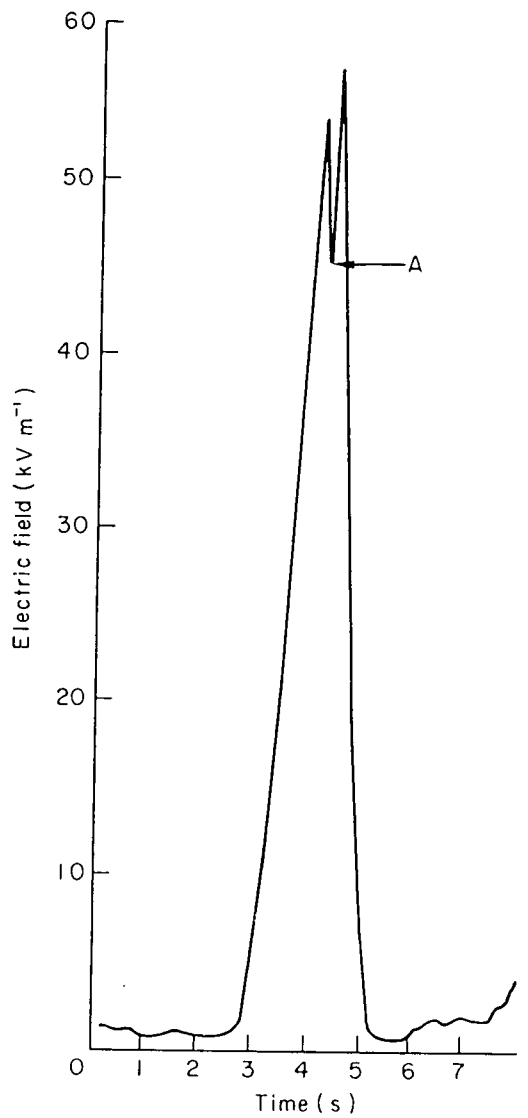

Figure 4. Observed variation of the electric field at a point under a moving charged spray. Spray velocity 0.71 m s^{-1}.

by more than 10–20%. However, as would be expected, the electric fields under the canopies of well-developed tall plants, such as broad beans, were quite small, typically only a few kV m^{-1} maximum. This indicates that in such cases most of the deposition must occur in the upper regions of the plant and incidentally implies that only a small percentage of the droplets would be lost to the soil below.

4.3. Theoretical droplet trajectories

Figures 5 and 6 show two sets of droplet trajectories calculated for typical spraying conditions (see sections 2.4, 4.1 and 4.2) where zero wind has been assumed. The two sets, which depict most of the possibilities for droplet motion, have been computed by solving equation 12 numerically for

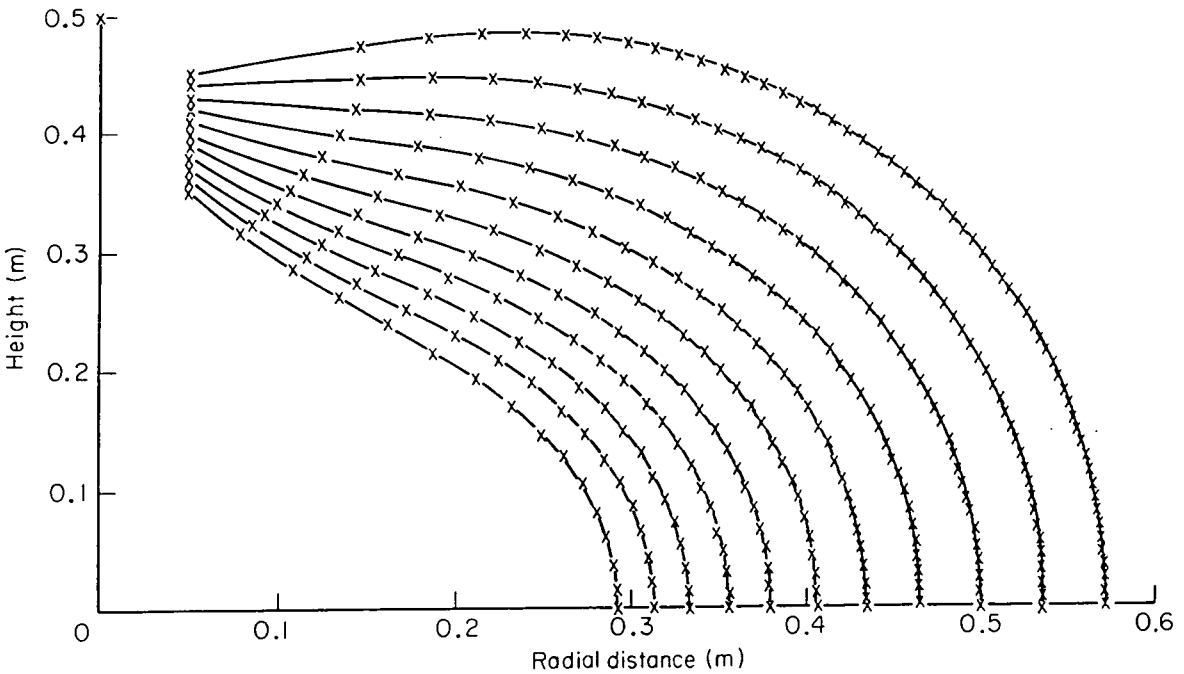

Figure 5. Theoretical trajectories for droplets calculated for typical spraying conditions.

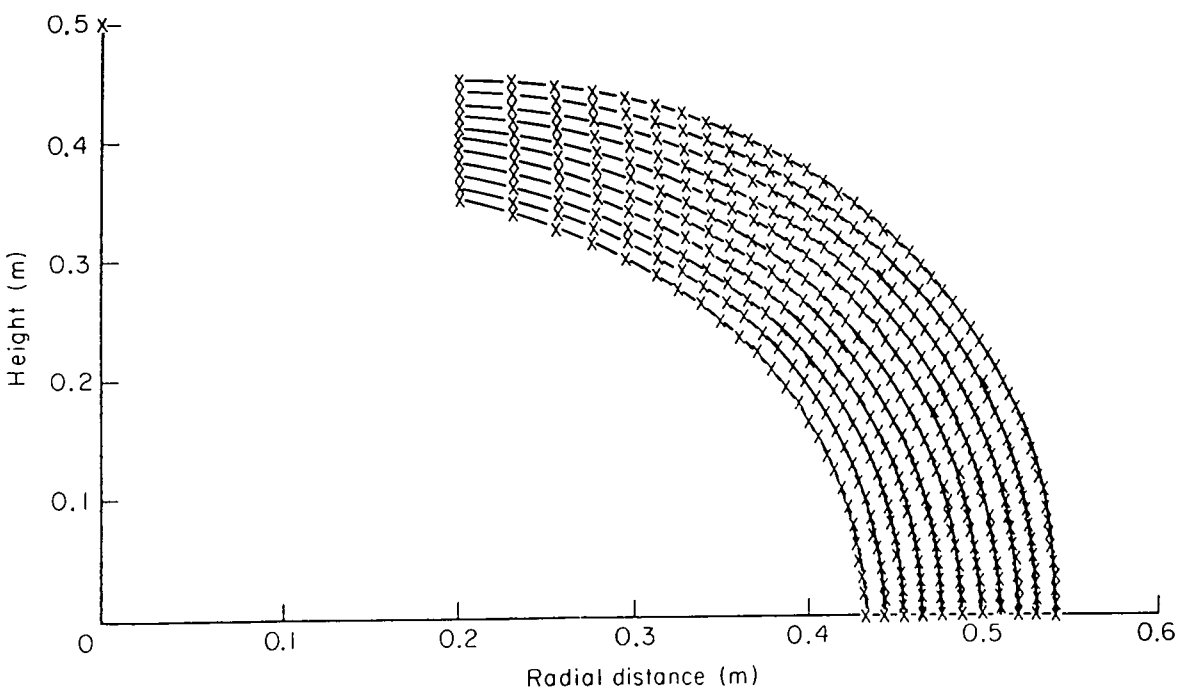

Figure 6. Theoretical trajectories for droplets calculated for typical spraying conditions.

initial droplet heights ranging from 0.35 to 0.45 m and radii 0.05 and 0.2 m, the crosses representing increments of 0.1 s.

Visual observation of the spray indicated that most of the droplets were thrown out to a distance of about 0.2 m from the disc. During this short time interval the droplets fall in the region of 0.02 m and from Figure 6 it is seen that they arrive at the ground at a radial distance of 0.51 m and take 3.8 s to do so. It is interesting to compare this with the time taken to fall to the ground in the absence of the electric field, 5.9 s. Hence the application of the field produces a significant reduction in the time taken to reach the ground, its mean velocity being increased from 0.07 m s^{-1} to 0.11 m s^{-1}.

Whilst many of the droplets behave as described above, a number were seen not to be thrown out as far as 0.2 m, a typical minimum distance being approximately 0.05 m. Referring to Figure 5, it would seem that in most cases this was a considerable disadvantage, the trajectory times tending to be larger than in the previous case except where the droplet was projected well downwards. A further point is that if droplets are released at heights exceeding 0.43 m some upward motion is predicted prior to descent which is clearly most undesirable. Both the predicted distance determined above and the initial upward trajectory of the droplets agree with laboratory observations.

4.4. Electric field observations of the charged spray in strong winds

It had already been noted from direct visual observation that application of the EHT voltage to the system considerably reduced the amount of spray being blown away and the electric-field measurements described below strongly reinforce this. In the experiments a field mill was placed 3 m downwind of a two-spray system (section 2.5) operating in a wind with a velocity (w) of 6 m s^{-1} with 60 kV applied. The separation of the atomisers was 1.07 m and their height above ground, which was planted with sugar beet 0.23 m high, was 0.53 m. For these conditions it was found that the term in square brackets in equation (20) can be made equal to about 3.75 for $\theta \rightarrow -20°$ to $+20°$ without serious loss of accuracy. In fact, wind direction variations were probably rather smaller than this and thus equation (19) could be written approximately as

$$E_2 = 3.75 i'/2\pi\epsilon_0 w \tag{21}$$

which gives

$$i' = 2\pi\epsilon_0 w E_2/3.75 \tag{22}$$

Observations revealed that the field E_2 was at no time greater than 300 V m^{-1}, from which it could be deduced that the maximum value that i' could have attained was about 2.7×10^{-8} A. As the current per spray was in the region of 4 μA, this is most encouraging in that it implies that less than 1 % of the spray was lost.

This analysis, of course, assumes that all the aerosol is well charged, because less charged or uncharged droplets would not be detected by the field mill. However, with the atomising and charging system used in this work it is thought that it would be most unlikely that any droplet could avoid acquiring a considerable charge.

5. Conclusions

The analysis of the electrical data in this paper demonstrates that spray performance can be considerably enhanced by employing electrically charged droplets. Examination of the theory developed indicates that further improvement might be obtained. Figures 2 and 5 show clearly the adverse effects of reverse electric fields when the droplet is above the main space charge centre of the aerosol cloud. It is possible with the present system for a droplet to be driven upward in a few cases; however, it is more usual that the field is not sufficiently strong to cause this and merely impedes rather than augments the downward motion.

The theoretical treatment developed above provides information on the performance of an electrically-charged crop-spraying system. Direct measurements of spray current and droplet mobility, which could be made using the standard techniques of Atmospheric Electricity,[8] together with those of droplet size, velocity and trajectory, obtained best perhaps by the holographic method,[9]

would be very useful and should enable a more rigorous theoretical approach to be formulated.

In this paper the electrical aspects of deposition on the plants themselves have not been considered. Theoretical analysis is difficult but it is at least evident that deposition on the undersides of leaves requires, with the present system, a reverse field of at least 7 kV m^{-1} to overcome the effects of settling velocity, assuming that other factors do not intervene. It is likely that maximum underside deposition will occur with small droplets, having a low settling velocity but carrying a high charge. Deposition will presumably occur preferentially on pointed areas where the electric fields are largest, most plants being sufficiently conductive, from an electrostatic viewpoint, to act as earthed objects.

Acknowledgements

One of us (P.R.H.) acknowledges the generous financial support given by the National Research Development Corporation and for permission to publish the paper. The other (C.D.J.) acknowledges the assistance of the Procurement Executive, Ministry of Defence and the NRDC in this work. Special thanks are due to Mr A. J. Arnold of the Rothamsted Experimental Station whose efforts in organising and assisting with the field experiments are much appreciated. The authors wish to thank Mr R. Bexon, Chemical Defence Establishment, Porton Down, for his contribution to the development of the numerical analysis associated with the trajectory calculations.

References

1. Hopkinson, P. R. *The prospects for enhanced impaction of fine sprays by electrostatic charging, Br. Crop Prot. Council Monograph No. 11, 1974* pp. 166–179.
2. Green, H. L.; Lane, W. R. *Particulate clouds: dusts, smokes and mists* Spon, London, 1957.
3. Turner, C. R.; Huntington, K. J. *J. Agric. Eng. Res.* 1970, **15**, 385.
4. Matthews, G. A. *PANS* 1975, **21**, 213.
5. Jones, C. D.; Hutchinson, W. C. A. *J. Atmos. Terr. Phys.* 1976, **38**, 485.
6. Jones, C. D.; Jennings, S. G. *Atmos. Environ.* 1977, **11**, 1197.
7. Mapleson, W. W.; Whitlock, W. S. *J. Atmos. Terr. Phys.* 1955, **7**, 61.
8. Chalmers, J. A. *Amospheric Electricity* Pergamon, Oxford, 1967.
9. Fourney, M. E.; Malkin, J. H.; Waggoner, A. P. *Rev. Sci. Instrum.* 1969, **40**, 205.
10. Bleaney, B. I.; Bleaney, B. *Electricity and magnetism* Oxford University Press, Oxford, 1965.

Appendix 1

Calculation of the vertical component of the electric field at any point on the axis of a cylindrical space charge.

Referring to Figure 1, the potential $\delta V'$ at the point P, due to the annular element y to $y+\delta y$ of thickness δh, is

$$\delta V' = \frac{2\pi y \rho \delta y \delta h}{4\pi\epsilon_0 x}$$

hence the potential V' due to the entire cylindrical charge is

$$V' = \frac{\rho}{2\epsilon_0} \int_0^H \int_0^R \frac{y \, dy \, dh}{\sqrt{(h-z)^2+y^2}}$$

Now the electric field $(E'_z) = -\partial V'/\partial z$, and by using the commutative properties of integration and differentiation, it is possible to write

$$E_z' = \frac{-\rho}{2\epsilon_0} \int_0^H \int_0^R \frac{\partial}{\partial z} \frac{y}{\sqrt{(h-z)^2+y^2}} \, dy \, dh$$

$$E_z' = \frac{\rho}{2\epsilon_0} \int_0^H \frac{\partial}{\partial z} \left[\sqrt{(h-z)^2+y^2}\right]_0^R dh$$

therefore

$$E_z' = \frac{\rho}{2\epsilon_0}\left[\sqrt{(H-z)^2+R^2} - |H-z| - \sqrt{z^2+R^2} + z\right] \tag{23}$$

The presence of the ground, which has not been considered so far, modifies the electric field distribution due to the cylindrical space charge. This effect can be most simply included by employing the image charge method.[10] It is found that

$$E_z = \frac{\rho}{2\epsilon_0}\left[\sqrt{(H-z)^2+R^2} + \sqrt{(H+z)^2+R^2} + 2z - 2\sqrt{z^2+R^2} - |H-z| - (H+z)\right] \tag{24}$$

Appendix 2

Calculation of the vertical and radical electric-field components at any point in space due to a line charge segment.

Referring to Figure 2, the potential at the point P due to the line charge element h to h+δh is

$$\delta V' = \frac{\lambda \delta h}{4\pi\epsilon_0 x}$$

hence the potential due to the entire charge is given by

$$V' = \frac{\lambda}{4\pi\epsilon_0}\int_0^H \frac{1}{\sqrt{(h-z)^2+r^2}}\,dh$$

and, taking into account the image charge, the final expression for the potential becomes

$$V = \frac{\lambda}{4\pi\epsilon_0}\int_0^H \left(\frac{1}{\sqrt{(h-z)^2+r^2}} - \frac{1}{\sqrt{(h+z)^2+r^2}}\right) dh$$

Now the vertical component of the electric field,

$$E_z = -\frac{\partial V}{\partial z},$$

thus

$$E_z = -\frac{\lambda}{4\pi\epsilon_0}\left[\frac{-1}{\sqrt{(h-z)^2+r^2}} + \frac{-1}{\sqrt{(h+z)^2+r^2}}\right]_0^H$$

therefore

$$E_z = \frac{\lambda}{4\pi\epsilon_0}\left[\frac{1}{\sqrt{(H-z)^2+r^2}} + \frac{1}{\sqrt{(H+z)^2+r^2}} - \frac{2}{\sqrt{z^2+r^2}}\right] \tag{25}$$

For the radial field,

$$E_r = -\frac{\partial V}{\partial_r};$$

therefore

$$E_r = -\frac{\lambda}{4\pi\epsilon_0}\int_0^H \frac{\partial}{\partial r}\left(\frac{1}{\sqrt{(h-z)^2+r^2}} - \frac{1}{\sqrt{(h+z)^2+r^2}}\right) dh$$

therefore

$$E_r = \frac{\lambda}{4\pi\epsilon_0 r}\left[\frac{H-z}{\sqrt{(H-z)^2+r^2}} - \frac{H+z}{\sqrt{(H+z)^2+r^2}} + \frac{2z}{\sqrt{z^2+r^2}}\right] \tag{26}$$

The field due to the charge Q (at H) can be readily shown to contribute an amount

$$-\frac{Q}{4\pi\epsilon_0}\left[\frac{H-z}{[(H-z)^2+r^2]^{3/2}}+\frac{H+z}{[(H+z)^2+r^2]^{3/2}}\right] \tag{27}$$

to the total vertical component and

$$\frac{Q}{4\pi\epsilon_0}\left[\frac{r}{[(H-z)^2+r^2]^{3/2}}-\frac{r}{[(H+z)^2+r^2]^{3/2}}\right] \tag{28}$$

to the total radial component.

Murlis J. and Jones C. D. (1981).

Fine-scale structure of odour plumes in relation to insect orientation to distant pheromone and other attractant sources.

Physiol. Entom. **6**, 71 - 86.

Physiological Entomology (1981) **6**, 71–86

Fine-scale structure of odour plumes in relation to insect orientation to distant pheromone and other attractant sources

J. MURLIS and C. D. JONES Centre for Overseas Pest Research, London, and Chemical Defence Establishment, Porton Down, Wiltshire

ABSTRACT. This paper describes an experimental method for simulating an odour plume in the field so that its fine-scale characteristics may be determined. It was found that the 'odour' arrived at a series of fixed points up to 15 m from the source in a series of discrete bursts, which were widely distributed in time but were typically 0.1 s long and 0.5 s apart. The strengths of the bursts were also found to be widely distributed and some contained considerable fluctuations. Thus an odour plume is not continuous, but intermittent, and appears at a fixed point downwind of the odour source as a series of bursts of odour which are variable in strength and duration. The distribution of the length of bursts and the time between them does not greatly vary with distance from source. Although concentration does decay with distance from source, instantaneous measurement would not be a reliable guide to the mean concentration and hence to position relative to source. To obtain reliable positional information from the odour plume an insect would have to average received stimuli over many seconds. More information is therefore required about the dynamics of insects' olfactory responses.

Introduction

As the wind blows it carries with it materials picked up along its path: from each particular source a plume will be created, similar to the plume of smoke from a chimney. Such a plume may contain materials attractive to insects (food odours, for example, or sex attractant pheromones) in which case receptive insects may respond in a way that enables them to locate the plume source. Recent progress in the study of behavioural mechanisms used by insects to find a distant odour source has been reviewed by Kennedy (1977), and it is clear that, although work has been done (mainly in wind tunnels) on insect behaviour under the influence of attractant odours (including the insects' reactions to wind, light, the sudden removal of odour, and visual clues), there has been very little done on the way in which odour stimuli are presented to insects in nature. To see how odour is presented it is necessary to determine odour plume structure, that is, the pattern of odour distribution within the plume.

Some work has been done on the production of mathematical models of plumes. Wright (1958) used a micro-meteorological calculation method developed by Sutton (1953) to estimate the active space, a region in which an insect would be stimulated by odour emanating from a point source. Bossert & Wilson (1963), using a similar method, went on to calculate concentration gradients and concluded that the estimated gradients would alone provide insufficient

Correspondence: Dr J. Murlis, Centre for Overseas Pest Research, Wrights Lane, London, W.8.

0307-6962/81/0300-0071 $02.00

clues for distant orientation towards the plume source. Similar methods have been used by Sower *et al.* (1973) and Nakamura (1976) to determine regions of attraction.

These methods all have a basic shortcoming: they give the time-averaged concentration distribution within a plume and say little if anything about the pattern of instantaneous concentrations. Even as a model of time-average distributions their value is limited: they involve a series of empirically derived expressions which cannot easily be modified for different conditions, and, during the averaging times required, the wind would generally not stay within the desired limits of strength or direction. Wright (1958) discussed the deficiencies of the average-plume approach: he saw that an illuminated cross-section of a smoke plume presented a filamentous nature and noted that this instantaneous structure might be expected to dominate the mean concentration structure as a mediator of insect behaviour. Bossert & Wilson (1963) similarly noted that the mean concentration gradients might be expected to be swamped by local fluctuating gradients.

Lewis & Macaulay (1976) described differences in the flight pattern made by moths towards a pheromone source and, using smoke, they described corresponding differences in the shape and structure of a plume issuing from the same source position. These observations are of great value as they demonstrate the importance of plume structure and suggest a need to quantify it. As calculation methods are at present inadequate, measurements of instantaneous plume structure are needed to map out in space the pattern of concentrations in which the attractant odour would arrive at an insect's receptors. A major difficulty in making such measurements is that they should ideally be to a time scale faster than the response time of the insect's receptors.

The magnitude of neural response to odour stimulus is, above a certain threshold, proportional to odour concentration, but it also has a strongly time-dependent form, rising rapidly at the onset of stimulus, reaching a peak and as stimulus is maintained decaying to some limiting value. Kaissling (1971) gives a lower limit of the half decay time of approximately half a second. If the stimulus is removed immediately after application, its re-application during the decay period may induce a further peak. Thus, intermittent stimulation may produce an intermittent neural response, which may have important effects on behaviour. It is therefore desirable that the chosen rate of sampling to determine odour concentration in the plume should cover the full expected range of neural response times. The sampling rate required to give accurate definition of a random signal is given by digital analysis theory as two samples in the shortest cycle time of interest for spectral properties, power spectra for example, and four times for shape definition (Bendat & Piersol, 1971).

Although it is currently difficult to ascribe an exact value to the shortest cycle of interest, it is possible to obtain an approximate idea from receptor response times. Kaissling (1971) quotes insect chemoreceptor reaction times from the beginning of stimulus to the onset of the first nerve impulse. The fastest may be of around 10 ms, and even slow response times (in individuals responding to weak stimuli) around 100 ms. Thus it may be expected that a sampling rate of $4 \times 100 = 400$ Hz would be required and that instantaneous values would then involve sampling times of *c.* 2.5 ms.

It is not yet possible to determine the instantaneous concentration of sex pheromone or food odour, even quite close to the source (i.e. at *c.* 1 m). Recently, however, plume structure measurements made in the study of air pollution have used tracers whose concentration can be assessed during short sampling times, in the order of a second or less. In the atmosphere the diffusive mechanisms responsible for creating the plume are dominated by air movements, molecular diffusion being neglible, and so these tracer results would apply equally to odour plumes.

Hadjitofi & Wilson (1979) describe a flame photometric technique for making fine-scale plume measurements using the chemical tracers sulphur dioxide and phosphorus pentafluoride. The sampling times for these are about 900 and 20 ms respectively, which is a little slow for present purposes. Moreover, as it is intended eventually to fly insects in the tracer plumes, such materials are unsuitable. Jones (1977) described a method which uses

ionized air as a tracer. This is believed to be non-toxic to insects and it has a time resolution of detection better than 1 ms. It is also experimentally relatively straightforward and can be deployed in field studies.

In this paper we describe measurements of instantaneous concentration made using such an ionized air tracer at a series of fixed positions up to 15 m downwind of a point source. Measurements of both the mean concentration and temporal fluctuations in concentration are presented. For the purposes of this paper small-scale structure has been taken to include features with periods less than *c.* 1 min, during which time an insect could reasonably be expected to negotiate the region of the plume under investigation, i.e. 15 m to 2 m from the source. We have chosen to use the term 'odour plume', but the results would apply equally to any kind of material carried passively by the wind.

Materials and Methods

Experimental method and recording technique

The tracer used to model an odour plume in these trials was a stream of unipolar ionized air. A controlled corona discharge was produced in an ion generator by the application of a very high potential (2.75 kV) to the central electrode of a coaxial pair, the outer annular electrode being at earth potential. Air blown through the corona was ionized and emerged from a downwind-pointed outlet of diameter 0.02 m with a velocity of 3 m s^{-1}, a magnitude of similar order to the mean wind speed in these trials.

At a downwind point, air was continually sampled by being drawn through an ion collector (inlet 0.03 m diameter) at 6 m s^{-1}. The ions in the sampled air were driven to the central electrode of a coaxial pair in the collector by a high voltage (about 0.6 kV) applied to the outer annular electrode. At the axial central electrode the recombination of the ions caused a small current (of a few pA) to flow to earth. A current amplifier placed between the ion collector and earth enabled the recombination current to be measured and recorded on a frequency-modulated tape recorder. The response time of the ion collectors used in these trials was *c.* 1 ms.

Unipolar ions are capable of persisting in the atmosphere for several minutes before they are neutralized by recombination (Chalmers, 1967). In our trials the required times of flight of the ions from source to collectors were governed by wind speed and maximum desired source–collector separation. Even in a light wind of, say, 1 ms^{-1}, and at a separation of 50 m the required times of flight would be only 50 s. For these trials carried out in moderate winds up to 15 m from source the ions can be considered a conservative tracer. A plume of unipolar ions spreads slightly due to repulsion forces, and tends to be affected by electrostatic image forces due to the proximity of the ground. Both these effects, however, are negligible when the system is operating as for the trials described here (Jones, 1979).

The typical shape of the ion collector signal is, as shown in Fig. 1, a series of spikes separated by intervals of zero signal. These intervals should represent periods when there are no ions at all arriving from the ion generator, not periods of weak signal indistinguishable from the background level of naturally occurring ions. Our reasons for this belief are that in a separate series of experiments (Jones, 1979) a similar intermittency together with a similar steep leading and trailing edge shape was seen in collector signals produced by ions arriving from both continuous and pulsed sources. In the same trials, comparisons with a sensor responding to the position of the whole plume showed that many intervals of zero signal occurred when the plume was away from the ion collector.

The sensitivity of the system is limited by the background level of ionized air in the atmosphere, the noise level of the current amplifiers, and the tape recorder noise. These combine to give, on replay, a noise level equivalent to about 0.2 pA peak to peak at the most sensitive amplifier range. On this basis the signal:noise ratio on the least sensitive amplifier range (employed at 2 m downwind) would be 60 dB, which is far in excess of the tape recorder performance (about 45 dB). The specification noise level on the current amplifier is 0.05 pA, but it is unlikely that this could be achieved in practice, and it seems probable that the

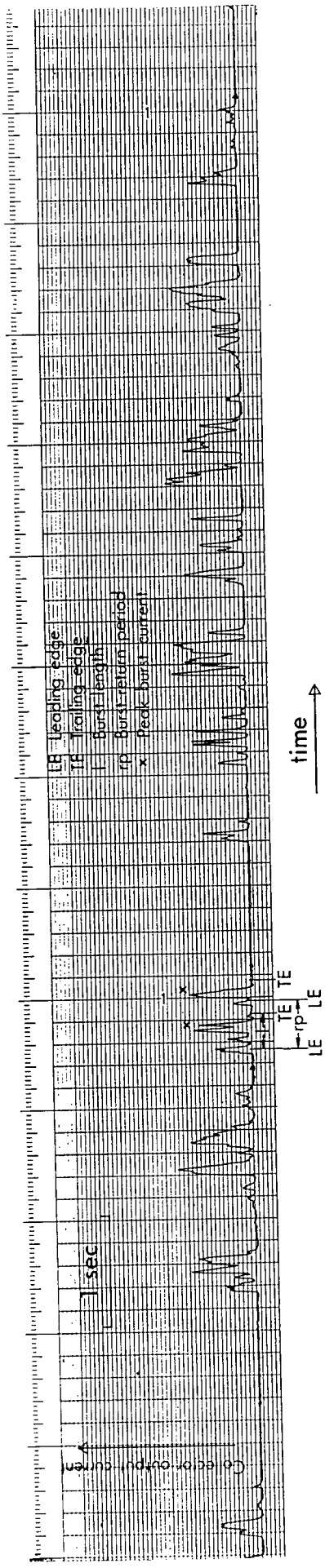

FIG. 1. Typical ion collector signal, showing the definition of signal characteristics.

amplifier and the background noise are of similar value. On this basis, at large separations between emitter and detector, where a higher sensitivity range is required, the recorder input signal: noise ratio would be about 25 dB. Thus, close to source the tape recorder limits sensitivity, but at large source–detector separations the theoretical limit of the system working at the generator current level specified here is reached.

It is impossible at present to make a direct comparison of the sensitivity of our apparatus with that of the insect antenna, not least because the sensitivity of the insect system varies. Bartell & Lawrence (1977) have shown that even short (*c.* 10 s) exposure to pheromone can affect insect responses. This, however, does not affect the force of our argument since we are concerned not simply with a varying concentration of material but with intermittency of signal resulting from periods when material released at the upwind source is totally absent from the airflow. Further details of the system are given in Jones (1977).

These trials were carried out on a flat level coastal strip in the north-west of Crete. It might be expected that topography would have an effect on the results obtained in this work, but before the more complex flows produced in uneven terrain can be understood it is essential to have a clear understanding of flows over the simplest possible sites. This site was chosen as giving the best available approximation to a flat even surface with a clear undisturbed wind fetch. The ion generator was placed with its outlet facing downwind 1 m above the ground. Close by, and at the same height, a wind vane and rotating-cup anemometer were fixed. An ion collector was placed downwind on the line of average wind direction assessed at the start of trials, also at a height of 1 m. Recordings were made on the tape recorder of wind speed and direction and of ion collector signal for a single collector placed successively 2, 5, 10 and 15 m downwind from the ion generator, each recording lasting 45 min. A single collector and amplifier was used to eliminate variation in sensitivity and time resolution which might occur between different collector–amplifier combinations.

During the trials the mean wind speed and temperature were measured at 1 and 11 m

above the ground so that the Richardson's number, a parameter relating to the atmosphere's stability (its propensity to sustain turbulent air movements), could be assessed.

Data and analysis

The recordings of each trial were replayed on a high-frequency-response chart recorder at a chart speed of 0.02 m s^{-1}, filtered electronically to remove frequencies above 100 Hz. This produced the type of chart shown in Fig. 1. From this it may be seen that the trace consists effectively of a train of pulses each of which signals a burst of ions arriving at the collector. The base line (zero signal) was marked on the trace together with the leading and trailing edges of each burst. The bursts and the interburst lengths were measured and noted in sequence in units of 1 mm (= 50 ms). From these measurements, burst length and burst return period (Fig. 1) could be found. The number of these separate events lying in each successive 50-ms band, expressed as a percentage of the total number of events, gives the percentage probability of occurrence of events in each band.

To check on the adequacy of our scale, replayed charts were made at 0.10 m s^{-1} and 0.02 m s^{-1} for the same piece of the recording and similarly analysed to give burst length probabilities. These results, compared in Fig. 2, showed that although minor detail is lost, the coarser scales adequately represent the broad outline of the probability distribution of burst length. It should be noted, however, that there are probability fluctuations at the fine scale, which is why in further work at least 100-Hz band-width would be required. Similarly for each burst, the peak height, or in the case of bursts with many peaks, the highest peak was measured (Fig. 1), in millimetres. From these measurements, the calibration constant of the current amplifier (in picoamps per 1 V output), and the recording and replay system signal-amplification factor, it was possible to evaluate peak signal strength for each burst in current units.

As with all atmospheric data there are considerable sampling problems in the analysis of

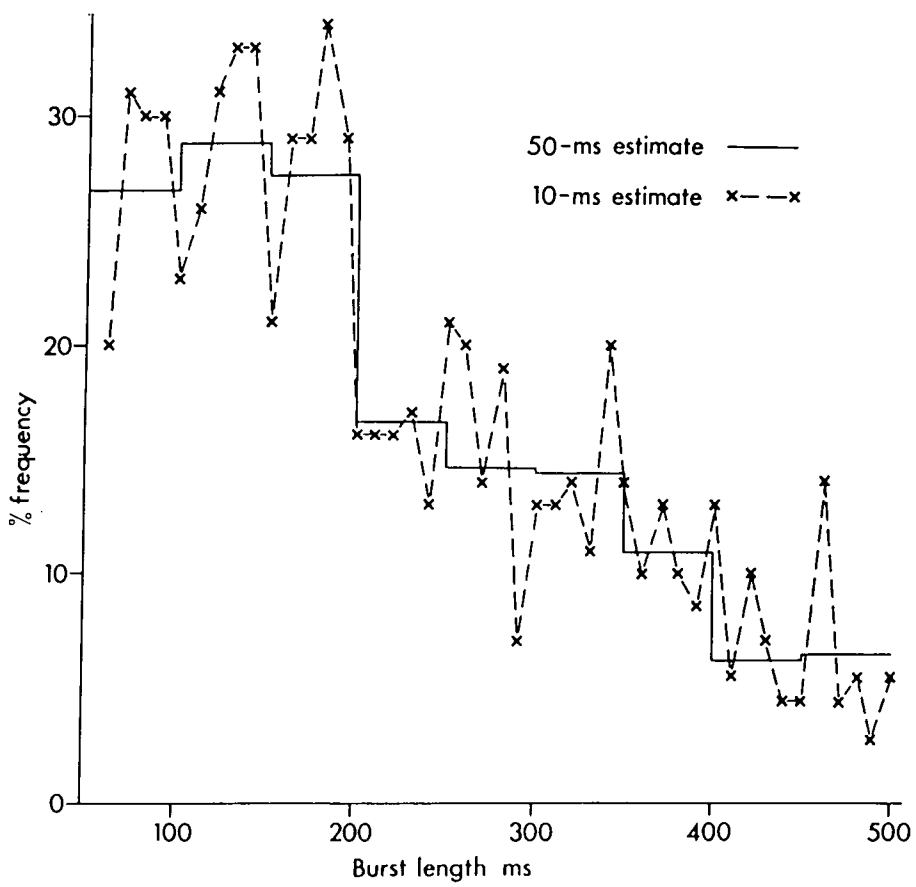

FIG. 2. Burst length probability distribution estimated in 50-ms and 10-ms units.

the ion detector signals. Essentially the problem is one of producing meaningful statistics to describe a signal containing variation over a wide range of frequencies; to describe the variations which take place at high frequency it is necessary first to remove the effects of low frequency variation, and in describing low frequency variation the fine, high frequency detail is inevitably lost. In the atmosphere, the range is from many fluctuations per second to fluctuation times of many hours (Lumley & Panofsky, 1964). The work we are describing is at the high frequency end of the spectrum, and it is therefore to be expected that the sources of variance between samples will be the sample mean wind speed and direction, the atmospheric stability, and the sampling duration, as described in Pasquill (1974).

Our approach has been to compare plume statistics at a series of downwind positions in fixed values of wind speed and stability, rather than to attempt to describe the effects of those variables on each position. The latter task would be considerable and basic conclusions would not be altered, except to shift typical values slightly.

The charts for each trial were examined, and those with suitable noise levels and with record lengths in excess of 10 min free of abnormal signals due to collector contamination by dust or water and of amplifier drift, were categorized according to the value of wind speed, atmospheric stability and downwind position. A set of trials having the closest mean wind speeds and Richardson number, and representing each downwind position was selected for full analysis. All trials selected were carried out between 10.30 and 15.30 hours on 15 August 1978.

The statistics relating to concentration distribution within bursts are taken from Jones (1979) to which reference should be made for details of methods used. Higher moments of distributions, kurtosis and skewness have been calculated according to the methods for grouped data outlined in Spiegel (1961) corrected for displacement of means.

Results

These trials were carried out in fine weather during daylight with virtually cloudless skies. The mean wind speed was between 4 and 5 m s^{-1} and the mean temperature 1 m above ground was 26°C. The atmosphere during the trials was in an unstable condition; that is, turbulent motions would tend to be maintained (a mean temperature lapse rate of 0.2°C m^{-1} and a mean Richardson number of *c.* − 0.15).

The traces shown in Fig. 3 are representative of the ion detector output at each downstream station. It can be clearly seen that each is highly intermittent: comparatively long periods of zero signal, up to several seconds duration, separate spikey signals (bursts of ions collected by the detector) of short duration, typically a few tenths of a second. At the larger generator–collector distances the traces are considerably noisier; this is a consequence of the higher amplification required, and at 15 m downwind, the signal–noise ratio approaches the theoretical limit of present current-amplifiers. The noise, though noticeable, has typical amplitudes of less than the signal, and in differentiating the one from the other a threshold equivalent to 20-mV amplifier output (compared to a peak value of over 1 V) was applied.

What is immediately apparent from a comparison of the signals is that their intermittency and spikeyness are well preserved downwind, even to 15 m. Ensemble statistics for the samples analysed in detail (some 400 to 200 events for each downwind station – equivalent to about 10 to 7.5 min of recording) are given in Table 1. The mean burst lengths were short, as might be expected from an inspection of the trace in Fig. 3, and they increased slightly with downwind separations from about 0.25 s at 2 m to about 0.35 s at 15 m. A number of long separations between bursts, of a minute or more, were found probably due to a large temporary deflection of wind direction, but the figures in Table 1 relate only to burst return periods of less than 10 s (at each distance more than 98% of all events). The mean burst return periods, which are of the order of four burst lengths, also increased downwind, with the exception of the high value measured at 5 m, perhaps caused by an excessive excursion of the mean wind direction during this trial: no other 5-m trials approached this one, when analysed in terms of consistency in Richardson number or low amplifier noise.

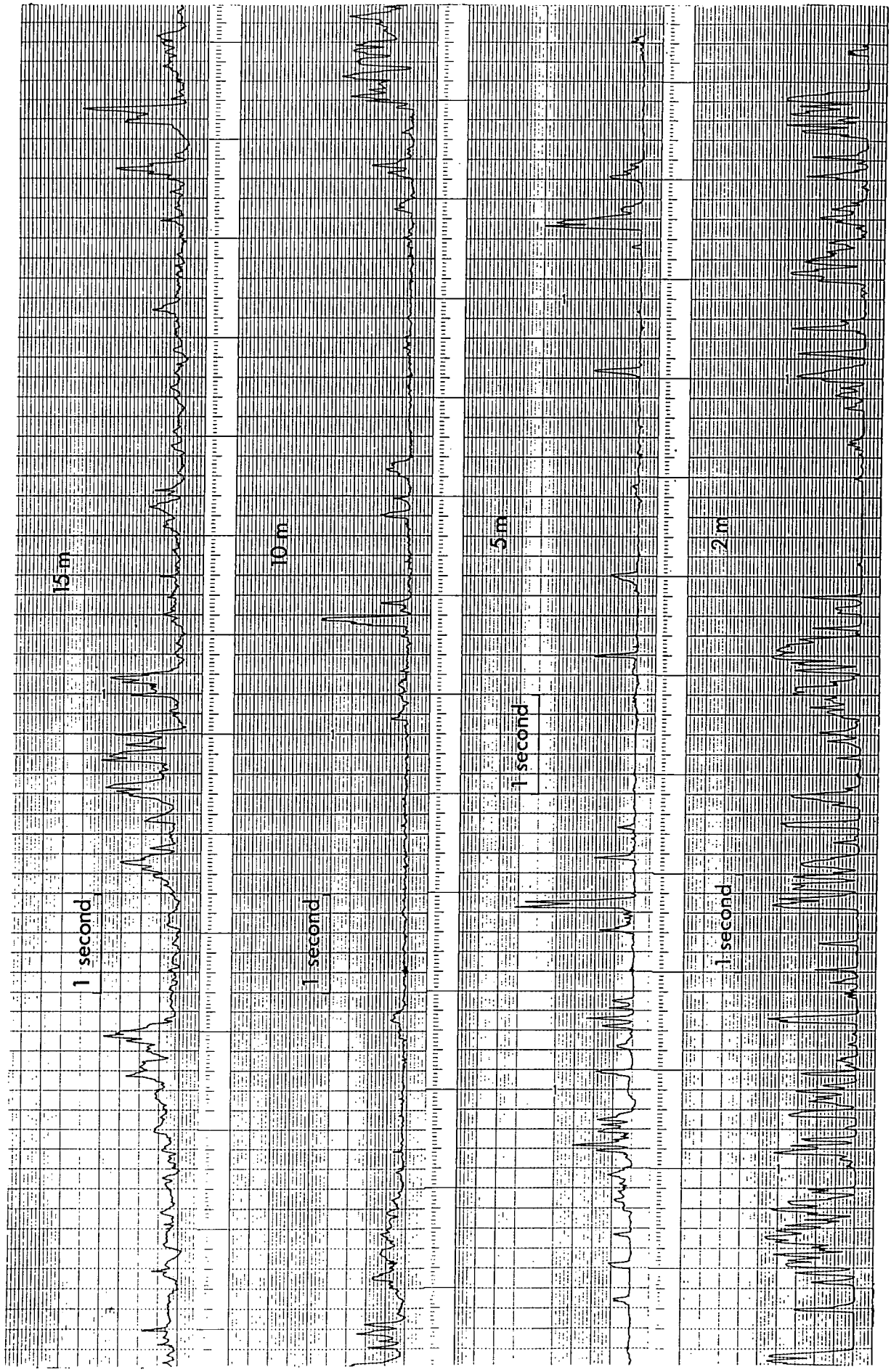

FIG. 3. Typical ion collector signals.

The intermittency, the proportion of total time for which signal was not present, was *c.* 80% and increased slightly downwind, with the exception of the 5-m value, which is again high.

The distributions of both burst length and return period are positively skewed, that is, below-mean values are more numerous. The kurtosis of the return period distribution shows the greatest departure from the Gaussian value which is 3, but even the burst length distribution is distinctly leptokurtic.

The probability distributions of burst length and burst returns period are detailed in Figs. 4 and 5, in 50-ms and 250-ms classes. Modal burst length is about 100 ms, and the probability of long bursts is relatively small (only 9% were more than 500 ms). There is no obvious shift in this modal value, but a slight increase in the frequency of longer bursts with increasing downwind distance. Similarly, the most frequent return period remains in the range 250–500 ms but the longer intervals became more frequent with increasing downwind distance (at 2 m, 12% of all periods were more than 2 s; at 15 m, 20% were).

The analysis of the signal level, that is, of the magnitude of the concentration of material in the plume, raises more difficult problems. Because the intermittency is high, the mean concentration over total time will be small compared with peak concentration. Table 1 gives these peak : mean ratios, which for our data are about 20. The analysis described here is therefore concerned with the statistics of the bursts themselves, specifically with the distribution of material within bursts and the peak values of bursts.

The mean of the highest signal levels found in each burst for each downwind station is given in Table 1 in the units of detector current (which are most appropriate to an instantaneous measurement). What is clear from these figures is that a rapid decline in peak strength occurred in the first few metres, and that 15 m or so downwind the mean peak was unlikely to exceed 2% of its value at 2 m. Fig. 6 shows the probability distributions of these peak strengths. The highest probabilities, at least for up to 10 m downwind, occur at the smallest peak values, and there is evidence from the raw data that this would continue to be so as peak-value class-size is reduced, down to the smallest peak value which could be discriminated (above the noise threshold). At the other end of the scale, the highest peak

TABLE 1. Statistics of intermittent structure of the plume

	Downwind distance from source			
	2 m	5 m	10 m	15 m
Mean burst length (ms)	246.1	268.7	271.7	344.6
SD	0.1733	0.1802	0.2051	0.2560
Skewness	2.183	1.235	1.413	1.464
Kurtosis	9.310	4.421	5.002	5.213
Mean return period (s)†	0.9050	1.364	1.192	1.275
SD	1.202	1.604	1.388	1.423
Skewness	3.87	2.58	2.86	2.89
Kurtosis	22.26	10.48	13.97	13.48
Intermittency (%)	76.78	84.5	79.5	83.8
Mean peak height (pA)	150.00	32.82	6.88	2.00
Peak as % of source (approximate)	1.0	0.22	0.046	0.013
Skewness	0.315	1.54	0.995	1.324
Kurtosis	2.25	5.48	4.72	5.08
Sample size for above (n)	447	331	288	209
Mean concentration (nC m^{-3})*	5.8	1.2	0.43	0.15
SD	7.7	1.1	0.25	0.12
Skewness	5.2	9.7	10.0	7.2
Kurtosis	37	128	156	88
Peak : mean ratio*	22	26	20	21

† Periods less than 10 s.

* Values taken from Jones (1979).

values were clearly defined and of the order of 3—4 times the mean. The calculated higher moments of these probability distributions, given in Table 1, show that the distribution of burst peaks is closer to normal than either of the temporal distributions are.

The mean concentration values in Table 1, taken from Jones (1979), are the mean values within bursts (below threshold values outside bursts being discounted). As might be expected, these means values decline rapidly with increasing distance downwind. The distributions in this case (the frequency distribution at a set of fixed concentration levels) are positively skewed, but strongly leptokurtic.

The concentration values have been re-calculated as follows. For a set of given probability levels ranging from 0.05% (at which concentrations will be highest) to 20% (at which they will be lower) the associated concentration levels were obtained from Jones (1979, Fig. 1) by interpolation between points in the log probability plot of ion collector current for each measuring position. The levels were calculated as a proportion of a

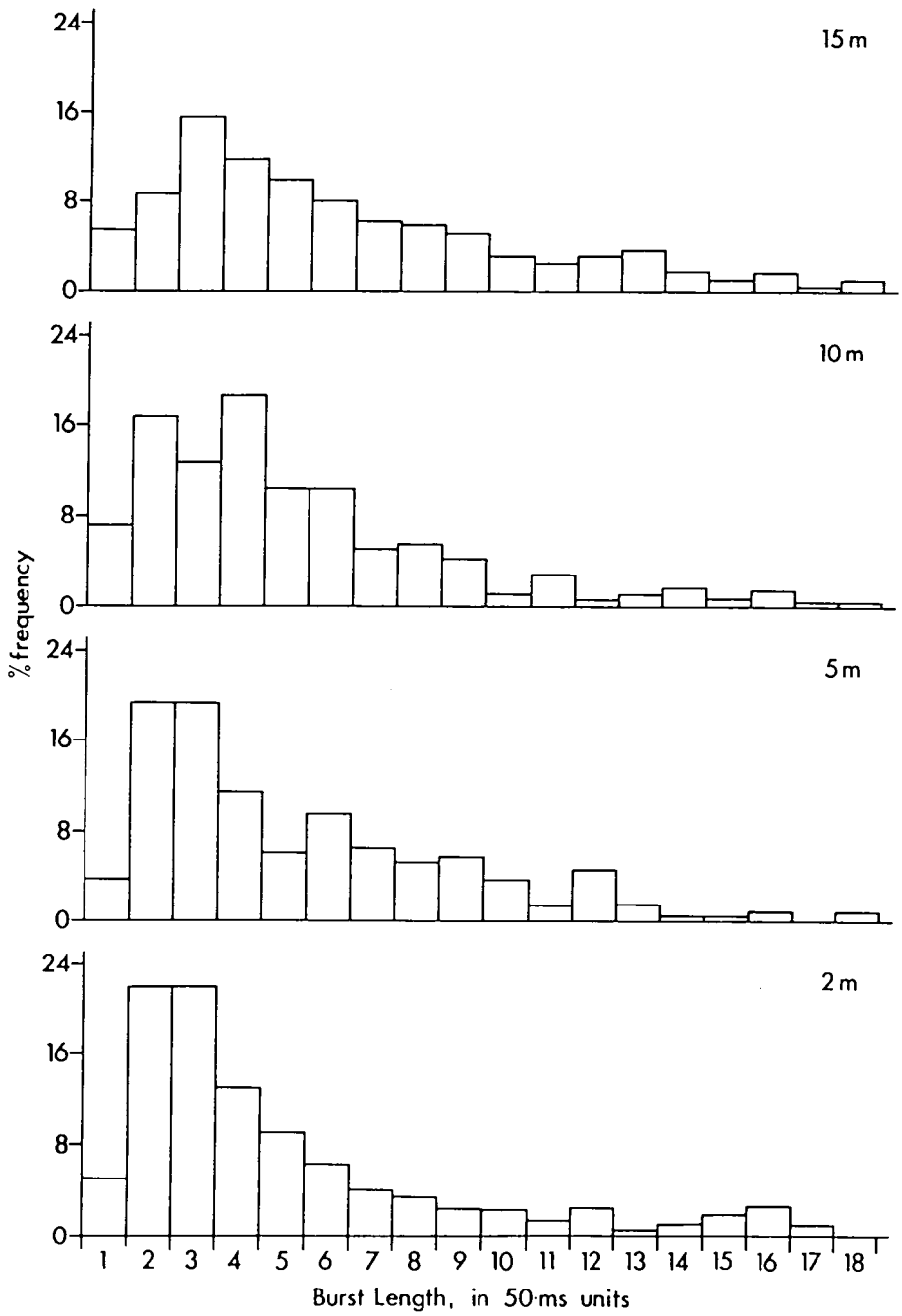

FIG. 4. Probability distribution (i.e. % frequency) of burst length.

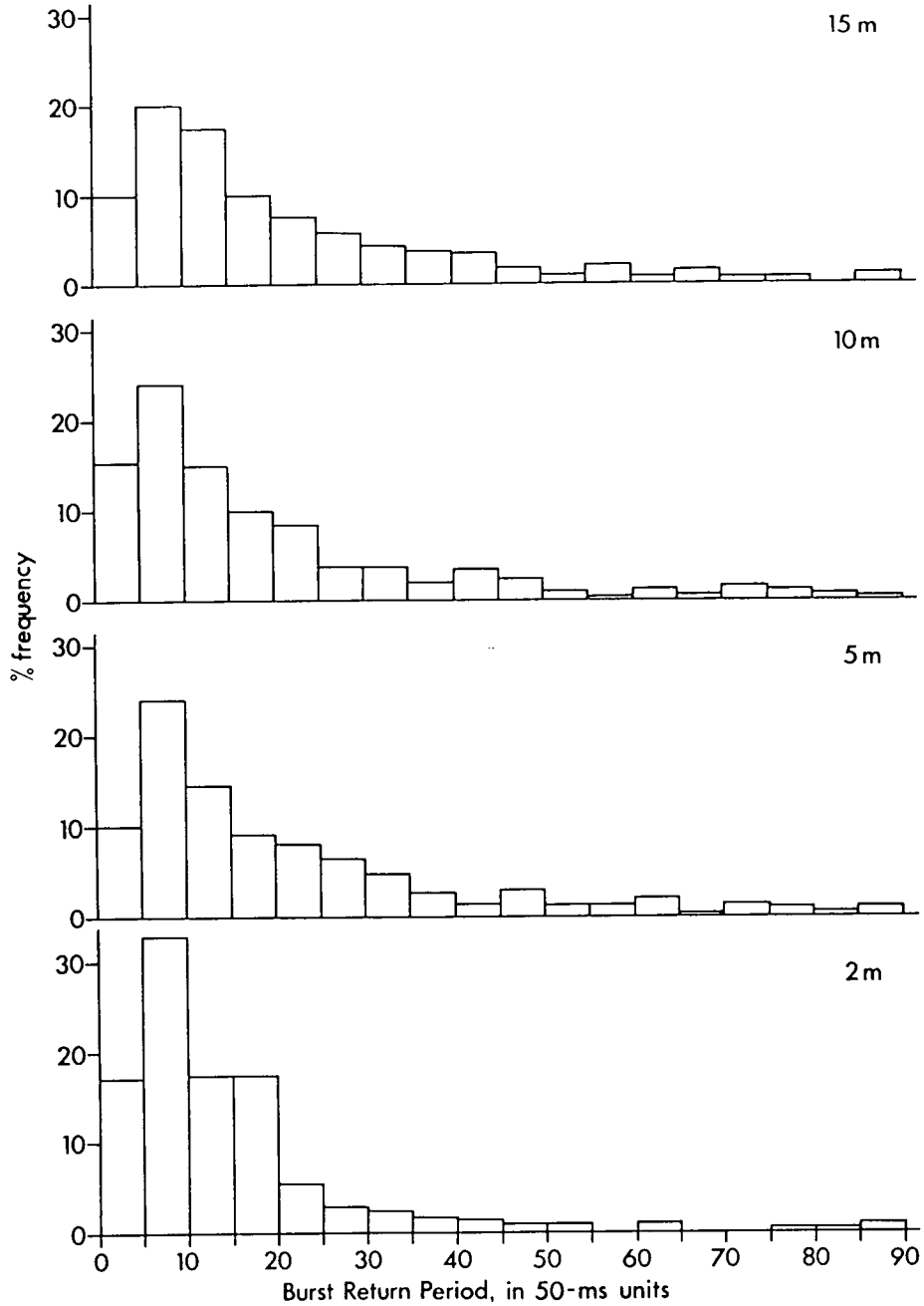

FIG. 5. Probability distribution (%) of burst return period.

notional source strength derived in the following manner.

As it is impossible at present to derive a satisfactory value for source strength, the concentration value obtained at the closest measuring station to source (2 m downwind) with the lowest probability (0.05%) was taken as representative of source strength. The assumption made is that the peak value obtained close to the source will closely represent source strength, in other words that some few bursts do preserve undiluted material to 2 m downstream. In practice, concentration proportions will be over-estimated by this method.

Fig. 7 shows the downstream distribution of concentration so-calculated relative to source at various probability levels. Note that zero values have been discounted, so that the curve gives the expectation of a certain relative concentration *within a burst.* Thus at 2 m downwind bursts will exceed 28% of source concentration for 20% of the time; for the same expectation at 10 m downwind the concentration would be 1% of source. The curve shows in a different way how the

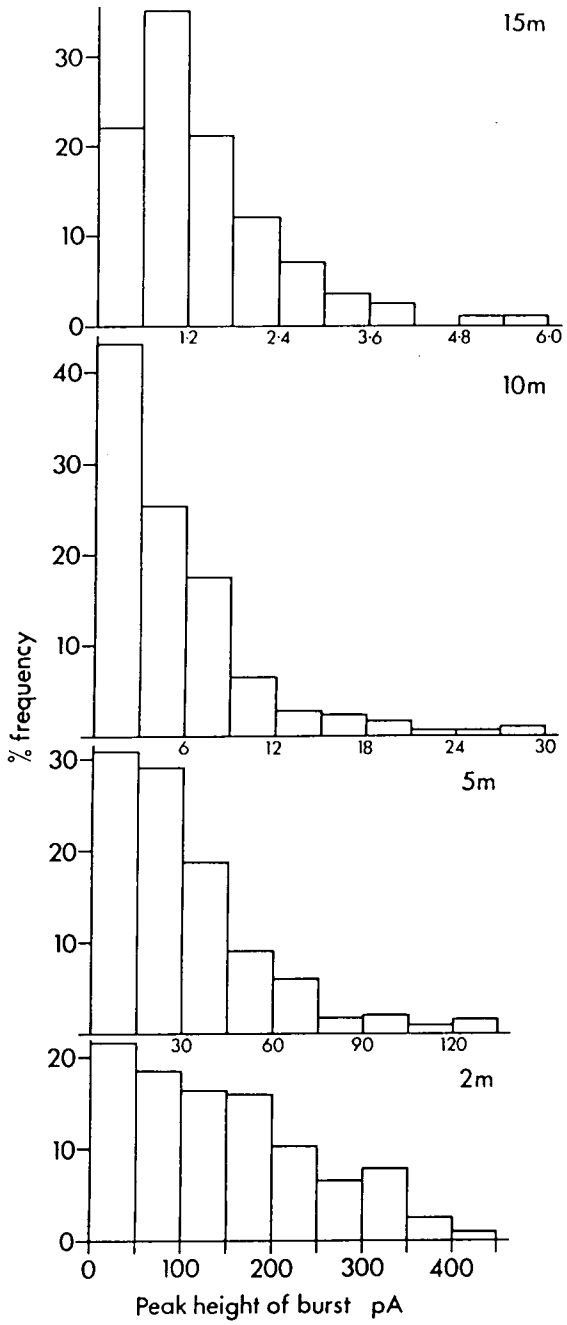

FIG. 6. Probability distribution (%) of peak heights within bursts.

process of atmospheric diffusion acts to dilute the material released at the source.

Discussion

The most helpful physical model to bear in mind when considering the process of atmospheric diffusion might be based on the mechanism of the atmospheric turbulence itself as described by Pasquill (1974). Turbulence is generated by forces which cause large-scale air masses to tumble into vortices as they move over the ground. Energy is injected into large-scale motions with typical length scales of a kilometre or more and with a strongly preferred direction, and it is transferred to successively smaller scales, the tumbles (vortices) becoming more randomly orientated. The preferred direction of large-scale motions gives the mean wind direction, and smaller motions contribute to the fluctuations in wind direction (which have a standard deviation of 10° or so).

At the smallest scales, the result is the creation of a tangled nest of vortex filaments. As it passes a source of some material, driven by the wind, the nest entrains the material released which is taken up initially by filaments of a scale similar to the source and taken downwind with the nest. Filaments within the nest are stretched by motions of their own scale and the nest itself expands and moves laterally and vertically due to the action of larger turbulence scales as it moves downwind. The process of stretching distributes the material and contributes to the decay in mean concentration, whilst intermittency would arise from the snaking and meandering caused by directional fluctuations of the large scales. Within the nest itself, its filamentous nature and expansion give rise to further intermittency on a smaller scale, seen in smoke plumes and in the concentration fluctuations within larger bursts, as in Fig. 3.

It was found in these trials that odours would present themselves in the given outdoor conditions as a series of bursts typically lasting about 100 ms, separated by periods of about 500 ms. These typical time scales may be converted approximately to typical length scales by multiplying by the relevant mean wind speed. Thus the typical length scales associated with the above findings, made in trials of mean wind speed 4–5 m s^{-1}, would be a burst length of 0.4–0.5 m, and a burst spacing of 2–2.5 m. These scales are large compared to those seen in smoke-filled plumes (e.g. by Wright, 1958), and suggests that much of the measured intermittency occurs as the plume snakes and meanders. Fig. 8 shows the 2 m downwind signal replayed at 0.5 m s^{-1} and without low-pass filtering. The fine-scale structure within bursts is clearly seen. Even a modest detector threshold level, *c.* 10% maximum signal, would cause these fluctuations to contribute

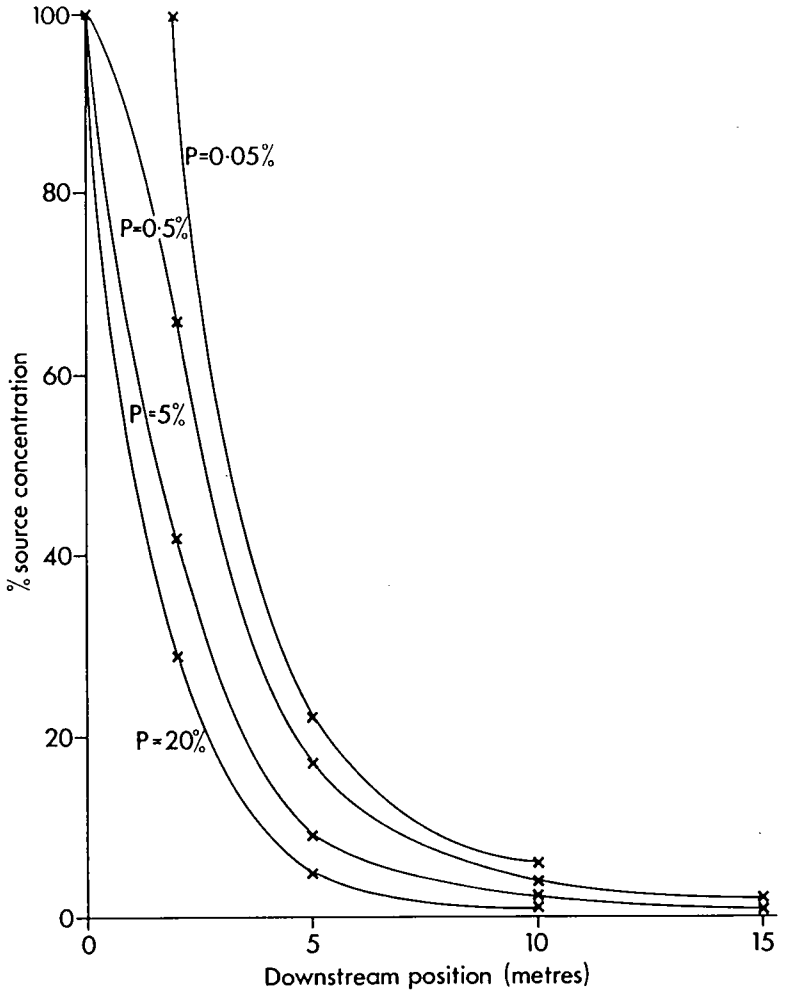

FIG. 7. Downwind concentration distribution at various probability levels.

to intermittency and thus to extend the burst length spectrum to far smaller values. This may have biological significance and further analysis of existing data, and new data to be produced with technically improved sensors, should enable us to quantify these very fine scales. The results given here, however, apply to the smallest events which can at present be separated using merely a noise threshold.

The conditions during these trials were typical of daytime and clear weather, but the results obtained by Jones (1979) suggest that data obtained in neutral stability, with cloudy weather, by night or day would, at comparable wind speeds, be similar to those reported here. At night time in clear weather, on the other hand, the atmosphere would be stable at low wind speeds, that is, turbulent motions would tend to damp out, and it might be expected that turbulence structure and hence plume structure would differ. Thus in turbulent conditions the picture will be qualitatively similar though, quantitatively, burst length and return period may vary according to wind speed and stability. In non-turbulent conditions there may be qualitative differences.

There is at the moment no information about the neurophysiological effects of continual intermittent olfactory stimuli at such short cycle times, but Blaney & Duckett (1975) have described the effects of intermittent contact chemoreception. *Locusta migratoria* palpates on leaf surfaces at about fifteen times a second, and they were able to show that, compared to sustained contact, this increases the sensory input to the central nervous system. Similarly, the intermittency of olfactory stimuli might serve to sustain the sensory input from olfactory receptors. Blaney & Duckett also found that simulated palpation at ten times per second caused separate registration of each contact in single sensilla. The cycle times for olfaction implied

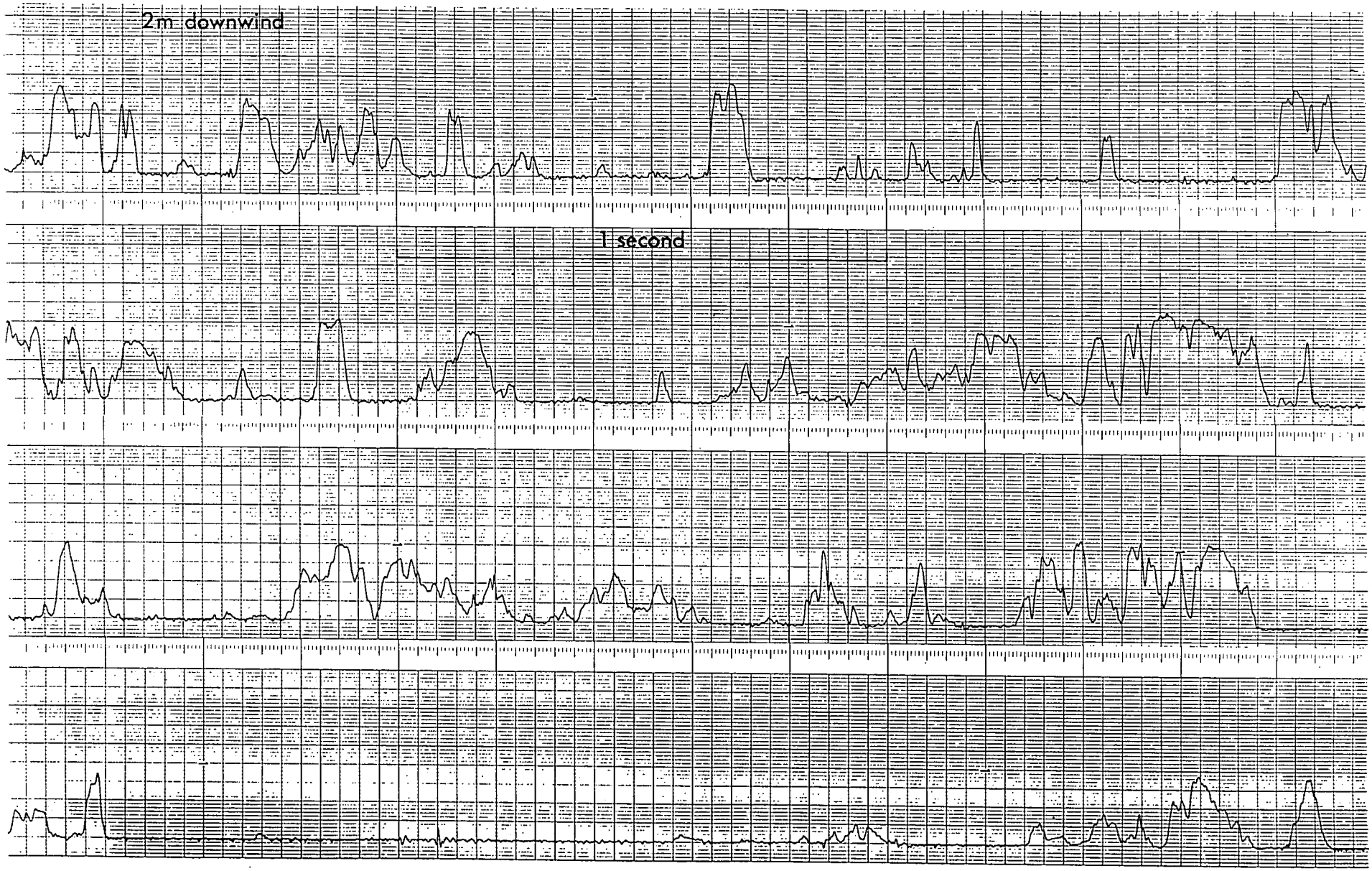

FIG. 8. Ion collector signal replayed at high chart speed.

in Kaissling (1971), obtained by adding electroantennagram formation and decay times, would be around 500–600 ms, which is the typical burst return period found in the present work. It might be expected, therefore, that even this relatively slow response would enable the separate registration of odour bursts in some species.

Close to the source there is a slight tendency for bursts to be shorter and more frequent, and with fewer long intervals. Clearly, as the source we used was continuous, there must have been some limiting position where burst separation would have been zero. Our closest measuring station was 2 m from the source, and closer-range measurements are required in this critical region. A rapid decrease in intermittency might be expected to be highly conspicuous to a flying insect; it is also the principal mechanism by which time-averaged mean concentration can increase close to source.

Although a detailed discussion of relationships between plume structure as described above and flight behaviour must await a fuller investigation of insect response to intermittent odour stimulation at various concentration levels, we can begin to see how odour is presented in the open air and to discuss some consequences of the presentation pattern.

To a stationary insect, sitting on vegetation within a few metres of a relevant, continuously emitting odour source, stimuli will be presented intermittently at a wide range of frequencies from about four times a second to once in 20 s, though exceptionally the time between stimuli may be many minutes. In the conditions of our measurements, the typical rate of presentation would be about twice a second. It seems that neither the duration nor the frequency of presentation should be greatly different at different downwind positions. To the stationary insect the strength of stimuli will also vary from burst to burst, whether measured in terms of the total quantity of active material contained in a burst or as the peak concentration in the burst. Averaged over time, however, the total quantity of material arriving will depend upon the insect's position: particularly large changes with position occur in the first few metres downwind of source. The reliability of a concentration estimate made by taking a sample of instantaneous values will itself be a function of the averaging time, and if a particular insect's ability to average and memorize could be defined, it should be possible to determine to what extent concentration could provide a clue to a stationary insect of its position relative to a point source.

If an insect responded more often or more strongly to high instantaneous concentrations (i.e. regardless of their duration), then the burst peaks themselves would provide some positional information. Fig. 6 shows that a given peak level may be found about five times more frequently at 10 m than at 15 m downwind. Further, at 10 m a third of all peaks exceed the largest to be found at 15 m, so that too may provide positional information.

The movement of the insect affects both the rate of presentation and the relative strength of successive stimuli. For an insect flying steadily upwind along the mean wind line (the line along which our sensors were placed), assuming a 4 m s^{-1} wind, and insect ground speed of 1 m s^{-1} and a typical burst spacing of 2 m, the stimulus presentation rate will be typically five times in 2 s. Insects flying in odour plumes are observed to follow an irregular path of horizontal and vertical zigzags (Marsh *et al.*, 1978). This would affect the presentation rate, but would substantially increase it only if the insect had developed a strategy for remaining within the plume core or if its lateral movements were dominated by the lateral component of air movements responsible for large-scale intermittency. The distance along the ground between bursts will then be *c.* 0.4 m, so an upwind-flying insect meeting a burst 5 m from source will typically encounter the next burst at 4.6 m from the source. At this latter point the mean concentration will be about 30% greater (Fig. 7), but the probability of any burst peak value exceeding the peak value of the median burst at 5 m would be only 6% greater (i.e. 56%, interpolating between points in Fig. 6).

Thus in moving from one point to another point upwind, the instantaneous available stimulus would not give a particularly reliable positional clue despite an increase in the time-averaged concentration; and this will be true even relatively close to source where change

rates are high. To improve the chances of the instantaneous value exceeding a set value, an insect should compare each burst with the mean of a series of previous bursts. Again, however, more information about averaging and memory is needed.

Marsh *et al.* (1978) found that a small moth, *Plodia interpunctella,* flown in a wind tunnel responded gradually to the removal of pheromone stimulus by casting sideways, but that only after 2–5 s did the moth's casting become such that no further forward movement occurred. This indicates that a stimulus might be expected to have a residual behavioural effect after its passing – a well-known behavioural phenomenon. Our results in the open air showed only about 20% of intervals between stimuli to exceed 2 s, and only about 4% to exceed 5 s, even 15 m from source. Thus the maximum memory time required in the open air between bursts might seldom exceed that demonstrated for *Plodia interpunctella* in a wind tunnel. On average, an insect might expect to meet five or so bursts in 2 s. By contrast, in work on odour plume-following, Wright (1964) found that *Drosophila melanogaster* responded very rapidly, within 100 ms, to loss of stimulus. In this case it might be expected that the presence of odour would be equally rapidly detected and it is therefore likely that *Drosophila* would be able to detect individual bursts.

Farkas *et al.* (1974) describe the effect of sex pheromone *concentrations* on visual responses in flying male moths. When the pheromone concentrations in the air stream were low, males of *Pectinophora gossypiella* ignored a strong visual cue, but at high concentration they orientated towards it. Implicit in this is the use of a pre-set con-concentration level as a switch to engage a new response mode allowing visual inputs to have a more important role in determining behaviour. Murlis & Bettany (1977) described changes in flight behaviour from straight and level flight at high speed to much slower oscillation flight in male *Spodoptera littoralis* flying in the field towards a sex pheromone source. This change occurred some metres from the source, but at a position which remained fairly constant over an evening's observation.

Orientation to visual cues is presumably a prelude to landing, and consequently is required close to the source. Although Farkas *et al.* had their visual cue placed well away from the odour source, they did use a wind tunnel and steady conditions in which stimuli could be maintained at a various fixed levels. Our results suggest, however, that in the open air the use of concentration level by itself would be highly unreliable as a measure of position relative to source, except very close to the source, where instantaneous concentrations rise rapidly. It is most unlikely, therefore, that the change in flight behaviour observed by Murlis & Bettany was brought about simply by a set concentration level. A major fault in the use of preset activation levels would be that the response might be engaged too early on the receipt of an unusually strong burst of odour or, as in the results of Farkas *et al.*, on encountering a strong but steady stimulus distant from the source.

Further criticisms of current plume models emerge from these findings. Concentration gradients of the kind calculated by Bossert & Wilson (1963) do not, as they predicted, exist in the instantaneous plume structure. Two positions in the plume can be related only probabilistically, in a similar manner to that analysed above for consecutive stimuli. Response boundaries have been calculated based on estimated mean concentration levels. We have shown that peak concentration may be 20 times the mean, so that if insects respond to instantaneous stimuli, either they would be drawn from a region larger than that predicted, or the threshold response level should be re-evaluated. This latter point is of some importance in bioassay of odour activity. At present most bioassay techniques involve the presentation of an odour for a long time compared with the burst length which we observed in the field. A more reliable technique (although considerably more difficult) might be to present a series of short bursts of pheromone at a range of burst concentrations.

Bartel & Lawrence (1977) were able to show that the response of a male apple moth, *Epiphyas postvittana,* to sex pheromone intermittently presented differed from that found to continuous exposure. Their application regime, however, consisted of a 10 s

exposure once a minute, which is a much longer burst length then the longest we found in our analysis, and is 100 times our most frequent burst length; their burst return period was, of course, also much longer than ours.

Conclusion

An odour plume is not continuous, but intermittent, and appears as a series of bursts of odour which are variable in strength and duration. The distribution of the length of bursts and the time between them does not greatly vary with distance from source. Although concentration does decay with distance from source, instantaneous measurement would not be a reliable guide to the mean concentration and hence to position relative to source except, perhaps, close to source. To obtain reliable positional information from the odour plume an insect would have to average received stimuli over many seconds. More information is therefore required about the dynamics of insects' olfactory responses.

Acknowledgments

We wish to thank Professor J. S. Kennedy for his helpful suggestions during the preparation of this paper and all those members of COPR staff who have read and criticized it in draft, especially Dr R. F. Chapman, Dr D. G. Campion and Mr D. E. Pedgley. We also thank Mr B. W. Bettany and Mr P. Lickiss for assistance in field work.

References

Bartell, R.J. & Lawrence, L.A. (1977) Reduction in responsiveness of male apple moths, *Epiphyas postvittana,* to sex pheromone following pulsed pheroward exposure. *Physiological Entomology,* 2, 1–6.

Bendat, J.S. & Piersol, A.C. (1971) *Random Data: Analysis and Measurement Procedures.* John Wiley, New York.

Blaney, W.M. & Duckett, A.M. (1975) The significance of palpation by the maxillary palps of *Locusta migratoria* (L): an electrophysiological and behavioural study. *Journal of Experimental Biology,* 63, 701–712.

Bossert, W.H. & Wilson, E.O. (1963) The analysis of olfactory communication among animals. *Journal of Theoretical Biology,* 5, 443–469.

Chalmers, J.A. (1967) *Atmospheric Electricity.* Pergamon Press, London.

Farkas, S.R., Shorey, H.H. & Gaston, L.K. (1974) Sex pheromones of Lepidoptera. Influence of pheromone concentration and visual cues on aerial odour trail following by males of *Pectinophera gossypiella. Annals of the Entomological Society of America,* 67, 633–635.

Hadjitofi, A. & Wilson, M.J.G. (1979) Fast-response measurements of air pollution. *Atmospheric Environment,* 13, 755–760.

Jones, C.D. (1977) Ion concentration variations at short distances downwind of continuous and quasi-instantaneous point sources. *Pesticide Science,* 8, 84–95.

Jones, C.D. (1979) Statistics of the concentration fluctuations in short range atmospheric diffusion. In: *Mathematical Modelling of Turbulent Diffusion in the Environment* (ed. by C. J. Harris). Academic Press, London.

Kaissling, K.E. (1971) *Insect Olfaction. Handbook of Sensory Physiology,* Volume IV. *Chemical Senses 1 Olfaction* (ed. by L. M. Beidler). Springer, Berlin.

Kennedy, J.S. (1977) Olfactory responses to distant plants and other odour sources. *Chemical Control of Insect Behaviour* (ed. by H. H. Shorey and J. J. McKelvey), pp. 67–91. Wiley-Interscience, New York.

Lewis, T. & Macauley E.D.M. (1976) Design and elevation of sex attractant traps for pea moth *Cydia nigricana* (Steph) and the effect of plume shape on catches. *Ecological Entomology,* 1, 175–187.

Lumley, J.L. & Panofsky, H.A. (1964) *The Structure of Atmospheric Turbulence.* John Wiley & Sons, New York.

Marsh, D., Kennedy, J.S. & Ludlow, A.R. (1978) An analysis of anemotactic zigzagging flight in male moths stimulated by pheromone. *Physiological Entomology,* 3, 221–280.

Murlis, J. & Bettany, B.W. (1977) The night-flight towards a sex pheromone source by male *Spodoptera littoralis* (Boisd.) (Lepidoptera, Noctuidae). *Nature,* 268, 433–434.

Nakamura, K. (1976) The effect of wind velocity on the diffusion of *Spodoptera litura* (F.) sex pheromone. *Applied Entomology and Zoology (Japan),* 11, 312–319.

Sower, L.L., Kaae, R.S. & Shorey, H.H. (1973) Sex pheromones of Lepidoptera. XLI. Factors limiting potential distance of sex pheromone communication in *Tricoplusia ni. Annals of the Entomological Society of America,* 66, 1121.

Spiegel, M.R. (1961) *Statistics.* Schaum, New York.

Sutton, O.G. (1953) *Micrometeorology.* McGraw-Hill, London.

Wright, R.H. (1958) The olfactory guidance of flying insects. *Canadian Entomologist,* 80, 81–89.

Wright, R.H. (1964) *The Science of Smell.* Allen & Unwin, London.

Accepted 4 August 1980

McCartney H. A., Bainbridge A., Legg B. J. and Jones C. D.(1982).

Electric charge and the deposition of spores of barley mildew *ERYSIPHE GRAMINIS.*

Atmos. Environ. **16**, 1133 - 1143.

Atmospheric Environment Vol. 16, No. 5, pp. 1133–1143, 1982
Printed in Great Britain.

0004–6981/82/051133–11 $03.00/0

ELECTRIC CHARGE AND THE DEPOSITION OF SPORES OF BARLEY MILDEW *ERYSIPHE GRAMINIS*

H. A. McCartney*, A. Bainbridge† and B. J. Legg*

* Physics Department and † Plant Pathology Department, Rothamsted Experimental Station, Harpenden, Herts., U. K.

and

C. D. Jones

Chemical Defence Establishment, Porton Down, Salisbury, Wilts., U. K.

(*First received* 15 *April* 1981 *and in final form* 25 *June* 1981)

Abstract—The deposition to cereal crops of spores of barley mildew, *Erysiphe graminis*, could be influenced by any electric charge that the spores might carry. Such influence was investigated (a) by calculating through mathematical models the effect of electric charge on the impaction of spores to vertical cylinders and on their sedimentation to flat plates, and (b) by seeking to determine through three different field experiments whether naturally produced spores do carry charge sufficient to affect deposition. The calculations showed that to cause any significant effect, charge per spore would need to exceed 3×10^4 electron charges (3×10^4 e or 5×10^{-15} C), a value close to the maximum charge that a sphere (spore) of 10 μm radius can retain against the influence of its own electric field. In the field experiments, attempts to measure spore charge directly revealed no charge large enough to affect deposition to plant surfaces. Field measurements of spore impaction to charged vertical cylinders did indicate that spores may carry charges of magnitude $\lesssim 10^4$ e (2×10^{-15} C), but these would be insufficient to influence deposition to natural surfaces.

INTRODUCTION

Many plant diseases are spread by windborne microscopic spores. For some plant species pollen grains are similarly dispersed by wind. The mechanisms governing the transport and deposition of small windborne particles to plant surfaces are therefore important to the understanding of the development of many disease epidemics and in cross pollination of some plant species.

Two main forces act on small, moving airborne particles: one is the force of gravity and the other is the viscous force exerted by the air through which the particles are moving. If the particles are electrically charged they will also be subject to electrostatic forces, which may alter the dispersal and deposition patterns of charged particles compared with uncharged ones. For example it has been shown that the penetration of particles into fibrous filters is significantly altered when the particles carry an electric charge (Lundgren and Whitby, 1965; Yoshioka *et al.*, 1968). (It may be remarked that in manufacturing industry where electrostatic forces have been used for many years to enhance deposition of paints and powders (Bright and Coffee, 1964; Felici, 1967), the field strengths employed are much higher than those naturally occurring within plant canopies.) Increased deposition of pesticide and fungicide sprays to plant leaves has also been reported for spray drops that are electrically charged (Bowen *et al.*, 1952; Splinter, 1968; Hopkinson, 1974; Coffee, 1974). However, little information appears to be available on the magnitude of the charge needed to be carried by each spray drop before the effect of the electrostatic forces becomes significant.

Many wind-dispersed fungal spores are violently discharged into the atmosphere (Ingold, 1971), and may thereby become electrically charged at the instant of release. Indeed it has been suggested that electrostatic forces may play an important part in the release mechanism (Leach, 1976). Observations in strong electric fields have shown that violently ejected spores can carry electric charges (Gregory, 1957; Swinbank *et al.*, 1964). Through similar observations Swinbank *et al.* (1964) measured the charges carried by basidiospores of *Merulius lacrymans* and found them to have relatively small magnitude (about 30 electron charges, i.e. 30 e, or 5×10^{-18} coulomb).

Nothing appears to be known about electric charges carried by spores which are passively released, such as spores of barley mildew, *Erysiphe graminis*. It is known that for liquid drops and for solid, non-biological materials, particles (drops) may become charged when they are formed, as when they separate from a surface. For 10 μm radius liquid drops, charges of 1000 e have been found on sprayed water drops (Whitby *et al.*, 1965), of 100 e for non-aqueous spray drops (Dodd, 1953), and of 600 e on castor oil drops flicked from fine steel wires (Hopper and Laby, 1941). For solids, Kunkel (1950) found that 10 μm quartz particles blown from a quartz surface could carry charges up to 500 e, and when blown from platinum could carry 1000 e. Harper (1951) has shown that particles become

charged when they make contact with a dissimilar material, and that the charge is retained when contact ceases. If the contact potential between the two materials is high, as between two different metals, large charges can be induced. Lui and Pui (1974a) calculated that for a 2 V contact potential, 7×10^4 e can be transferred to a 10 μm particle. (However, such high contact potentials are unlikely to exist between a fungal spore and a plant leaf).

If the spores are not charged during release, they would nonetheless acquire a charge when airborne and in the presence of atmospheric ions (Friedlander, 1977). The atmosphere usually contains both positive and negative ions therefore such charging would be "bipolar", that is particles could acquire either positive or negative charges. In equilibrium the spores thus charged will have a charge distribution that depends on their radius, but which is independent of the ion concentration (Lui and Pui, 1974b). For particles (spores) of 10 μm radius the root mean square (rms) charge per particle is about 12 e, and few particles carry charges of more than 500 e (Lui and Pui, 1974b). For 50 μm particles the rms charge is about 200 e. The upper limit for the charge that can reside on a 10 μm radius solid sphere in air at S.T.P. is about 2×10^5 e (Moore, 1973). It is thus unlikely that barley mildew spores, which are ellipsoidal, could retain charges of 10^5 e for more than a few seconds—the electric field intensity close to the spore's surface, particularly near its ends, would be such as to attract highly mobile atmospheric ions. These ions would neutralise some of the spore charge, which would attain an equilibrium appropriate to the atmospheric ion concentration.

In the light of these considerations, the work here reported was directed (a) to a theoretical investigation of the effect that charges of various magnitude would have on the motion and deposition of passively-released spores, and (b) to a programme of field measurements that sought to determine whether electric charge does indeed reside on such spores. The work is part of an intensive study, at Rothamsted Experimental Station, into the wind dispersal of small particles.

THEORETICAL CONSIDERATIONS AND ANALYSES

The influence of electric charge on the deposition of barley mildew spores to plant surfaces was assessed, to within a factor of two or three, through two mathematical models that simulated (a) the inertial impaction of spores on a 2.5 mm radius vertical cylinder that represented plant stems and (b) the sedimentation of spores onto horizontal flat plates that represented plant leaves. In both models the mildew spores were considered to be spheres, of radius 10 μm chosen to give the spheres a terminal velocity, in air at 20° C, of 1.2 cm s^{-1}, the same value as real mildew spores, which are approximately ellipsoidal in shape, with major and minor axes of about 28 and 15 μm, respectively (Gregory, 1973).

The vector equation of motion of a spherical particle of radius r obeying Stokes' Law and travelling in a fluid of velocity $\mathbf{u}$ and viscosity η is given by the vector equation

$$m\frac{d\mathbf{v}}{dt} = -6\pi\eta r(\mathbf{v} - \mathbf{u}) + m\mathbf{g} + \mathbf{F}_e \qquad (1)$$

where m is the particle mass, $\mathbf{v}$ its velocity, $\mathbf{g}$ the acceleration due to gravity and $\mathbf{F}_e$ the electrostatic force on the particle. Equation (1) holds only when the fluid's Reynolds number (relative to the particle) is much less than 1.0 (Davies and Peetz, 1956), that is, when the relative velocity between the fluid and the particle is small. This is generally assumed to be the case for both sedimenting and impacting particles (Davies and Peetz, 1956); thus, to give a Reynolds number of 0.1 the relative velocity between a 10 μm particle and air would have to be 7 cm s^{-1}.

Equation (1) will not be rigorously valid for this application to spore dynamics because the spores are ellipsoidal rather than spherical. Moreover, barley mildew spores are sometimes released in clumps, rather than individually. For such clumps, charge (and hence $\mathbf{F}_e$) per unit mass might be expected to be equal to that for a single spore, but the viscous force would ideally increase only in proportion to the cube root of the mass, and indeed there is evidence (P. Dunn and M. J. Walls, private communication) that for barley mildew spores the increase is considerably less. Equation (1) will thus give biased estimates for the influence of electric charge on the deposition of barley mildew spores if many of the spores are in fact released in clumps.

For small particles, the electrostatic force $\mathbf{F}_e$ can arise in three ways: (a) a charged particle passing close to an uncharged surface will induce a charge on the surface that will in turn cause an attractive force on the particle (image force); (b) a charged particle will experience a force in the presence of external electrical fields caused by nearby charged objects (Coulombic force) and (c) an uncharged particle will become polarised in the presence of an electric field and will experience a net force if the electric field is non-uniform. For case (b), external electric fields can arise from the earth's electric field and from the space charge field due to other charged spores (Coffee, 1974). And for case (a), the image force experienced by a charged particle will be due not only to its own induced charge, but also to those induced by other charged particles passing the surface. However, our measurements have shown that the earth's electric field intensity within a barley crop is small (< 20 V m^{-1}); furthermore, Bainbridge and Stedman (1979) report that spore concentrations within a canopy are also small (< 0.1 cm^{-3}). Thus the effects of space charge field and of charge polarisation can be neglected, as can those of forces due to a multiplicity of image charges. Hence,

only force (a), for a single image, need be considered when calculating the influence of spore charge on the deposition of barley mildew spores.

As mildew spores are small compared with plant surfaces the image force can be approximated by using the expression for the image force between a charged particle and an infinite plane (Davies, 1973); the magnitude of the force is given (SI units) by Corson and Lorrain (1962) as

$$\mathbf{F}_e = [q^2/(16\pi\varepsilon_0 d^2)][(\varepsilon_r - 1)/(\varepsilon_r + 1)] \qquad (2)$$

where the force $\mathbf{F}_e$ acts towards the plane and at right angles to it, d is the distance between the particle and the plane, q is the charge on the particle, ε_0 is the permittivity of free space and ε_r the relative permittivity of the material beneath the plane. For plant material, ε_r was taken to equal that of water (82.0); although ε_r for living plant tissue is probably less than this, for example dry beech wood has ε_r equal to 9 (Kaye and Laby, 1973). Equation (2) nonetheless shows that a large error in ε_r, for $\varepsilon_r \sim 80$, would introduce a relatively small error into $\mathbf{F}_e$.

Inertial impaction onto vertical cylinders

In order to calculate through (1) the trajectory of a particle in the vicinity of a vertical cylinder it is necessary to know values for the velocity vector $\mathbf{u}$ throughout the space surrounding the cylinder. Furthermore, (1) requires that the fluid's Reynolds number, Re, be much less than 1.0. But in an air stream flowing at a wind speed of 1 m s^{-1}, a cylinder of a few mm radius exposed at 90° to the flow will cause, in its immediate vicinity, values of Re that exceed 100. However, Davies and Peetz (1956) have shown that even at large Re the fluid flow round the *leading surface* of a cylinder is reasonably approximated by the flow round the cylinder of an *ideal* fluid. Thus, since the flow field downstream of the cylinder is not so important as the upstream flow in calculating particle impaction, ideal flow was assumed in solving (1), using expressions taken from Davies and Peetz (1956). Davies (1973) showed that (2) may be used validly to estimate $\mathbf{F}_e$, for cylinders as well as planes, when the cylinder (stem) radius R ($\sim$2.5 mm) so greatly exceeds the particle (spore) radius r ($\sim 10\,\mu$m).

Equation (1) was written in Cartesian co-ordinates with the cylinder axis vertical (z axis) and the x axis parallel to the free stream air flow. Individual particle trajectories were calculated by integrating (1) numerically using a time step of 1.0×10^{-6} s. Tests showed that this time step was short enough for errors due to the finite integration interval to be negligible, and about 10^4 steps were usually required to calculate one trajectory. The starting point for each trajectory was 16 cylinder radii upstream of the cylinder and a variable distance, y, from the x axis; and at the starting point, the particle was assumed to have the same velocity as the free stream air flow (magnitude u_0, along the x axis).

The collection efficiency, α, of a cylinder, radius R, is defined as the number of particles actually striking the cylinder (assuming that the cylinder is exposed to a uniform stream of particles and the particles do not bounce off after impacting) divided by the number that would strike it if the particles travelled in straight lines parallel to the upstream fluid flow (Davies and Peetz, 1956). In terms of particle trajectories α is given by

$$\alpha = y_c/R \qquad (3)$$

where y_c is the y co-ordinate of the starting point of the critical trajectory of the particles—thus particles starting with $y > y_c$ will miss the cylinder, and those starting with $y < y_c$ will impact.

y_c, and hence α, will be a function of R, r, particle mass m and charge q, and wind speed u_0. To model mildew spores impacting on plant stems, r was taken as 10 μm and R as 2.5 mm, and the density of the particle was assumed equal to that of water.

Collection efficiencies were calculated for charged and uncharged particles for several different wind speeds and the results are summarised in Fig. 1. As expected, collection efficiencies for uncharged particles, α_0, increase with windspeed, and our results are in excellent agreement with those of Davies and Peetz (1956). The influence of electric charge is more marked at low windspeeds, as is clearly illustrated in Fig. 2, which shows, as a function of windspeed and particle charge, the ratios α/α_0 of collection efficiencies for charged and uncharged particles. This wind-dependence of α/α_0 arises because the inertial forces acting

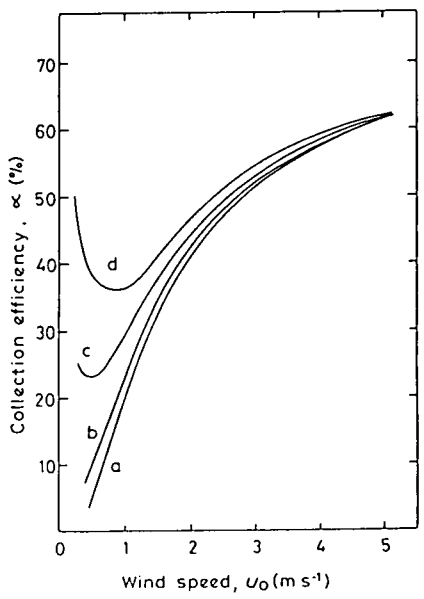

Fig. 1. Computed collection efficiency, α, for charged 10 μm radius particles (representing barley mildew spores) impacting onto a 2.5 mm radius vertical cylinder (representing barley stems) as a function of wind speed, u_0, for charges per particle of: (a) zero, (b) 1×10^5e, (c) 5×10^5e and (d) 1×10^6e.
Note: 1 electron charge (e) = 1.6×10^{-19}C.

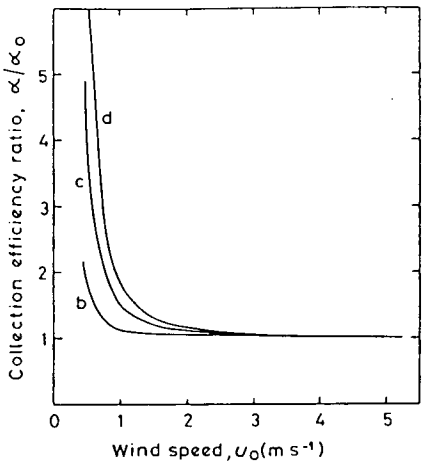

Fig. 2. Computed ratio, α/α_0, of collection efficiencies of charged and uncharged 10 μm radius particles (representing barley mildew spores) impacting onto a 2.5 mm radius vertical cylinder (representing barley stems) as a function of wind speed, u_0 for charges per particle of (b) 1×10^5e, (c) 5×10^5e and (d) 1×10^6e.
Note: 1 electron charge (e) = 1.6×10^{-19}C.

on the particle increase with wind speed, whereas the electrostatic forces are independent of wind speed.

With the uncertainties inherent in calculating spore deposition an increase of about 50% (i.e. $\alpha/\alpha_0 = 1.5$) due to charge on spores is probably required before electrostatic forces need to be considered. Table 1 shows the calculated particle charge that would result in α/α_0 values of 1.5, 2.0 and 5.0 for a wind speed of 0.5, 1.0 and 2.0 m s^{-1}. The particle charge needed to increase deposition to stems near the top of the canopy by 50% (with wind speed about 1 m s^{-1}), would be 5×10^5 e, that is 8×10^{-14} C.

Within the canopy, wind speeds are smaller ($\sim$0.5 m s^{-1}) and as the table shows, charges of 6×10^4e would be required for a 50% increase in collection efficiency. However, at low wind speeds α is small (about 6% for uncharged particles at 0.5 m s^{-1}), and the contribution of inertial impaction onto stems relative to the total deposition within the canopy is small. Consequently, impaction efficiencies at low wind speeds would have to be substantially increased (possibly by a factor of 10) before total deposition rates were significantly increased. Table 1 therefore suggests that particle charges greater than 5×10^5e are required before increased impaction to stems significantly alters the total rate of deposition of mildew spores to cereal crops—a charge probably larger than the spores can retain.

Table 1. Magnitude of charge per particle (in electron charges) needed, at various wind speeds, to effect 1.5, 2.0 and 5.0 fold increases in collection efficiency, α, for impaction to vertical cylinders, of 10 μm radius particles (representing barley mildew spores)

α/α_o	Wind speed (m s^{-1}) 0.5	1.0	2.0
1.5	6×10^4	5×10^5	3×10^6
2.0	1×10^5	1×10^6	6×10^6
5.0	8×10^5	5×10^6	3×10^7

Notes: (1) These data may be assumed uncertain to within a factor of two: their derivation is underlain by various assumptions (e.g. validity of Stokes' Law) that are described in the text.
(2) 1 electron charge (e) = 1.6×10^{-19} coulomb.
(3) α_0 is the collection efficiency for uncharged particles.

Deposition to flat plates

The influence of electric charge on the deposition of mildew spores onto leaves, by sedimentation, was investigated by calculating the trajectories of charged and uncharged particles moving over an infinitely thin horizontal flat plate. The air flow over the plate was approximated by assuming that it was uniform and parallel to the plate and of magnitude u_0. This assumption is not strictly valid as it ignores the change in velocity close to the plate due to the development of a boundary layer; however, comparison between results predicted for charged and uncharged particles should be valid.

Equation (2) was used to describe the electrostatic force on the particle; the force was assumed to act towards the plate and at right angles to it. As the electrostatic image force on a small particle is approximately inversely proportional to the square of the distance between the particle and a surface, it only becomes important when the particle is relatively close to the surface (a few mm distant), and the electrostatic force was therefore considered to act only when the particle was directly above or below the plate.

Particle trajectories were calculated using (1) as outlined in section 2.1. The plate was considered to lie in the horizontal x–y plane with its leading edge lying along the z axis, and calculations were started from various points on the z axis either above or below the plate. At the start point, $x = 0$, the particle was assumed to be falling at its terminal speed, v_s, and moving in the x-direction with the same speed as the air, u_0.

Particle deposition rates to horizontal plates are often expressed in terms of a deposition velocity (Chamberlain, 1975) which can be defined as

$$v_g = D/(Ac) \qquad (4)$$

where D is the particle deposition rate (number per unit area per unit time) to the plate, of area A and c the concentration of particles in the free air flow. Deposition velocities to the upper and lower surfaces of the plate were calculated from particle trajectories as outlined in the Appendix. It may be noted that the model predicts that for an uncharged particle v_g and v_s should be the same, and measurements for some fungal spores of v_g to flat plates at low windspeeds have indeed been

shown to be close to the spores' v_s (Gregory and Stedman, 1953; Bainbridge and Stedman, 1979). For the model represented by (4) it can be shown (Appendix) that for charged particles v_g is a function of q and l/u_0 only, where q is the charge carried by the particle and l is the length of the plate (x-direction). In cereal crops the value of l rarely exceeds a few cm and wind speeds are generally between 0.1 and 1 m s^{-1}, thus l/u_0 can range between 0.01 and 1.0 s, and is typically 0.05 s.

The values thus calculated for v_g of 10 μm particles are shown in Fig. 3 plotted as a function of l/u_0 and of q. Correspondingly, Table 2 shows for these 10 μm particles and for different values of l/u_0 the charge required to increase v_g by a factor of 1.5, 2.0 and 5.0. These latter data suggest that electrostatic forces will play a significant role in deposition of mildew spores, by sedimentation, only when the charge per particle exceeds 3×10^4 e (5×10^{-15} C)—close to the limit of charge that a spore can retain.

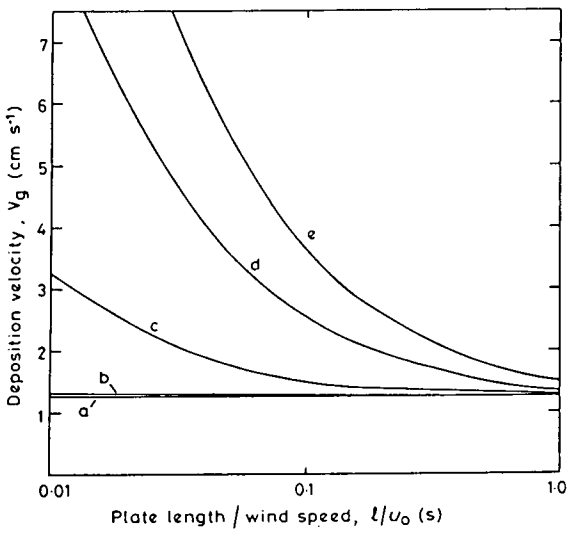

Fig. 3. Computed deposition velocity, v_g, for 10 μm radius charged particles (representing barley mildew spores) sedimenting onto a flat horizontal plate (representing barley leaves) as a function of l/u_0 where l is the plate length and u_0 is the windspeed, for charges per particle of (a) zero, (b) 1×10^4e, (c) 1×10^5e, (d) 5×10^5e and (e) 1×10^6e.
Note: 1 electron charge (e) = 1.6×10^{-19}C.

Table 2. Magnitude of charge per particle (in electron charges) needed, at various values of l/u_0 (see text), to effect 1.5, 2.0 and 5.0 fold increases in deposition velocity, v_g, to flat plates, of 10 μm radius particles (representing barley mildew spores)

	l/u_0 (s)			
$v_g/v_g(0)$	0.01	0.05	0.1	0.5
1.5	3×10^4	1×10^5	3×10^5	1×10^6
2.0	7×10^4	3×10^5	5×10^5	2×10^6
5.0	2×10^5	1×10^6	3×10^6	1×10^7

Notes: (1) These data may be assumed uncertain to within a factor of two: their derivation is underlain by various assumptions (e.g. validity of Stokes' Law) that are described in the text.
(2) 1 electron charge (e) = 1.6×10^{-19} coulomb.
(3) $v_g(0)$ is the deposition velocity for uncharged particles.
(4) l/u_0 within a barley crop is typically about 0.05 s.

EXPERIMENTAL TECHNIQUES FOR DETERMINING THE CHARGES ON BARLEY MILDEW SPORES IN THE FIELD

The second part of this investigation sought to determine, in three separate experiments, whether naturally produced barley mildew spores do carry electric charges as large as the minimum charge (3×10^4 e per spore) that, by the foregoing theory, would be needed to influence spore deposition to a crop. The experimental site consisted of eight small plots, each 9.0 m square, separated by fallow strips 6.0 m wide and arranged as in Fig. 4 and situated within, and approx. 50 m from the edge of, a large field (area 6 ha). The plots were sown with a mildew-susceptible variety (Julia), and the surrounding field with a mildew-resistant variety (Athos), of spring barley. The cultivation of all plots, and of the surrounding field, was identical except that alternate plots were regularly sprayed with a fungicide (tridemorph) and the unsprayed plots were inocculated with barley mildew spores. The experimental site thus consisted of four

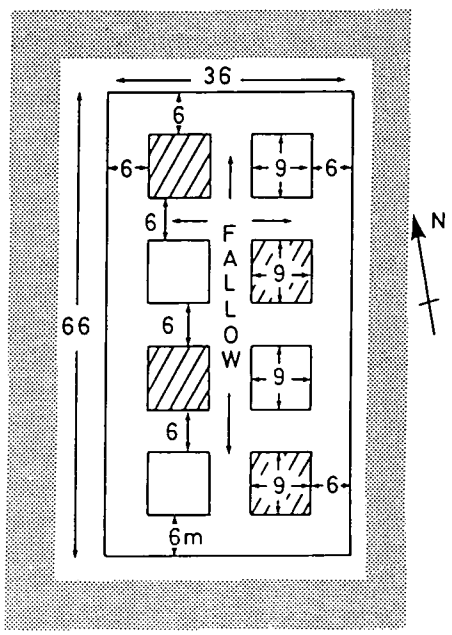

Fig. 4. Arrangement of the experimental plots. The eight plots were all sown with spring barley var. Julia, which is susceptible to barley mildew; four of them, depicted by hatched lines, were sprayed with fungicide to prevent the development of barley mildew. The surrounding field area 6 ha and shown by stippling, was sown with spring barley var. Athos, which is mildew resistant.

small area sources of mildew spores surrounded by a mildew free crop. By this design it was possible to ensure that, whatever the wind direction, there would be at least one infected plot for which the area upwind was not a source of mildew spores. Descriptions of the three separate experiments, and calculations of their respective sensitivities for determining spore charge, comprise the remainder of this section of the paper.

Direct measurement of spore charge

Direct measurement of charges on spores was attempted with an apparatus developed specifically for the purpose. It consisted (Fig. 5) of a small suction trap (a), made, to a design of Gregory *et al.* (1961), from an electrically conducting alloy and placed within, and electrically isolated (b) from, a brass cylinder (c) of 60 mm diameter. The trap casing was electrically connected to a sensitive electrometer (Type 602, Keithly Instruments Inc., USA). A small fan (d) drew air along the cylinder and past the trap. The fan housing was attached to the brass cylinder by a flexible sleeve (e) which served to prevent the transmission from the fan to the trap of mechanical vibrations that otherwise would cause spurious signals on the electrometer. The fan casing and the brass cylinder were both electrically connected to earth.

The suction trap sampled the air stream at $9\,\ell\,\mathrm{min}^{-1}$, and spores entering the trap impacted, with an efficiency approaching 100%, upon a 3 mm wide cellophane strip coated with glycerine jelly and supported on a rigid plastic insert (f). A *charged* particle entering the trap and impinging on the cellophane strip induced an opposite charge on the trap case, and the latter charge was detected as a small voltage pulse on the electrometer. The output of the electrometer was recorded on a FM tape recorder (Type 8–4, SE Laboratories, Feltham) and subsequently played back through a u.v. oscillograph (series 45000, Bryans Southern Instruments Ltd., Mitcham). The smallest signal that could be detected, above the signal noise level, was equivalent to a particle (spore) charge of about 10^5 e, just sufficiently small (Tables 1 and 2) for the purpose of this investigation. Tests, using dust particles charged by shaking them from a nylon brush, showed that the apparatus did respond to charged particles. A direct calibration of the charge-response of the apparatus could not be undertaken because of the difficulty of obtaining particles of known charge.

Ground level electric field measurements

The charge carried by a cloud of spores can be inferred from the effect, ΔE, that such charge has on E, the electric field intensity, at the ground. If the cloud acts like an infinite sheet, of charge area density σ, then, approximately,

$$\Delta E \approx \sigma/\varepsilon_0. \tag{5}$$

If the total number of particles per unit area column above the ground is N, and each particle carries a charge q, then the charge density of an equivalent infinite sheet is

$$\sigma = Nq \tag{6}$$

and, correspondingly,

$$\Delta E = Nq/\varepsilon_0. \tag{7}$$

Experimentally, the electric field, E, was measured continuously upwind and downwind of an infected plot using two field mills (Mapleson and Whitlock, 1955). These devices operate by detecting the alternating voltage developed across a high resistance connected from earth to a conductor that is alternately exposed to and shielded from the electric field by a rotating disc. The field mill signals were recorded on magnetic tape. N was estimated from the mean concentration of mildew spores measured at 6, 40, 80 and 160 cm above the ground using rotorods (Perkins, 1957). The sensitivity of the technique thus depended on the concentration of spores passing over the field mills and the minimum change in E which could be detected, in this case $20\,\mathrm{V\,m}^{-2}$. Bainbridge and Stedman (1979) report typical values for the average concentration of barley mildew spores downwind of an infected crop of between 1000 and 2000 spores m^{-2}.

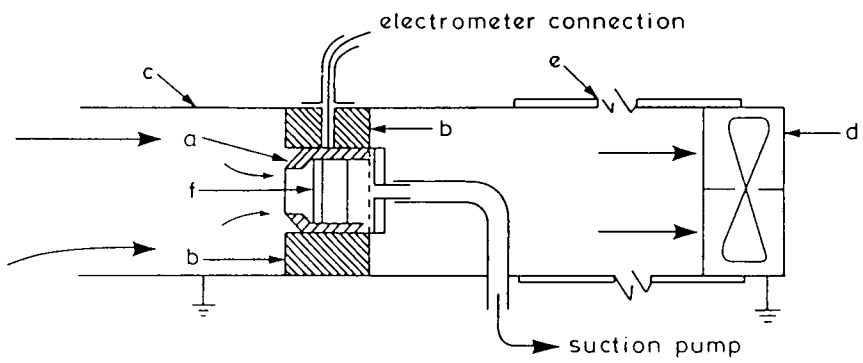

Fig. 5. Spore trap designed to measure spore charge directly. (a) All metal suction trap, (b) P.T.F.E. insulating ring to insulate the trap electrically from the case, (c) earthed cylindrical brass case (60 mm dia.), (d) small fan to draw air past trap, (e) flexible sleeve to reduce mechanical vibration in the case and trap and (f) plastic insert onto which spores impact. Air flow through the trap is indicated by arrows.

Thus for example taking N as $1500\,m^{-2}$ the minimum detectable q would be about 10^{-13} C (i.e. 6×10^5 e), a value somewhat greater than the minimum significant charge (Sect. 2). However, instantaneous spore concentrations may exceed their mean appreciably therefore the sensitivity of the technique may be greater than indicated by the above example.

Measurements with charged rods

The third technique of spore charge detection involve electrically charged rods. The electric field $\mathbf{E}_r$ due to a charged rod of linear charge density λ will be radially symmetric and its magnitude E_r may be calculated, for distances d from the rod axis that are sufficiently small (a few cm) that the rod's length may be considered infinite, as

$$E_r = \lambda/2\pi\varepsilon_0 d \tag{8a}$$

$$= Q/2\pi\varepsilon_0 Ld \tag{8b}$$

where L is the length of a rod, and Q its total charge. Under the influence of this field, a particle (or spore) of charge q experiences a force of magnitude

$$F_r = qE_r \tag{9}$$

that will either attract the spore to, or repel it from, the rod. (The particle also experiences an image force, that is much smaller than F_r, and a polarisation force, that is much smaller still.) It would therefore be expected that for spores carrying a charge of a particular sign a positively charged rod would collect the spores with an efficiency (β_+) that was different from that (β_-) of a negatively charged rod, and that each of these efficiencies would differ from that (β_0) of an electrically neutral rod (for which the major electrostatic force is the image force). Thus, if the charges q are all positive (and the argument is simply reversed for charges that are all negative) then β_+ will decrease, and β_- will increase, as q increases. Consequently, β_+/β_- will depend on the magnitude of q, as will the ratio of the corresponding numbers of caught spores if each rod be exposed to the same wind speed and the same concentration of spores. Alternatively, if the particles are, with equal number, positive and negative, then β_+ and β_- will be equal to each other, but different from β_0 (and the numbers of trapped spores will show corresponding behaviour), and hence, for this case, β_+/β_0 (or β_-/β_0) will depend on q. Thus, whether the spore charges be of one or of both signs, the ratios β_+/β_- and β_+/β_0, when calculated for various assumed values of q, will indicate the minimum value of q that could be resolved through the detection of differences between catches of spores by positive, negative, and neutral rods.

The efficiencies β_+, β_-, β_0 were therefore derived, for the particular charged rods that were used in the field application of this technique, by computing [through (1), (8) and (9)] trajectories for 10 μm radius spores and for a range of values of q and of wind speed. The rods, thirteen of them, were of brass, 5.0 mm diameter and 13.0 cm long, and were held vertically, in a wooden frame, a few cm above the barley on an infected plot (Fig. 4). The rods were spaced at 6.0 cm intervals along the frame, and were maintained at potentials relative to earth of either +6 kV, 0 V, or −6 kV. Along the frame, the sequence of rod potentials was 0 V, +6 kV, 0 V, −6 kV, 0 V, +6 kV, . . . 0 V, so that of the thirteen rods, seven were neutral, three were at positive potential, and three at negative. For the charged rods, the trajectory computations required, in (8b), a value for the total charge on a rod, Q, for which a rough estimate can be obtained through measurement by a field mill of the electric field intensity, E_m, at a point mid way between a positively and a negatively charged rod (the intervening neutral rod being removed). If, in this situation, it is assumed that the charged rods act as quasi point charges, Q, and that the effects of charges on the other rods can be ignored, then the system can be considered equivalent to a point charge (the rod) at a distance D from an infinite conducting plane (the vertical measuring plane of the field mill, which perpendicularly bisects the line joining the rods). The mode of operation of the field mill is such that the joint effect of the two charged rods is equivalent to one point charge and its image in the conducting plane, whence

$$E_m = 2Q/4\pi\varepsilon_0 D^2. \tag{10}$$

In our configuration D was 0.060 m and E_m was measured as $21\,kV\,m^{-1}$, implying that Q was 4.2×10^{-9} C and that λ, for a rod length of 0.13 m, was $3.3 \times 10^{-8}\,C\,m^{-1}$. These were the values used in the calculation of β_+, β_- and β_0, the results for which are presented, in Table 3, in terms of the magnitudes of spore charge that would be needed at various wind speeds to produce values of the ratios of the collection efficiencies β_-/β_+ and β_-/β_0 of 1.5, 2.0 and 5.0. For wind speeds less than $1.5\,m\,s^{-1}$, the entries suggest that, if a difference (between rods) in efficiency of collection of 50% (i.e. a factor of 1.5) can be measured, then if there are equal numbers of positively and negatively charged spores the minimum detectable charge would be less than 8×10^4 e; if the spores carry charges all of the same sign the minimum detectable charge would be less than 10^4 e, smaller than the value of charge that would be needed to affect sedimentation to a horizontal leaf.

In computing the particle trajectories [through (1), (8) and (9)], it was assumed that each rod stood alone, and that its electric field was radially symmetric (8). In the array of thirteen rods, at 6.0 cm spacing, this assumption was not valid, and the entries in Table 3 are therefore somewhat too large: thus any charge inferred from measurements of β_-/β_+ or of β_-/β_0 will be an overestimate of charge actually carried. Since we are concerned in this study only to set an upper limit to the magnitude of spore charge, such overestimation is likely to cause concern only if inferred spore charges are near to the minimum predicted to be required to influence spore deposition.

Table 3. Magnitude of charge per spore (in electron charges) needed, at various wind speeds, to produce values of 1.5, 2.0 and 5.0 for:
(a) the ratio β_-/β_+ of the efficiencies, for collecting from an air stream containing spores only of positive charge, of negatively and positively charged rods;
(b) the ratio β_-/β_0 of efficiencies, for collecting spores from an air stream containing equal numbers of positively and negatively charged spores, of a negatively charged and of a neutral rod

	Wind speed ($m s^{-1}$)			
	0.5	1.0	1.5	2.0
(a) β_-/β_+				
1.5	$<10^4$	$<10^4$	$<10^4$	1×10^4
2.0	$<10^4$	$<10^4$	1×10^4	2×10^4
5.0	$<10^4$	$<10^4$	2×10^4	4×10^4
(b) β_-/β_0				
1.5	$<10^4$	3×10^4	8×10^4	1×10^5
2.0	$<10^4$	4×10^4	1×10^5	2×10^5
5.0	2×10^4	7×10^4	2×10^5	3×10^5

Notes: (1) These data may be assumed to be uncertain to within a factor of three: their uncertainty (compared to the data of Tables 1 and 2) is greater because of the uncertainty in determining the electric field intensity within the array of rods.
(2) 1 electron charge (e) = 1.6×10^{-19} coulomb.

Experimentally, the collection of spores was accomplished in the field by attaching to each of the thirteen rods, at its mid-point, a 2.0 cm wide Cellophane strip coated with glycerine, to which the impacting spores would adhere. After exposure of the rods and strips above an infected barley plot (Fig. 4), the strips were removed and mounted on glass slides and the numbers of spores caught were counted using a light microscope. As the rods were exposed to the same concentration of spores and same windspeeds the number of spores caught on each rod was also a measure of the rod's collection efficiency. Thus the ratio of the number of spores caught on charged or uncharged rods was the same as the ratio of their collection efficiencies (β_-/β_+, β_-/β_0).

EXPERIMENTAL PROCEDURES AND RESULTS

All three techniques described above were used to seek electric charges on mildew spores on three different days. The chosen days, 19 June, 20 June and 5 July 1979, were all warm with clear skies and light winds, the ambient vertical electric field intensity was low, varying between 80 and 200 V m^{-1}. Additionally, the charged-rod traps were exposed for about 6 h per day during the two periods 28–29 June and 17–19 July, by these long exposures appreciable numbers of spores were caught.

Direct measurement of spore charge

Four spore charge detectors (Section 3.1) were used in each experiment, two within an infected plot, and two in an uninfected plot, and all mounted 15 cm above ground level. The detectors were operated for about 160 min and the signals from the electrometers were continuously recorded on magnetic tape. After exposure the plastic inserts were removed from each spore trap and the Cellophane trapping surface removed and mounted on a glass slide. The number of spores caught by each trap was counted and is given in Table 4, which shows that there were few spores present in the uninfected plots. Of material other than mildew spores, similar amounts were collected by each trap, confirming that each was working satisfactorily.

Table 4. Direct measurement of spore charge: numbers of spores caught on three separate days within plots of infected and uninfected barley (two replicates per plot)

Date	Experiment duration (min)	Infected		Uninfected	
19 June	157	3689	153*	3	2
20 June	160	64*	861	0	0
5 July	155	1643	1448	52	34

* Pump fault.

The recorded signals from each trap were played back through the u.v. oscillograph. Examination of the signals showed no significant difference between uninfected and infected plots. Furthermore, none of the signals showed any evidence of charge particles being collected by the traps. For the infected plots, the numbers of spores caught were (apart from the two exceptions ascribed to equipment malfunctioning) sufficiently large that if the spores had been carrying charges of 10^5 e or more, measurable electrometer signals should have been recorded every few seconds. It is therefore concluded that spores did not carry charges greater than about 10^5 e (1.2×10^{-14} C).

Spore charge inferred from electric field measurements

Concentrations of spores, and hence N, the number of spores above unit ground area, were determined from the four rotorods (Section 3.2) that were deployed on each of two masts—one upwind and one downwind of an infected plot (Fig. 4). The high impaction speed of spores on the arms of the rotorods ensured that, even for charged spores, the collection efficiencies were close to 100%. Near to the masts the ground level electric field intensity E was continuously recorded (in analogue form on magnetic tape) throughout the $2\frac{1}{2}$ h of each experimental run.

Values for N, in Table 5, show that there were few spores upwind of the infected plot. From the downwind values, minimum detectable spore charges were calculated through (7), setting ΔE equal to the 20 V m^{-1} resolution of the field mill. Because the values for N were less than those expected on the basis of the observations of Bainbridge and Stedman (1979), the technique was a less sensitive detector of spore charge

Table 5. Upper bounds for the magnitude of spore charge as inferred from measurements of electric field intensity. (The upper bound, or minimum detectable spore charge, is the charge, calculated through (7), that would cause a change ΔE of 20 V m^{-1} in the ground level electric field intensity downwind of an infected plot)

Date	*Time average of N (number m^{-2}) upwind	downwind	Minimum detectable spore charge (electron charge)	†Electric field intensity (V m^{-1})
19 June	29	121	9×10^6	100
20 June	47	457	2×10^6	200
5 July	91	556	2×10^6	80

* N is the number of spores above unit ground area.
† Time average of mean upwind and downwind ground level electric field intensities.

than had been hoped, and the tabulated upper bounds (Table 5) are all somewhat higher than 10^6 e.

The measured values for E showed no difference in their time averages for observations made upwind and downwind of the infected plot. As an indication of the observed magnitudes of E, time averages for the means of upwind and downwind values of E are included in Table 5. Throughout each experiment both upwind and downwind values of E remained steady and without fluctuations. The absence of fluctuations in the *downwind* E gives further evidence that spores carry little charge, because, noting that the rate of release of mildew spores is likely to fluctuate, then if the spores be charged, there would be consequent fluctuations in ΔE, and hence in E, contrary to observation.

The finding from these measurements of E, ΔE and N is thus that the mildew spores did not carry charges greater than about 2×10^6 e (4×10^{-13} C)—and realistically, the limit must be set lower, at $\sim 10^5$ e—the maximum charge retainable by a 10 μm sphere.

Spore charge inferred from observations of catches by charged rods

The two frames, each with their thirteen rods were exposed above an infected plot (Fig. 4) on 19 June, 20 June and 5 July for about 3 h each day, and concurrent measures of mean wind speed were made alongside the rods. Few spores were caught during the 3 h periods, and analysis was therefore made on only two sets of counts (from 20 June and 5 July, one frame each) from the available total of six. The two chosen sets, and the four additional sets that derived from the longer exposures of 28–29 June and 17–19 July (two frames each), gave results that are summarised in Table 6. The tabulations show the averages, over the seven replicates of neutral or three replicates of charged rods, of the numbers of spores caught on the variously charged rods during each of the exposure periods. The coefficients of variation for these replicate catches were high; averaged over positive, negative and neutral rods, within a particular exposure, the coefficients were typically 37–39%, with extremes of 26 and 49%. Hence, in order to seek differences between the catches by the variously charged rods, the data from the six exposures were analysed as a combined set. Proceeding on the assumption that the coefficient of variation was the same for each of the data groups summarised in Table 6, the individual replicate counts of caught spores were transformed logarithmically, and an analysis of variance performed on the transformed data.

The analysis showed that there was no significant difference between the numbers of spores caught by the positively and the negatively charged rods. It also showed that there was a tendency for rods near the

Table 6. Spore charges as inferred from catches by electrically charged rods: average of numbers of spores caught by rods held at potentials of 0 V, +6 kV and −6 kV during each of six experiments

Exposure date	*Average number of spores caught by rods 0 V 7 replicates	+6 kV 3 replicates	−6 kV 3 replicates
20 June	68	72	102
28–29 June†	542	554	705
28–29 June†	464	444	406
5 July	30	46	45
17–19 July†	154	195	209
17–19 July†	154	162	181

* Average coefficients of variation of the counts within an exposure were typically 38%, with extremes of 26% and 49%.
† Results presented for each of two frames of rods.

centre of the line (frame) of 13 to have higher catches than those at the ends. To test for differences between catches by neutral and charged rods (either sign), a second analysis was made in which data from positive and negative rods were combined, and the influence of position in the frame was removed by covariates of linear and quadratic distances along the frame. This second analysis showed a significant difference between catches by charged and neutral rods: means for the logarithmically transformed data were 2.16 for neutral and 2.23 for charged rods, and their difference, 0.073, was significant at the 95% level in relation to a standard error of difference of 0.036. The 95% confidence limits for the difference between transformed means were 0.004 and 0.146. The mean difference and the 95% limits respectively correspond in the untransformed data to mean ratios of catches by charged to catches by neutral rods (the equivalent of β_-/β_0 in Table 3) of 1.18, 1.001 and 1.40: values that suggest that the spores did indeed carry charge.

As to the magnitude of this possible charge: to achieve a value for β_-/β_0 of 1.18 for a mean wind speed above the crop equal to the $1.3\,m\,s^{-1}$ that prevailed during the exposures would require a particle (spore) charge of 2×10^4 e (4×10^{-15} C); the charges corresponding to the 95% confidence limits for β_-/β_0 are about 10^3 and 4×10^4 e. However, as was remarked in Section 3.3, the closeness (6.0 cm) of the rods in their frames is likely to have introduced some distortion of the radial symmetry of the electric fields surrounding the charged rods, causing the inferred spore charge to be an overestimate of the true charge. Furthermore, the effect of any clumping of spores (Section 2) would be to decrease the viscous forces, in comparison to the intertial and electrostatic forces, and hence to cause an enhanced capture by the charged rods of any charged spore clumps, leading, again, to an overestimate by β_-/β_0 of average charge per spore. It may thus be realistic to conclude that the magnitude of any spore charge is not greater than 10^4 e: a value that is acceptably smaller than the maximum charge (Section 1) that a barley mildew spore can retain.

DISCUSSION AND CONCLUSIONS

Theoretical considerations indicated that barley mildew spores are unlikely to be able to retain electric charges greater than $\sim 10^5$ e. Calculation of spore trajectories (Section 2) showed that rates of sedimentation to flat plates (simulating horizontal leaves) and to vertical cylinders (plant stems) could be affected to a measurable extent if spore charge per particle respectively exceeds about 3×10^4 e and 5×10^5 e. Our experimental programme therefore sought to determine whether spores do indeed carry charges of 3×10^4 e (or more) that could influence spore deposition to leaves.

Results (Section 4.3) of our measurements of rates of collection of spores by vertical cylinders at large positive and negative electric potential indicated that spores may carry charges. Our estimate of their magnitude, $< 10^4$ e, is necessarily somewhat imprecise because the detection technique cannot be calibrated experimentally. Nonetheless, our conclusion is that the charge magnitude is too small to affect significantly the deposition of spores to plant surfaces. Furthermore, if the catches by cylindrical rods (Table 6) show so small an influence of electric field even for field intensities created by potentials of ± 6 kV, then there is little likelihood of spore deposition to plant surfaces being affected by the much smaller field intensities that exist naturally within crop canopies. These conclusions are likely to hold also for fungal spores other than those of barley mildew. However, electrostatic forces, being short range, may influence the retention (as opposed to the capture) of spores by plant surfaces, even for spores carrying relatively little charge.

Acknowledgements—The authors are grateful to Mr. S. A. Strange and Mr. P. K. Marsden for assistance in constructing and deploying the spore traps.

REFERENCES

Bainbridge A. and Stedman O. J. (1979) Dispersal of *Erysiphe graminis* and *Lycopodium clavatum* spores near to the source in a barley crop. *Ann. appl. Biol.* **91**, 187–198.

Bright A. W. and Coffee R. A. (1964) Electrostatic powder coatings. *6th International Metal Finishing Conference*, May 1964.

Bowen H. D., Hebblethwaite P. and Carleton W. M. (1952) Application of electrostatic charging to the deposition of insecticides and fungicides on a plant surface. *Agricl Engng* **33**, 347–350.

Chamberlain A. C. (1975) The movement of particles in plant communities. *Vegetation and the Atmosphere Vol. I Principles.* (Ed. by J. L. Monteith), pp. 155–203, Academic Press, London.

Coffee R. A. (1974) Depositional control of macroscopic particles by high strength electric-field population. *IEEE Trans. on Industry Applications* **IA 10**, 511–519.

Corson P. and Lorrain P. (1962) *Electromagnetic Fields and Waves.* W. H. Freeman and Co., San Francisco.

Davies C. N. (1973) *Air Filtration.* Academic Press, London.

Davies C. N. and Peetz C. V. (1956) Impingement of particles on a transverse cylinder. *Proc. R. Soc.* **234A**, 269–295.

Dodd E. E. (1953) The statistics of liquid spray and dust electrification by the Hopper and Laby method. *J. appl. Phys.* **24**, 73–80.

Felici N. J. (1967) Electrostatics and electrostatic engineering. 1967 *Static Electrification Conference, Conference series No.* 4, pp. 127–138, Institute of Physics, London.

Friedlander S. K. (1977) *Smoke, Dust and Haze.* John Wiley and Sons, NY.

Gregory P. H. (1957) Electrostatic charges on spores of fungi in air. *Nature* **180**, 330.

Gregory P. H. (1973) *The Microbiology of the Atmosphere.* 2nd Ed., Leonard Hill Books, London.

Gregory P. H., Longhurst T. J. and Sreeramulu T. (1961) Dispersion and deposition of airborne *Lycopodium* and *Ganoderma* spores. *Ann. appl. Biol.* **49**, 645–658.

Gregory P. H. and Stedman O. J. (1953) Deposition of airborne *Lycopodium* spores on plant surfaces. *Ann. appl. Biol.* **40**, 651–674.

Harper W. R. (1951) The volta effect as a cause of static electrification. *Proc. R. Soc.* **205A**, 83–103.

Hopkinson P. R. (1974) The prospects for enhanced impaction of fine sprays by electrostatic charging. *British Crop Protection Council Monograph*, No. 11, 166–179.
Hopper V. D. and Laby T. H. (1941) The electronic charge. *Proc. R. Soc.* **178A**, 243–273.
Ingold C. T. (1971) *Fungal Spores: Their Liberation and Dispersal.* Clarendon Press, Oxford.
Kaye G. W. C. and Laby T. H. (1973) *Tables of Physical and Chemical Constants.* Longman, London.
Kunkel W. B. (1950) Static electrification of dust particles on dispersion into a cloud. *J. appl. Phys.* **21**, 820–832.
Leach C. M. (1976) An electrostatic theory to explain violent spore liberation by *Drechslera turcica* and other fungi. *Mycologia* **68**, 63–86.
Lui B. Y. H. and Pui D. Y. H. (1974a) Electrical neutralisation of aerosols. *J. Aerosol Sci.* **5**, 465–472.
Lui B. Y. H. and Pui D. Y. H. (1974b) Equilibrium bipolar charge distribution of aerosols. *J. Colloid Interface Sci.* **49**, 305–312.
Lundgren D. A. and Whitby K. T. (1965) Effect of particle electrostatic charge on filtration by fibrous filters. *I and EC Process Design and Development* **4**, 345–349.
Mapleson W. W. and Whitlock W. S. J. (1955) Apparatus for the accurate and continuous measurement of the earth's electric field. *J. atmos. terr. Phys.* **7**, 61–72.
Moore A. D. (1973) *Electrostatics and its Application.* Wiley, New York.
Perkins W. A. (1957) The rotorod sampler. Second Semi Annual Report of the Aerosol Laboratory, Stanford University, CML 186.
Splinter W. E. (1968) Electrostatic charging of agricultural sprays. *Trans. Am. Soc. agricl Engrs* **11**, 491–495.
Swinbank P., Taggart J. and Hutchingson S. A. (1964) Measurement of electrostatic charges on Spores of *Merulius lacrymans* (Wulf) Fr. *Ann. Bot.* **28**, 239–249.
Whitby K. T., Lundgren D. A. and Peterson C. M. (1965) Homogeneous aerosol generators. *Int. J. Air and Water Pollut.* **9**, 263–277.
Yoshioka N., Emi H., Hattori M. and Tamori I. (1968) Effect of an electrostatic force on the filtration efficiency of aerosols. *Chem. Engng, Tokyo* **32**, 815–820. (Health and Safety Executive translation number 7452).

APPENDIX: DEPOSITION VELOCITY TO A FLAT PLATE

For charged or uncharged particles, the deposition velocity, v_g, to a flat plate of length l and breadth b is given by

$$v_g = D/lbc \tag{A1}$$

where D is the rate of deposition of particles to the plate (number s^{-1}) and c is the concentration of particles in the free air upwind of the plate. Let the plate be orientated so that it is horizontal and aligned parallel to the air flow (Fig. A1). If particles which strike the plate on its trailing edge have passed through a line at height h above the leading edge of the plate, then all particles which pass closer to the leading edge will also strike the plate. (It will be noted that h will depend on q, the charge per particle). Thus the rate at which particles strike the plate is equal to the rate at which particles cross the vertical plane, of height h and width b, located at the leading edge of the plate, i.e.

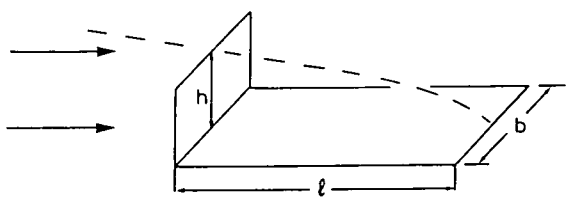

Fig. A1. The calculation from particle trajectories of deposition velocity to a flat plate l, b, length and width of plate; h, height on passing leading edge of plate of that trajectory (shown as broken line) that just strikes trailing edge of plate. Air flow over the plate is indicated by arrows.

$$D = hbcu_0 \tag{A2}$$

where u_0 is the windspeed upwind of this plane. Combining (A2) and (A1):

$$v_g = hu_0/l. \tag{A3}$$

The variable l/u_0 is thus the time taken for a particle to fall through the height h and is a function of l/u_0 and q only.

For charged particles, it should be noted that the electrostatic image force always acts towards the plate. Thus some particles which would have missed the plate had they carried no charge will strike its lower surface. Hence, in comparing deposition velocities for charged and uncharged particles, total deposition, to upper and lower surfaces, must be allowed for when computing charged particle deposition (as was done for Fig. 3 and Table 2).

Storebø P. B., Bjorvatten T., Hønnåshagen K., Lillegraven A., Jones C. D. and Van Buijtenen C. J. P. (1983).

Tracer experiments with turbulently dispersed air ions.

Bound. Layer Met. **26**, 127 - 139.

TRACER EXPERIMENTS WITH TURBULENTLY DISPERSED AIR IONS

P. B. STOREBØ, T. BJORVATTEN, K. HØNNÅSHAGEN, A. LILLEGRAVEN

Norwegian Defence Research Establishment, N-2007 Kjeller, Norway

C. D. JONES

Chemical Defence Establishment, Porton Down, Wiltshire SP4 OJQ, UK

and

C. J. P. VAN BUIJTENEN

Prins Maurits Laboratorium TNO, Postbus 45, 2280 AA Rijswijk, The Netherlands

(Received in final form 26 April, 1983)

Abstract. Unipolar air ions released into the wind constitute a tracer which can be measured with high resolution. An ion source produces a cloud with homogeneous charge density, insensitive to source strength, dependent on time since formation only. It is well suited for tracing concentration changes due to turbulence, less suited for cloud size tracing.

A tight array of 8 sensors has been used to examine turbulently dispersed ions. High-resolution records are presented and discussed. The highest concentrations measured could be undiluted source material. The frequency distribution within a plume did not differ from that in a multitude of puffs. The distribution seems to be log-normal with a geometric standard deviation of about 2.45. The time resolution used corresponds to volume resolutions of 40, 225, and 650 cm^3. Sample size had no apparent effect.

1. Introduction

Scientists from three Defence Research Institutes in England, the Netherlands and Norway have examined small-scale cloud structures during turbulent dispersion. Air ions have been used as a tracer. The method and the instruments were developed by Jones (1977), partly in cooperation with Hønnåshagen (1980). The method for describing small-scale concentration structures proposed by Storebø (1975, 1980) has served as a guide for experimental design.

A series of multi-sensor experiments were carried out at Gardermoen airport in Norway in 1978. Records for a full set of 8 sensors exist only for 26 May. On that day, the ion generator was operated in a continuous mode from 11 : 16 to 13 : 12 h and in a pulsed mode 14 : 00 to 15 : 50 h Norwegian Standard Time.

The tracer behaviour influences the results, and the instruments could be improved. However, the records are probably the most detailed available for studying small-scale turbulent dispersion structures. For this reason, they deserve close attention.

Boundary-Layer Meteorology **26** (1983) 127–139. 0006–8314/83/0262–0127$01.95.

2. Experimental Conditions

On 26 May, the weather was warm and sunny, with wind of up to 3 m s^{-1}, variable within the sector S to NW. Only towards the end of the experiment did some cumulus clouds appear.

The ion sensor mast was located in the middle of a 40 m wide, disused concrete runway surrounded by a flat field where only sparse low grass grew within at least 500 m

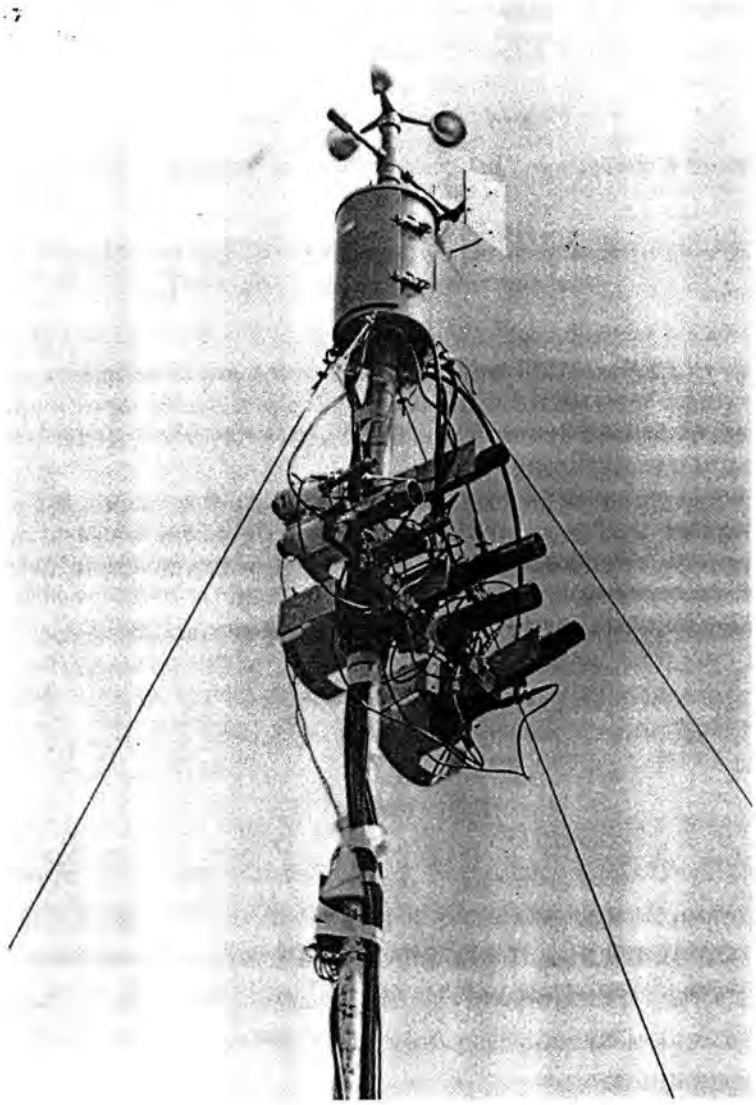

Fig. 1. Ion sensor array on the mast. Larger circle: Sensor tube radius 1.95 cm, air flow 19 l/s, detection threshold 0.11 nC/m^3, electrical rise time 3.8 ms. Smaller circle: Radius 1.8 cm, flow 6.7 l/s, threshold 0.3 nC/m^3, rise time 2.8 ms. Dot: Radius 0.5 cm, flow 1.1 l/s, threshold 1.8 nC/m^3, rise time 0.14 ms. Individual sensors are identified by numbers. With 30 Hz resolution of the total system, independent air samples correspond to 650, 225, and 40 cm^3.

of the runway. A photograph of the sensors is shown in Figure 1. They are aligned to sample air from the same upwind distance. The lower 6 sensors are mounted 8.5 m above ground. The mast itself could be rotated in order to direct the sensors towards the generator.

The ion generator mast was positioned in the field just off the runway 37.5 m from the sensor mast. The 10 cm diameter generator was mounted on a boom 60 cm off the mast, 8.5 m above the ground.

The time between ion generation and detection should thus be 10–15 s. Some electronic equipment was located at the base of both masts but in general nothing protruded upward more than 0.7 m.

3. Tracer Behaviour

Negative ions were produced continuously or pulsed at a rate of 0.2 μA. A substantial repulsion takes place in the ion cloud, but cloud dimensions remain small compared to travel distances. The sensors are infrequently hit by the ions, and most of the records therefore are blank. On the other hand, when the cloud is detected, it is usually seen by all sensors.

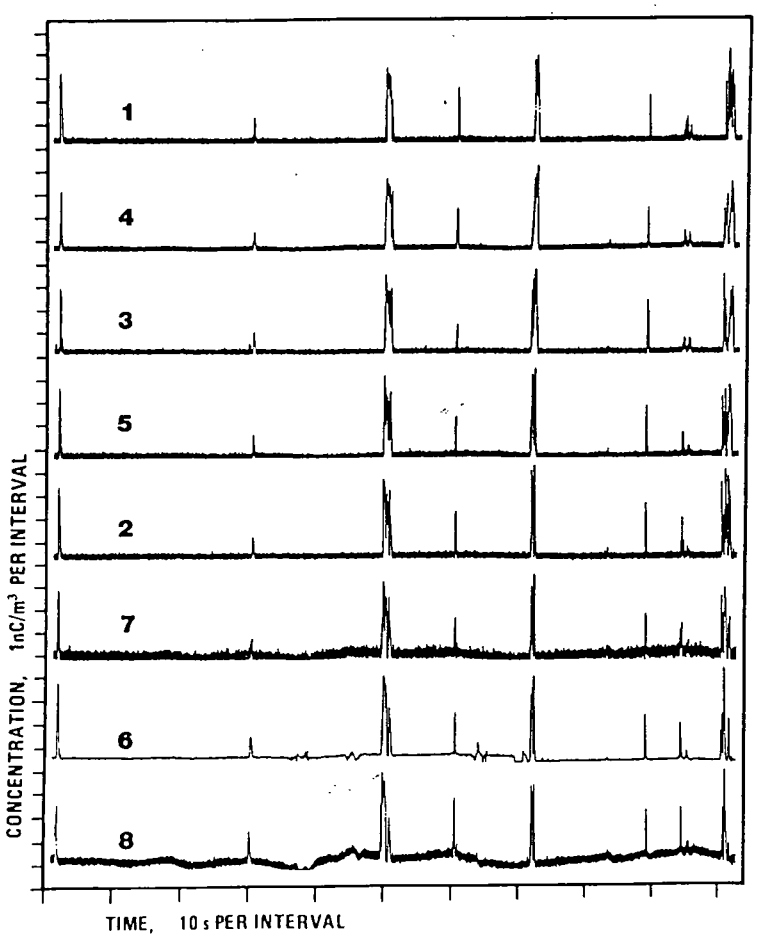

Fig. 2. Sample of records for pulsed mode operation of ion generator.

A section of the pulsed mode record is presented in Figure 2, while Figure 3 shows a section of the continuous mode record. The wind in both diagrams is blowing from mast to mast, but the variability is striking nevertheless. The detector system resolution is 30 Hz.

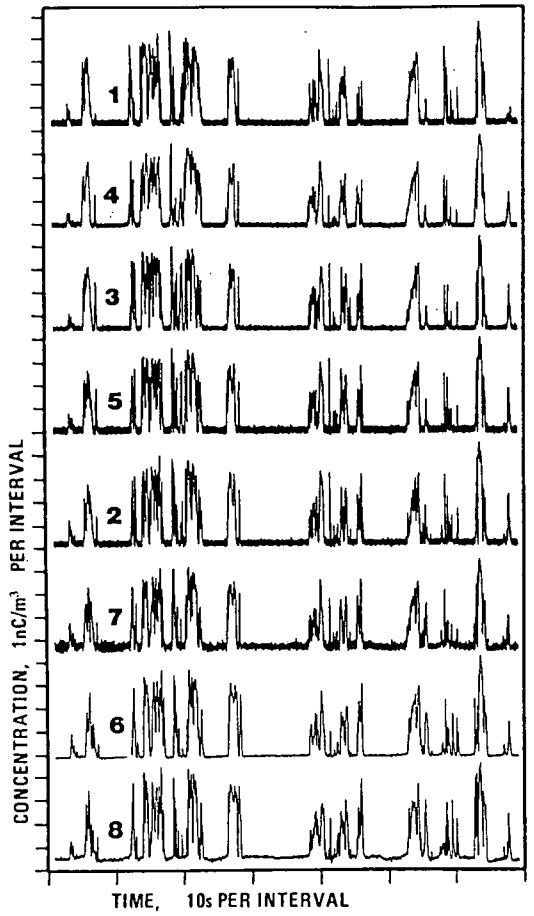

Fig. 3. Sample of records for continuous mode operation of ion generator.

The sensors were intercalibrated in situ by assuming that the highest concentration levels of individual records were equal. For the six largest sensors, laboratory estimates agreed well. For the two smallest sensors, laboratory measurements had been difficult to make, and the original response estimates had to be raised a little.

The electric charge has a dominant influence on tracer behaviour. Under ideal conditions, a tracer cloud developed from a generator pulse should have a point-symmetrical distribution, i.e., a puff. Continuous generation should lead to an axis-symmetrical distribution, i.e., a plume. The electric force is normal to any concentric sphere or coaxial cylinder, respectively.

For the puff, the electric field E at a distance r from the centre is:

$$E = Q/(4\pi r^2 \varepsilon) \tag{1}$$

where Q is total charge inside the sphere, and ε is the dielectric constant for air. For

the plume,

$$E = (\mathrm{d}Q/\mathrm{d}l)/(2\pi r\varepsilon) \tag{2}$$

where $\mathrm{d}Q/\mathrm{d}l$ is charge per unit axis length inside a cylinder of radius r.

If μ is the mobility of the ions in the air, a surface always consisting of the same ions expands due to the field

$$\mathrm{d}r/\mathrm{d}t = \mu E\,. \tag{3}$$

For the puff this leads to,

$$\mathrm{d}r/\mathrm{d}t = \mu Q/(4\pi r^2\varepsilon)\,.$$

The quantity Q is invariant for any surface of the type defined, and the equation may be integrated. With radius r_0 at generation time $t = 0$,

$$r^3 = r_0^3 + 3\mu Q t/(4\pi\varepsilon)\,. \tag{4}$$

The charge density may be introduced;

$$\begin{aligned} 4\pi r^3/(3Q) &= 4\pi r_0^3/(3Q) + \mu t/\varepsilon\,, \\ 1/\gamma &= 1/\gamma_0 + \mu t/\varepsilon\,, \end{aligned} \tag{5}$$

where γ and γ_0 are actual and initial mean charge densities inside the defined surface.

For the plume, the corresponding equations are

$$\begin{aligned} \mathrm{d}r/\mathrm{d}t &= \mu(\mathrm{d}Q/\mathrm{d}l)/(2\pi r\varepsilon)\,, \\ r^2 &= r_0^2 + \mu(\mathrm{d}Q/\mathrm{d}l)t/(\pi\varepsilon)\,, \end{aligned} \tag{6}$$

$$\begin{aligned} \pi r^2/(\mathrm{d}Q/\mathrm{d}l) &= \pi r_0^2/(\mathrm{d}Q/\mathrm{d}l) + \mu t/\varepsilon\,, \\ 1/\gamma &= 1/\gamma_0 + \mu t/\varepsilon\,. \end{aligned} \tag{7}$$

The ion generator had an output of 0.2 μA. The puffs were generated by pulses of 0.2 s duration. For spheres comprising whole clouds, $Q = 4 \times 10^{-8}$ C. Production cloud size is estimated to be $r_0 = 5$ cm, while $\mu = 2 \times 10^{-4}\ \mathrm{m^2\,V^{-1}\,s^{-1}}$ and $\varepsilon = 8.85 \times 10^{-12}\ \mathrm{C\,V^{-1}\,m^{-1}}$.

Equation (4) gives quantitatively

$$r^3\,(\mathrm{m^3}) = 0.000\,125 + 0.216\,t \approx 0.216\,t\,(\mathrm{s})\,. \tag{8}$$

The approximation is good for t larger than some small fraction of a second, and therefore certainly at sampling time some 10 s after production.

Equation (5) leads to a quantitative charge density,

$$\begin{aligned} \gamma\,(\mathrm{C/m^3}) &= \gamma_0/(1 + \mu\gamma_0 t/\varepsilon) = 7.64 \times 10^{-5}/(1 + 1726\,t) \\ &\approx \varepsilon/(\mu t) = 4.43 \times 10^{-8}\,t^{-1}\,(\mathrm{s})\,. \end{aligned} \tag{9}$$

The approximation is again good almost immediately. It implies a density independent of the production density.

Equations (6) and (7) for plumes may be evaluated by assuming a wind velocity of 3 m s^{-1}, i.e., $dQ/dl = 6.67 \times 10^{-8}$ C m^{-1},

$$r^2\,(\mathrm{m}^2) = 0.0025 + 0.48\,t \approx 0.48\,t\,(\mathrm{s})\,, \tag{10}$$

$$\gamma\,(\mathrm{C/m}^3) = \gamma_0/(1 + \mu\gamma_0 t/\varepsilon) = 8.5 \times 10^{-6}/(1 + 192\,t)$$

$$\approx \varepsilon/(\mu t) = 4.43 \times 10^{-8}\,t^{-1}\,(\mathrm{s})\,. \tag{11}$$

The approximate form should not be used as early as for the puff. It is however good for times greater than 0.1 s.

The mathematical expressions in Equations (9) and (11) apply to the volume inside any concentric or coaxial surface within the cloud. Individual elementary volumes consequently behave likewise. The characteristic tracer behaviour may therefore be described in the following manner for the ideal cloud:

> Differences in charge concentration are rapidly smoothed out. Irrespective of source characteristics, the density depends on time after production only. But the total charge determines the size of the homogeneous cloud.

The atmospheric fair-weather electric field might cause an ascent of 20–40 cm over a period of 10 s. For the plume, this is counteracted by attraction due to ground induction (Jones, 1977), amounting to 10–15 cm descent over the same time. The attraction is negligible for puffs.

Natural ions in the air constitute a variable background level. The deviation from the background is the tracer level. Possible neutralizations of tracer by natural ions are of no consequence here, because the net air charge is conserved.

The ideal clouds are either spheres or infinitely long cylinders. Regarding size, Equations (8) and (10) give cloud radii of 1.3 and 2.2 m. Turbulent dispersion causes a similar spread. The ion experiments are for this reason not used for cloud size assessments.

But the clouds are torn apart and twisted. A highly idealized case may be studied.

At time t_s, let two identical fragments of radius r_s and charge Q be formed a centroid distance R_s apart. To simplify matters, assume electrical interaction limited to a centroid repulsion, for which Coulomb's law can be applied. Because both clouds move, the centroid distance R is determined by

$$dR/dt = 2\mu Q/(4\pi\varepsilon R^2)\,,$$

i.e.,

$$R^3 = R_s^3 + 3\mu Q(t - t_s)/(2\pi\varepsilon)\,.$$

Equation (9) makes it possible to replace Q by $4/3\pi r_s\,\gamma(t_s)$, where $\gamma(t_s)$ may be replaced by $\varepsilon/\mu t_s$, leading to

$$R^3 = r_s^3(R_s^3/r_s^3 + 2(t - t_s)/t_s)\,. \tag{12}$$

The sphere size r may be developed from (4) with a similar replacement,

$$r^3 = r_s^3(1 + (t - t_s)/t_s) . \tag{13}$$

A numerical example is informative. For an initial separation $R_s = 4r_s$, the time needed for the spheres to touch is $t - t_s = 9.3\, t_s$. R is then increased to $1.09\, R_s$, r to $2.18\, r_s$.

The two equations imply that the impacts of turbulence on the ion cloud are gradually blurred while dimensions increase. Only recent events are faithfully reflected in the cloud. The time interval needed for a certain obliteration to occur increases with time between cloud production and turbulent impact. The numerical values indicate small distortions of concentration structures over the latter half of the path between generator and detector. The ion cloud should thus be a useful tracer for the concentration pattern developed during turbulent dispersion.

4. Measured Concentration Sequences

4.1. Puff records

Three puff-cloud passages are shown with high time resolution in Figure 4. Fluctuations with time shorter than some 0.03 s should be regarded as noise.

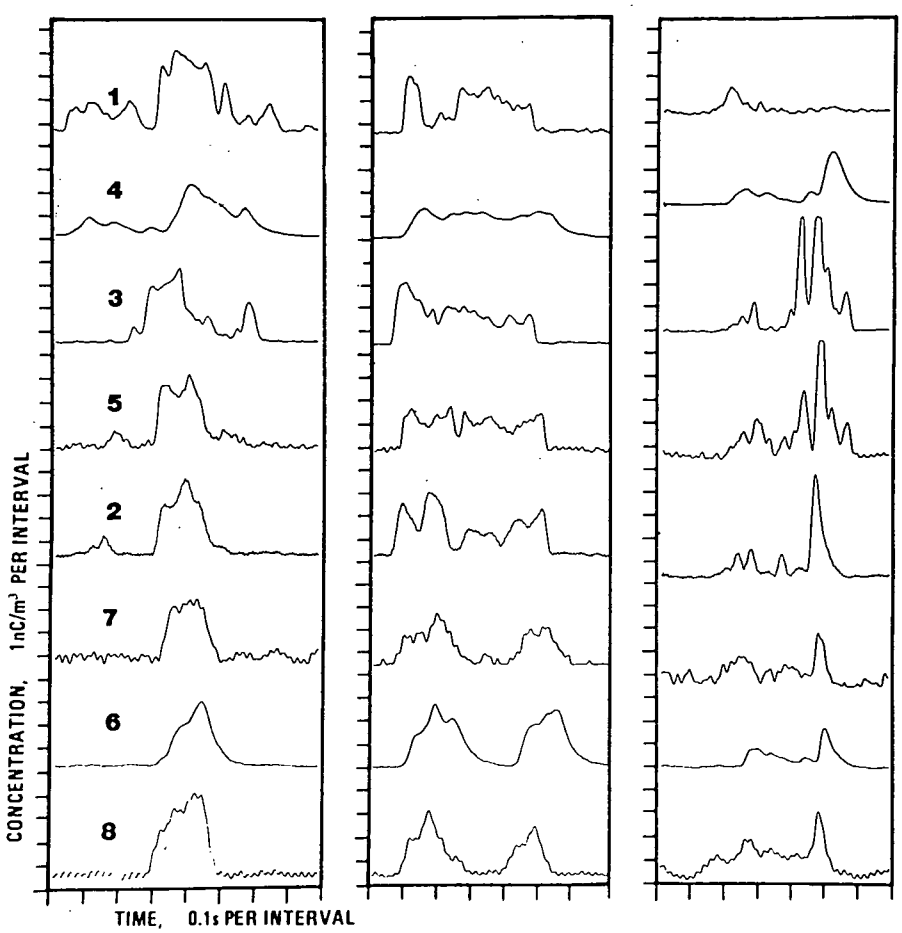

Fig. 4. Records during passage of ion puffs. The records are presented in sensor sequence along the boom with the upper sensors at the top. Time resolution 30 Hz.

The first puff is recorded approximately Gauss-shaped by many sensors. On one side and at the higher levels a more fragmented structure is evident. Large features can be traced from one sensor to the next. The structures are, however, not regular enough for spatial interpolation to be undertaken with confidence.

The second puff in the figure is split into two discrete parts on one side, but it appears more homogeneous in other records. Considerable small-scale structures are seen. Slightly larger structures often extend from one detector to the next.

The third puff reveals a cloud with rapid and strong fluctuations. Some of the more dominant features may be found along the horizontal boom, but can be shifted slightly in time between the sensors. They could be interpreted as twisted thin layers of high concentration.

Since hardly anything is measured at the highest level, it is tempting to assume a quasi-horizontal structure. The peak concentrations are about 4 nC/m^3. If the time 10 s is introduced in Equation (9), the concentration in a cloud not exposed to turbulent dispersion should be 4.4 nC/m^3. It thus appears that the highest peaks could be due to cloud elements which have not been diluted at all.

About 40 puffs were recorded out of some 1000 produced. The three puffs presented are typical for records of short duration. The longest records last 1.5 to 2 s. The equipment did not permit determination of the puff path. It is not known *per se* if a central or a peripheral part of the puff was observed, or if the puff headed straight into the sensor array or passed by in an oblique manner.

In general the puffs show considerable variation. They are often torn into separate pieces. No consistent difference is noted between front and rear ends. Structural details may sometimes be traced over many crosswind sensors, indicating high-concentration pockets extended in one or two dimensions rather than compact three-dimensional shapes.

4.2. Plume records

A section of plume record is shown with high time resolution in Figure 5. The arrival of the plume is abrupt and simultaneous at all the sensors (left side of diagram). Near the left centre of the diagram, the plume strength dwindles away, very pronounced on one side (lower traces), less pronounced and slightly later on the other side and at higher levels.

The plume appears to be somewhat torn. The last 0.2–0.3 s of the records are almost detached. Many large peaks may be followed throughout the diagram, although time shifts occur. Certain characteristic small peaks and troughs can also be followed over several sensors. More often than not, they suddenly disappear or are submerged by the appearance of a new feature.

Tracing of peaks on the diagram is a dubious undertaking: a peak may be seen on all records about 0.4 s before the end of the diagram. But is it the same feature? Sensor No. 7 shows a double peak, which could be a confluence of two pronounced ones appearing on either side of the sensor.

The general impressions given by the plume record do not differ much from those

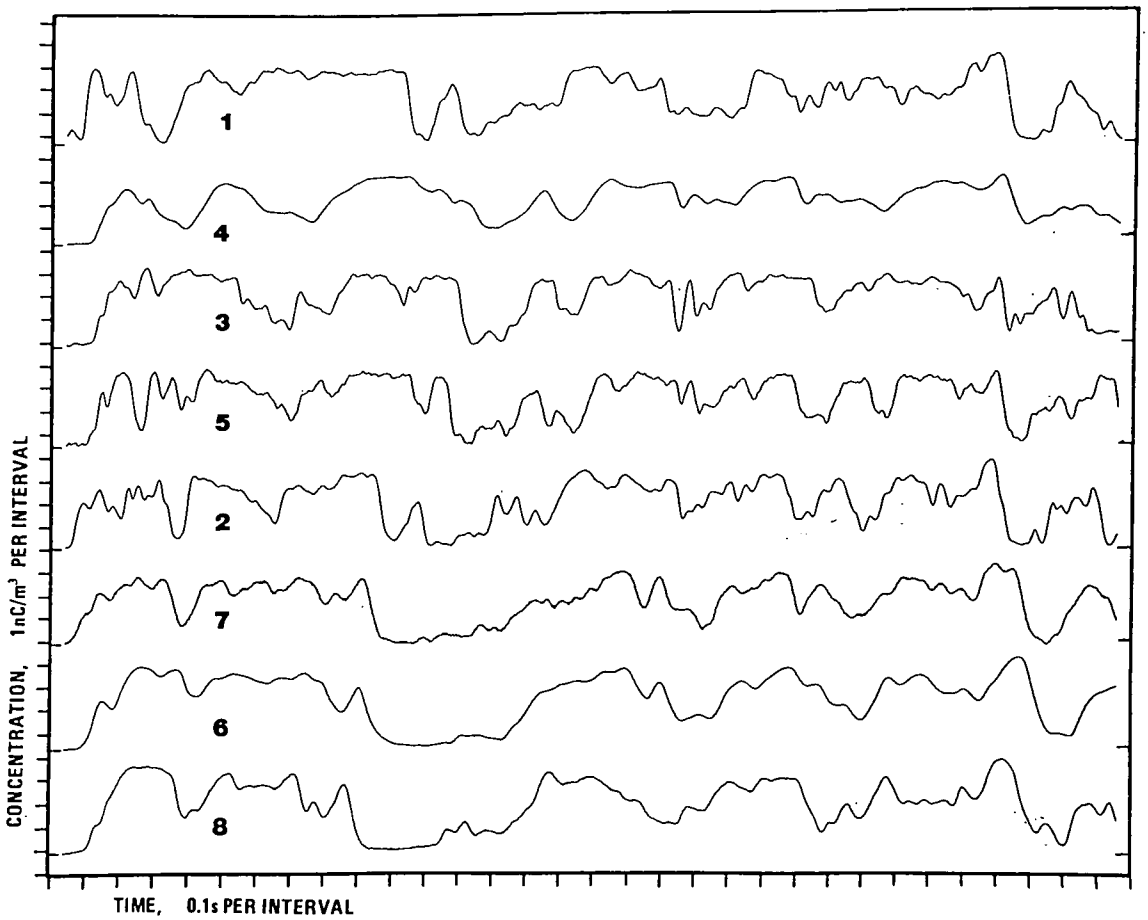

Fig. 5. Records from ion plume registrations. The records are presented in sensor sequence along the boom with the upper sensors at the top. Base levels are indicated. Time resolution 30 Hz.

given by the puffs. Large-scale features are likely to be present on all sensors. This may perhaps be seen most clearly with the coarser time resolution of Figure 3.

High-concentration pockets often have sharp boundaries; they might even be interpreted as discontinuities. Laminar forms with large crosswind extensions are sometimes evident. A directional effect might however be due to the observational technique and should not be over-stressed.

Smaller pockets can show up as peaks in one sensor record only or may be traced over several adjacent sensors. Each sensor measures a specific concentration time-profile which cannot be constructed by interpolating the sensor records on either side.

5. Concentration Frequency Distributions

Other investigations on the concentration frequency distribution of material dispersed by turbulence (Csanady, 1973; Cats and Holtslag, 1980) indicate a log-normal distribution. This distribution has been adopted without being seriously questioned, and data-processing procedures are developed with this in mind.

The log-normal distribution is described by two parameters. It is most convenient to use the geometric mean γ_g and the geometric standard deviation σ_g. If individual

measurements are represented by γ_i:

$$\gamma_g = \sqrt[n]{(\gamma_1 \cdot \cdot \gamma_i \cdot \cdot \gamma_n)} \tag{14}$$

and

$$\log^2 \sigma_g = 1/n \sum_{i=1}^{n} \log^2(\gamma_i/\gamma_g) . \tag{15}$$

In the log-normal distribution, the arithmetic mean $\bar{\gamma}$ is related to the geometric parameters by

$$\bar{\gamma} = \gamma_g \exp(0.5 \log^2 \sigma_g) . \tag{16}$$

Our immediate aim of data processing is to provide parameters for the shifting concentration structure method (Storebø, 1980), where the log-normal distribution at a position relative to the centroid or the axis of the cloud is sought. But the centre in question is not known, although it must be reasonably close whenever the sensor threshold is surpassed. A sort of average distribution for positions in the bulk cloud may thus be found by pooling all measurable concentrations.

Lillegraven (1980) has done this by means of a pulse height analyser. The time the signal strength exceeds a series of set levels is measured, and the resultant distribution is fitted to a log-normal one. By least-square method, the regression line is determined on a probability/log-concentration diagram.

Very low concentration events are obviously missed in the analysis. The method therefore requires an estimate of the frequency below the threshold. This has, after some testing of goodness of fit, summarily been set at 0.1 for the puff records. For the plume records, a better fit resulted with a lower frequency estimate.

The representativity of the few very high concentration measurements is questionable. Therefore the upper tenth of the data is discarded during the regression analysis. What remains is treated as a log-normal distribution between 0.1 and 0.9 cumulative frequency. The results for the various sensors and for the two modes of operation are shown in Table I.

TABLE I

Experimental distribution parameters

Sensor No.	Pulsed generation			Continuous generation		
	$\bar{\gamma}$, nC/m^3	γ_g, nC/m^3	σ_g	$\bar{\gamma}$, nC/m^3	γ_g, nC/m^3	σ_g
1	1.68	0.97	2.86	1.53	0.97	2.61
2	1.59	1.03	2.53	1.53	0.96	2.64
3	1.69	1.15	2.41	1.57	1.12	2.27
4	1.62	1.12	2.36	1.52	1.14	2.14
5	1.78	1.32	2.16	1.56	1.17	2.14
6	1.31	0.86	2.51	1.54	0.93	2.72
7	1.67	1.47	1.65	1.63	1.29	1.99
8	1.72	1.43	1.84	1.67	1.22	2.20

The first 6 sensors agree fairly well. The last two sensors have different distribution parameters. They are less sensitive, however. The quoted arithmetic mean concentration is in the region of their detecting threshold. They probably leave a higher proportion of the cloud unrecorded, and would indeed agree better if the frequency estimate for concentration below threshold were raised well above that used.

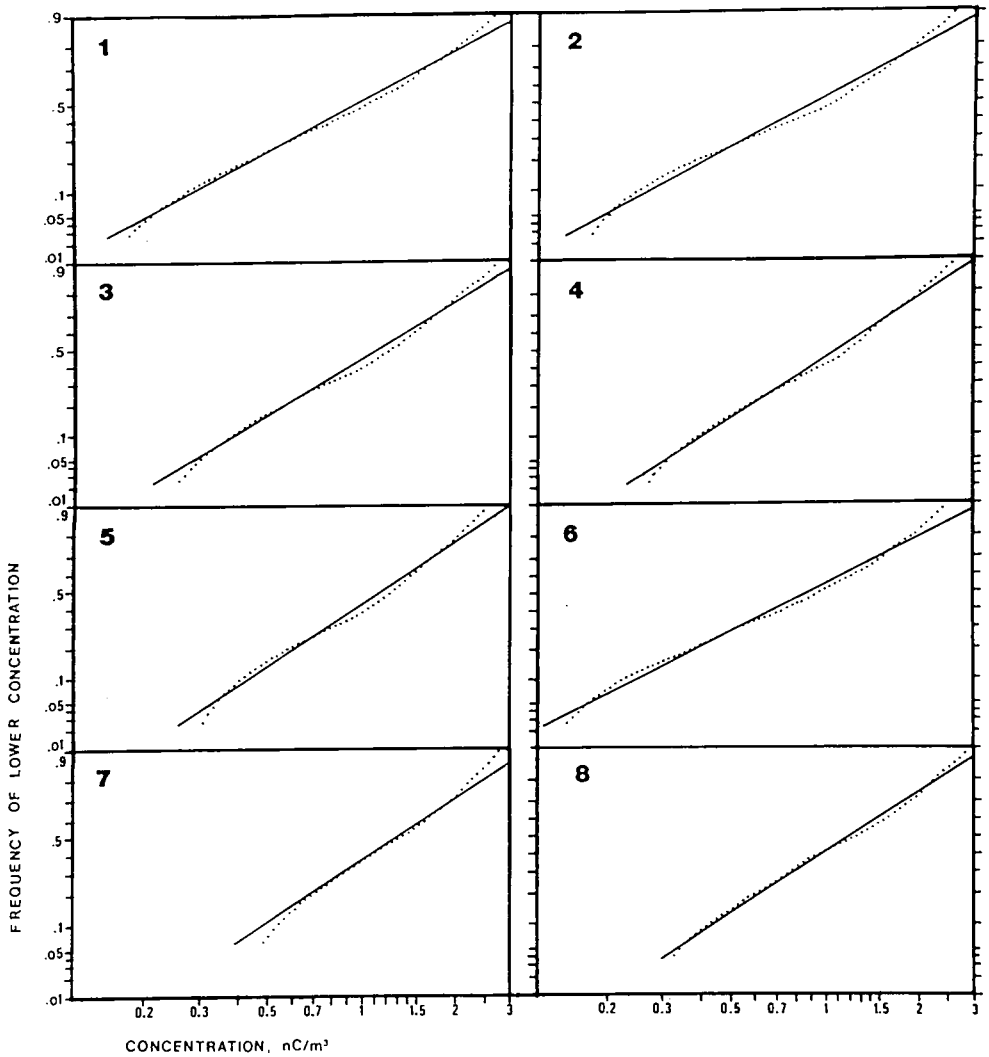

Fig. 6. Cumulative frequency distributions for puffs as recorded by the various sensors. It is assumed that 0.1 of the events are below instrumental threshold. The regression-determined log-normal distributions are shown on the diagram.

The frequency distributions for the puffs are shown in Figure 6, together with the log-normal regression lines. Figure 7 shows the same for the plume.

No obvious differences are present between parameters for puff and plume. The electrical forces should produce the same concentration. But also the turbulence appears to disperse puffs and plume in the same manner, even quantitatively.

The statement is limited to the central part of actual clouds, or to points not far removed from an actual centroid or an actual plume axis. The likelihood for hitting the cloud is not considered or compared, and the arithmetic mean concentration is that of

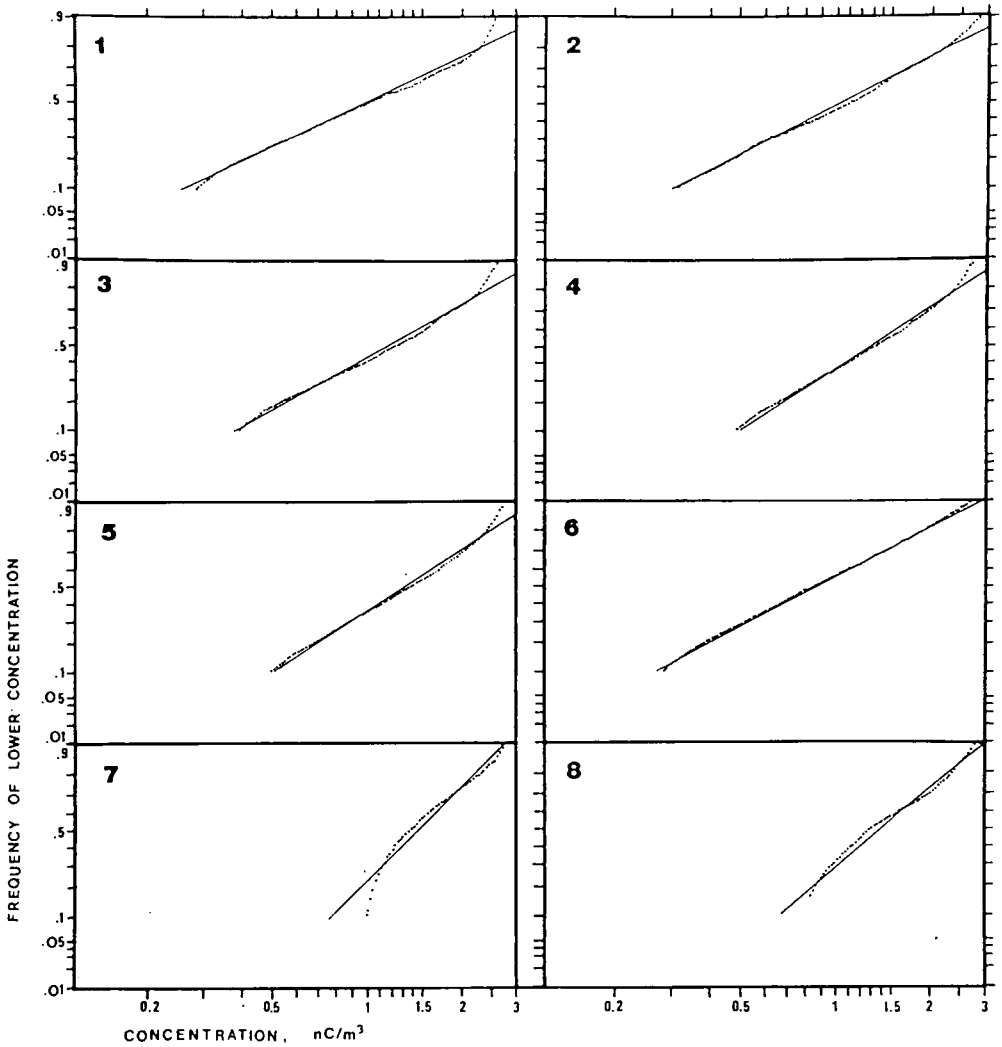

Fig. 7. Cumulative frequency distributions for a plume as recorded by the various sensors. Below threshold fractions are individually assessed, but are less than 0.1.

the frequency distribution and has no connection with the mass distribution in space described by most dispersion formulas.

6. Conclusion

Air ions used as a tracer for turbulent dispersion allow high resolution. An experiment with 8 sensors located close together reveals a concentration structure with high variability with pockets of undiluted source material even after 37.5 m transport. An analysis of the concentration frequency distribution in terms of a log-normal distribution yields approximately similar parameters for puffs and a plume. The distribution could well be independent on sample size.

Acknowledgement

The research reported is supported by NATO research grant No. 1307.

References

Cats, G. J. and Holtslag, A. M. M.: 1980, 'Prediction of Air Pollution Frequency Distribution, Part I. The Log-Normal Model', *Atmos. Envir.* **14**, 255–258.

Csanady, G. T.: 1973, *Turbulent Diffusion in the Environment*, D. Reidel Publ. Co., Dordrecht, Holland, 248 pp.

Hønnåshagen, K.: 1980, 'Electronic Problems During the Experimental and Data Processing Phases of the Ion Turbulent Dispersion Project', in *The Shifting Concentration Structure Method for Analyses of Dispersion-Dependent Phenomena*, FFI/Rapport-80/3007, Kjeller, Norwegian Defence Research Establishment.

Jones, C. D.: 1977, 'Ion Concentration Variations at Short Distances Downwind of Continuous and Quasi-Instantaneous Point Sources', *Pestic Sci.* **8**, 84–95.

Lillegraven, A.: 1980, 'Fitting of Log-Normal Distributions to the Concentration Records from Turbulent Dispersion Experiments', in *The Shifting Concentration Structure Method for Analyses of Dispersion-dependent Phenomena*, FFI/Rapport-80/3007, Kjeller, Norwegian Defence Research Establishment.

Storebø, P. B.: 1975, *Proposal for Improved Empirical Models for Atmospheric Puffs and Plumes*, Note written at Chemical Defence Establishment, UK.

Storebø, P. B.: 1980, 'A Method for Analysing Turbulent Dispersion Problems with Attention Paid to Shifting Concentration Structures', *Proc. Second Joint Conf. on Applications of Air Pollution Meteorology*, New Orleans, American Meteor. Soc., Boston, 450–454.

Jones C. D. (1983).

On the structure of instantaneous plumes in the atmosphere.

J. Haz. Mat. **7**, 87 - 112.

Journal of Hazardous Materials, 7 (1983) 87—112
Elsevier Scientific Publishing Company, Amsterdam — Printed in The Netherlands

ON THE STRUCTURE OF INSTANTANEOUS PLUMES IN THE ATMOSPHERE

C.D. JONES
CDE Porton Down, Salisbury, SP4 0JQ (Gt. Britain)
(Received March 30, 1982; accepted May 21, 1982)

Summary

Current methods for the analysis and prediction of the concentration fluctuations occurring in substances dispersing in the atmosphere are reviewed particularly with reference to existing experimental data.

The results obtained from a series of very high time resolution concentration measurements conducted in neutral conditions over flat terrain using specially developed tracer techniques are then examined in detail. Various statistical, and other parameters, are formulated and quantified in an attempt to characterize the observations. The implications for dispersion modelling, particularly in situations where fluctuations are important i.e. in the evaluation of risks due to flammable, toxic or reactant materials and of nuisance due to malodourous substances are then considered.

It is evident that risk/hazard analyses based on time mean concentrations distributions can at best be misleading and at worst result in serious underestimation when fluctuation-sensitive phenomena are involved.

1. Introduction

The use of Gaussian (or similar mathematical form) descriptions for the crosswind and vertical concentration/dosage profiles in atmospheric dispersion models is a well established and widespread practice and the fact that such profiles arise in an apparently natural way as solutions to the 'equations of turbulent diffusion' confers upon them a degree of respectability which is undeserved. The reason for this is that these equations are not precise mathematical representations of physical phenomena: they are based on an analogy not of mechanism but rather of result between molecular and turbulent dispersion processes. Nevertheless in some situations, generally those in which the longer term aspects of exposure to pollutants are of concern and the effect of concentration upon 'response' is linear, predictions based on these techniques yield results which accord reasonably well with experiment and are thus helpful. However the uncritical acceptance of the molecular: turbulent dispersion analogy can, if applied inappropriately, give rise to very misleading estimates of the concentration fields expected in the vicinity of pollutant sources. Closer scrutiny reveals that the disparity between prediction

and reality can be traced to the fact that the implied physical similarity between molecular and turbulent dispersion processes can only be a sensible hypothesis when the spatial scale of relevance to the problem (i.e. the size of the dispersing cloud and/or that of the detector) is considerably greater than the elements (i.e. eddies) actually causing the dispersion. If this is not so then those eddies which have scales of similar size to the cloud itself or are larger will cause it to move bodily thereby resulting in large, rapid and unpredictable (at least on a conventional Gaussian model) fluctuations in concentration.

Hence, if it is the 'instantaneous' concentration experienced at a particular point which is important, as for example it would be in examining a flammability, toxic or malodour problem, then it is vital to bear in mind the limitations of most of the currently used methods of analysis. Whilst some allowance can be made by introducing semi-empirical adjustments to the model predictions to account for the physical fact that instantaneous concentrations can, and do, exceed Gaussian mean values by substantial factors such a procedure is not satisfactory. This is because an approach of this type avoids any attempt to quantify the *mechanism* of the processes responsible for causing the fluctuations. The main theoretical difficulty arises from the fact that material released from a source is initially advected away in the direction of the instantaneous wind vector and this latter varies continuously in magnitude and direction. (This very obvious feature of atmospheric dispersion is immediately confirmed by a few minutes' observation of an industrial stack or similar plume.) Also evident, and of considerable importance because it implies the existence of high local concentrations, is that the plume *itself* is frequently not very well dispersed but consists of a long sinuous volume of material.

Consequently, if the concentration of plume material is measured with a sufficiently rapid response detector a series of relatively short bursts of high concentration are seen interspersed with generally rather longer intervals during which the concentration is either zero or very close to zero. Figure 1 illustrates this point. Csanady [1] refers to this phenomenon as intermittency (note that Townsend [2] introduced this concept, in relation to a turbulent velocity field, much earlier) and suggests that it may be quite normal for the concentration to be zero at a given sampling point for up to 80% of the observation time: a feature subsequently confirmed by the writer (Jones [3]) in some recent experiments. Alternatively, if the *time averaged* concentrations are observed, using for example dosage type receptors at a set of locations distributed in a horizontal arc about the mean wind vector (i.e. mean plume axis) then, provided the sampling time exceeds the longest significant eddy scale ($\sim$ 15 mins) an *approximately* Gaussian spatial profile of dosage will probably result. It was of course this discovery which reinforced the development and exploitation of the analogy between molecular and turbulent phenomena discussed above.

Recognition, particularly recently, of the inherent deficiencies in current

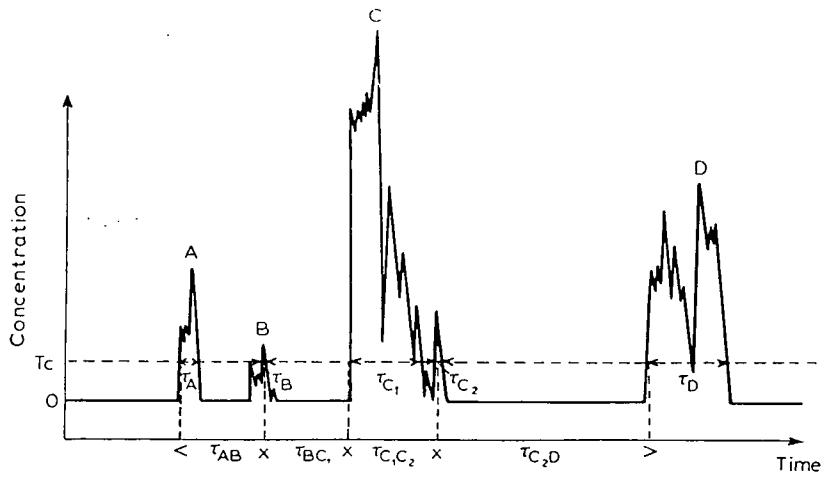

Fig. 1. Illustrating the use of CAAS (Concentration Amplitude Analysis System) and SHADA (Signal Height and Duration Analyser).

dispersion modelling procedures has stimulated a reexamination of the experimental data available in order to develop physically more realistic approaches to the analysis of fluctuation sensitive phenomena. However, lack of high resolution sampling techniques has hindered the exploration of this aspect of atmospheric dispersion and very little data exist on which to base more refined models. Certainly many qualitative observations (and remarks) have been made concerning the fluctuating properties of plumes, but apart from a few isolated exceptions (see next section) there has been no attempt to develop theories capable of explaining or predicting fluctuation structure.

In the last two or three years however several atmospheric dispersion programmes have been carried out by the writer and others [e.g. 3, 4] using a novel tracer method capable of better than 10^{-2} s resolution. These two earlier papers have outlined some of the more basic aspects of instantaneous plume structure and have produced direct evidence for the existence of heterogeneities in concentration down to very small scales — a few centimetres — thereby implying very large spatial gradients of concentration. This paper re-examines the nature of these and other features in a more penetrating manner and in particular attempts to derive reliable quantitative data from the experimental results which are more directly applicable to modelling. It should be emphasised however, that the intention cannot be to promulgate definitive information on the fluctuations and the parameters describing them because this would require a much larger experimental data base than is currently available before precise statements could be made. Rather it is to provide reasonably reliable indications of the type of distributions that are likely to be encountered in practice.

2. Earlier experimental investigations and their impact on theories of cloud structure

The theoretical formulation of rigorous descriptions of atmospheric

plume and puff structure can only be contemplated in statistical terms. It is possible that, eventually, realistic estimates of peak concentration and related 'instantaneous' parameters will be feasible at least in reasonably straight forward situations. It will, however, remain difficult to ascribe confidence levels to such estimates and it is to be expected that a substantial proportion of the theory will develop in an ad hoc and empirical fashion to explain what is observed. Many of the problems in formulating statistical models of plume or puff structure are related to two characteristic features of atmospheric turbulence: namely its spatial inhomogeneity (e.g. arising from surface irregularities) and its temporal non-stationarity (due mainly to synoptic and diurnal influences). These properties, whilst implicit of course and effective in the earliest dispersion experiments, were not so relevant then because of the preoccupation with dosages and long term average concentration distributions.

A consequence of the above is that the fundamental concept underlying the analysis and characterisation of instantaneous concentration properties has therefore, of necessity, to be that of the ensemble, rather than a spatial or temporal, average. Clearly one cannot in practice perform ensemble type experiments*, i.e. to release material and observe the ensuing concentration at a series of points in space-time (the latter in the relative sense) repeatedly. Reasonable, and indeed the only practical, alternatives one can conceive are experiments in which, with spatially homogeneous conditions, many sources and detectors are deployed sufficiently well spaced for the results to be statistically independent and the concentrations noted at a given time; or, in temporally stationary conditions, the statistics could be built up by observing the concentration at a single detector as a function of time. Obviously the latter is the preferred option since it is far less demanding on experimental resources; however, there remains the inherent difficulty of developing an acceptable criterion for defining stationary or at least quasi-stationary conditions. In practical terms this necessitates avoiding, in clear weather, the hours near sunrise and sunset when the stability undergoes marked and rapid changes. Also conducting experiments in which mesoscale (e.g. showers, thunderstorms) and synoptic (e.g. fronts) events are taking place is precluded.

Chatwin [5], in his 1982 paper, discusses a mathematical analysis which although intended for puffs, can be satisfactorily extended to plumes by suitable redefinition of the parameters concerned. Retaining his notation, consider the concentration at a point x in coordinates relative to the source at a time t. Suppose the value of concentration observed in the r^{th} experiment is $\Gamma^{(r)}(x, t)$ then, by definition, the ensemble mean,

$$C(x, t) = \lim_{n \to \infty} \frac{1}{n} \sum_{r=1}^{n} \Gamma^{(r)}(x, t) = \overline{\Gamma}(x, t) \tag{1}$$

*i.e. in the field, however one could conceive and enact experiments of ensemble type in the laboratory and then attempt to apply the results to atmospheric situations by invoking appropriate scaling laws.

In *completely* stationary conditions the ergodic hypothesis may be invoked and the ensemble mean can be expressed in the form of a time integral,

$$C(x) = \frac{1}{T} \int_0^\infty \Gamma\,(x,\, t)\, \mathrm{d}t, \tag{2}$$

which is independent of t.

Equations 1 and 2 are not informative regarding the fluctuations per se and to specify their characteristics it is necessary to investigate the behavious of the higher moments of $\Gamma\,(x,\, t)$, and strictly this should be done in the ensemble context.

Prior to proceeding it is helpful to consider in more detail how the mean concentration is actually accumulated over a period of time. Observations with high-resolution tracer techniques by Barynin and Wilson [6], Hadjitofi and Wilson [7] and Jones [8] downwind of various types of atmospheric sources have unequivocally shown the intermittent nature of $\Gamma\,(x,\, t)$. In the simplest situation of a single detector it was found that for a significant fraction, normally the majority, of the observation period the concentration was zero — i.e. the detector was not in the plume at all. (Recognition of this fact earlier led Gifford [9] to propose his fluctuating plume model which was, however, based on 'Gaussian' concpets.) In addition, the experiments indicated the presence of considerable amounts of fine structure actually within the plumes themselves and, even at 5 km downwind from the source, heterogeneities of remarkably small-scale were found.

Taken together these experimental findings convey a substantially different impression of a plume than would be deduced from Gaussian models. In particular, due to the discontinuous nature of the concentration field, the use of conventional descriptors of fluctuation characteristics (i.e. the higher statistical moments) is somewhat questionable. Never theless, providing such techniques are applied and interpreted intelligently, they are capable of specifying certain features of the fluctuations in a reliable and therefore helpful manner. In stationary conditions the n^{th} central moment, denoted by $M_n(x)$ is defined as

$$M_n(x) = \frac{1}{T} \int_0^\infty [C(x) - \Gamma\,(x,\, t)]^n\, \mathrm{d}t \tag{3}$$

It is often convenient to express the second moment (i.e. the fluctuation variance) in non-dimensional form so that direct comparisons between experiments are facilitated. One thus defines the relative intensity of the fluctuations, $I(x)$, as

$$I(x) = \sqrt{M_2(x)}/C(x) \tag{4}$$

Normalized third and fourth moments, the skewness and kurtosis respectively, also provide valuable information on the character of the fluctuations — i.e. their shape and "peakiness". Note, however, that certain problems can arise in the determination of these moments, particularly the latter, because lengthy observation periods are required in order to establish stable values (see Lumley and Panofsky [10]) and these are generally precluded by the need to collect data in as near stationary conditions as possible.

One aspect of the observed concentration data that necessitates particular consideration is the approach to handling the intervals, which are often lengthy, when the concentration is zero or at least less than some very small value. It is evident that for the calculation of the second and higher moments inclusion of very many zeroes would tend to confuse the results by introducing large contributions into the integrals which had nothing whatever to do with the nature of the *fluctuations themselves.* Hence a pragmatic approach was taken, which though somewhat hard to defend rigorously, did enable realistic values of these moments to be obtained. This was achieved by adopting a conditional sampling procedure in which integration was only carried out when $\Gamma(x, t) > 0$*.

Concentration-frequency distributions provide additional information on plume structure and, in many cases, logarithmic-normal cumulative probability distributions have been fitted to sequences of observed data [e.g. 1, 11]. Although the theoretical justifications for compliance with this particular distribution are fairly vague there is, as yet, no other distribution which appears to offer a better fit to the available data. An argument against the use of the log-normal distribution is that all the zero values of concentration have to be discounted before the fluctuation data can be fitted — hence this distribution really describes a distribution *within* the plume and not that experienced at a particular sampling point.

The experiments of Barynin and Wilson [6], using methyl mercaptan (CH_3SH) as the 'tracer' and fast-response detectors revealed various interesting features about odour perception which relate directly to plume structure. Rapid rises in concentration were found to be especially noticeable when compared with similar variations occurring over a longer time interval. This is significant because the leading, i.e. oncoming, edges of plumes (and puffs) frequently exhibit very rapid increases in concentration (probably reinforced by the shear processes occurring) and hence olfactory response appears well adapted to providing the maximum warning of the arrival of unpleasant (or, more importantly, dangerous) airborne material. It was also found, and this is known from everyday experience, that response declines on prolonged exposure to odour but is restored if the stimulus is temporarily withdrawn and then re-presented. Thus, to summarize, the nose is well attuned to respond efficiently to the two most significant features of instantaneous concen-

*Note: Single point measurements are the only type discussed in this paper; multi-point statistics will form the subject of a later publication.

tration fields: i.e. the presence of large spatial gradients and the existence of considerable intermittency.

The rate of presentation of stimuli is important not only from the odour nuisance assessment standpoint but also in the study of a variety of biological processes, e.g. the insect pheromone sex-attractant mechanism, as discussed by Murlis and Jones [4]. In these processes it may be possible to consider the response in a quantized, possibly even binary, fashion — i.e. nothing happens below a given threshold concentration whilst some particular activity occurs once that threshold is exceeded. (Certainly in the human case the threshold of odour perception varies considerably among individuals and, thus in establishing the likely level of odour nuisance, a more sophisticated analysis will be required.)

The implication of these findings is therefore that a rather different type of data analysis is required than provided by the approaches outlined earlier. Information on the temporal, as opposed to the amplitude, structure of the fluctuations in the form of peak duration and, just as important, gap-length distribution might therefore provide a basis on which to develop more realistic descriptions of plume structure appropriate for odour nuisance assessment etc. In effect the analysis involves investigating the relation

$$\sum_{i=1}^{n_{pi}} t_{pi} + \sum_{j=1}^{n_{gj}} t_{gj} \; (=T) \tag{5}$$

where T is the total observation time, t_{pi} the duration of the ith peak, n_{pi} the peak number, t_{gi} and n_{gi} being the corresponding parameters for the gaps.

Figure 1 illustrates the type of analysis that is implied (for practical reasons a slightly different procedure had to be employed) and also indicates that the operations expressed by equation 5 are only meaningful in relation to a given threshold level of concentration. The analysis was extended by firstly examining the frequency distributions of the t_{pi}'s and t_{gj}'s themselves and secondly by performing the operation at a sequence of threshold levels by automatic means (see Section 4).

It would be anticipated that both the maximum concentration and its gradient would steadily diminish with distance from the source. However, this trend is not really evident in the data, such as it is, and as mentioned earlier Barynin and Wilson observed substantial variations of sulphur dioxide concentration occurring in time intervals of ~ 1 s at 5 km downwind of a power station stack. Chatwin and Sullivan [12] have attempted to explain these and related observations by considering the physical mechanism by which turbulence causes dispersion. In their view the turbulent flow fields act in a complex way, but always so as to enhance the effect of molecular dispersion, but note however that it is only the *latter* which has the ability to *change* concentration (defined on the continuum scale). The fundamental

feature of turbulence is that the kinetic energy of the fluid motion is transferred progressively from larger to smaller scales by various mechanisms, but particularly by vortex stretching (Lumley and Tennekes [13]) — the three dimensional nature of which tends to reduce the anisotropy of the turbulent velocity components at the smaller scales. Eventually as the velocity scales become very small, about 1 mm in the atmosphere, the velocity gradients are sufficient to cause a significant destruction of energy by viscous effects and thus the turbulent energy is ultimately dissipated as heat. Hence any passive (i.e. not affecting the velocity field) material released into a fluid medium becomes involved in this complicated system of motion and the net result is generally that the material is drawn out into contorted sheets and strands — often being stretched in one direction and compressed in another. After a time the cloud of material will thus resemble a loosely wound ball of wool and, whilst its *overall* size will steadily increase, the rate of diffusion within the individual strands and sheets is slow because it depends solely on molecular diffusion. Hence the net effect of the turbulence is not actually to reduce the concentration gradients but rather to expand and regenerate the 'internal' surface area of the cloud and, by effectively *increasing* the gradients of concentration, to augment the molecular diffusion process. In many cases this latter effect is so slow that it does not preclude the existence of very high instantaneous concentrations (and gradients) at considerable distances from a source and in practice it is possible that virtually undiluted material may be observed up to several hundred metres away.

These authors also point out that spatial structure will occur down to very small scales and, even in atmospheric processes, this means fluctuations occurring over distances of as little as 1 mm. No measurements approaching this resolution have yet, to the author's knowledge, been reported in the atmosphere, but Birch et al. [14] have undertaken some interesting laboratory studies in which considerable structure was observed at these and even smaller scales. However, their results were obtained using a small methane jet (as opposed to a passively dispersing plume) and, although certain numerical results they obtained correspond quite well with those obtained by the author [2] in the atmosphere, it would be unwise to assume too close a parallel between the two situations. In the jet experiments meandering did not of course occur (since there was no very low frequency turbulence) and thus any contribution to the observed intermittency from this cause would have been excluded.

A rather different approach to the analysis and production of concentration fluctuations has been proposed by Csanady [1] and is based on the existence of an analogy between the behaviour of the variance of the concentration fluctuations and that of turbulent kinetic energy. Whilst it is plausible to expect that some relationship between these parameters will prevail it is rather difficult to justify any formal mathematical connection. This is because velocity is a vector quantity and directly related to momentum transfer (due to cross-correlation between its components) whilst the concentration

is a scalar and entirely decoupled from momentum or energy transfer processes. Csanady develops the concept mathematically and obtains an equation connecting the rate of disappearance of concentration fluctuations with that of the turbulent energy decay time and a gradient-transfer coefficient. This idea is then extended by applying the concept of self-similarity so that, in principle the concentration fluctuation variance can be predicted as a function of distance downwind and from the plume axis. In practice however, the complications of inhomogeneity in the turbulence field and of meandering, causing intermittency, make it difficult to see how this approach, notwithstanding its appeal, can be satisfactorily applied in anything but a restricted range of situations.

Turning to the future, it would seem that the statistical approach is most likely to offer the most scope as a rational basis for fluctuation description. Generally, one will be faced with non-stationary conditions and thus adjustment and probably considerable adaptation of the conventional methods of statistics will be essential if the maximum flexibility and realism in modelling is to be achieved. Horowitz and Barakat [15] discuss this aspect in relation to the estimation of the extreme values of concentration that can be expected and two procedures, based on the supposition that some fluctuation data already exists, are suggested for analysis. Despite this limitation, both procedures point the way in which it is felt the subject will develop in the next few years and thus merit attention.

The first, and somewhat difficult, method described is to actively search for and identify the non-stationary stochastic processes operating that can explain the data. As an indication of the type of philosophy required one might for example introduce diurnal, weekly or even seasonal trends into test models and check whether these improved the accuracy of matching and thence prediction. However, it is evident that a large data base may need to be accumulated in order to decipher all the non-stationary effects present — for only in this way could reliable estimates of extreme values be made.

An alternative, and in the majority of situations, more feasible approach is to select a section of the data which fulfills reasonable stationarity criteria and employ 'traditional' methods of analysis. Once some familiarity with the vagaries of fluctuation behaviour has been obtained one could then reasonably attempt to 'add on' the fluctuation statistics to the particular circumstances for which predictions were required. It is suggested that this latter method, if coupled with the physical concepts of the turbulent dispersion process proposed by Chatwin, may offer the best chance for making significant progress. The necessity to acquire enormous amounts of data in presumably a wide variety of dispersion environments to fulfil the first suggestion is clearly rather impractical. It is therefore with the latter type of approach in mind that the results presented later in this paper are discussed.

3. Outline of experimental method

The experimental techniques developed to release tracer material (in this case negatively ionized air) in a controlled manner and monitor its concentration downwind with the requisite time resolution have been described in detail earlier [8, 16—18] and therefore are only outlined here for the sake of completeness.

At first sight the choice of ionized air as a tracer for atmospheric dispersion investigations may seem inappropriate, nevertheless, provided its limitations are appreciated it can form the basis of a very effective, convenient and cheap system for obtaining information about plume and puff structure. Ionized air can be readily produced by exploiting the properties of corona discharges as discussed by Loeb [18], and, in the experiments reported here, was generated by creating a corona in the vicinity of fine wire (10^{-5} m diameter) mounted coaxially within an earthed aluminium cylinder (diameter 0.012 m, length 0.19 m). A copious and constant supply of ions was provided by maintaining, in conjunction with the —3 kV bias to the fine wire, a current of air along the axis of the device of ~ 3 m s^{-1}. The ion current output was —16 nA.

The ionized air concentration was determined by drawing air, at a carefully controlled rate, through a suitably biassed coaxial capacitor arrangement and monitoring the current with a sensitive amplifier. The ion collector inlet diameter was 0.036 m and the volume flow rate of air 6.67×10^{-3} m^3 s^{-1}. With careful choice of amplifier design and biassing arrangements it proved possible to obtain good sensitivity (~ 10^{-10} C m^{-3}) and a response time considerably better than 10^{-2} s. In these experiments 1 volt was equivalent to charge concentrations of 151.35, 40.545, 15.555 and 4.995 n C m^{-3} at 2, 5, 10 and 15 m downwind from the source, respectively. The concentration fluctuations were recorded on an FM instrumentation tape recorder for subsequent laboratory analysis.

4. Note on data analysis systems

Two essentially pragmatic methods have evolved for this purpose and although both are automated neither involves excessively complex hardware. The first system senses when the ion concentration (i.e. its equivalent voltage level) exceeds a preset threshold value upon which a counter/timer (incremental time 10^{-3} s) is actuated and continues until the signal voltage falls below threshold. Counting is cumulative and thus the total time the signal exceeds a given value for an entire field experiment can be determined (see Fig. 1). This sytem will be subsequently referred to as CAAS — Concentration Amplitude Analysis System. Repetition of the playback procedure for a progressively increasing sequence of threshold levels enables the concentration amplitude statistics to be built up and, in particular, frequency distributions to be calculated.

A second method of analysis, developed later, is based on a different, and complementary concept which involves the temporal (as opposed to amplitude) structure of the fluctuations (see Section 2). Again preset threshold sensing devices (ten in total) are employed but are arranged to examine the mark:space ratio(s) of the signal and here two distinct modes of operation are possible. In the first the 'mark' is examined and the duration of the concentration bursts are measured and then automatically accumulated in time 'bins'. These bins, 32 in all, are arranged in the geometrical progression (with $\sqrt{2}$ multiplier): 0.015 s, 0.015 s—0.022 s, 0.022 s—0.030 s . . . . . 5.79 min—8.19 min, > 8.19 min and thus cover most, if not all, of the time scales important in fluctuation studies. This entire sampling process can now be accomplished automatically, having been done manually originally, using an instrument developed specifically for the purpose — SHADA (Signal Height and Duration Analyser). Readout of the number of events in each time bin is a simple procedure and merely involves monitoring the memories with a digital voltmeter (1 bit ≡ ~ 3 mV and so is easily resolvable). Alternatively the number distribution from all 32 bins can be automatically 'emptied' onto a chart recorder or oscilloscope if this is more convenient. The second type of analysis offered by SHADA involves a similar examination of the gap duration statistics — subsequently referred to as the burst return period distribution.

5. Experimental results and discussion

5.1 Experimental aspects

The dispersion experiments discussed were carried out over unobstructed moorland terrain in Northern England. Meteorological conditions were heavily clouded and this, in conjunction with a mean wind speed of 5 m s^{-1}, indicated close to neutral stability. (Note that the choice of site was dictated entirely by topographical considerations as the equipment is completely portable and independent of mains power.) Negatively ionized air was released from the source (described in Section 3) placed at a height of 1 m above the earth's surface; equivalent to approximately 0.75 m above the top of the heather. Ion concentrations (at 1 m height) were sampled and recorded at distances of 2, 5, 10 and 15 m downwind in a sequence of four experiments each of 48 min duration.

Strenuous attempts were made to position the ion collector as close to the mean wind line downwind of the ion source as possible although fulfilment of this ambition is usually a matter of luck rather than judgement! Nevertheless the meteorological and stability conditions were sufficiently stationary to require only very minor angular adjustments (i.e. a few degrees) of the source-collector line during the sequence of experiments. Hence the results obtained should be helpful in establishing some 'baseline' parameters for simple terrain situations.

It is perhaps worth mentioning that although only four relatively short ex-

periments were carried out, implying that the numerical results presented must be at least somewhat tentative, this is to a considerable extent countered by the very high temporal resolution employed. Thus, for each 48 min period, about 2.7×10^5 data points were collected — a figure which certainly compares favourably with the majority of other diffusion investigations!

5.2 Data processing and main results

5.2.1 Results obtained using CAAS and SHADA. The intermittency, here defined as the fraction of the observation time in which the concentration was zero, was determined by playing-back the data tapes through CAAS with its threshold adjusted to a nominal zero. It was of course impossible in practice to employ a true zero voltage for this purpose because the inevitable presence of a small amount of noise and drift on the ion concentration signal would have produced spurious counts and thus led to misleading and inconsistent results. It was found, by trial and error, that for reproducible and accurate (as compared with a manual analysis of chart records) values of intermittency a threshold level of +25 mV was required. Since typical peak values of the signal were in the region of 1 V this seemed acceptable.

The amplitude-frequency distribution was determined by using CAAS with progressively increasing threshold levels (25 mV increments) up to the

TABLE 1

Mean concentration, taken over 48 minutes, as a function of distance from source (unfiltered data)

Distance downwind (m)	2	5	10	15
Mean concentration ($\bar{\Gamma}$) (nC m^{-3})	4.21	0.525	0.239	0.159

TABLE 2A

Processed data from the 2 m downwind experiment[a]

Parameter	Unfiltered	With low pass filtering				
		30 Hz	10 Hz	3 Hz	1 Hz	0.3 Hz
σ_Γ (nC m^{-3})	12.6	11.0	8.71	5.60	3.77	2.40
S_Γ	4.95	4.87	4.62	4.31	4.18	3.93
K_Γ	30.2	29.6	27.6	25.5	23.2	21.5
$\hat{\Gamma}/\bar{\Gamma}$	36.4	31.9	25.6	18.4	13.9	6.74
I (%)	85.2	82.7	80.9	78.8	79.1	86.5

[a] σ_Γ standard deviation of ion concentration.
S_Γ skewness of ion concentration.
K_Γ kurtosis of ion concentration.
$\hat{\Gamma}/\bar{\Gamma}$ peak:mean.
I (%) percentage intermittency.

TABLE 2B

Processed data from the 5 m downwind experiment

Parameter	Unfiltered	With low pass filtering				
		30 Hz	10 Hz	3 Hz	1 Hz	0.3 Hz
σ_Γ (nC m^{-3})	2.21	2.08	1.83	1.39	1.03	0.722
S_Γ	7.18	6.46	6.27	5.47	4.24	3.29
K_Γ	66.6	53.3	51.4	39.3	23.7	13.0
$\hat{\Gamma}/\Gamma$	78.2	62.7	58.9	43.4	22.2	10.6
I (%)	90.1	87.9	82.6	84.8	81.0	82.9

TABLE 2C

rocessed data from the 10 m downwind experiment

Parameter	Unfiltered	With low pass filtering				
		30 Hz	10 Hz	3 Hz	1 Hz	0.3 Hz
σ_Γ (nC m^{-3})	0.818	0.765	0.679	0.536	0.395	0.279
S_Γ	8.82	7.82	7.48	5.62	4.49	3.50
K_Γ	129	97.0	89.8	47.0	30.6	14.9
$\hat{\Gamma}/\Gamma$	112	90.4	79.0	48.0	28.5	12.2
I (%)	83.7	83.9	85.2	83.7	83.7	85.2

TABLE 2D

Processed data from the 15 m downwind experiment

Parameter	Unfiltered	With low pass filtering				
		30 Hz	10 Hz	3 Hz	1 Hz	0.3 Hz
σ_Γ (nC m^{-3})	0.346	0.329	0.310	0.254	0.211	0.179
S_Γ	5.38	5.06	4.79	4.26	3.91	4.12
K_Γ	42.1	38.0	32.1	23.3	19.6	23.0
$\hat{\Gamma}/\Gamma$	43.5	42.7	34.1	19.2	13.7	10.6
I (%)	71.0	72.8	73.5	72.1	68.6	71.2

highest peak level on the particular recording involved and the parameters presented in Tables 1 and 2 were calculated. Also included in the latter table are the results of a later analysis in which the procedure was repeated with a high quality (48 dB attenuation per octave) low pass filter interposed between the tape recorder output and the CAAS input. The main objective of this was to evaluate, quantitatively, the effect of detector response time on the nature of the concentration fluctuations perceived, see also Figs. 2, 3, 4 and 5.

In theory the mean value of concentration should be independent of filtering, but in practice, mainly due to the finite threshold increment, this

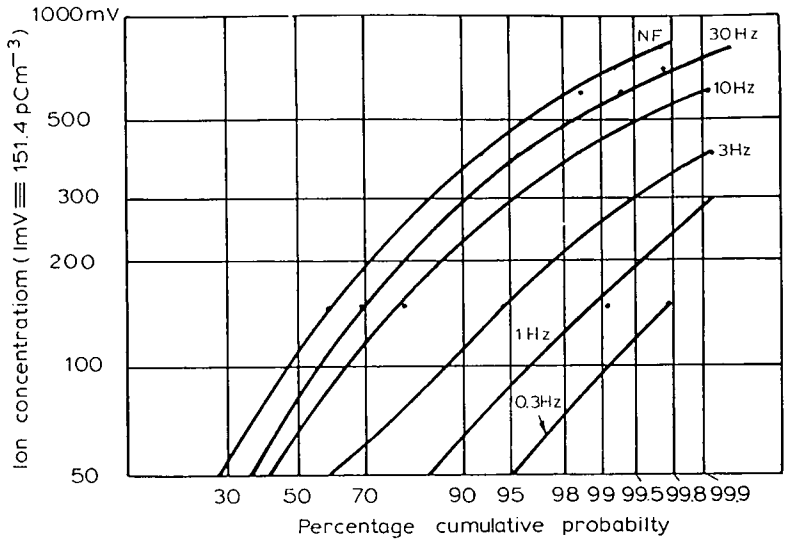

Fig. 2. Ion concentration frequency distributions at 2 m downwind.

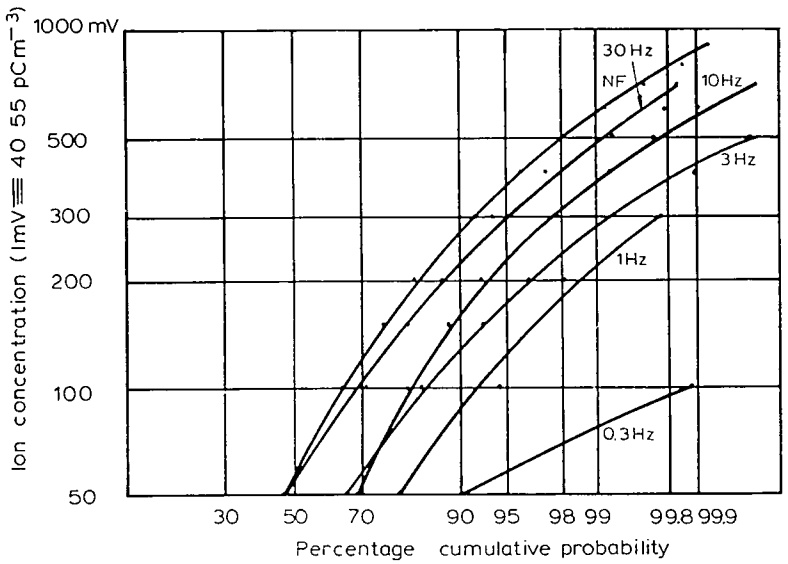

Fig. 3. Ion concentration frequency distributions at 5 m downwind.

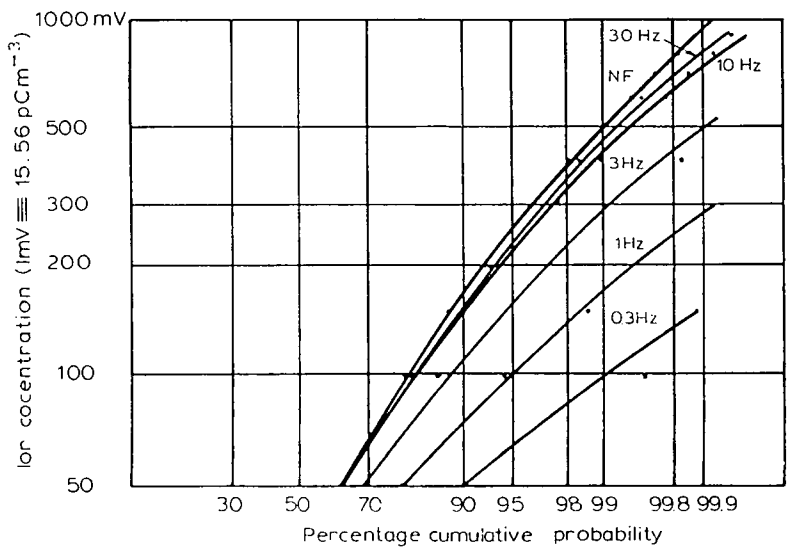

Fig. 4. Ion concentration frequency distributions at 10 m downwind.

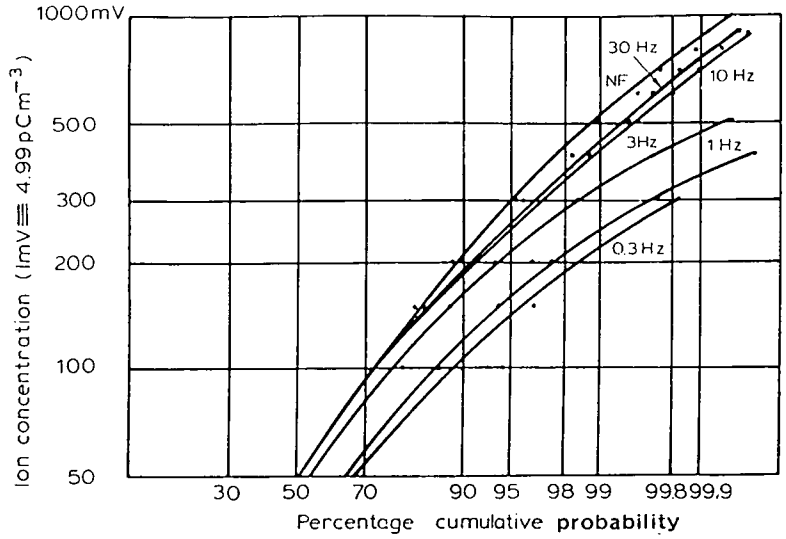

Fig. 5. Ion concentration frequency distributions at 15 m downwind.

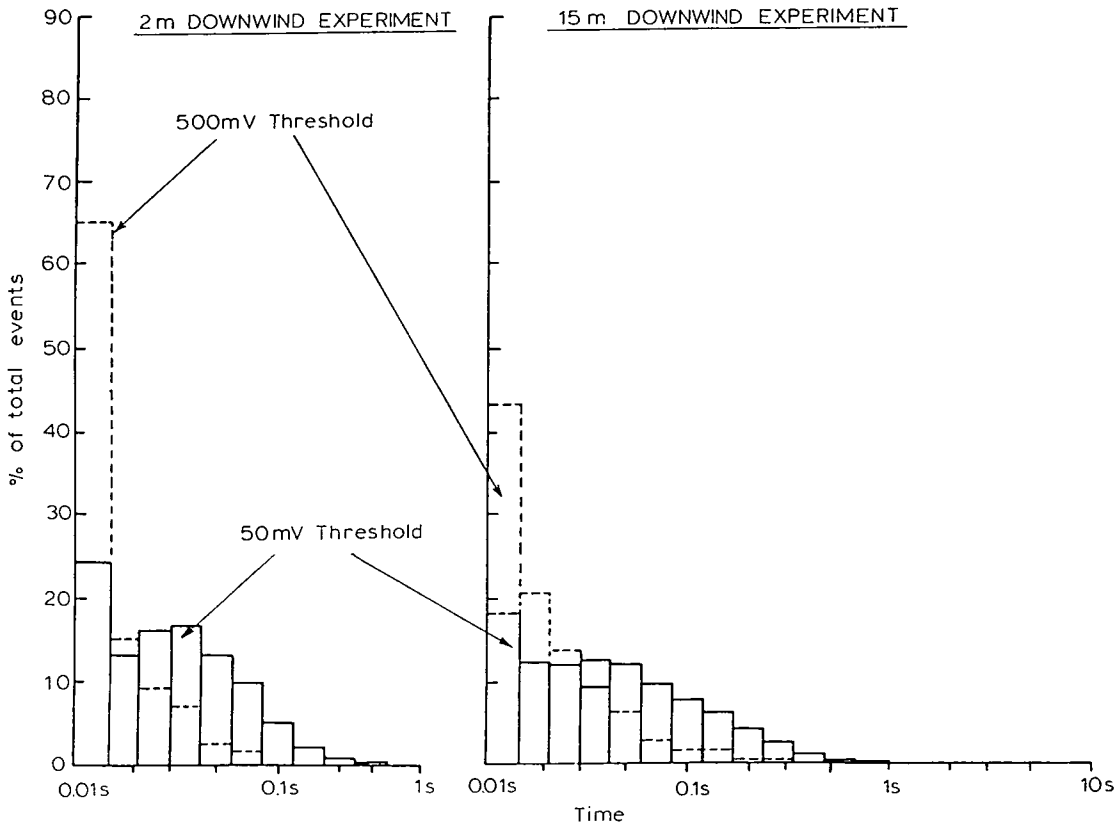

Fig. 6. Burst length distributions obtained using 'SHADA'.

was not quite so. However the discrepancy between means obtained with various filtering bandwidths was never greater than about 10% and this was regarded as acceptable.

A representative selection of results obtained with SHADA is presented in Figs. 6, 7 and 8. Table 3 below shows, in addition, the behaviour of the event total (i.e. the sum of the event counts in each of the time bins) for the

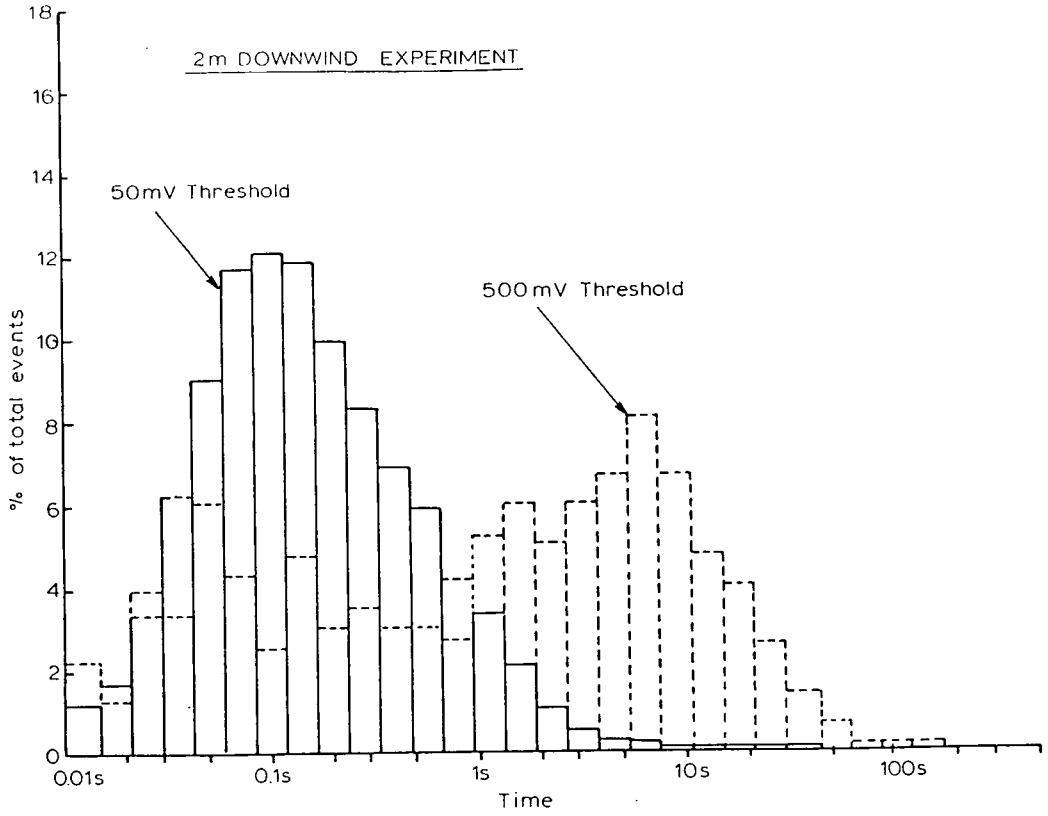

Fig. 7. Burst return period distributions obtained using 'SHADA'.

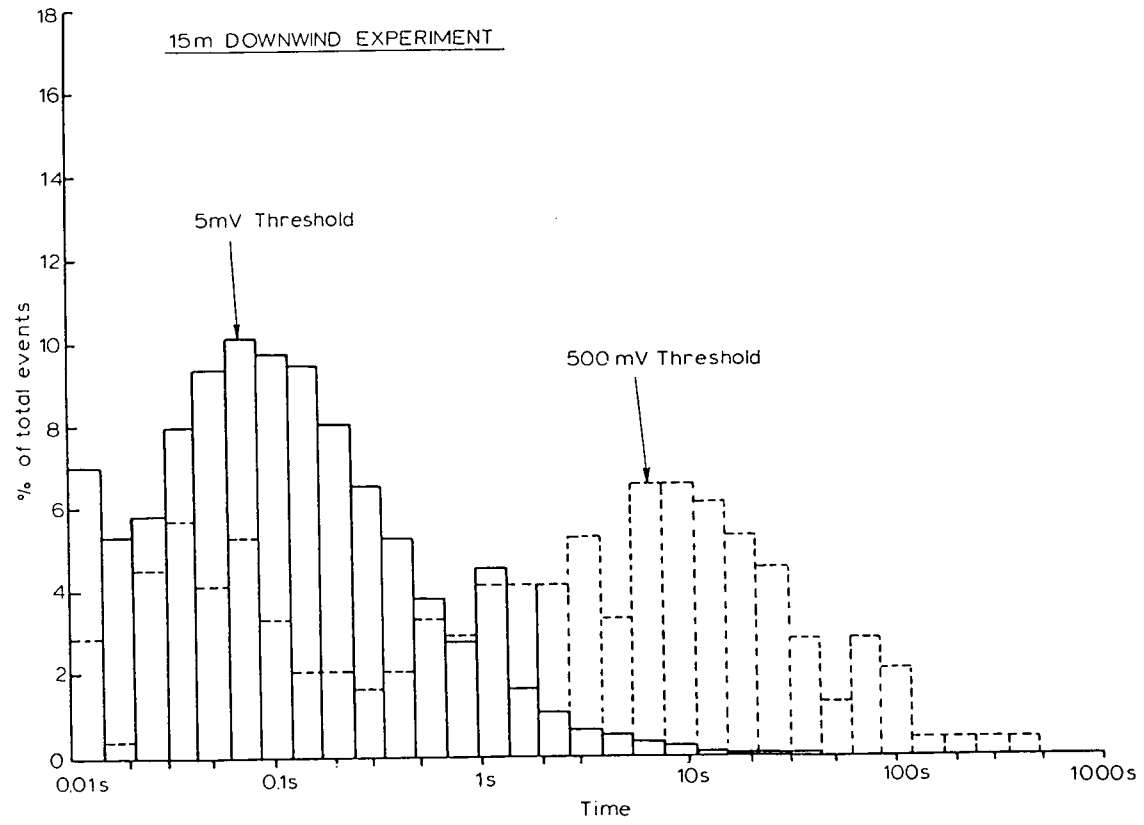

Fig. 8. Burst return period distributions obtained using 'SHADA'.

TABLE 3

Total event count as a function of threshold voltage

Threshold level	Total even count			
(mV)	2 m	5 m	10 m	15 m
50	9132	2892	4242	7750
100	7464	2221	2219	4583
200	5075	1352	1078	2322
300	2873	723	500	830
400	1633	435	310	494
500	625	211	155	245
800	49	23	38	46
1000	3	5	13	7
1500	0	0	2	0

experiments over all the threshold levels used. The values given in the Table were derived from the burst length data.

5.3 Discussion

5.3.1 Mean concentration. The discontinuous nature of the concentration fluctuations suggests that it could be instructive to define two distinct types of mean. The conventional approach, i.e. to average the observed values over the entire experimental period, leads to the results in Table 1. However, this produces averages which are sensitively dependent on the angular relationship between the detector and the mean wind vector and there is thus a rather unsatisfactory degree of arbitrariness about them. In other words if the detector had been sited, fortuitously, very close to the mean wind line then a higher value of 48 min mean concentration would be obtained than if it had been placed off-axis.

A way of defining the mean concentration*, which at least circumvents this difficulty, is to perform the averaging process only over the intervals when the concentration is non-zero. This approach, which is closely equivalent to finding the average concentration within the plume, yields the results in Table 4, which were obtained using the relation

$$\overline{\Gamma}(\text{plume}) = \frac{\overline{\Gamma}}{1 - \frac{I}{100}} \tag{5}$$

Comparison of Tables 1 and 4 indicates that the decline of mean concentration with distance is rather more regular for the 'in plume' averages:

*Another possibility, which could be examined in future experiments, might be to use several ion collectors, and then interpolate the results to find the position of maximum mean concentration.

presumably this is a result of removing the unpredictable effects of meandering.

TABLE 4

Mean concentration in the plume for the four experiments

Distance downwind (m)	2	5	10	15
$\overline{\Gamma}$(plume) (nC m^{-3})	28.4	5.33	1.46	0.549

5.3.2 'Instantaneous' plume radii. Visual examination of concentration-time records shows several common yet distinct features and this tempts one to try to deduce the actual plume dimensions for the following reasons. Generally, on entering the plume, a very rapid rise in concentration occurs — typically the concentration changing from near zero to a high value within a few tens of milliseconds. Thereafter, although very substantial variations in concentration are usually observed — due to either repeated transections of the plume or the presence of internal structure or more likely both; in a number of cases the concentration appears to remain reasonably uniform well inside the plume. Hence, provided the ion source strength (i) and the mean wind speed ($\bar{u}$), are known, it is theoretically possible to estimate a *mean* 'instantaneous' plume radius, R_{inst}, using the charge conservation principle. Hence

$$R_{inst} = \left[\frac{i}{\pi \, u \, \overline{\Gamma}(\text{plume})} \right]^{1/2} \tag{6}$$

where it has been assumed, and this is substantially confirmed by smoke tracer experiments, that the plume cross-section is approximately circular. Table 5 shows the values of this quantity obtained with $|\,i\,| = 16$ nA and $\bar{u} = 5$ m s^{-1} which were appropriate to these experiments.

In the past [20] it has often been the practice, in order to facilitate modelling and prediction, to fit power laws to the relationship between plume

TABLE 5

Calculated values of 'instantaneous' plume radii

Distance downwind (m)	2	5	10	15
Instantaneous plume radii, R_{inst} (m)	0.190	0.437	0.834	1.36
R_{inst}, corrected for electrostatic expansion: R_{inst} (m)	0.118	0.351	0.762	1.18

width and distance downwind from source. Adopting this procedure here yields a best fit power law, obtained using a least squares regression technique, of

$$R_{inst} = R_0 + 0.087x^{0.996} \tag{7}$$

where R_0 is the plume radius at the release point, i.e at $x = 0$, and thus corresponds to the ion generator outlet radius (0.013 m).

An obvious limitation to the application of eqn. 7 is that it refers to an electrically charged plume and, whilst in fact many industrial stack plumes are very highly charged [20], the result would be more useful if the electrostatic effects could be quantified and then removed. Provided certain assumptions can be justified, and these are not unduly restricted, it is possible to deduce that,

$$R_{turb} = R_0 + Ax^p - \frac{ui}{2\bar{u}^2 \pi \epsilon_0} \int_0^x \frac{dx}{R_0 + Ax^p} \tag{8}$$

as shown in the Appendix. In the equation the constants A and p are those in the power law expansion expression, x is the distance downwind and R_{turb} the corrected radius.

Equation 8 was integrated numerically and the results obtained are also listed in Table 5. As before it is possible to determine best fit values to a modified power law description for the corrected radius and one finds that

$$R_{turb} = R_0 + 0.046x^{1.21} \tag{9}$$

It is noteworthy that the value of the index in this equation considerably exceeds those commonly accepted for the power law expressions for plume expansion — which are generally in the region of 0.8—0.9. However, these are invariably derived from 'mean' plume data and thus cannot really be compared with the present results. Nevertheless it is not likely that the trend expressed in equation 9 can be maintained out to distances much in excess of 100 m or so since, even at that distance, the predicted plume radius (~ 12 m) is somewhat too large. A possible explanation for this discrepancy may be in the relation between the observed range of plume size (i.e. ~ 0.1—1.0 m) and the dominant turbulent energy scales. This ratio would appear to exert a substantial influence on the rate of plume growth and further must in itself be a function of the plume size. In fact Csanady [1] also mentions a rapid growth phase in his discussion of puff dispersion which appears to originate from the same phenomenon.

5.3.3 Statistical moments, intermittency and peak to mean ratios. Tables 2A, B, C and D give values for these parameters as a function of distance from source and also illustrate the effect of low pass filtering. Some not unexpected trends can be discerned, in particular the progressive reduction in σ_I with distance. Note, however, that the corresponding coefficients of variation (or

relative intensity) of the fluctuations vary from 3.03, 4.22, 3.42 and 2.17 at 2, 5, 10 and 15 m respectively and thus fall off much more slowly with distance. (The correlation coefficient between them is in fact —0.59.) Further if the mean concentration *in the plume* is used as the basis for calculating the relative fluctuation intensity then these values become respectively 0.45, 0.42, 0.56 and 0.63. Here the correlation coefficient is +0.94 thus suggesting a slight but systematic increase with distance downwind from the source. (A least squares regression analysis yields the relation $I(x) = 0.02x + 0.39$.)

The ratios between the σ_I's for the unfiltered and 0.3 Hz values are 5.25, 3.06, 2.93 and 1.93 at the four distances downwind the correlation coefficient being, in this case, —0.89. Hence these results appear to be consistent with a systematic shift towards longer scales as dispersion proceeds. However, the more sophisticated and physically realistic descriptions of this process discussed in Section 2 indicate that this may be an oversimplification and the true explanation for the observed trend may be more subtle.

In all the experimental results the fluctuation statistics are markedly positively skewed, typical values being in the region of 7 for the unfiltered data. Note that these values have been normalized by their respective standard deviation raised to third power and thus direct comparisons between experiments are permissible. No very obvious trends with distance are evident, the correlation coefficient being only +0.13, however, a fairly systematic reduction in skewness with increased filtering is apparent.

Similar comments also apply to the kurtosis — the very high values reflecting the 'peaky' nature of the distribution. Again no significant trend with distance emerges, the correlation coefficient being +0.23.

Values of peak to mean concentration ratio were obtained by noting the maximum threshold level (during CAAS processing) at which a non-zero count was maintained. Although the internal clock in this system operates in 10^{-3} s increments, information was only recorded in 0.1 s intervals in order to minimise the risk of any isolated very short duration spurious transients (due to for example a charged dust particle entering the ion collector) producing misleading results. Nevertheless it is theoretically possible for a single peak of only 0.1 s length actually to determine the peak to mean ratio obtained during an entire 48 min experiment. Consequently the numerical values of this ratio tend to be variable and the reader is cautioned not to attach too much significance to individual results. In practice, it usually happens that the peak level occurs two or three times during an experiment — the implication being that 'experiencing' the peak is an unlikely event — typically the probability of doing so being $\sim$ 1 in 10^5. However, even though it is an apparently rare event the fact that such high instantaneous concentrations can occur is obviously important for the accurate assessment of flammable and toxic risks and odour nuisance particularly. (No significant trend of peak:mean with distance is evident; the cross correlation coefficient being +0.13.)

One aspect of considerable theoretical interest concerns the relationship

between the peak concentrations observed downwind and that at release. If concentrations approaching that at source are observed it would lend support to the mechanism of turbulent dispersion put forward by Chatwin and described earlier in Section 2. However, for an electrically charged tracer some form of correction must be applied to compensate for the effects of electrostatic repulsion before comparisons can be made. A convenient method of analysis is to assume that the ion plume spreads by repulsion alone, i.e. there are no additional dispersive processes operative, calculate the ensuing ion concentration using the formula [16],

$$\Gamma(t) = \Gamma_0 \Big/ \left(1 + \frac{\mu \Gamma_0 t}{\epsilon_0} \right) \tag{10}$$

and then compare the results obtained with the peak values actually observed, see Table 6. (In eqn. 10, Γ_0 is the concentration at release and $\Gamma(t)$ that at a time t after release.) Note that in Table 6 the theoretical maxima were calculated with an assumed mean wind speed of 5 m s^{-1}. Hence the estimates could probably be in error by as much as 30% since it is the instantaneous speed which determines the transit time between ion generator and collector.

TABLE 6

Comparison of theoretical maximum ion concentration with those actually observed

Distance downwind (m)	2	5	10	15
Theoretical maximum concentration (nC m^{-3})	110	44.1	22.1	14.7
Peak value observed (nC m^{-3})	153	41.0	26.7	6.92

Nevertheless these results suggest quite definitely that it is possible to observe, occasionally, completely undiluted material at least within 10 m of the source and probably much further. If this is in fact the case, and a more recent series of experiments appears to substantiate this, then again there are implications for many areas of hazard and nuisance assessment.

5.3.4 Cumulative concentration probability distributions. Figures 2, 3, 4 and 5 show the distributions obtained at the four distances for each of the six bandwidths used. These distributions are plotted in terms of mV rather than in ion concentration units — see the conversion factors in Section 3. Note, that in developing these distributions, non-zero values of concentration have been discounted, because of the inherent difficulty of handling zero quantities on a logarithmic scale. Some curvature is apparent on the figures suggesting that adherence to the log—normal distribution is by no means perfect. It is possible that this deviation may, at least partly, be due to the nature of the tracer used but this is certainly not the sole reason because, if

it were, the discrepancy would tend to be smaller at the longer distances, where ionic repulsion effects have by then become virtually negligible. In any case, the theoretical justification for expecting a log—normal distribution is rather questionable and it is mainly a matter of convention that the results are presented in this format. (It is arguable that the use of a linear axis may have been an equally acceptable choice — possibly superior in that it would allow the reader to come to his own conclusions about the nature of the distribution without having the fashionable log—normal foisted upon him!)

Aside from this rather contentious aspect the effect of filtering is quite unambiguously illustrated by the progressive diminution in the probability of observing high peak values together with a reduction in slope —reflecting a decrease of (geometric) standard deviation. In particular note the tendency towards bunching of the curves as the distance increases — presumably being a result of the loss of high frequency structure as one moves away from the source.

5.3.5. Temporal structure analysis using SHADA. Table 3 details the total events (i.e. the sum of all the counts in the individual time bins) for the four experiments and sequence of threshold values used. (Note that these totals do not, at least in theory, depend on whether 'burst length' or 'burst return period' is considered because the summation should yield the same or very nearly the same result. Experimental results did in fact support this assertion.) It would seem there ought to be at least a tenuous connection between the total events and intermittency (note, however, that the latter has been defined on the basis of a 25 mV threshold) because, to take an extreme case as an example, if the bursts were all of identical length, then the event total and intermittency would behave in complementary fashion. Comparison of Tables 2 and 3 indicates that such a trend is not really discernible (correlation coefficient —0.52), thus suggesting that the intermittency can remain high even though much fluctuation activity (i.e. many events) has occurred and vice versa.

The 2 m downwind experiment burst length distribution taken at 50 mV threshold contains a rather ill-defined most probable value in the 0.30—0.42 s interval; the higher level occurring in the lowest class (< 0.015 s) being due to the presence of high frequency noise. However at 500 mV the most probable value shifts to the shortest class interval and this effect is certainly a reflection of the pulse shape itself and not related to spurii. Note also that the total events at the higher threshold is much smaller, by a factor of nearly 15, thus implying that only about 7% of the bursts exceeded 500 mV in amplitude. Further, the longest burst observed throughout the 48 min run at the 500 mV load is a full 4 class intervals (i.e. $(\sqrt{2})^4$, $4\times$) shorter than at 50 mV.

These results also provide some important clues regarding the burst or pulse shapes occurring in the fluctuations. If, for example, the pulses were rectangular and of similar, amplitude, then no change in the length distribu-

tion or event number would have occurred with threshold variation until the latter exceeded the pulse height. The existence of a rapid fall-off of these parameters in practice strongly suggests that the pulse shape is triangular — i.e. the structure is peaky — a feature also evinced by the large kurtosis values observed.

Similar behaviour is evident in the 15 m histograms. However here, the distributions are broader and bursts of up to $(\sqrt{2})^5$ i.e. 5.7 × the duration of the longest seen in the 2 m experiment were observed. This feature may be related to the increased plume width at the longer distance and in fact this ratio, 7.2, accords quite well with the burst length increase.

Burst return period data are given in Figs. 7 and 8 and provide complementary information to that above. In particular, since return period analysis is essentially an examination of the statistics of the gaps in the concentration distribution it is thus a far more precise technique for describing the intermittency than merely specifying a global percentage value. Alternatively, particularly in the context of hazard assessment, one can view this type of analysis as providing an indication of how long one has to wait before a given value of concentration is likely to recur.

The nature of the distributions themselves is rather different to those of burst length. For instance in the case of the 2 m downwind experiment with 50 mV threshold, there is some tendency towards a log—normal distribution since the histogram appears to have roughly Gaussian form on its logarithmic variate scale. However this could be fortuitous since the other three distributions are markedly skewed: negatively for both 500 mV results and positively for 15 m, 50 mV data. Perhaps the most striking feature is the marked shift to longer values of return period with the increase of threshold in both the 2 and 15 m case, the most probable value being displaced by almost 2 orders of magnitude. Even then, however, at the relatively high concentration equivalent to 500 mV (in comparison with the overall mean) one has only to wait, *on average*, about 8 s for the same levels to be experienced again. This does not preclude the existence of some very long gaps as in both cases the distribution extends out to several minutes — physically this being the result of large horizontal eddies causing the plume to meander. Some tendency towards bimodality can be seen in both the 500 mV analyses — the shorter peak at about 0.1 s possibly coinciding with some feature of the internal plume structure.

6. Conclusions

The results presented in this paper confirm the following main features of instantaneous plume structure:

(i) Very high levels of intermittency, typically 80—90%, coupled with correspondingly large peak to mean ratios in the range 30—150.

(ii) Plumes, and therefore by implication, puffs are generally of small cross-section and in the former case have a sinuous form. Consequently the con-

centration, when within them, is high and moreover the time mean (i.e. averaged over 10—15 min) of concentration is actually accumulated in the form of a series of short, discontinuous but intense bursts of concentration. This has relevance to many applications of dispersion analysis but particularly for the accurate assessment of flammability/explosion and toxic risks and nuisance due to malodours.

(iii) Detector response time is a crucial factor in determining the impression obtained of plume structure — a rapid reduction in all the statistical parameters relating to the variability and peakiness of the fluctuation being noted when the response is deliberately degraded by the introduction of a low pass filter.

Finally the point should be made that although the experiments on which the above conclusions have been developed were performed at close ranges there are certain theoretical reasons, mostly founded on self-similarity and related postulates, for asserting that many of the structural features observed will persist for considerable distances downwind. In addition the results of more recent experiments having source-detector separations of several hundred metres indicate the existence of similar (and just as much) fine structure and thus lend further support to this assertion.

Appendix

Power law expression for instantaneous plume radius: examination of electrostatic repulsion effects

The radial electrostatic field due to the net charge contained in the plume causes radial and, to a much lesser extent, longitudinal expansion. The latter can safely be ignored [16], but the radial component can be comparable with the expansion due to turbulence and thus requires investigation. If the plume, for simplicity, is considered to be a uniformly charged cylindrical volume then, in a *non-turbulent* flow, it can be shown, using the fundamental equations of electrostatics, that,

$$\left(\frac{\partial R}{\partial x}\right)_{\text{electrostatic}} = \frac{\mu i}{2 R \bar{u}^2 \pi \epsilon_0} \tag{A1}$$

where $(\partial R/\partial x)_{\text{electrostatic}}$ is the rate of increase of plume radius with distance (x), μ the ionic mobility, i the output current of the ion generator, $\bar{u}$ the flow velocity and ϵ_0 the permittivity of free space. It must be stressed that equation A1 is only an approximation to reality, in practice the charge is not uniformly distributed and neither is the wind speed constant, but nevertheless it provides a useful indication of the relative magnitudes of the dispersive agencies operating on the plume.

If the flow is turbulent, as is generally the case in the atmosphere, then the total, and therefore *observed*, plume expansion rate can be written

$$\frac{dR}{dx} \simeq \left(\frac{\partial R}{\partial x}\right)_{\text{electrostatic}} + \left(\frac{\partial R}{\partial x}\right)_{\text{turbulent}} \tag{A2}$$

where $(\partial R/\partial x)_{\text{turbulent}}$ represents the contribution to plume expansion arising directly from turbulent processes. Thus

$$\left(\frac{\partial R}{\partial x}\right)_{\text{turbulent}} \simeq \frac{dR}{dx} - \frac{\mu i}{2 R \bar{u}^2 \pi \epsilon_0} \tag{A3}$$

and integrating

$$R_{\text{turbulent}} \simeq R - \frac{\mu i}{2 \bar{u}^2 \pi \epsilon_0} \int \frac{dx}{R} \tag{A4}$$

Since R refers to the observed radius it can be replaced by the power law approximation already deduced (i.e. eqn. 7) and eqn. A4, with this modification, can then be integrated numerically to reproduce the results given in Table 4.

References

1 Csanady, G.T., Turbulent diffusion in the environment, D. Reidel, Dordrecht, Holland, 1973.
2 A.A. Townsend, The Structure of Turbulent Shear Flow, 2nd edn. Cambridge University Press, Cambridge, 1976.
3 C.D. Jones, Statistics of the concentration fluctuations in short range atmospheric dispersion, Conference on "Mathematical modelling of turbulent diffusion in the environment". Liverpool University Sept 12—13, 1978. Proceedings published by Academic Press, C.J. Harris, Ed.), 1978.
4 J. Murlis and C.D. Jones, Fine-scale structure of odour plumes in relation to insect orientation to distant pheromone and other attractant sources, Physio. Entomol., 6 (1981) 71.
5 P.C. Chatwin, The use of statistics in describing and predicting the effects of dispersing gas clouds, J. Haz. Mat., (1982) to be published.
6 J.A.M. Barynin and M.J.G. Wilson, Outdoor experiments on smell, Atmos. Environ., 6 (1972) 197.
7 A. Hadjitofi and M.J.G. Wilson, Fast response measurements of air pollution, Atmos. Environ., 13 (1979) 755.
8 C.D. Jones, Ion concentration variations at short distances downwind of continuous and quasi-instantaneous point sources, Pestic. Sci., 8 (1977) 84.
9 F.A. Gifford, Statistical properties of a fluctuating plume dispersion model, in F.N. Frenkiel and P.A. Sheppard, eds., Atmospheric Diffusion and Air Pollution, Advances in Geophysics, 6, Academic Press, New York, 1959, p. 117.
10 J.L. Lumley and H.A. Panofsky, The structure of atmospheric turbulence, John Wiley and Sons, London, 1964.
11 G.J. Cats and A.A.M. Holtslag, Prediction of air pollution frequency distributions, Atmos. Environ., 14 (1980) 255.
12 P.C. Chatwin and P.J. Sullivan, On the probability density function of concentration in turbulent dispersion, Transactions of the CSME, 5 (78—79) (1979) 192.

13 J.L. Lumley and H. Tennekes, A first course in turbulence, MIT Press, London, 1972.
14 A.D. Birch, D.R. Brown, M.G. Dodson and J.R. Thomas, The turbulent concentration field of a methane jet, J. Fluid Mechanics, 88 (1978) 431.
15 J. Horowitz and S. Barakat, Statistical analysis of the maximum concentration of an air pollutant: effects of auto-correlation and non-stationarity, Atmos. Environ., 13 (1979) 811.
16 C.D. Jones and W.C.A. Hutchinson, Plumes of electric space charge in the lower atmosphere, J. Atmos. and Terr. Phys., 38 (1976) 485.
17 C.D. Jones, Ionized air as a wind tunnel tracer, J. Phys. E: Sci. Instr., 10 (1977) 1287.
18 C.D. Jones and N.T. Gulliford, Developments in the use of ionised air as a wind tunnel tracer, J. Phys. E: Sci. Instr., 12 (1979) 321.
19 L.B. Loeb, Electrical Coronas: their basic physical mechanisms. Univ. of California Press, Berkeley and Los Angeles, USA, 1965.
20 F. Pasquill, Atmospheric Diffusion, 2nd ed., Ellis-Horwood, Chichester, UK, 1974.
21 C.D. Jones and S.G. Jennings, Large Electric fields due to industrial chimney stack plumes, Atmos. Environ., 11 (1977) 1197.

Jones C. D. and Griffiths R. F. (1984).

Full-scale experiments on dispersion around an isolated building using an ionised air tracer technique with very short averaging time.

Atmos. Environ. **5**, 903 - 916.

Atmospheric Environment Vol. 18, No. 5, pp. 903–916, 1984
Printed in Great Britain.

0004–6981/84 $3.00 + 0.00

FULL-SCALE EXPERIMENTS ON DISPERSION AROUND AN ISOLATED BUILDING USING AN IONIZED AIR TRACER TECHNIQUE WITH VERY SHORT AVERAGING TIME

C. D. JONES
Chemical Defence Establishment Porton Down, Salisbury SP4 OJQ, Wiltshire, U.K.

and

R. F. GRIFFITHS
Pollution Research Unit, PO Box 88, UMIST, Manchester M60 1QD, U.K.

(*First received* 2 *August* 1983 *and received for publication October* 1983)

Abstract—Experiments are reported in which negatively ionized air is used as a tracer on the flow and dispersion in the vicinity of an isolated building. The technique permits very rapid response concentration measurements to be made, so that the characteristics of concentration fluctuations can be determined. Experiments have been carried out using both continuous and pulsed ion sources, and with several detectors deployed to reveal aspects of their sequential activation as a puff of ions is carried on a trajectory in the wake region. Statistical aspects of the multi-detector experiments are presented, and suggestions based on these results are put forward concerning further use of the method in examining this type of flow and dispersion behaviour.

1. INTRODUCTION

The nature of the air flow around buildings, and other obstructions, is a topic that has attracted much investigation, generating a substantial body of literature describing theoretical treatments, experiments carried out in wind tunnels and, in fewer cases, investigations conducted at full scale. The overall features of these flows, involving streamline displacement and a wake region characterized by the presence of a velocity defect and one or more zones of recirculating secondary flows, have been detailed by numerous authors. Whilst the existence of these overall features is now well established, the simple picture of a closed wake cavity region as described in the earlier literature, e.g. by Halitsky (1963) seems over simplified in the light of current knowledge. More recent work indicates a very much more complicated pattern of secondary flows, and streamline trajectories that may enter the wake recirculation zone, presumably by entrainment, even though they start from outside the leading edge separation streamline (Britter *et al.*, 1976; Vincent, 1977; Castro and Robins, 1977; Hunt, 1982).

The understanding gained through these and numerous other studies has been substantial, but has not yet advanced to the stage where the need for tests at full scale can be eliminated and there are relatively few reported studies. Notable among recent full-scale trials are those by Drivas and Shair (1974), Ogawa and Oikawa (1982) and the multi-sponsor project reported by Barker *et al.* (1982). In all of these studies the tracers used (SF_6, and smoke in Barker *et al.*) limit the resolution of the concentration fluctuations expected in turbulent dispersion, and whose existence has already been demonstrated in experiments using fast response detectors (Hadjitofi and Wilson, 1979; Jones 1977a; Murlis and Jones, 1981). The use of Gaussian (or similar) models to describe pollutant concentration distributions is a well established practice, but the inherent limitations of such procedures are often overlooked. A particularly important example lies in the fact that these models provide temporal or spatial mean values and do not account for the concentration fluctuations characterizing real plumes and puffs. Whilst such average values are satisfactory for materials where the accumulated dosage is the important variable (e.g. radioactive isotopes) it is clear that they do not give an adequate means of hazard estimation for situations in which the 'instantaneous' concentration and the intermittency of exposure are important or even crucial factors. Examples of such cases would be:

(a) combustible materials, for which the important factor is whether or not the 'instantaneous' concentration lies within the Upper and Lower Flammable Limits;

(b) toxic gases such as ammonia, or chlorine, for which the toxic response is considerably more severe for high concentration over a given duration of exposure than it is for the same total dosage received over a longer period at lower concentration and

(c) malodour nuisance, which is much dependent on the property of the olfactory sense to respond to rapid changes of concentration, and to become desensitized or tolerant to steady concentrations.

These considerations suggest that it would be par-

ticularly valuable to investigate tracer concentrations monitored with rapid response detectors at fixed points in the vicinity of a building. The ionized air tracer technique developed by Jones (1977a, b) offers a convenient means of approaching this and in the experiments described herein was used to examine the dispersion processes operating in a building wake, employing both continuous and pulsed releases of tracer. Although the tracer behaves in a somewhat non-passive way, mainly due to mutual electro-static repulsion of the ions, this feature does not detract too seriously from the overall quality of the results; the ability of the technique to resolve very rapid changes in concentration being an advantage that more than compensates for this deficiency (see discussion in Appendix). It was also hoped that further information could be gained regarding the unsteadiness of building wakes in the atmosphere, that is to say the transient nature of the existence of the wake region as an entity. In most previously reported studies, with the notable exception of Drivas and Shair (1974), Hinds (1969) and Ogawa and Oikawa (1982), this very important aspect has received little attention. In a recent excellent review Hosker (1981) does mention this property of unsteadiness, but does not offer anything but tentative discussion on how this could modify the temporal and spatial concentration patterns.

2. THE PROBLEM OF MAKING REPRESENTATIVE WIND VELOCITY MEASUREMENTS

The interaction between buildings and wind is a subject that has been given a great deal of study, particularly in connection with the aerodynamic loading of structures (Owen, 1971; BSI, 1972). Full-scale investigations of urban wind conditions using anemometers on mobile masts show that the modification to the mean free-stream velocity due to groups of buildings is extremely complicated, and no generalization of the effects is likely to be adequate (Eaton and Buller, 1974; Cook *et al.*, 1974). Wind tunnel investigations by Hussain and Lee (1980) and Hussain (1979) were carried out using arrays of cubes with variable spacing, configuration and plan area density. These experiments showed that the nature of the flow modifications associated with those regular arrays could be categorized into three distinct regimes. With sufficient space intervening between the elements the flow was such that each cube acted as an isolated obstruction, with streamline reattachment occurring in each wake. If the elements were somewhat closer there was interference between the wake of one cube and the flow round its downstream neighbour. At yet closer spacings a skimming flow regime was apparent, with stable regions of rotating flow between the cubes. Measurements of the air speed, U, as a function of height expressed as the ratio U/U_f, where U_f is the free stream air speed, showed that for a given height h, the ratio U/U_f was dependent on the flow regime that was in force, but the values of U/U_f increased and tended to converge as h/H was increased, H being the cube height.

The results show that at $h/H = 2$ the ratio U/U_f was between 0.5 and 0.7, the higher values being associated with lower plan area density (at this value of h/H the 'street' centreline and 'building' centreline values of U/U_f had converged). These results suggest strongly that measurements of wind speed taken at heights less than two building heights will be complicated by the flow modifications to such an extent that they are not readily interpretable, or indeed usable, as a measurement representative of the free stream wind speed.

In studies involving both full-scale and wind tunnel model experiments, Evans and Lee (1981) made comparisons of anemometer readings obtained at different heights and locations in the campus of Sheffield University, and investigated the behaviour experimentally using a simplified model of the site in a wind tunnel. The results showed that the wind speed U_A, measured at a particular location, expressed as the ratio U_A/U_g, where U_g is the undisturbed mean wind speed at that height, was dependent on the wind direction as well as on small variations in the anemometer height. These findings suggest that in order to be made representative of the free stream flow, wind speed measurements taken in the vicinity of complex arrays of buildings would require correction by factors that were wind direction as well as location dependent.

The general conclusion of their discussion is that there is great difficulty in specifying local wind conditions and in relating them to the free stream values. The suggestion is clear from the work of Lee and his co-workers that in practical terms it is necessary to use wind tunnel models of complex sites, and that once a site has been 'calibrated' in this way it is probably best to scale local wind measurements to the geostrophic wind by means of these calibrations.

In the experiments reported here, which were in relatively simple configurations of buildings and obstructions, several types of measurement were made to characterize the wind. A bidirectional vane/propeller anemometer was used in some experiments, giving wind azimith, elevation and speed. The bivane was usually located close to one of the ion collectors. Run-of-wind meters were deployed in several different configurations in the later experiments, and a system of tissue streamers on poles, or tethered small He filled balloons was set-up close to the building to give some information about the flow field in and around the wake. A tethered parafoil kite was flown to show the wind direction at a height of about 50 m and conventional cup anemometers located on two nearby masts (at heights of 47 and 9 m) served to provide data on the mean flow behaviour.

Whilst these instrumentation systems did not provide a full characterization of the wind field, they were sufficient for the purpose of making the approximate calculations needed to interpret some aspects of the experimental results.

3. EXPERIMENTAL APPROACH AND TECHNIQUE

3.1. *Introductory notes*

Two short series of field experiments were carried out with the particular aim of investigating the transient aspects of flow and dispersion in the vicinity of a small and reasonably well isolated building. The first series, in May 1982, was essentially exploratory in nature having the central objective of establishing the feasibility of using ionized air as a dispersion tracer in topographically complex conditions as previously it had been employed only in flat and unobstructed terrain, albeit very successfully. In these initial experiments a relatively powerful tracer source (i.e. ion generator) was used because it was thought valuable to be able to observe the ion concentration at considerable distances downwind from the building; up to perhaps 100 m or so in this context. In practice this did not however prove feasible mainly due to the unusually light wind conditions which prevailed throughout the experimental period. Nevertheless it was apparent from the results obtained that a much lower output ion generator would have sufficed to provide adequate data and furthermore would be most desirable for any future work in order to reduce electro-static interferences, mostly arising from mutual repulsion, to completely acceptable levels.

In view of this the second trials series, conducted in November 1982, employed a specially developed ion generator with much reduced output and the results obtained were of considerably higher quality (see Appendix for a detailed discussion). Consequently it is appropriate that these latter data be treated with more emphasis and credence than those obtained in the 'May' experiments.

3.2. *Note on the ionized air tracer system*

This has already been described in detail in the published literature (Jones, 1977a, b; Jones and Gulliford, 1979; Murlis and Jones, 1981) and therefore only a superficial account of its salient features is given here.

In the ion generator *unipolarly* ionized air was produced by applying a high potential, between -2 and -5 kV*, to a pair of radially mounted, thin ($\phi = 10\ \mu$m), platinum wires fixed within, but insulated from, an earthed aluminium cylinder ($\phi = 0.024$ m). Owing to the asymmetric electrode arrangement a very large electric field was developed in the immediate vicinity of the tips of the wires which results in *local* breakdown and thus production of ions. Further the electric field distribution was such that most of the volume between the outer cylinder and inner wires becomes filled with unipolar ions (negative in this case) moving relatively slowly outward. Consequently it is feasible to expel a proportion of this unipolar ion current into the free atmosphere by simply blowing a gentle current of air (provided by a small fan) through the cylinder.

This system is clearly very convenient because it offers a method of introducing a tracer into the atmosphere with relatively little disturbance to the system under study and moreover possesses the added advantage that continuous, intermittent or even quasi-instantaneous releases can be simulated simply by applying appropriately timed high voltage waveforms to the ion generator corona points.

Ion concentration was determined as follows. The windborne ionized air was drawn, by means of a small suction fan, through an inlet tube ($\phi = 0.036$ m) at a well controlled velocity (6.6 m s^{-1}) so that the volumetric flow rate was known accurately. The detector itself, or collector as it is generally referred to, consists essentially of an outer cylindrical electrode of the same diameter as the inlet tube (of length 0.1 m) to which a d.c. bias of about -500 V was applied. The polarity of this voltage is such that it drives the incoming ions towards an axially mounted collecting rod ($\phi = 0.002$ m) the arrival of ions constituting a small electric current which then flows to earth through a broad band low impedance integrated circuit amplifier. It was possible, with reasonable precautions, to measure and record ion currents as small as 10^{-12} A and, provided the input capacity of the collector/cable/amplifier system was kept low (less than ~ 50 pF) to obtain frequency responses up to about 200 Hz. Thus the detection method can be made highly sensitive, is linear and has no hysterisis or other problems. These advantages, together with the very good high frequency resolution, are thus the major reasons for using this particular tracer technique. In addition both the ion generator and collector(s) possess very modest power supply requirements and can be readily operated for periods of several hours from batteries.

3.3. *Experimental details: 'May 1982' series*

Both these experiments and those in November 1982 were carried out in the vicinity of a small, single storey flat-roofed hut with a number of almost flush fitting windows and doors. The terrain near the hut was completely flat but there were several small shrubs and trees located relatively close to the experimental area, predominantly in the north and southward directions. However to the east there was an extensive area of closely mown grass and this provided a reasonably representative (see Section 2) location at which to obtain reference, ie characteristic of the unobstructed flow, wind speed and direction measurements. The trees and shrubs referred to above were of course fully in leaf during the first series of experiments and thus must have presented a greater disturbance to the flow than would have been the case in the November experiments by which time all the leaves had been shed. A plan drawing of the hut is given in Fig. 1.

This figure also, in conjunction with Table 1, shows the arrangement of ion generator and collectors for the sequence of four experiments that are to be discussed subsequently. The equipment was sited near the NE corner of the building rather than nearer the mid-point of either the N or E face because, under the very light winds pertaining throughout the experiments, preliminary smoke tracer† experiments indicated that this positioning would most likely provide at least some usable data (both cine and still photography was used to record the smoke experiments for subsequent analysis if warranted).

As indicated earlier the wind field around the building was delineated in a qualitative fashion by means of paper streamers fixed at heights of 1.6 and 1.0 m to a matrix of

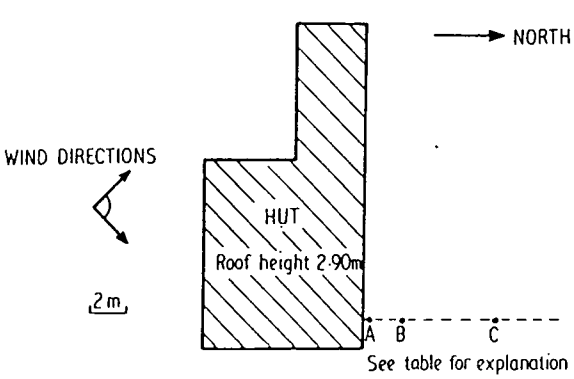

Fig. 1. Arrangements for the continuous source (May 1982) experiments.

* The precise value depends on the ion current output required (and also the electrode geometry).

† A convenient source of 'cool' smoke was found to be a small pyrotechnic device intended for leak testing of drain pipes.

Table 1. (To be read in conjunction with Fig. 1) Arrangement of ion generator (IG) and ion collectors (IC1, IC2) for the 'May' experiments

Expt No.	Located at: A	B	C
1	IG, height 1 m	IC1, height 1 m	IC2, height 1 m
2	IG, height 1 m	IC1, height 0.3 m	"
3	IC1, height 0.3m	IG, height 1 m	"
4	IC1, height 1 m	IG, height 1 m	"

bamboo canes. This arrangement functioned very well under most conditions but in the very lightest winds tethered He filled balloons ($\sim 3\ell$ volume) attached by threads 2 m in length to the ground proved effective down to velocities as low as an estimated 0.1 m s^{-1}.

3.4. *Experimental details: 'November 1982' series*

The layout adopted for the experiment to be described is given in Fig. 2. Various modifications to techniques were incorporated in the light of previous experience notably in relation to the electrical output of the ion generator. In the May series a continuously operating ion source was used which delivered 50 nA of negatively ionized air at a volume flow rate of 2×10^{-2} m^3 s^{-1}, however for these trials a miniaturized source was developed which produced 5 nA of current at the much reduced flow rate of 1.25×10^{-3} m^3 s^{-1}. Consequently the effects of electro-static repulsion were markedly decreased but additionally any disturbances to the ambient flow due to the emergent jet of ionized air were virtually eliminated. A further refinement was the inclusion of a controlled pulsing facility for the generator so that 'short puffs' of ionized air could be released and this proved particularly useful for studying transport, in contradistinction to dispersion, phenomena. Pulsing was accomplished by directly switching the high voltage supply to the generator using a large gap (0.025 m) rotary relay; the latter being driven by a control signal derived from a high stability timing circuit.

The bidirectional wind vane was not available for these experiments and was substituted by four 'run-of-wind' meters, three of which were co-located with the ion collectors; in reality within about 0.20 m of them. The fourth meter was situated 50 m crosswind, in an easterly direction from the building, at a height of 2 m in a well exposed position to obtain an indication of the 'background' flow characteristics.

Other developments included the replacement of the cine camera, for documenting the supplementary smoke tests, by video camera and recorder. This proved a highly advantageous change enabling immediate and repeated review of flow and dispersion patterns to be made thereby providing considerable assistance in the siting of the ion generator and collectors.

3.5. *Instrumental data handling and processing*

All the transducer outputs ie the ion collectors, bivane and ion generator pulse 'marker' were logged, together with voice comments, on an eight channel analogue FM instrumentation tape recorder. Subsequent playback was undertaken in the laboratory, the output signals being examined using a variety of electronic/analytical equipment including a fast response multichannel chart recorder and threshold gating and filter system (Jones, 1983).

4. RESULTS AND DISCUSSION

It is intended, for reasons of clarity and convenience, to deal with the results obtained from the two series of experiments separately. In the case of the 'May' series a sequence of four runs has been selected for examination and represents a typical sample of the type of data obtained, whereas for the 'November' data a single, but of a similar total duration, run will be discussed.

4.1. *The 'May' experiments*

The reader is referred to Fig. 1 and Table 1 regarding the various arrangements of tracer source and detectors for these experiments.

The weather conditions throughout the sequence of

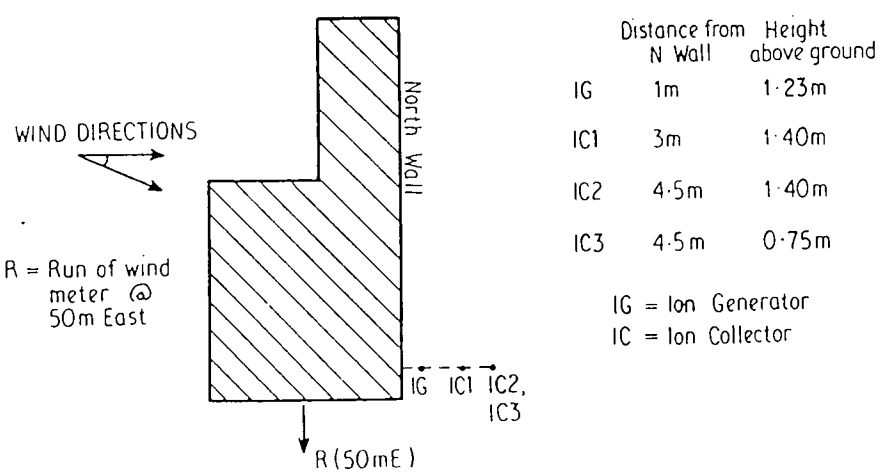

Fig. 2. Arrangements for the pulsed source (Nov. 1982) experiments.

runs were characterized principally by the exceptionally light winds which prevailed near ground level. As is normal on such occasions the wind direction was very variable but mainly from a SSE to WSW point. The sky was well clouded (with 7–8 oktas altostratus plus 6–7 oktas cumuli below) and, at the time of day (1100–1400 GMT) and year concerned, the lower boundary layer would have been slightly unstable, i.e. Pasquill Class C.

Prior to siting the ion generator and collectors several smoke releases were made in an attempt to establish optimal locations for these instruments. Unfortunately the prevailing wind, or rather the lack of it, rendered this a difficult, highly subjective and frustratingly inconclusive exercise. Nevertheless, even in these most atypical meteorological conditions, it was gratifying to observe, albeit occasionally, the occurrence of flow features in the vicinity of the building which at least bore some resemblance to those only seen previously by the authors in the wind tunnel models. Although the existence of a wake recirculation zone was demonstrated, as might be expected it proved very difficult to make any reliable estimate of its size or the velocity distribution within it.

Figure 3 shows an ion concentration trace observed during the course of an experiment and obtained from the collector placed nearer to the ion generator. Note the very intermittent nature of this record, a feature already observed in previous high resolution concentration measurements carried out in flat unobstructed terrains (Jones, 1983). However the result of most significance, at least as far as this series of experiments is concerned, is that there is definite evidence for the existence of interludes during which the ion concentration remains above zero, and more importantly, virtually steady for as long as 10 s; a feature in sharp contrast to the type of behaviour experienced with earlier investigations referred to above. Further this phenomenon was only observed at the nearer collector, never at that placed 8 m away from the hut. The consistency of this ion concentration 'plateau' was initially regarded with suspicion but we have carefully examined both the records and the experimental hardware and can find no reason to conclude that what was observed was an artefact. The 'plateau' episodes appeared from time to time in all four runs and thus did not seem to be too sensitively dependent on the heights of the ion generator and relevant collector.

One possible explanation of this phenomenon is that it arose from the development of a well mixed cavity that was presumably rather unstable in both time and space. Indeed the variability of the oncoming flow was such that it was likely that the recirculation zone would continually be formed, displaced and eventually destroyed and then reformed with the ion collector being periodically engulfed within it. Thus the higher concentration peaks, which exceed the plateau level by factors as much as ten occasionally, could correspond to the transport of ions by the 'direct' route from generator to collector when the cavity (i.e. the well mixed region) is not enclosing them both.

The actual concentrations observed during the 'plateau' episodes for the four experiments listed in Table 1 were respectively 2.7, 3.0, 4.5 and 6.5 nCm^{-3} and it is instructive to compare these figures with those derived from simple predictions based on plausible theories developed from wind tunnel studies. Letting H be the building height, W its crosswind width, Q the point source emission rate, U (as in Equation (1)), the 'local' wind speed at height H, l the cavity length and C the concentration within it, then from Hall (1980).

$$C = \frac{Q}{UH^2}. \tag{1}$$

Typically, for the experiments under discussion $U = 1\ m\,s^{-1}$ and, with $Q = 50$ nA, the equation above yields

$$C = 5.9\ nCm^{-3}.$$

Alternatively, Hunt (1982) obtains

$$C \cong (5\text{–}8.2)\frac{Q}{UH^2} \tag{2}$$

for a cube and, replacing H^2 by HW, gives

$$C \cong 4.7\text{–}7.8\ nCm^{-3}.$$

The same author also considers the concentration resulting from a line source (strength q) with a two-dimensional building and this is probably a rather better approximation to the conditions of the current

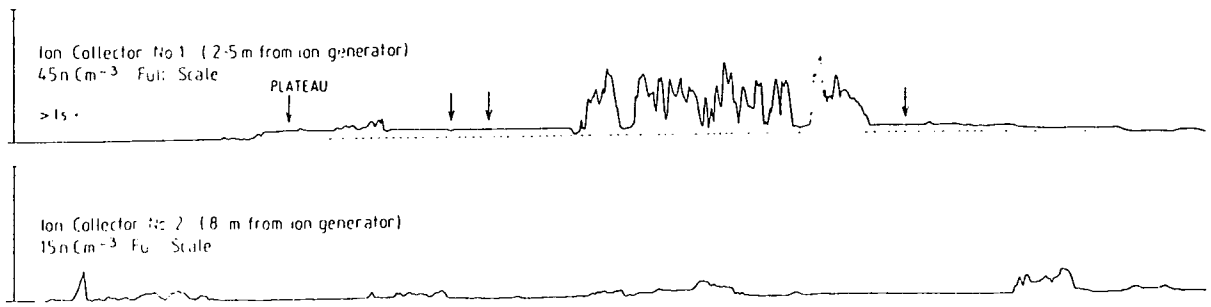

Fig. 3. Section from continuous source (May 1982) experiments.

experiments. In this case he obtains

$$C \cong (5\text{–}8.3)\frac{q}{lU} \qquad (3)$$

and putting, tentatively, $l = 2H$ and $q = \frac{Q}{W}$ yields

$$C \cong 2.3\text{–}3.9\,\mathrm{nCm}^{-3}.$$

The agreement between the experimental values and those calculated is really quite good bearing in mind the extremely difficult conditions under which the experiments were carried out. It would therefore appear that the cavity region recirculation explanation of the 'plateau' effect could be at least qualitatively correct.

4.2. *The 'November' experiments*

The particular experiment selected for discussion was carried out on a cloudy afternoon with a surface (i.e. 2 m) mean wind speed of 4–5 $\mathrm{m\,s}^{-1}$ and direction varying between S and SW. Insolation was very weak and the atmospheric stability fell into the neutral or near-neutral classification. Figure 2 gives details of the arrangement of the ion generator and collectors employed.

The experiment was operated continuously for a period of ~ 110 min during which a total of 1131 ion 'puffs' were released. The releases were uniformly distributed throughout the run the pulse length being 1.0 s with separation 4.8 s. Figure 4 shows a typical sample of the ion concentrations recorded by the three detectors. On the figure the rectangular pulses indicate when the ions were actually released and the delay between this and their subsequent arrival at the detection sites is clearly evident. A cursory examination of the entire chart record reveals that the corresponding flow velocities for the particular part of the wake studied derived on a time of flight (i.e. Lagrangian) basis are ~0.5 $\mathrm{m\,s}^{-1}$. This compares quite well with the findings of Drivas and Shair (loc. cit.) who concluded, presumably from Eulerian measurements, that the velocities encountered in the recirculating wake region were generally about 10–30% of those in the unobstructed flow at similar heights.

As before an important feature of short time resolution concentration measurements is the very high intermittencies invariably observed. It was found,

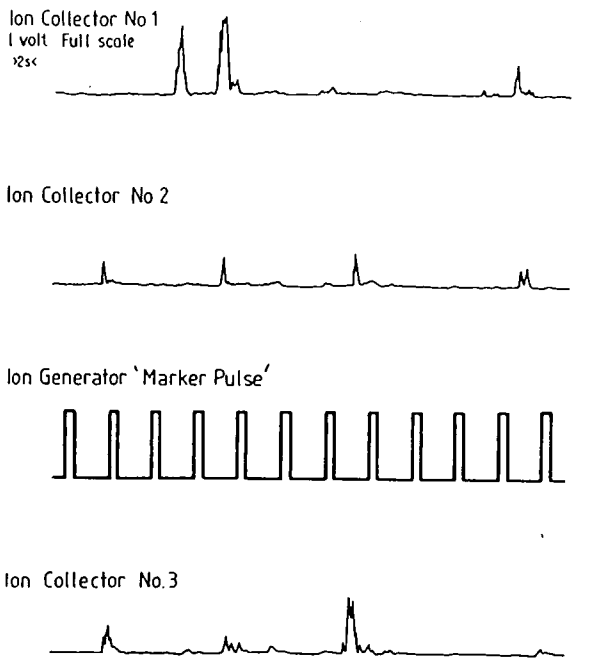

Fig. 4. Section from pulsed source (Nov. 1982) experiment.

even in flat unobstructed terrains (Jones, 1983), with a continuous source and a detector located close to the mean plume centre line, that the concentration was zero (or strictly below the detection threshold) for 80–90% of the sampling time. This phenomenon is of course merely a consequence of the plume meandering in response to the lower frequency components of the turbulence spectrum and thus it would be reasonable to expect an analogous situation to occur, though to a different degree and for somewhat different physical reasons, in the recirculating wake region of a building. In this case however it is probable that the entire wake geometry and structure will alter in response to variations in upstream conditions and moreover it is possible that relatively small changes in wind direction and/or speed may induce substantial and sudden effects in this regard. Table 2 shows the percentage, P, of the total pulses released that were subsequently detected at each collector (irrespective of their actual concentration); the remnant percentage (i.e. 100-P) being thus approximately equivalent to the concept of intermittency as applied to the analysis of continuous source data.

Table 2. Total number of pulses observed at each collector in relation to total released

Ion collector number	Total number of pulses observed	Percentage of total released (P)	Equivalent percentage intermittency ($100 - P$)
1	122	10.8	89.2
2	70	6.2	93.8
3	105	9.3	90.7

Note: Although these intermittency values do in fact correspond rather well with previously obtained figures for flat terrain the comparison is not a precise one.

It is interesting that ion collector (IC) 2 received considerably fewer pulses than either IC's 1 or 3, thus suggesting that the flow frequently possessed a significant downward component in the vicinity of IC1, although other physical mechanisms could be postulated to account for this difference in numbers. Also of interest is that evidence from the run of wind meter data, Table 3, reinforces the existence of a very 'slack' flow pattern in the vicinity of IC2.

Whilst dealing with the topic of flow regimes at the ion collectors it is worth pointing out that, with the oncoming wind direction perpendicular to the front face of the building, i.e. due south, it is probable that the 'Lateral Edge' and 'Elevated vortex pairs' as described by Hunt *et al.* (1978) would have been present. Indeed smoke dispersion tests carried out prior to the main experiment indicated the existence of helical motions about approximately vertical axes in the vicinity of the NE corner of the building. On the other hand on those occasions when the wind became more oblique to the front face (i.e. from the SW) it is possible that the instrumentation would have been fully immersed within a recirculating wake proper. It should be noted however that this latter region, when and where it existed, would have been about three building heights in length i.e. ~ 9 m and thus even the further downstream collectors, at 4.5 m, were likely to have been in front of the main return flow area.

An important part of the study of wake flows in the open air is the examination of the variety of regimes that can develop in response to alteration of external conditions and, with the three detectors used in the current experiments, it is possible to characterize the observations in a number of ways. Initially therefore a simple analysis was undertaken to establish the order and frequency of arrival of pulses of ions at the collectors. Since measurements were made at three points it would be possible, following ion puff release, for signals to be observed at one, two or all three collectors and, at least in theory, in any order. Thus quite a number, 15 in fact, of permutations of ion collector activity exist even with the relatively simple arrangements employed here. It seems appropriate to describe this as an 'event-type' analysis and the results obtained are given in Table 4.

Entries in the table are made irrespective of signal amplitude and, in most categories of events, include pulses of quite small size, particularly for IC2. Examination of the table indicates that there is good evidence to support the existence, at least for a substantial fraction of the time during which pulses were actually observed, of an instantaneous flow structure of the type anticipated on the basis of time mean velocity measurements; i.e. events of category 12, 13, 23, 31 and 123 account for about 45% of the total. In addition if one takes into account those events in which only a single collector was activated, on the assumption that here too the flow regime was as above, then nearly 99% of events can be included. Note, however, that although uncommon, 'reversed' flow events apparently do occur as shown by the non-zero totals in the 132 and 32 classes but it should be pointed out that, with the benefit of hind sight, it is just possible that either or even both of these events may, in reality, have been a result of insufficient pulse separation at release; i.e. *different* puffs were being observed at the collectors.

A further point of considerable interest, because it has implications for diffusion rate calculations within the wake region, is the fact that very many of the pulses arriving at the collectors did so in a highly discontinuous form and this is quite surprising bearing in mind the very short distances of travel involved. Frequently a 'pulse' would consist of several apparently disjointed portions of ionized air spread over as much as 2–3 s.

Table 3. Run of wind meter data

Meter located close to:	Mean wind speed over 1413–1539 GMT ($m\,s^{-1}$)
IC1	+0.39
IC2	+0.03*
IC3	+0.55
at 50 m east of building	+4.60

* It should be remarked that the meter co-located with IC2 was observed to be running backwards for a substantial fraction of the time and thus the figure in the table is indicative of the mean algebraic flow. However, it is very unlikely that the response of the meter would have been identical in both the forward and reverse directions and would be designed to favour the former (note that here 'forward' refers to flow away from the building, ie parallel to the main flow). Consequently the closeness of the IC2 meter reading to zero needs interpreting with care and it is certainly conceivable that the mean flow was, in reality of a small magnitude in the *reverse* direction.

Table 4. Event type analysis

Event type designation*	Total number of events	%
1 (Single collector activated)	58	32.6
2 " " "	6	3.4
3 " " "	31	17.4
12 (Two collectors activated)	9	5.1
13 " " "	17	9.6
23 " " "	17	9.6
21 " " "	0	—
31 " " "	1	0.6
32 " " "	1	0.6
123 (Three collectors activated)	37	20.8
132 " " "	1	0.6
213 " " "	0	—
231 " " "	0	—
321 " " "	0	—
312 " " "	0	—
Total:	178	

* Events have been designated by the following fairly obvious notation. The numbers themselves refer to the particular ion collectors at which signals have been detected whereas their order corresponds with that of the arrival of the pulses at the respective collectors.

Clearly this implies that quite energetic eddying and shearing motions are active in the wake region and their effects will need to be included in future dispersion models capable of describing and predicting concentration fluctuation statistics.

One final and obvious point regarding this data should be made in that it is only possible to make deductions regarding flow and dispersion for those occasions when pulses were actually detected by one or more collectors and this in fact only amounts to a total of $\sim$ 1/6 of the total release time. Little can be said regarding what took place on the remaining occasions apart from the obvious comment that the flow must have been either horizontally or vertically (or both) skewed in relation to the instrumentation line.

The analysis was extended further by examining the distribution of peak heights of the pulses: an aspect of particular relevance to the assessment of toxic and flammable hazards and also to odour nuisance. It must however be noted that due to self-repulsion effects the results obtained with the ion tracer technique represent the *lower* possibilities in terms of peak concentration (in relation to source strength) likely to be experienced. Gauging from previous results the peak concentrations observed, even at considerable distances downwind, appear to correspond with that of *undiluted* source material (Jones, 1983). Nevertheless the data presented in Table 5 are internally self-consistent and hence valuable.

Table 5 reveals quite a marked difference in the overall magnitude of the concentration fluctuations observed by the ion collectors, however this is not entirely surprising in view of the much closer location of IC1 to the generator than IC's 2 or 3. What is certainly rather more unexpected is the paucity of substantial peaks at IC2 in relation to IC3 since both were situated quite close together and at the same distance from the ion generator. All three peak height distributions are skewed positively and that of IC1 possesses a very approximate compliance with the log-normal frequency distribution as suggested by Csanady (1973); although, strictly speaking, he was referring to concentration fluctuations in their entirety rather than just the peak heights.

An estimate of the 'time' mean concentration, taken only over periods when the ion concentration was non-zero and therefore equivalent to averaging over the entire sampling time and then dividing by the fraction of that time for which ions were actually observed, has been found with other data to be in the region of 0.05–0.25 of the mean peak height. Thus the conventionally defined peak to mean ratios would probably be about 10 times as large as the figures given under (d) in the Table and such values are in order of magnitude agreement with data obtained in similar meteorological conditions in unobstructed terrain employing identical experimental techniques. Note that the ion concentration averaged over the entire sampling period and *including* the zero positions will yield a very low value because of the pulsed source used. Since the numerical value of this type of time average is obviously determined to a major extent by the pulse mark-space ratio selected for the source (and is therefore specifically related to a particular experiment) rather than any physical features of wake behaviour it is not appropriate to consider it further.

The manner in which the ion concentration 'events' are distributed is also important for some aspects of hazard estimation particularly where non-linear dosage/effect relationships obtain. Generally, in un-

Table 5. Peak height distribution analysis

Charge concentration (peak) interval (nCm^{-3})	Number of observations having peak level		
	IC1	IC2	IC3
0–1	75	65	83
1–2	21	6	14
2–3	9	0	6
3–4	4	0	1
4–5	2	0	1
5–6	3	0	0
6–7	2	0	0
7–8	2	0	0
8–9	1	0	0
9–10	2	0	0
10–11	0	0	0
11–12	0	0	0
12–13	0	0	0
13–14	1	0	0
14–15	1	0	0
(a) Mean peak height (nCm^{-3})	1.70	0.359	0.622
(b) Standard deviation of peak heights (nCm^{-3})	2.51	0.404	0.790
(c) Highest peak observed (nCm^{-3})	14.5	1.65	4.50
(d) Ratio of highest : mean peak	8.49	4.60	7.23

obstructed situations with short detector-source* separations (i.e. < 200 m) tracer is observed to arrive in sequences of short bursts, sometimes of only one or two tenths of a second duration, and these appear to correspond with the wind direction being exactly along the source-detector line. On the other hand quite long intervals may occur during which no tracer material at all is detected because of a temporary shift in wind direction and in fact it is not uncommon for such intervals to be of ten minutes or even longer duration. Thus in the context of hazard assessment it would be clearly beneficial to have information, preferably on a statistical basis, regarding the distributions both of these 'burst lengths', i.e. the durations of ion concentration events and of the 'burst return periods', i.e. of the gaps separating them. This type of analysis can readily be accomplished automatically and, if so desired, simultaneously at a number of voltage (≡ concentration) threshold levels. It was only possible however to conduct this type of analysis on the IC1 signals as the somewhat higher noise and drift levels present on the records of the remaining collectors rendered the results too unreliable to be very meaningful with so few, relatively speaking, signals to process.

When considering this Table it should be borne in mind that the ions were released in the form of 1 s 'puffs' with ~ 5 s spacing in between and thus it would be rather unexpected if a burst of duration much exceeding 1 s were recorded. This is of course subject to the proviso that a longer burst could occur if the flow pattern in the wake were so tortuous or convoluted so as to enable one or more puffs to become concatenated. However, judging from the burst length distributions in the table this does not appear to have happened since the longest event encountered falls in 1.36–1.92 s interval, but note that this type of analysis would not reveal the occurrence of two quite lengthy events separated by a few milliseconds gap and suggestive of joined puffs. However examination of the chart records convincingly negates this possibility.

It must be remarked that the results in Table 6 do not correspond precisely, in terms of peak height distribution, with those of Table 5 because, in the latter analysis which was done manually, the effects of slow baseline drift, typically equivalent to about 1 nCm^{-3} in concentration units, were eliminated. Furthermore a 12 Hz low pass filter was incorporated in the burst length and return period analytical system to reduce extraneous tape noise whereas in the manual analysis a wider pass-band could be tolerated (50 Hz).

In some ways the burst return period data in Table 7 are more interesting because, in effect, a forced period of 5 s has been deliberately imposed on the data by the choice of pulse separation interval. Thus if the arrival of ion puffs occurred in groups there should be evidence of this in the return period analysis however, on the other hand, if all the pulses had occurred singly then there would, by implication, be a considerable range of periods present. Examination of the results obtained at the lowest threshold used (note that even

* Continuously releasing source.

Table 6. Burst length analysis for IC1

Time interval limits	Numbers of events at concentration threshold level (nCm^{-3})				
	2.93	4.40	5.87	7.34	11.7
0–15 ms	1	0	1	0	0
15–21	0	1	1	0	0
21–30	1	1	1	0	0
30–42	1	1	1	0	0
42–60	3	1	0	1	1
60–85	1	0	0	0	0
85–120	4	1	1	0	1
120–170	7	4	0	0	0
170–240	4	1	0	1	0
240–340	1	0	0	0	0
340–480	5	0	1	4	0
480–680	4	3	4	0	0
680–960	3	1	0	0	0
960–1.36 s	3	1	1	0	0
1.36–1.92 s	1	0	0	0	0
Event totals	39	15	11	6	2

Table 7. Burst return period analysis for IC1

Time interval limits	Numbers of events at concentration threshold level (nCm^{-3})				
	2.93	4.40	5.87	7.34	11.7
0–15 ms	0	0	0	0	0
15–21	0	0	0	0	0
21–30	0	0	0	0	0
30–42	1	0	1	0	0
42–60	0	0	1	0	0
60–85	1	0	1	0	0
85–120	0	1	0	0	0
120–170	1	0	0	0	0
170–240	0	0	0	0	0
240–340	1	1	0	0	0
340–480	1	0	0	0	0
480–680	1	0	0	0	0
680–960	1	0	0	0	0
0.96–1.36 s	1	0	0	0	0
1.36–1.92	0	0	0	0	0
1.92–2.72	1	0	0	0	0
2.72–3.84	1	0	0	0	0
3.84–5.44	1	2	3	1	1
5.44–7.68	2	1	0	0	0
7.68–10.88	0	0	0	0	0
10.88–15.36	0	0	0	0	0
15.36–21.76	0	0	0	0	0
21.76–30.72	1	0	0	0	0
30.72–43.52	2	1	0	0	0
43.52–1.02 min	0	0	0	0	0
1.02–1.45	4	1	0	0	0
1.45–2.05	0	1	0	0	0
2.05–2.90	1	1	2	1	0
2.90–4.10	2	1	1	0	0
4.10–5.79	3	1	0	0	0
5.79–8.19	7	7	6	6	2
> 8.19 min	0	0	0	0	0
Event total	33	18	15	8	3

this excludes about 85% of the peaks, see Table 5) reveals only very tenuous substantiation for the presence of extra activity in the 5 s time 'slot'. Indeed the existence of single events in both of the preceeding (i.e. shorter) slots and two events in the immediately following (longer) slot really suggests that a specifically 5 s periodicity is absent. However if one takes a more relaxed view of the concept of a return period then, in the conditions of a outdoor recirculating wake with its inevitably erratic and disorganized flow system, it could be argued that a weak periodicity ranging from 1.92 to 7.68 s is brought out by the analysis since the five events occupying this time slot comprise a significant proportion of the total. At the higher thresholds there is a more unequivocal indication that a 5 s cycle is present in the results as shown for example by the occurrence of three events, at the 5.87 nCm^{-3} level, having return periods in the range 3.84–5.44 s.

Apart from this aspect the number of events is of itself quite interesting particularly when considered in relation to the total number of peaks (see Table 5) above similar threshold levels. Take, for example, the 5.87 nCm^{-3} level as before: the total number of peaks with maxima exceeding this is 9, whereas in the burst return period analysis 3 events occurred in the range 3.84–5.44 s. These three periods could embrace between 4 and 6 pulses dependent upon whether they were all in direct sequence or occurred in pairs on separate occasions, respectively. However the general conclusion from this must be that the conditions conducive to transport of tracer at high concentrations tend to persist, once established, for periods somewhat longer than 5 s since there appears to be at least some grouping of the pulses. This feature is in fact also evident from a visual examination of chart records. Expressed in another way the conclusion is: if a high concentration 'event' has recently been experienced then the probability of a recurrence is rather higher than would be expected on a purely random basis.

As in the unobstructed terrain data alluded to earlier there is evidence for the existence of very long return gaps in the analysis. This is well brought out by the presence of seven events of duration between 5.79 and 8.19 mins in the lowest threshold category and this alone would account for in the region of 50 min of the total observation time, i.e. ~ 45%. Physically these long intervals must presumably correspond to temporary shifts in oncoming wind direction and/or speed which sufficiently alter the recirculating wake location and probably also structure to the extent that tracer is persistently and systematically transported away from the detector concerned (IC1). However the occurrence of such lengthy periods without any ions at all being detected at the relatively close range from the source employed (2 m) remains something of a mystery particularly when one considers the apparently inherent and incessant instability and variability present in the flow system so near a building.

Note that the activity in the time range 30 ms to about 1 s corresponds with the 'internal' structure of the ion puffs and reinforces the comments made in earlier papers (loc. cit.) regarding the effects of high frequency turbulent fluctuations and the production of intense gradients of concentration (Chatwin and Sullivan, 1980).

5. CONCLUSIONS

The results obtained from these experiments have revealed various interesting features of dispersion and transport within and in the vicinity of recirculating wakes. In particular direct evidence has been obtained for the movement of tracer material in cyclic fashion between collectors and an extension of this experimental technique, principally involving an increase in the number of detectors deployed, should permit detailed trajectory investigations to be made. A further possibility and one with more practical application might be, for example, to place a pulsed ion source on the roof of a building and monitor the ensuing transport patterns and concentration distributions so as to optimize the subsequent siting of a proposed exit flue or stack.

The variety of tracer movements that can occur appears to be very considerable, judging not only from the ion concentration data but also from the preliminary smoke experiments that were carried out. This is of course to be expected in the open air where the oncoming flow is rarely, if ever, even approximately steady in the statistical sense. Whilst certain features of wake flows elucidated by wind tunnel studies (Vincent, 1977) were actually observed at the full-scale such flow regimes were invariably transitory and never persisted long enough to attempt correlation with particular sequences of ion concentration patterns (it may be feasible to obviate this difficulty by employing a conditional release system for the ion generator in which the upwind conditions are monitored and used to trigger the high voltage system). Hence the analysis has been intentionally orientated towards the objective of increasing the information available on the concentration distribution and structure in the wake *per se* without any (except superficial) attempts to delineate the fluid mechanical phenomena operating and responsible for their production.

Turning to the future, current experience suggests that the use of an increased number of detectors would permit much more illuminating studies to be carried out particularly of the transport phenomena occurring in wake regions. There is also evidence that the time separation between the ion puffs at release in the current trials was insufficient and should be extended so as to eliminate any risk of ambiguities arising regarding the attribution of particular events at the detectors with those of release of tracer.

The Appendix shows that mutual electro-static repulsion between the ions must, at least to some

extent, have modified the tracer behaviour. Whilst this inevitably detracts from the ultimate quality and universality of the results in terms of understanding and therefore modelling the transport and dispersion of 'passive' material, the effect was probably not too serious here. Nevertheless use of a lower output ion generator in any subsequent experiments is strongly recommended to minimize any deleterious effects as much as possible. One method of achieving this, and of simultaneously realizing a more ideal instantaneous point source, might be to release tracer over a much shorter time interval, say 0.1 s rather than 1 s. Even without reducing the generator current output itself this would decrease the total puff charge by a factor of ten (i.e. to 500 μC) and would afford a very significant improvement in passivity.

A final possibility for the future is that, since the tracer is unipolarly charged, electric field measurements could be made the basis for determining the details of the ion puff trajectory. This technique, which is both elegant and technically straightforward to carry out, has already been explored theoretically by Jennings and Jones (1977) and is a most attractive proposition.

REFERENCES

Barker C. D., Fackrell J. E., Foster P. M., Robins A. G., Sharpe B. F. and Varey R. H. (1982) The C.E.G.B. building wake dispersion study—a description of research carried out in 1980 and 1981. C.E.G.B. report Berkeley Nuclear Laboratories TPRD/B/0070/N82.

Britter R. E., Hunt J. C. R. and Puttock J. S. (1976) Predicting pollution concentrations near buildings and hills. *Proc. Conf. on Systems and Models in Air and Water Pollution*, Institute of Measurement and Control, London September).

BSI (British Standards Institution) (1972) Code of basic data for the design of buildings. Chapter V, Part 2, Wind Loads.

Castro I. P. and Robins A. G. (1977) The flow around a surface mounted cube in uniform and turbulent streams. *J. Fluid. Mech.* 79(2), 307–335.

Chatwin P. C. and Sullivan P. J. (1980) The structure of the probability density function of concentration in turbulent diffusion *Proc. 13th A.I.A.A. Fluid & Plasma Dynamics Conf.*, Snowmass, Co., U.S.A.

Cook N. J., Atkinson P. A. and Watts P. A. (1974) Investigating localised urban wind conditions in full-scale using a mobile anemometer mast. *J. Fluid Mech.* 79(2), 18–25.

Csanady G. T. (1973) *Turbulent Diffusion in the Environment*. D. Reidel, Dordrecht, Holland.

Drivas P. J. and Shair F. H. (1974) Probing the air flow within the wake downwind of a building by means of a tracer technique. *Atmospheric Environment* **8**, 1165–1175.

Eaton K. J. and Buller P. S. J. (1974) Wind speeds measured in urban areas with anemometers mounted on portable masts. 42nd Industrial Fluid Mechanics research meeting, N.P.L. and Leicester University Eng. Dept., 8–17.

Evans R. A. and Lee B. E. (1981) The problems of anemometer exposure in urban areas—a wind tunnel study. *Met. Mag.* **110**, 188–199.

Hadjitofi A. and Wilson J. J. G. (1979) Fast-response measurements of air pollution. *Atmospheric Environment* **13**, 755–760.

Halitsky J. (1963) Gas diffusion near buildings. *ASHRAE Trans.* **69**, 464–484.

Hall, D. J. (1980) The discharge of fume cupboard effluents into the atmosphere WSL report (Dept. of Industry) LR 345 (AP).

Hinds W. T. (1969) Peak-to-mean concentration ratios from ground level sources in building wakes. *Atmospheric Environment* **3**, 145–156.

Hosker R. P. (1981) Methods for estimating wake flow and effluent dispersion near simple block-like buildings. U.S. Dept. of Commerce, National Oceanic and Atmospheric Administration, Technical Memorandum ERL ARL-108.

Hunt J. C. R. (1982) Mechanism for dispersion of pollution around buildings and vehicles. *Proc. Colloquium, Abgasbelastungen durch den Kraftfahrzengverkehr im Nahbereich verkehrsreicher Strassen*, Verlag TUV Rheinland GmbH, 235–267.

Hunt J. C. R., Abell C. J., Peterka J. A. and Woo H. (1978) Kinematical studies of the flow around free or surface mounted obstacles: applying topology to flow visualization. *J. Fluid. Mech.* **86**, 179–200.

Hussain M. (1979) A study of the wind forces on low rise building arrays, and their application to natural ventilation design methods. Ph.D. thesis, Sheffield University.

Hussain M. and Lee B. E. (1980) A wind tunnel study of the mean pressure forces acting on large groups of low rise buildings. *J. Wind Engng indust. Aerodyn.* **6**, 207–225.

Jennings S. G. and Jones C. D. (1977) Tracking electrically charged puffs, as used in short range atmospheric diffusion investigations, by ground level electric field measurements. *J. Electrostatics* **2**, 367–373.

Jones C. D. and Hopkinson P. R. (1979) Electrical theory and measurements on an experimental charged crop spraying system. *Pestic. Sci.* **10**, 91–103.

Jones C. D. (1977a). Ion concentration variations at short distances downwind of continuous and quasi-instantaneous point sources. *Pestic. Sci.* **8**, 84–95.

Jones C. D. (1977b) Ionized air as a wind tunnel tracer. *J. Phys. E. Sci. Instrum.* **10**, 1287–1291.

Jones C. D. (1983) On the structure of instantaneous plumes in the atmosphere. *J. Haz. Mat.* **7**, 87–112.

Jones C. D. and Gulliford N. T. (1979) Developments in the use of ionized air as a wind tunnel tracer. *J. Phys. E. Sci. Instr.* **12**, 321–327.

Jones C. D. (1974) A Study of Turbulent Dispersion in the lower atmosphere using artificially produced electric space charge. Ph.D. thesis, University of Durham.

Murlis J. and Jones C. D. (1981) Fine-scale structure of odour plumes in relation to insect orientation to distant pheromone and other attractant sources. *Physiol. Ent.* **6**, 71–86.

Ogawa Y. and Oikawa S. (1982) A field investigation of the flow and diffusion around a model cube. *Atmospheric Environment* **16**, 207–222.

Owen, P. R. (1971) Buildings in the wind. *Q. Jl. R. met. Soc.* **97**, 396–413.

Vincent J. H. (1977) Model experiments on the nature of air pollution transport near buildings. *Atmospheric Environment* **11**, 765–774.

APPENDIX: ELECTRO-STATIC REPULSION AND IMAGE EFFECTS ON IONIZED AIR CLOUD BEHAVIOUR IN THE PULSED GENERATOR EXPERIMENTS

1. INTRODUCTION

The validity of most tracer techniques for atmospheric dispersion studies relies on the frequently unproven assumption that the material employed responds entirely passively to the atmospheric motions to which it is subjected. Moreover, in many cases, the dispersion information sought may well be in the context of a particular substance, e.g. NO_x, SO_2 and hence additional peculiarities of response could need consideration. Many tracers do in fact differ markedly from their

atmospheric host gases in several respects apart from those necessary for their detection, e.g. density, specific heat. Additionally, for other types of tracers factors such as particle size, release temperature and opacity to radiation can be important. Ionized air suffers from the obvious deficiency that the unipolarly charged volume which actually defines the 'marked' air will tend to expand due to electro-static repulsion, even in the complete absence of any fluid motion: laminar or turbulent. However, it is relatively easy to gain an approximate appreciation of the quantitative effects of this phenomenon by applying simple electro-static principles.

2. INITIAL CONDITIONS

In the pulsed generator experiments described in the main body of this paper ionized air was released for a 1 s period every 5 s* and thus the initial appearance of those ion puffs would have been of an approximately thin cylindrical form, see Fig. A1. Also shown is an impression of what the actual puff shape was probably like at the end of the 1-s period.

The length, L_0, is determined largely by the ambient flow conditions in the vicinity of the ion generator together with the exit velocity profile from the generator, the latter becoming progressively more influential as the wind speed decreases. If the ambient flow were constant, both in speed (u) and direction over the release period (rather unlikely in reality, particularly in the wake of a building), then L_0 would simply be ut where t is the release duration. R_0, the initial radius of the ion puff depends upon the nature of the wake from the ion generator system and also the interaction of the exit jet with the ambient flow. Wind tunnel measurements indicate that a value of 0.1 m for this particular generator is appropriate.

For the purpose of illustration we select a few representative values of u, namely 0.2, 0.5 and 1 m s^{-1} (the mean value observed at IC1 was 0.39 m s^{-1}) and assume that for these cases the initial puff is as in Table A1.

(Subsequent laboratory measurements have shown, with the particular value of EHT applied to the generator (−2 kV), the ion output current was −5 nA and, since the pulse duration was 1 s, the *total* charge per puff must have been −5 nC.)

3. ANALYSIS

3.1. *Mutual repulsion*

Whilst it is theoretically feasible to calculate the exact electric field distribution at all points on the surface of a cylindrical space charge cloud and thence determine the ensuing expansion (assuming the charge carriers are mobile) such a procedure is too complex to be justifiable here. Further the postulated cylindrical initial distribution is in itself a considerable approximation and thus the following simple method of assessing repulsion effects was developed.

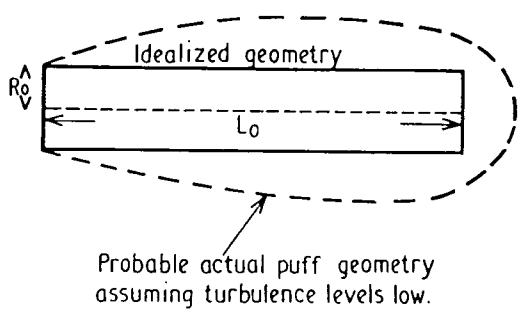

Fig. A1. Idealized and 'probable actual' initial ion puff geometry.

Table A1. Initial puff geometries selected for analysis

Ambient air speed (m s^{-1})	Length L_0 (m)	Radius R_0 (m)	Initial charge concentration nCm^{-3}
0.2	0.2	0.1	−796
0.5	0.5	0.1	−318
1.0	1.0	0.1	−159

First it is assumed that the expansion process is due solely to electrostatic repulsion ie no turbulent dilution effects are considered, consequently the analysis predicts the *maximum* concentration of ions likely to be observed at a given point. Second it is assumed that the charge is uniformly distributed within the cloud at all times, clearly this is unrealistic when turbulent phenomena are involved but when absent perfectly acceptable.

It was shown by Jones and Hopkinson (1979) that the axial electric field at the ends of a cylinder is

$$E_{ax} = \frac{-q}{2\pi R^2 L\varepsilon_0}\left[\sqrt{L^2+R^2}\,|-(L+R)\right], \qquad \text{(A1)}$$

where q is the total charge, R the radius and L the length.

The outward (radial) field, at any point on the curved surface of the cylinder, can be obtained from simple application of Gauss's Law, and is

$$E_{rad} = \frac{q}{2\pi RL\varepsilon_0} \qquad \text{(A2)}$$

but it should be noted that this expression becomes increasingly less accurate as $L/R \to$ unity.

The axial and radial expansion rates are now calculated from the expressions

$$\frac{dR}{dt} = \mu E_{rad}, \qquad \frac{dL}{dt} = 2\mu E_{ax}, \qquad \text{(A3)}$$

where μ is the ionic mobility. Hence

$$\frac{dR}{dt} = \frac{\mu q}{2\pi\varepsilon_0}\frac{1}{RL} \qquad \text{(A4a)}$$

and

$$\frac{dL}{dt} = \frac{-\mu q}{2\pi\varepsilon_0}\frac{2}{R^2 L}\left[\sqrt{L^2+R^2}\,|-(L+R)\right], \qquad \text{(A4b)}$$

which are simultaneous. Eliminating t (time) between them yields

$$\frac{dL}{dR} = \frac{-2}{R}\left[\sqrt{L^2+R^2}\,|-(L+R)\right] \qquad \text{(A5)}$$

which has the solution:

$$R = \frac{K\exp(-2\theta/3)}{\left[1-\tfrac{1}{2}\coth\frac{\theta}{2}\right]^{4/3}\left[2+\sinh\theta-2\cosh\theta\right]^{1/3}}, \qquad \text{(A6)}$$

where K is a constant of integration dependent on the initial conditions–ie L_0 and R_0 and

$$\theta = \sinh^{-1}\left(\frac{L}{R}\right).$$

Equation A6 thus allows the development of the puff shape (i.e. L/R) to be predicted but it is in an awkward form since it would be more useful to have R and L as functions of time. However evaluation of A6 for the range of initial conditions of concern here reveals that $(L-L_0) = a(R-R_0)$† within a

* Note that the effect of electro-static interaction, i.e. repulsion between separate puffs can readily be shown to be very small for these experiments and is not considered further.

† a is a constant.

few per cent throughout the expansion process. Thus, we may rewrite (A4a) in the integrable form

$$\frac{dR}{dt} = \frac{\mu q}{2\pi\varepsilon_0}\frac{1}{R}\frac{1}{a(R-R_0)+L_0} \quad (A7)$$

and integrating and putting $R = R_0$ at $t = 0$ gives

$$t = \frac{2\pi\varepsilon_0}{\mu q}\left[\frac{a}{3}(R^3 - R_0^3) + \left(\frac{L_0 - aR_0}{2}\right)(R^2 - R_0^2)\right]. \quad (A8)$$

The behaviour predicted is shown in Figs A2 and 3. It can be readily seen that the tracer performance is not ideal because the expansion is quite rapid particularly for the lowest wind speed case examined and results in a considerable reduction in ion concentration, see Fig. A4. It is interesting to note that, as t grows large $\rho \to C/t$, where C is constant, and thus the puff 'forgets' its initial conditions. In an earlier publications (Jones and Gulliford, 1979) simple theory was invoked to deduce that $\rho(t) = \varepsilon_0/\mu t$ and hence the very basic models employed in the analysis above do at least reflect this aspect of charged cloud behaviour accurately.

3.2. *Electro-static image effects*

The presence of any electric charge induces charges of opposite polarity in nearby objects and, consequently, an ion puff will experience attractive forces towards the ground and building walls in its immediate vicinity. Disregarding the latter for a moment, it has been shown by Jones (1974) that, for a charge in the neighbourhood of an infinite flat plane (it is reasonable to consider the Earth's surface as approximating to this)

$$h = \left[h_0^3 - \frac{3\mu q t}{16\pi\varepsilon_0}\right]^{1/3}, \quad (A9)$$

where h is the height above ground after time t and h_0 that when $t = 0$.

In the above it is assumed that the charge q resides in a point, in reality this is not so but, provided the charge centre and boundaries are well away from the flat surface being considered, errors remain small. Insertion of appropriate numerical values into A9 indicate that even after 10 s, h is only reduced by ~ 0.02 m from the release height of the ions, which was 1.23 m. Even if puff trajectories at much lower levels are considered eg at 0.5 m the height reduction is still quite small (h now 0.35 m) after 10 s.

Similar considerations will apply to the effects of walls etc and indicate that, at least in the majority of situations, image effects are very much secondary in importance compared with advective transport due to air motion.

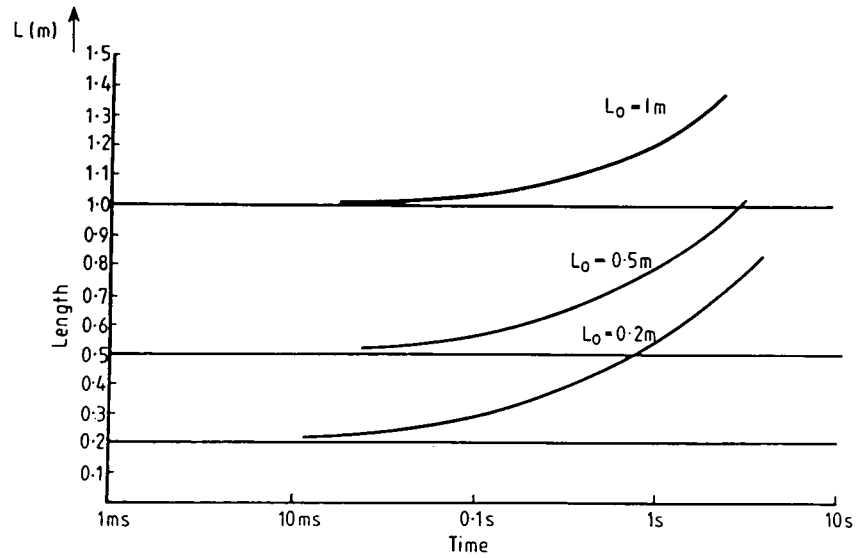

Fig. A2. Predicted values of ion puff length as a function of time.

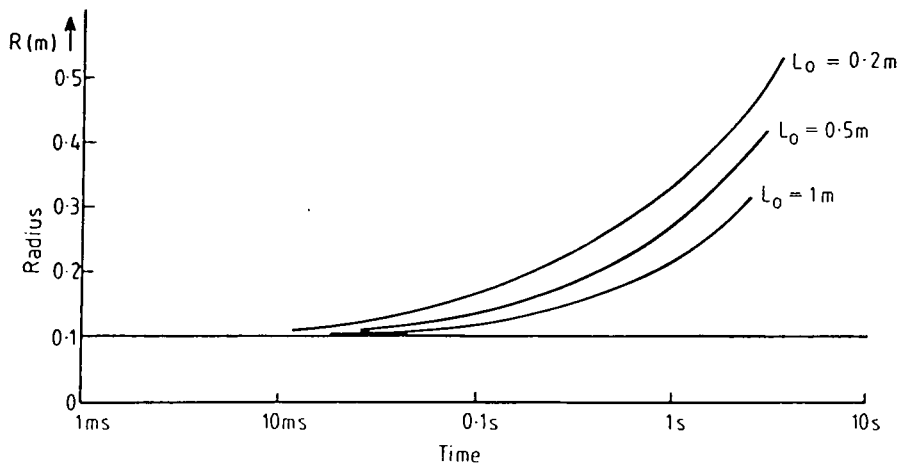

Fig. A3. Predicted values of ion puff radius as a function of time.

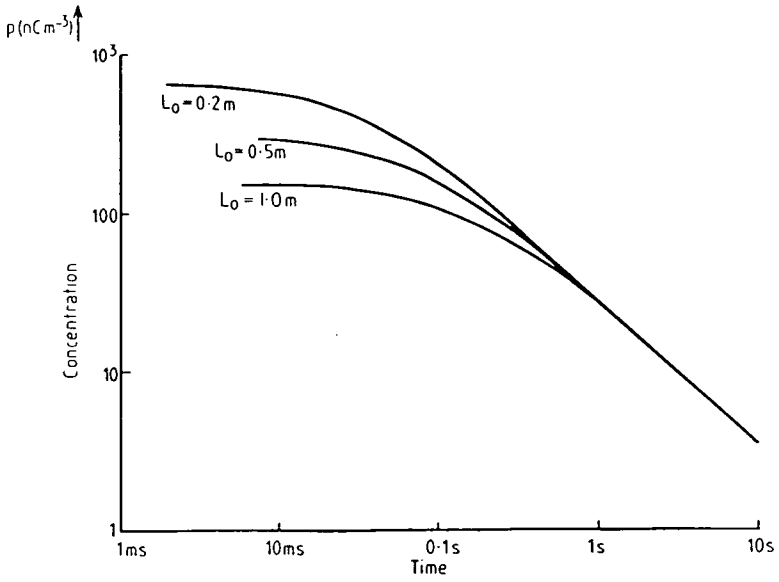

Fig. A4. Predicted values of ion puff concentration as a function of time.

Boreham B. W., Jones C. D. and Griffiths R. F. (1985).

Field evaluation of a new Langmuir-type probe for atmospheric dispersion studies using ions as a tracer.

J. Phys. E: Scientific Instruments. **18**, 218 - 223.

J. Phys. E: Sci. Instrum., Vol. 18, 1985. Printed in Great Britain

Field evaluation of a new Langmuir-type probe for atmospheric dispersion studies using ions as a tracer

B W Boreham†‖, C D Jones‡ and R F Griffiths§
† Department of Aeronautics, Imperial College of Science and Technology, London SW7 2BY, UK
‡ CDE, Porton Down, Salisbury, Wilts, UK
§ Pollution Research Unit, UMIST, Manchester M60 1QD, UK

Received 12 March 1984, in final form 29 August 1984

Abstract. A new type of ion detector probe has been evaluated under field conditions. Experiments were conducted at distances of up to 15 m downwind of a continuous point source of negative ions. The results obtained demonstrated clearly that this new device offered a significant improvement in performance over the previously used aspirator type of detectors. In particular the device possessed superior performance in terms of response time and reliability under adverse conditions. Future experiments are planned to exploit the potential of this device.

1. Introduction

During the last few years it has become increasingly recognised that the standard methodology used to determine the potential hazards arising from the presence of airborne toxic, inflammable or other substances with deleterious properties can produce results which could lead one to significantly underestimate the probable risks. This situation arises simply because the majority, if not all, of atmospheric dispersion models, and the predictions based upon them, are derived from a convenient but erroneous analogy between molecular and turbulent dispersion mechanisms. Generally speaking, the motion of the atmosphere near the Earth's surface is nearly always turbulent to some degree, at least near the Earth's surface, and thus the implications of this fundamentally dubious assumption are considerable. However, to be fair, the predictions of such models – the so-called 'Gaussian plume model' being the classical example – can be accurate and reliable if it is only the long term, i.e. accumulated, effects of exposure to a pollutant that determine the hazard. Consequently this type of analysis can be a perfectly acceptable basis for the assessment of risks associated with materials such as radio-isotopes and lead.

In many cases, however, it is the short term (10 s–1 min) or even the instantaneous (0.1–1 s) behaviour of the pollutant concentration that is the relevant parameter in assessing hazard. This is because, for example, toxic response for many irritant gases is determined by $\int C^n \, dt$ ($n > 1$) rather than $\int C \, dt$, the latter being the conventionally defined dosage. Whereas in the past it was tacitly assumed that the conventional models could be adapted to provide estimates of short term concentration variability by 'tinkering' with their predictions using simple mathematical devices such as peak to mean ratios, procedures of this type are not really acceptable for producing reliable hazard estimates. The reason is that the turbulent velocity field that transports and disperses materials released into the atmosphere does so in a markedly discontinuous way and thus, in reality, the concentration observed at a given point is highly intermittent in character. This is of course in marked contrast to the smoothly varying profiles, in both time and space, predicted by the Gaussian models referred to earlier. Indeed recent experimental evidence (Hadjitofi and Wilson 1979, Jones 1983) has fully substantiated this assertion and Chatwin and Sullivan (1979) has been a strong advocate, on both theoretical and practical grounds, that dispersion modelling will need to become statistically rather than deterministically based if significant progress is to be made in this area.

Undoubtedly a major difficulty in developing such a radically different approach to dispersion modelling has been the almost complete lack of field data with adequate time resolution. Thus a number of *ad hoc* treatments of concentration fluctuation statistics have appeared – probably the most prevalent (for no particularly good reason) being the log-normally based distributions. Indeed a recent analysis using a simple model fitted to experimental data by Ride (1983) suggests that other distributions may well be more appropriate.

In terms of experimental techniques, a major step forward occurred with the development and application of the ionised air tracer technique (Jones 1977a, b, 1979). This method enabled a considerable amount of good quality, very high resolution concentration data to be obtained which have been subsequently analysed in considerable detail (Jones 1978, 1983). A particularly important feature was the discovery of the existence of very high instantaneous concentrations, even at distances ~ 100 m from a tracer source, which appeared to correspond with those expected in completely undiluted material. Thus the values observed were almost certainly the result of pure advection of material, an occurrence certainly not predicted by conventional models, but however substantiating the concepts concerning the mechanism of turbulent dispersion set out by Chatwin and Sullivan (1979).

(This author argues cogently that turbulence in the atmosphere acts to produce advection, associated with the mean wind, together with progressive stretching, distortion and convolution of cloud elements. The concentration gradients of these elements are eventually smoothed out by molecular diffusion but this is, by comparison, a very slow process.)

The present paper describes a further step in the development of high resolution, ionised air tracer techniques. The ionised tracer system used consists, in brief, of the following items.

As with all such systems, a source of tracer is required, in this case unipolarly ionised air. This can be very conveniently provided by employing a corona point system, the asymmetric electric field created by the specific design of the device ensuring that the interelectrode space is filled largely with unipolar ions. These ions are expelled into the atmosphere by means of a low powered fan and then drift and diffuse downwind in the manner of a smoke or any other airborne material. This device, usually referred to as an 'ion generator', is compact, requires little electrical power and is therefore a very convenient instrument for field use. In addition the generator can be easily pulsed to simulate instantaneous sources, these latter being an important area of interest in atmospheric dispersion research.

In the present system the ionised air is detected, and its concentration measured, by means of both conventional aspirated ion collectors (see references cited earlier for a full description of the tracer system) and a new detection device, which is the subject of this paper. These former instruments,

‖ Present address: Monaro Research Laboratories, PO Box 190, Fyshwick, ACT 2609, Australia.

0022-3735/85/030218 + 06 $02.25

whilst very sensitive and responsive, are really too delicate for protracted field use. The main difficulty arises from the inevitable presence of substances such as dust, pollen, cobwebs and so on in the atmosphere which progressively reduce the integrity of the insulation between the collecting, bias and shielding electrodes. The problem is of course considerably exacerbated by high humidity. In the past various attempts at remedial measures have included the provision of heated inlet tubes for the collectors, and whilst some improvement has been obtained, performance was never very satisfactory.

The use of wind tunnels for the physical modelling of atmospheric dispersion scenarios, particularly those sufficiently complex to preclude rational theoretical analysis, has had a long tradition and provided much helpful data on which to form local planning recommendations and decisions. Very recently a research project was inaugurated with the specific purpose of assessing the potential value of employing miniaturised versions of the ion generator and collector used hitherto in field studies. A major objective was to establish whether concentration fluctuations, in addition to their time mean values, could be realistically modelled using this novel technique. During the course of the project it was realised that a promising alternative method of at least detecting ionised air might be to employ a device based on Langmuir probe concepts. In fact such a system would appear to offer considerable advantages over ion collectors in that it ought to be far more resistant to the deleterious effects of moisture and contamination ingress referred to previously.

Consequently, several small probes of this type were built and have performed extremely well in a wind tunnel (Boreham and Harvey 1983, 1984b, Boreham 1985a, b) and thus it seemed worthwhile to design an enlarged version suitable for field use. This paper presents and discusses the initial, and very encouraging, results obtained with this new system.

2. The ion probe

Figure 1(*a*) is a picture of the ion probe used in these trials. The basic design consists of two concentric electrodes and is shown schematically in figure 1(*b*). The inner, small diameter, electrode is solid and functions as the collector, whilst the outer electrode consists of a thin wire mesh, or grid, and serves to define the sampling volume which remains constant. An electrostatic field is applied between the two electrodes. The current flow to the collector from the gas sample is amplified using built-in circuitry, the design being given in figure 2. Its location within the probe is illustrated in figure 1(*b*). The amplifier output signal is proportional to the ion flux.

The bias potential applied to the probe is chosen so that the probe operates in or near the saturation regime in order to maximise the signal response.

Figure 3 shows the measured characteristics for the present probe for three different constant wind velocity values, U. The measurement was carried out in a 20″ octagonal section, low speed wind tunnel. The probe was located approximately 2 m downstream from the unipolar source. The theory of operation has been given in detail elsewhere (Boreham 1985a). The current

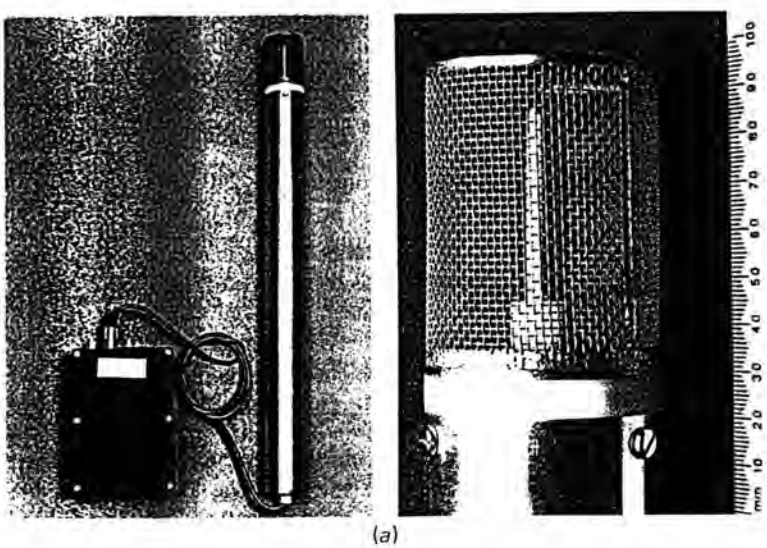

(*a*)

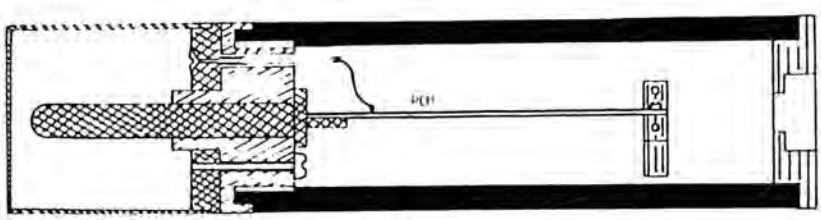

(*b*)

Gold plated brass mesh
Brass
Dural
Gold plated brass
PCB

Figure 1. (*a*) A general view of the ion detection probe and associated electronics and a close-up view of the probe head with reference scale. (*b*) Schematic view of the internal construction of the probe. PCB, amplifier printed circuit board.

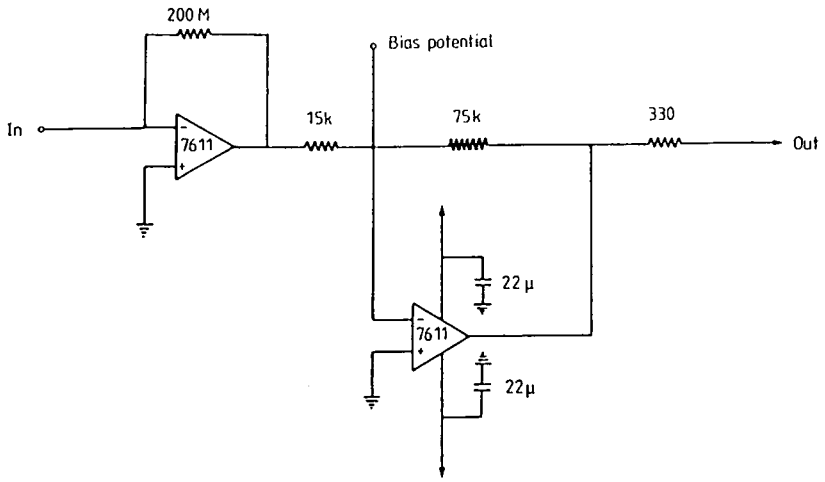

Figure 2. Head amplifier circuit for the ion probe.

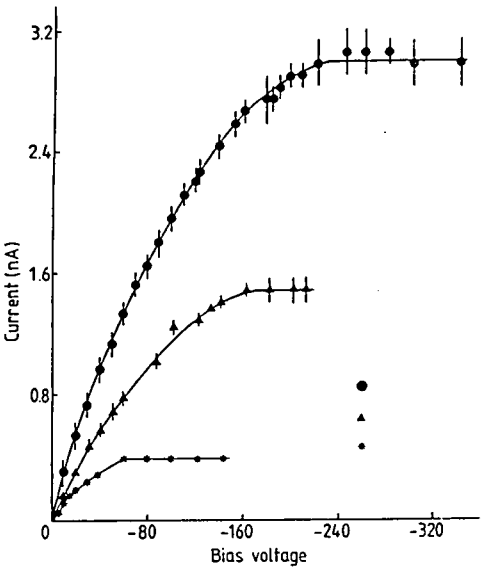

Figure 3. Characteristic curves for the probe. ●, $U = 5.4$ m s^{-1}; ▲, $U = 3.9$ m s^{-1}; *, $V = 1.5$ m s^{-1}.

measured by the probe is $i = \bar{F}wl$ where w and l are the collection area width and height respectively ($w = l = 0.05$ m in the present case) and $\bar{F}$ is the mean particle flux measured by the probe, defined by

$$\bar{F}(X, Y, Z) = \frac{\gamma}{wl} \int_{Y-w/2}^{Y+w/2} \int_{Z-l/2}^{Z+l/2} F(x, y, z)\, dy\, dz.$$

F is the flux field, γ a grid transmission factor (~ 1) and (X, Y, Z) is the collection area centre. The flux $F = U\chi$, where U is the wind velocity and χ the ion concentration. The collector electrode current will therefore increase with increasing wind velocity, as observed in figure 3. Hence a calibration curve (figure 4) is required for the measured current as a function of velocity to allow for operation with fluctuating wind speeds. The data of figure 4 were obtained from figure 3, assuming bias potentials of 60 V and 240 V.

For a sufficiently large variation in wind speed, nonsaturated probe operation may occur (i.e. the effective probe collection area decreases) and a calibration curve (such as that for a 60 V bias in figure 4) will be required for each value of the bias potential used, if absolute flux values are required. (For comparisons between relative values it is sufficient to assume $\bar{F}$ proportional to U.) If more than one probe is being used, it is also possible for the probes to operate in different regimes simultaneously, and a correction factor is required to allow direct comparison between signals obtained for operation in the saturated regime with those obtained in the nonsaturated regime. The required correction factor (equal to the ratio of the probe collection area to the effective collection area at nonsaturation) is obtained from a direct comparison of the calibration curves for saturated and nonsaturated operation (such as those in figure 4).

For these trials a bias potential of -240 V was chosen, with which probe saturation could be expected for wind speeds of up to 5.4 m s^{-1}. Air speeds during the experiments were typically ~ 2 m s^{-1}, which is well within this range. Saturated probe operation was therefore assumed and, consistently with the preliminary nature of these trials, no attempt was made to correct the measured signals for velocity fluctuations.

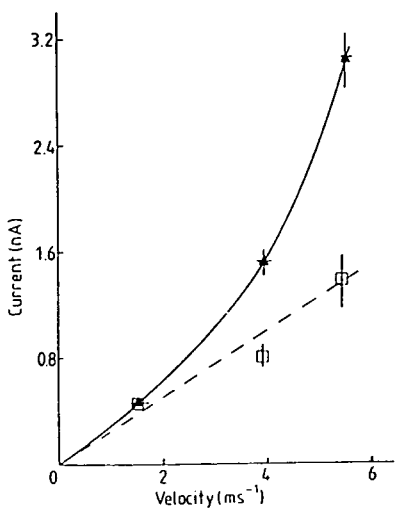

Figure 4. Probe calibration curve for saturated (▲) and nonsaturated (□) conditions.

3. Field trials

Field tests were carried out on two consecutive days early in November 1983 at the same site as the ion tracer experiments described by Jones and Griffiths (1984). The site consists of an extensive flat area of closely mown grass bordered by numerous shrubs and small trees. The surrounding area is also flat, but is given over to agricultural use, principally for root crops. The experiments described here were carried out with the instruments deployed on the closely mown grass so that the immediate upwind fetch was over the grass rather than the nearby shrubs and trees, and well away from the flat-roofed hut used for the dispersion experiments reported by Jones and Griffiths.

3.1. Probe and ion collector experiments

The experiments conducted on the first day employed two of the Langmuir-type probes operated simultaneously with an aspirated ion collector of the type developed by Jones and described fully in the references given in § 1. The ion generator used was the smaller of the two described elsewhere by Jones and Griffiths, giving a continuous current of ~ 5 nA of negatively ionised air at a volume flow rate of $\sim 1.25 \times 10^{-3}$ m^3 s^{-1}. With the ion generator positioned at a height of 1 m above the ground, the other devices were placed as follows, also at a height of 1 m above the ground. One Langmuir-type probe was located a distance of 1.5 m downwind of the ion generator; the second probe and the aspirated ion collector were located 2.5 m downwind of the ion generator, as close together as was consistent with ensuring that the air flow due to the aspirated collector did not interfere with the natural air flow to the probe. This was achieved by locating the head of the probe approximately 0.05 m to the side of the intake of the aspirated ion collector, which was facing upwind. A sensitive bi-directional vane/propeller anemometer was located 5 m upwind of the ion generator, at a height of 2 m, giving wind speed, azimuth and elevation in the vicinity of the instruments. The outputs from the anemometer, both probes and the aspirated ion collector were recorded on an eight-channel analogue FM instrumentation tape recorder, one channel being used for a voice-over commentary. The outputs from the two probes and the ion collector were also displayed on a recording oscilloscope so that the signals could be readily monitored and inspected throughout the experiment. Selected signals displayed on the oscilloscope were photographed. The experiment was operated successfully for several hours from mid-morning to mid-afternoon, during which time the wind direction was principally from the south, and the speed low, typically about 2 m s^{-1} as indicated by the bivane anemometer. The conditions were mild, the temperature being about 13° C (286 K) at mid-day, and the cloud cover was 6 oktas, with the cloud base at about 8000 ft. The stability category corresponding to these conditions would be class D (neutral) in the Pasquill scheme.

3.2. Probe only experiments

On the second day experiments were performed with the ion generator and the bivane anemometer located as for day 1, but only one Langmuir-type probe was used. The probe was operated for three successive periods of about 1 hour each, commencing mid-morning, being located for the first period at a distance of 5 m downwind of the ion generator, then at 10 m and 15 m in the second and third periods respectively. Both the ion generator and the probe were at a height of 1 m above the ground. The weather conditions throughout this experiment were very similar to those of day 1, with low windspeeds of about 2 m s^{-1} from the south. However, the sky was completely overcast, with the cloud base at about 2000 ft. Intermittent light drizzle commenced shortly after the experiment was started and accordingly neither the aspirated ion collector (which experience had shown would not work reliably in damp or wet conditions, due to leakage currents across the insulation between the electrodes) nor the tape-recording system were deployed. The signal from the probe was displayed on the recording oscilloscope and photographs were taken of some of the traces. The objective of this experiment (restricted by the unfavourable weather conditions) was to reveal the performance of the probe at increasing distances from the ion generator, the tests of day 1 having been carried out with a maximum distance between generator and probe of only 2.5 m. A further aspect was to test the probe in the light drizzle conditions referred to above, in which the aspirated ion collector would certainly not be operable without constant remedial attention, and probably would not be operable at all.

4. Results and discussion

4.1. Probe and ion collector experiments

Of the several hours of tape-recorded data from day 1 the sequence shown in figure 5 is a typical example. In considering these results it should be borne in mind that whilst the aspirated ion collector gives a signal that is proportional to the ion concentration in the aspirated flow, the Langmuir-type probe measures the flux of ions swept through its collection cross section by the air flow of the wind. Thus the probe output signal is proportional to both ion concentration and windspeed as discussed in § 3. With the particular configuration of the probe electrodes used here, the ion flux is independent of the direction of the horizontal wind component. Bearing these points in mind, one may note that the signals from the aspirated ion collector (uppermost trace) and the probe located at 2.5 m from the ion generator show a very marked degree of intercorrelation, similar to that obtained in experiments by Storebø *et al* (1983) using a multiple array of aspirated ion collectors located at a distance of 37.5 m from an ion generator of current strength 0.2 μA, with a typical cross-wind separation between ion collectors of 0.12 m. The traces also reveal the features of intermittency and fine scale

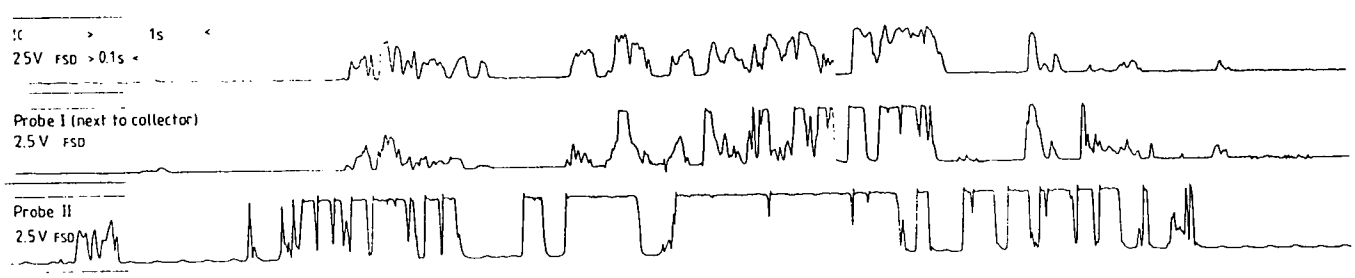

Figure 5. A segment of the simultaneous records obtained from the aspirated ion collector (top trace) and the two ion flux probes (see §§ 3.1 and 4.1).

structure in the concentration, with the probe apparently displaying a faster response than the collector, based on the timescale of the most rapid fluctuations in the two traces, which is somewhat less than 0.01 s. The signal obtained from the probe located at 1.5 m from the ion generator reveals saturation of the probe amplifier over a substantial portion of the record. This is also evident over a lesser portion of the record from the probe located at 2.5 m from the ion generator.

It is instructive to compare the magnitude of the outputs of the co-located probe and ion collector in relation to the corresponding ion concentrations. For the ion collector the full scale deflection in figure 5 represents 2.5 V, and the settings used yield 45 nC m^{-3} V^{-1} for the relationship between ion concentration and amplifier output. Thus the largest signals on the ion collector trace correspond to an ion concentration of ~80 nC m^{-3}. The operating conditions for the probe at the same location correspond to 0.2 nA V^{-1} in terms of ion-current-to-the-probe-electrode per volt of output signal. Full scale deflection on this trace is also 2.5 V, so the largest signals are approximately 0.4 nA. Treating the ion current to the probe as a simple collection cross-section problem, so that the current is the product of windspeed, ion concentration and collector cross-sectional areas as indicated in § 2, for operation at saturation, the ion current is 0.4 nA for a cross section of 0.05 m × 0.05 m (height and diameter of the electrode system) with an ion concentration of 80 nC m^{-3} and a windspeed of 2 m s^{-1}, which was a typical value in this experiment. The outputs from the two devices are thus self-consistent.

4.2. *Probe-only experiments*

A selection of signals obtained in the experiment of day 2 with the probe located at 5, 10 and 15 m downwind of the ion generator is shown in figure 6. This demonstrates that the probe is able to give significant signal amplitude over this range of distances. Deployment of the probe at distances of perhaps a few hundred metres from the source can be envisaged, since the ion flux can be increased simply by enlarging the electrodes. This would be expected to be more effective than increasing the ion generator current, since it appears that after a quite short time of travel from the generator the ion concentration becomes independent of the ion current at the source, other things being equal. This is attributable to the effects of electrostatic self-repulsion in the early stages of the ion travel, a larger source current resulting in ion clouds of larger size rather than of higher ion concentration (Jones and Gulliford 1979, Storebø *et al* 1983).

A noteworthy feature of this experiment was that the probe operated reliably in light drizzle without remedial attention.

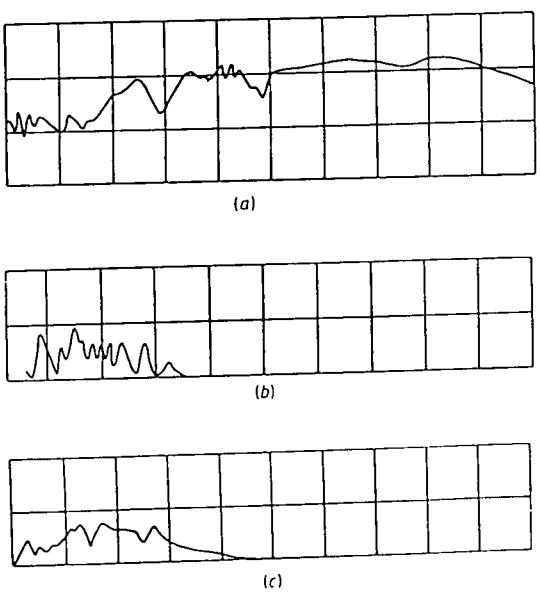

Figure 6. Typical signals obtained from the ion flux probe located at downwind distances of (*a*) 5 m, (*b*) 10 and (*c*) 15 m. Vertical scale: 0.1 V per division; horizontal scale: (*a*) 50 ms/div, (*b*) 0.2 s/div, (*c*) 0.2 s/div.

4.3. *Further development of probe*

As discussed above, the Langmuir-type probe measures ion flux, whereas the aspirated ion collector measures ion concentration. Although both are parameters of interest in atmospheric dispersion studies, concentration is the more commonly used in modelling and measurement. In order to calculate the ion concentration from the ion flux one must know the 'instantaneous' windspeed, the measurement for preference being made using a device at least as fast in response as the probe itself. It is envisaged that this could be achieved using a single hot wire anemometer, the wire axis being aligned with the electrode axis. In this way, the output of a hot wire device located near the cylindrical electrode system could be used with suitable signal processing, to give flux, concentration and horizontal windspeed (assuming the device is oriented as in the experiments described here).

5. Conclusions

The Langmuir-type probe described here has been shown by these field tests to be a promising device for the study of atmospheric dispersion using ionised air as the tracer. As an alternative to the aspirated ion collector developed for such studies it has several preferable features in terms of response time, reliability, the lack of moving parts and motors, lower power consumption, and susceptibility to airborne dust, debris, insects, rain and moisture. With the addition of a built-in wind speed measuring device and appropriate signal processing as envisaged in § 4 it offers substantial scope as a device for dispersion experiments, particularly in the important aspect of the fine structure of the concentration field. It is the intention of the authors to apply, develop and evaluate the device in further field experiments.

References

Boreham B W 1985a A new fast response probe for diffusion studies in air
J. Phys. E: Sci. Instrum. To be published

Boreham B W 1985b Preliminary investigation of dispersion of pollutants in model building wake flows using bipolar space charge. *Atmos. Environ.* to be published

Boreham B W and Harvey J K 1983 Monitoring the atmospheric diffusion of puffs and plumes and bipolar space charge at small scale in wind tunnels
Proc. IUTAM Symp. 'Atmospheric Diffusion of Heavy Gases and Small Particles' Delft University of Technology, August 29–September 2, 1983 (Berlin: Springer)

Boreham B W and Harvey J K 1984a Bipolar charged particles as markers for dispersion simulation in wind tunnels
J. Phys. E: Sci. Instrum. 17 994–8

Boreham B W and Harvey J K 1984b to be submitted

Chatwin P C and Sullivan P J 1979 On the probability density function of concentration in turbulent dispersion
Trans. CSME 5 192

Hadjitofi A and Wilson M J G 1979 Fast response measurements of air pollution
Atmos. Environ. **13** 755–60

Jones C D 1977a Ion concentration variations at short distances downwind of continuous and quasi-instantaneous point sources
Pestic. Sci. **8** 84–95

Jones C D 1977b Ionised air as a wind tunnel tracer
J. Phys. E: Sci. Instrum. **10** 1287–91

Jones C D 1978 Statistics of the concentration fluctuations in short-range atmospheric dispersion
Conf. on Mathematical Modelling of Turbulent Diffusion in the Environment, Liverpool ed. C J Harris

Jones C D 1983 On the structure of instantaneous plumes in the atmosphere
J. Haz. Mat. **7** 87–112

Jones C D and Griffiths R F 1984 Full scale experiments on dispersion around an isolated building using an ionised air tracer technique with very short averaging time
Atmospheric Environment **18** No 5 903–16

Jones C D and Gulliford N T 1979 Developments in the use of ionised air as a wind tunnel tracer
J. Phys. E: Sci. Instrum. **12** 321–7

Ride D J 1983 A probabilistic model for dosage
Proc. IUTAM Symp. 'Atmospheric Diffusion of Heavy Gases and Small Particles', Delft University of Technology, August 29–September 2, 1983

Storebø P B, Bjorvatten T, Hønnashagen K, Lillegraven A, Jones C D and van Buijtenen C J P 1983 Tracer experiments with turbulently dispersed air ions
Boundary Layer Meteorology **26** 127–39

Chatwin P. C., Hajian N. T., Mole N. and Jones C. D. (1989).

Investigations on the atmospheric dispersion of clouds containing charged tracers.

IMA J. Appl. Math. **42**, 97 - 117.

IMA Journal of Applied Mathematics (1989) **42**, 97–117

Investigations on the Atmospheric Dispersion of Clouds Containing Charged Tracers

P. C. CHATWIN, N. T. HAJIAN, N. MOLE

Department of Mathematics and Statistics, Brunel University, Uxbridge, Middlesex UB8 3PH, UK

AND

C. D. JONES

Chemical Defence Establishment, Porton Down, Salisbury, Wiltshire SP4 0JQ, UK

[Received 24 March 1987 and in revised form 21 November 1988]

Many different sensor systems are used in experimental studies of atmospheric dispersion and the results obtained with each of them need careful interpretation. This paper was motivated by an unusual sensor system, in which charged particles are used as a tracer material. Earlier results for special configurations of charge are generalized, and lead to a condition which ensures conservation of total charge and a negligible influence of image charges. The remainder of the paper discusses some basic physics of charged clouds dispersing in turbulent flow and shows (partly on the basis of exact results for simple models) that order-of-magnitude, and other, results for clouds of passive tracer can be extended rather simply to charged clouds. A principal conclusion of the work is that the sensor system's use should be extended and certain suggestions are made for future work.

1. Introduction

THE GREAT practical importance of atmospheric dispersion has led to the development of many different sensor systems for measuring the concentrations of substances (especially gases) that have been injected into the air. One major difficulty, present in some degree in all turbulent flows, that concerns the designer of any such sensor system is the wide range of length and time scales that occur during the evolution of the cloud of injected substance. Particularly difficult to record faithfully is the fine structure which is associated with very small length scales (typically of order 10^{-3} m) and rapid changes (on times of order 10^{-2} to 10^{-1} s). Such structure is of crucial importance in understanding the dynamics of concentration fluctuations (e.g. Chatwin & Sullivan, 1979a; Carn & Chatwin, 1985).

In the atmosphere, the existence of these fluctuations is evident to anyone who has ever observed the behaviour of the smoke from, say, a garden bonfire on a breezy day. It is the unceasing changes of wind velocity, over a wide range of spatial and temporal scales, which cause variations in both the instantaneous trajectory and the internal structure of the smoke 'parcels' comprising the plume, thus producing, at any instant, a complex and inherently unpredictable distribu-

tion of smoke. In the past, and indeed to a large extent even now, the modelling of atmospheric dispersion phenomena and the calculation of the concentration of materials released into the atmosphere has been based on the employment of Gaussian plume concepts which, at best, can yield only time-averaged concentrations. By their very nature, such estimates (they are not predictions!) of concentration represent averages over periods in which the effects of many turbulent eddies are smeared out: therefore neither the high instantaneous concentrations associated with material directly advected from source to receptor nor the long periods of zero concentration (i.e. the intermittency) are described.

In many situations of practical interest the existence of a highly structured concentration field is not important because it is only the long-period average concentration multiplied by the exposure time (i.e. the dosage) that is relevant as in, for example, radionuclide toxicology. However, in other cases, such as exposure to certain toxic gases (ammonia and chlorine are notable in this respect), there may be proportionately much greater effects for a *given* dosage if the concentration is high (Ride, 1984; Griffiths & Harper, 1985). Other examples of situations in which it is necessary to take account of the instantaneous distribution of material in order to make realistic practical assessments are (i) flammability/explosion studies, and (ii) malodour nuisance.

Deterministic modelling of the instantaneous structure of a cloud of dispersing material is inherently impossible and, therefore, a statistical approach is essential for the practical situations discussed above. Such an approach requires validation with data acquired using appropriately high-resolution detectors and a suitable tracer material. In the past, chemical tracers (e.g. SO_2, SF_6, C_4H_{10}) have often been used, but none has proved very satisfactory. Generally, chemical techniques suffer from two major deficiencies, namely,

(a) inadequate temporal response – i.e. the rapid fluctuations in concentration are missed (averaged out in practice);

(b) general lack of stability – characterized by features such as baseline drift, need for recalibration, hysteresis, etc.

This paper deals with a novel technique developed by Jones (1979, 1983) which has neither of the above deficiencies and, moreover, can be made responsive to *most* of the small-scale structure present in clouds dispersing in the atmospheric boundary layer. Briefly, the system consists of a constant source of unipolarly (usually negative) ionized air produced by a stabilized corona discharge and a series of detectors located at appropriate positions downwind (up to about 100 m) of the source. The detectors operate on a biased coaxial cylinder electrode principle in which the ionized air tracer is drawn into the detector by means of a low-power suction fan whereupon the ions experience a strong electric field and are repelled onto a collecting electrode. The collected current, typically 10^{-12} to 10^{-8} A, is sensed by a high-speed feedback amplifier that produces a voltage output proportional to that current and thus to the local instantaneous ion concentration. The special feature of this system which makes it potentially so useful and attractive is the extremely fast response time ($\sim 10^{-2}$ s), which allows

high-resolution measurements up to 100 Hz bandwidth. In addition, the system is unusually robust, and has been successfully deployed in both laboratory *and* field (full-scale) trials. In the latter regard, it is different from many (e.g. LDA) systems currently fashionable in laboratories.

However, the interpretation of data taken with this system requires consideration of the inevitable electrostatic effects that influence the dispersion in addition to the universal processes of advection and molecular diffusion. Such consideration is the concern of the present paper.

2. Basic background

The presence of the electric charge of density $\rho(\boldsymbol{x}, t)$ sets up an electric field $\boldsymbol{E}(\boldsymbol{x}, t)$ which, in the absence of magnetic effects, is conservative with potential $\varphi(\boldsymbol{x}, t)$ such that

$$\boldsymbol{E} = -\nabla\varphi, \qquad \nabla^2\varphi = -\rho/\epsilon_0. \tag{2.1}$$

Here, ϵ_0 is the permittivity, which can be taken to be the vacuum permittivity with value $\epsilon_0 \approx 8{\cdot}85 \times 10^{-12}\,\mathrm{C V^{-1} m^{-1}}$. In practice, the ground will be an equipotential, and therefore there is the possibility of charge leakage to earth; this is discussed later in this section. Also, the injected charge distribution is confined; thus $|\boldsymbol{E}| = |\nabla\varphi|$ must approach zero at great distances. Note that this condition implicitly assumes that the ambient atmospheric electric field can be ignored. Indeed, its magnitude is of order $100\,\mathrm{V\,m^{-1}}$, whereas values of $|\boldsymbol{E}|$ generated in trials using Jones's sensor system are usually orders of magnitude higher, e.g. $10^4\,\mathrm{V\,m^{-1}}$ (Jones & Hutchinson, 1976) and $10^5\,\mathrm{V\,m^{-1}}$ (Storebø *et al.*, 1983).

The velocity of charged particles differs from that of the ambient air, denoted here by $\boldsymbol{u}(\boldsymbol{x}, t)$, by an amount $\mu\boldsymbol{E}(\boldsymbol{x}, t)$, where μ is the mobility. The value of μ depends on many factors, especially ion size, but, for the small ions generated by the sensor system, $|\mu|$ is typically of order $10^{-4}\,\mathrm{V^{-1}\,m^2\,s^{-1}}$ (Jones, 1979). (In this paper, the sign convention adopted is that $\mu\rho$ is always positive, and that ρ has the sign of the ionic charge.) The evidence is that ion recombination can be ignored (Jones, 1977b), so that the equation of charge conservation takes the form

$$\frac{\partial\rho}{\partial t} + \nabla\cdot[\rho(\boldsymbol{u} + \mu\boldsymbol{E})] = \kappa\nabla^2\rho, \tag{2.2}$$

where κ is the molecular diffusivity. Equation (2.2) is standard except for the inclusion of the mobility term, but this, of course, makes the process nonlinear because of the dependence of $\boldsymbol{E}$ on ρ. The magnitude of $\mu\boldsymbol{E}$ is greatest in the early stages of dispersion when, obviously, electrostatic repulsion is most intense. For values of $|\boldsymbol{E}|$ of 10^4 to $10^5\,\mathrm{V\,m^{-1}}$ reported above, $|\mu\boldsymbol{E}| \sim 1$–$10\,\mathrm{m\,s^{-1}}$, certainly comparable with mean wind speeds.

The velocity field $\boldsymbol{u}(\boldsymbol{x}, t)$ is incompressible, i.e.

$$\nabla\cdot\boldsymbol{u} = 0, \tag{2.3}$$

and satisfies the Navier–Stokes equations. These need not be given here; what requires emphasis is that $\boldsymbol{u}$ and (therefore) ρ and $\boldsymbol{E}$ are random variables. The philosophy and principles of the statistical approach that is necessary are described by Chatwin (1982). Here it suffices to note some key points. In general, the random variables are *not* statistically stationary or homogeneous; for one thing, it is important to be able to deal with the dispersion of finite regions of material ('clouds') generated by release over a finite period of time and such processes are inevitably nonstationary. Mean values are therefore ensemble means and cannot, in general, be estimated by time or space averages. Such means will be denoted by overbars, and the fluctuations (differences between actual and mean values) by primes in the normal way. Thus, for example,

$$\rho = \bar{\rho} + \rho', \quad \boldsymbol{u} = \bar{\boldsymbol{u}} + \boldsymbol{u}' \qquad \text{with } \overline{\rho'} = 0, \quad \overline{\boldsymbol{u}'} = \boldsymbol{0}, \tag{2.4}$$

and all variables appearing in equation (2.4) are, in general, functions of $\boldsymbol{x}$ and t. However, it may often be possible and appropriate to ignore any dependence of mean wind $\bar{\boldsymbol{u}}$ on t and the horizontal components of $\boldsymbol{x}$.

The sensor system can be deployed in either of two modes. In one, leading to charged plumes, unipolar ions are injected at a constant rate over a substantial period. In the second, leading to charged clouds, a fixed quantity Q_0 of charge is injected almost instantaneously. Since, at least in principle, clouds form a canonical situation from which the properties of plumes can be inferred (exactly – in theory – when $\mu = 0$ and approximately when μ is relatively small), this paper will emphasize the second mode. The physics is, of course, essentially the same for both modes; results for plumes corresponding to those given below can be obtained easily and some are given in Chatwin (1985).

The advantages of the sensor system have been summarized above. Its use requires that the differences in dispersion properties between a cloud of passive tracer (smoke, foreign gas, etc.) and a cloud containing charged tracers are small enough for useful results about the former, practically more important, situation to be deducible from data taken in the second situation. In simple physical terms, the differences are due to (a) the effect of electrostatic repulsion leading to an increase in the size of the charged cloud compared with a conventional cloud of tracer of the same initial size, and (b) the possibility of loss of charge by leakage to earth (which corresponds – in a conventional cloud – to nonconservation of mass of the tracer).

It happens that there is a simple result that enables a global treatment of both (a) and (b) to be given. Suppose that the initial volume of the cloud is V_0. It is believed that the assumption that the initial charge density ρ_0 is uniform is a good one; thus

$$\rho_0 = Q_0/V_0. \tag{2.5}$$

Since Péclet numbers are typically of order 10^6, molecular diffusion plays little role in the global distribution of charge and will be neglected in the following treatment. Equation (2.2) then has a solution in which the charge density ρ at time t after release is independent of position $\boldsymbol{x}$ within the cloud, because use of

(2.3) and the approximation $\kappa = 0$ reduces equation (2.2) to

$$\frac{\mathrm{d}\rho}{\mathrm{d}t} + \mu\rho\nabla \cdot \boldsymbol{E} = 0, \tag{2.6}$$

assuming ρ does not depend on $\boldsymbol{x}$. Since, from (2.1),

$$\nabla \cdot \boldsymbol{E} = \rho/\epsilon_0, \tag{2.7}$$

it follows that (2.6) is a simple ordinary differential equation for $\rho(t)$ with solution

$$\rho = \rho_0(1 + t/T_e)^{-1} \quad \text{with } T_e = \epsilon_0/\mu\rho_0. \tag{2.8}$$

Assuming for the moment that total charge is conserved, it follows from (2.8) that the cloud volume V satisfies

$$V = V_0(1 + t/T_e). \tag{2.9}$$

Equation (2.8) was derived in a different context (the relaxation of electrostatic charge in hydrocarbon fuels) by Bustin *et al.* (1964), and extensions were discussed by Gavis (1967). The present derivation shows clearly that the existence of motion in the ambient fluid does not affect the result (provided the motion is incompressible); this is a powerful extension. Jones (1977a) derived the special cases of (2.8) and (2.9) for a spherical cloud. The time scale T_e is an important one since it is clear from (2.9) that it is a measure of the time within which electrostatic effects become significant. Typical values in actual use of the sensor system range from $T_e \sim 5 \times 10^{-4}$ s (Storebø *et al.*, 1983: $\rho_0 \approx 7{\cdot}6 \times 10^{-5}$ C m^{-3}) to $T_e \sim 20$ s (Jennings & Jones, 1977: $\rho_0 \approx 2{\cdot}3 \times 10^{-9}$ C m^{-3}), and other examples are given in Chatwin (1985).

It is now possible to assess when it is reasonable to assume that total charge is conserved. Integration of equation (2.2) (with $\kappa = 0$) over all space gives

$$\frac{\mathrm{d}Q}{\mathrm{d}t} = \mu \int [\rho E_z]_{z=0}\,\mathrm{d}x\,\mathrm{d}y, \tag{2.10}$$

where Q is the total charge at time t and $z = 0$ is the ground (assumed plane) at which $\boldsymbol{u} = \boldsymbol{0}$. It is therefore reasonable to assume total charge is conserved, i.e. $Q = Q_0$ for all t, provided $[\rho E_z]_{z=0}$ is negligibly small. This is not likely to be true whenever a mean cloud radius at time t, say $(3V/4\pi)^{\frac{1}{3}}$, is comparable with the cloud release height H_0, i.e. whenever

$$\frac{3V_0}{4\pi}\left(1 + \frac{t}{T_e}\right) \sim H_0^3, \tag{2.11}$$

using equation (2.9). For practical applications, it is more convenient to replace t by $d/\bar{u}$, where d is the downwind distance between ion generation and ion collection and $\bar{u}$ is the mean wind speed. If $R_0 = (3V_0/4\pi)^{\frac{1}{3}}$, it follows that charge leakage to earth can be neglected provided that

$$\frac{4\pi\bar{u}(H_0^3 - R_0^3)\epsilon_0}{3\mu d Q_0} \gg 1. \tag{2.12}$$

It can be shown also that satisfaction of condition (2.12) ensures that the movement of the cloud towards the ground caused by image charges is negligible (Jones, 1977a; Chatwin, 1985). Typical values of the left-hand side are ~250 (for $H_0 \approx 8{\cdot}5$ m, $R_0 \approx 5 \times 10^{-2}$ m: Storebø *et al.*, 1983) and ~450 (for $H_0 \approx 5$ m, $R_0 \approx 1$ m: Jennings & Jones, 1977) with, in both cases, $d/\bar{u} = 12{\cdot}5$ s. This time of travel is typical of those in the experiments that have so far been conducted. When (2.12) is not satisfied, the interpretation of the data is inevitably difficult. It is therefore recommended that the sensor system be deployed so that (2.12) is always satisfied.

The remainder of this paper explores some of the principal differences in the dispersion properties of charged and uncharged clouds, with the main aim of developing some understanding of the interactions between electrostatic effects and the processes (advection and molecular diffusion) controlling the dispersion of uncharged clouds. Such understanding is worthwhile in itself and, furthermore, it will aid and/or reinforce inferences from the data collected with the sensor system. Indeed, the authors would argue that data collection without an attempt at understanding the basic physics is not proper science.

However, it cannot be emphasized too highly that the dispersion of clouds of *passive* tracers in turbulent flow is not (yet) understood in the sense that, while most of the physics can be described in at least qualitative terms, there is no method available for predicting with reasonable confidence the quantitative behaviour of properties as fundamental as the size of the mean-square fluctuation. The reasons for this are well known; the most important ones are alluded to later in this paper. In charged clouds, there is the additional complication of electrostatic effects. It is therefore obvious that rapid progress in the theoretical description of the dispersion of charged clouds cannot be expected; realistically, this paper considers only some aspects of this problem in which progress has been made.

3. The dispersion of small clouds

Some understanding of the turbulent dispersion of uncharged clouds has been gained by studying the dispersion of small clouds, with linear dimensions not exceeding about five Kolmogoroff microscales, i.e. about 1 cm in normal atmospheric conditions (Townsend, 1951; Chatwin & Sullivan, 1979a). The understanding relates to the very important small-scale physical processes and, in the spirit exposed at the end of Section 2, this section aims to extend, in part, that understanding to small charged clouds.

For such small clouds, it is possible to approximate the velocity field $\boldsymbol{u}$ relative to the centre of the cloud by constant shear, so that

$$\boldsymbol{u} = (\alpha_1 x_1,\ \alpha_2 x_2,\ \alpha_3 x_3), \tag{3.1}$$

where (x_1, x_2, x_3) are the components of $\boldsymbol{x}$, and the α_i are the principal rates of strain. In equation (3.1), the axes are the principal axes of rate of strain and their orientation in space varies from realization to realization of the dispersion in random fashion. (Saffman (1963) explains why it is possible to ignore the

solid-body rotation contribution to $\boldsymbol{u}$; essentially the reason is that this makes no contribution to the *change* of shape of the cloud.) Incompressibility – equation (2.3) – requires that

$$\alpha_1 + \alpha_2 + \alpha_3 = 0. \tag{3.2}$$

In the absence of electrostatic effects and of molecular diffusion, a spherical cloud of initial radius R_0 is converted at time t into the ellipsoid

$$(x_1/a_1)^2 + (x_2/a_2)^2 + (x_3/a_3)^2 = 1, \tag{3.3}$$

where, for each i,

$$a_i = R_0 \exp(\alpha_i t). \tag{3.4}$$

The volume of the ellipsoid in (3.3) should of course, by incompressibility, be $\frac{4}{3}\pi R_0^3$ for all t; it is easily verified that this is true using (3.2).

With electrostatic repulsion, the volume of a small, initially spherical, charged cloud must increase with t according to (2.9), i.e. its volume must be $V(t)$, where

$$V(t) = \tfrac{4}{3}\pi R_0^3(1 + t/T_e). \tag{3.5}$$

The derivation of (2.9) gave no indication of the *shape* of the charged cloud, and this is a crucial factor in determining the magnitude of statistical properties (Chatwin & Sullivan, 1979a). The rates of change of the principal axes of the ellipsoid (3.3) for a charged cloud are given by

$$\frac{da_i}{dt} = [u_i + \mu E_i]_{x=a_i e_i} = \left[\alpha_i a_i - \mu \frac{\partial \varphi}{\partial x_i}\right]_{x=a_i e_i}, \tag{3.6}$$

where there is no summation, and the $\boldsymbol{e}_i$ are unit vectors. Kellogg (1953: pp. 192–6) gives φ for a uniformly charged ellipsoid, and it is therefore possible to find the a_i from equation (3.6). Here, since the single aim of the work is increased physical understanding, results for two special cases only will be given. Further algebraic details can be found in Chatwin (1985).

Consider first the case when the ellipsoid in (3.3) is an oblate spheroid (i.e. shaped like a discus); this occurs when

$$\alpha_1 = \alpha_2 = \alpha, \quad \alpha_3 = -2\alpha \qquad (\alpha > 0), \tag{3.7}$$

and it is then convenient to replace (x_1, x_2, x_3) by (x, y, z), and to write the equation of the ellipsoid as

$$\frac{x^2 + y^2}{a^2} + \frac{z^2}{c^2} = 1, \tag{3.8}$$

for some $a(t)$ and $c(t)$, with $a > c$. The eccentricity $\varepsilon(t)$ satisfies

$$c^2 = a^2(1 - \varepsilon^2), \tag{3.9}$$

so that $\varepsilon = 0$ gives a sphere and $\varepsilon = 1$ gives a flat circular disc (with proper attention to limiting processes). Use of (3.6) and the expressions in Kellogg's

book gives

$$\frac{da}{dt} = \alpha a + \frac{3\mu Q_0}{4\pi\epsilon_0 a^2}\left(\frac{\arcsin\varepsilon - \varepsilon(1-\varepsilon^2)^{\frac{1}{2}}}{2\varepsilon^3}\right),$$
$$\frac{dc}{dt} = -2\alpha c + \frac{3\mu Q_0}{4\pi\epsilon_0 a^2}\left(\frac{\varepsilon - (1-\varepsilon^2)^{\frac{1}{2}}\arcsin\varepsilon}{\varepsilon^3}\right). \tag{3.10}$$

It is easily verified that these equations satisfy (3.5) *exactly*. However, it is not clear how the shape of the charged ellipsoid differs from that of the corresponding uncharged cloud. After some algebra, it can be shown that good approximations for all except small αt are

$$a \approx R_0 e^{\alpha t}, \qquad c \approx R_0(1 + t/T_e)\, e^{-2\alpha t}. \tag{3.11}$$

For the corresponding uncharged cloud, the exact results, from (3.4) and (3.7), are

$$a = R_0 e^{\alpha t}, \qquad c = R_0 e^{-2\alpha t}. \tag{3.12}$$

It follows that electrostatic repulsion has no discernible effect on the two large axes of the ellipsoid, essentially because it acts much more slowly than advection. On the other hand, comparison of the expressions for c in (3.11) and (3.12) shows that repulsion slows down, but does not prevent, the exponential shrinking to zero of the smallest axis of the ellipsoid.

The other special case is when the ellipsoid in (3.3) is a prolate spheroid (i.e. shaped like a cigar); this occurs when

$$\alpha_1 = 2\alpha, \quad \alpha_2 = \alpha_3 = -\alpha \qquad (\alpha > 0), \tag{3.13}$$

and the equation of the ellipsoid can now be taken in the form

$$\frac{x^2}{a^2} + \frac{y^2 + z^2}{c^2} = 1. \tag{3.14}$$

The mathematical treatment for a prolate spheroid is very similar to that summarized above for the oblate spheroid. The approximations corresponding to (3.11) are now†

$$a \approx R_0 e^{2\alpha t}, \qquad c \approx R_0(1 + t/T_e)^{\frac{1}{2}} e^{-\alpha t}, \tag{3.15}$$

whereas the corresponding exact results for an uncharged cloud are

$$a = R_0 e^{2\alpha t}, \qquad c = R_0 e^{-\alpha t}. \tag{3.16}$$

Once more, it can be seen that the only effect of electrostatic repulsion is to slow down the shrinking to zero of the smallest dimension of the cloud.

† Both (3.11) and (3.15) arose from solving sets of two first-order equations in which the boundary conditions were that each set had the correct behaviour, given by (3.5), for large t. Curiously, and apparently fortuitously, both (3.11) and (3.15) then happen also to have the correct behaviour at $t = 0$.

4. Some statistical properties of real clouds

The work of Section 3 was restricted to very small clouds, but it has important implications for real charged clouds, which is why it was included and why it is more than an academic exercise. It shows, first, that the expansion of the volume $V(t)$ of the charged cloud, given by (2.9), does not take place isotropically (except, perhaps, in a statistical sense). It is of course already well understood, and illustrated in special cases by (3.12) and (3.16), that the random distortion of uncharged clouds is also anisotropic (Batchelor, 1952a). Advection causes a roughly spherical cloud of initially uniform concentration to develop into something resembling a very loosely wound ball of wool (Chatwin & Sullivan, 1979b), in which long strands of high tracer concentration are separated by clean (or cleaner) air. This random process is shown schematically in a famous sketch by Corrsin (1959), which is reproduced on p. 592 of Monin & Yaglom (1971).

The overall dimensions of the 'ball of wool' depend on the net sum of the *stretching* components of the velocity field. The work in Section 3 strongly implies that electrostatic repulsion has little effect on such components in small clouds and therefore (since real clouds can legitimately be regarded, for present purposes, as the combination of many small clouds) on the overall dimensions of a charged cloud. It follows that statistical properties of uncharged clouds that depend only on the overall dimensions, such as the distribution of the mean tracer concentration, and the mean cloud size and shape, can be estimated accurately from observations of charged clouds.

A measure of the shape of a dispersing cloud is provided by its dispersion tensor $L_{pq}(t)$ (Batchelor, 1952b). Assuming that (2.12) is satisfied so that total charge is conserved, an appropriate definition is

$$L_{pq}(t) = \frac{1}{Q_0} \int x_p x_q \rho \, \mathrm{d}V, \tag{4.1}$$

where the integral can be taken over the whole of space.† For a uniformly charged ellipsoid of semi-axes a_1, a_2, a_3, we have

$$L_{pq} = \frac{1}{5} \begin{bmatrix} a_1^2 & 0 & 0 \\ 0 & a_2^2 & 0 \\ 0 & 0 & a_3^2 \end{bmatrix}, \tag{4.2}$$

when referred to principal axes. In particular $L_{pp} \approx \frac{2}{5} R_0^2 \mathrm{e}^{2\alpha t}$ for the oblate spheroid considered in Section 3 and $L_{pp} \approx \frac{1}{5} R_0^2 \mathrm{e}^{4\alpha t}$ for the prolate spheroid. In both of these special cases, L_{pp} is independent of electrostatic repulsion.

† It should be noted that (4.1) is an incomplete definition since the origin $\boldsymbol{x} = \mathbf{0}$ has not been specified. In the rest of this paper, $\boldsymbol{x} = \mathbf{0}$ is taken as the instantaneous centroid of the charge distribution, so that the means are those for a relative diffusion ensemble (Chatwin & Sullivan, 1979a). In most practical situations, a more appropriate choice is a fixed origin (or one moving at fixed velocity), giving an absolute diffusion ensemble. However, since the conclusions of this section are that electrostatic repulsion does not affect certain statistical properties in a relative diffusion ensemble, standard turbulent diffusion results (Batchelor, 1952b) show that the same conclusions hold in an absolute diffusion ensemble.

The full expression for the rate of change of $L_{pq}(t)$ is given in Chatwin (1985), where it is noted that molecular diffusion makes a negligible contribution. Here, it is sufficient to remark that a good estimate of the order of magnitude of the volume occupied by the *mean* charge distribution $\bar{\rho}$ is L^3, where (Chatwin & Sullivan, 1979a)

$$L^2(t) = L_{pp}(t), \tag{4.3}$$

and, of course, $L^3(t)$ is normally much greater than $V(t)$ – the volume occupied by the charge in any one realization and given by (2.9) – because of the volume of the clean air entrained into the 'ball of wool', and because of the randomness of the orientation of the cloud in space. (In addition, in an absolute diffusion ensemble, there is the large effect on $L^3(t)$ due to meandering.) The conclusion of the arguments at the beginning of this section is that electrostatic repulsion has no effect on $L^3(t)$.

Conservation of total charge requires that, throughout each realization,

$$\int \rho(\mathbf{x}, t)\, \mathrm{d}V = Q_0. \tag{4.4}$$

As has been seen in Section 2, equation (4.4) is satisfied because ρ has the uniform value $\rho_0(1 + t/T_e)^{-1}$ throughout a volume of size $V(t) = V_0(1 + t/T_e)$, where $\rho_0 V_0 = Q_0$. The ensemble mean of equation (4.4) is

$$\int \bar{\rho}(\boldsymbol{x}, t)\, \mathrm{d}V = Q_0, \tag{4.5}$$

where the integrand is sensibly nonzero over a volume of space with order of magnitude $L^3(t)$. It follows that the order of magnitude of $\bar{\rho}$ is

$$\bar{\rho} \sim Q_0/L^3(t). \tag{4.6}$$

Thus, the order of magnitude of the mean concentration in clouds of passive tracer is the same as that of the mean charge in charged clouds, and conversely. This order of magnitude can be estimated by means of standard methods which predict the dependence of $L^3(t)$ on atmospheric conditions (Monin & Yaglom, 1971, 1975; Pasquill & Smith, 1983).

A basic difference between charged and uncharged clouds occurs when the mean-square fluctuations are considered. By multiplying equation (2.2) by 2ρ and integrating over all space, it follows, after use of equations (2.1), that

$$\frac{\mathrm{d}}{\mathrm{d}t}\left(\int \rho^2\, \mathrm{d}V\right) = -\frac{\mu}{\epsilon_0}\left(\int \rho^3\, \mathrm{d}V\right) - 2\kappa\left(\int (\nabla\rho)^2\, \mathrm{d}V\right). \tag{4.7}$$

The term involving κ in equation (4.7) will be considered in Section 6; here, attention is focused on the first term on the right-hand side, since it has no counterpart in the dispersion of uncharged clouds of passive tracer. For such clouds, $\rho\delta V$ and $\rho^2\delta V$ (and indeed $f(\rho)\delta V$ for any function f) are conserved throughout the dispersion in the absence of effects of molecular diffusion for every material volume element δV (Chatwin & Sullivan, 1979a). In charged clouds, on the other hand, repulsion causes $\rho\delta V$ to decrease with t, since δV is

invariant by incompressibility and ρ decreases according to equation (2.8). In equation (4.4), this decrease in ρ is balanced by an increase in the total volume V over which ρ is nonzero. Therefore the integral of ρ^2 over all space must decrease with t, and this is the significance of the first term on the right-hand side of equation (4.7). (Note that $\mu\rho$ is positive.) While equation (4.7) is true whether ρ is spatially uniform within V, or not, it is sufficient to note here that, when $\kappa = 0$, equation (4.7) is trivially satisfied by equations (2.8) and (2.9) and, in that case,

$$\int \rho^2 \, dV = \rho_0^2 V_0 (1 + t/T_e)^{-1}. \tag{4.8}$$

It is reasonable to suppose, in discussing orders of magnitude, that equation (4.8) holds in all circumstances for which molecular diffusion is negligible.

The ensemble mean of equation (4.8) is

$$\int (\bar{\rho})^2 \, dV + \int \overline{(\rho')^2} \, dV = \rho_0^2 V_0 (1 + t/T_e)^{-1}, \tag{4.9}$$

where $\bar{\rho}$ and ρ' are defined in equation (2.4). According to equation (4.6), the order of magnitude of the first term on the left-hand side of equation (4.9) is $\rho_0^2 V_0^2 / L^3$, and, since $L^3(t) \gg V_0(1 + t/T_e) = V(t)$, the balance in equation (4.9) requires the integral involving $\overline{(\rho')^2}$ to be of the same order of magnitude as the right-hand side. Thus,

$$\overline{(\rho')^2} \sim \frac{\rho_0^2 V_0}{L^3 (1 + t/T_e)} = \frac{Q_0^2}{L^3 V}, \tag{4.10}$$

where, as usual, $V = V_0(1 + t/T_e)$. This is different from the corresponding estimate in uncharged clouds, which is $Q_0^2 / L^3 V_0$ (Chatwin & Sullivan, 1979a). Nevertheless, it remains true that $\overline{(\rho')^2} \gg (\bar{\rho})^2$, since

$$\overline{(\rho')^2} / (\bar{\rho})^2 \sim L^3 / V \gg 1. \tag{4.11}$$

In summary, the conclusions of this section are that, compared with uncharged clouds, the order of magnitude of $\bar{\rho}$, the analogue of the mean concentration, is unchanged, as are the size and shape of the mean cloud, whereas $\overline{(\rho')^2}$, the analogue of the mean square fluctuation, is less by a factor of about $(1 + t/T_e)^{-1}$. (It should also be noted that there has been no consideration of any 'core' structure that the statistical properties of ρ may have: see Chatwin & Sullivan (1979a).)

5. Some data for plumes

Jones (1983) presents data from experiments in which the sensor system was deployed in the mode in which a steady current i_0 is generated, thereby resulting in a statistically steady charged plume in which the statistical properties are functions, not of time, but of downwind distance x, and in which the instantaneous cloud volume is replaced by the actual cross-sectional area $A(x)$ of the plume. The analogues of equations (2.9), (4.6), (4.10), and (4.11) are

(Chatwin & Sullivan, 1979c; Chatwin, 1985)

$$A = A_0\left(1 + \frac{x}{uT_c}\right), \qquad \bar{\rho} \sim \frac{\rho_0 A_0}{L^2}, \qquad \overline{(\rho')^2} \sim \frac{\rho_0^2 A_0}{L^2(1 + x/uT_c)}, \qquad \frac{\overline{(\rho')^2}}{(\bar{\rho})^2} \sim \frac{L^2}{A}, \tag{5.1}$$

respectively, where u is the wind speed, A_0 is the initial plume cross-section and $L = L(x)$ is a *mean* plume radius, analogous to $L(t)$ in the above discussion of the dispersion of clouds. From Table 6 on p. 107 of Jones (1983), it can be deduced that

$$u \approx 5\,\mathrm{m\,s^{-1}}, \qquad T_c \approx 0{\cdot}04\,\mathrm{s}, \qquad \rho_0 \approx 1{\cdot}2 \times 10^{-6}\,\mathrm{C\,m^{-3}}, \tag{5.2}$$

and on p. 105 Jones quotes a value for the initial plume radius R_0 of 0·013 m, so that

$$A_0 \approx 5{\cdot}3 \times 10^{-4}\,\mathrm{m^2}, \qquad i_0 = u\rho_0 A_0 \approx 3{\cdot}2 \times 10^{-9}\,\mathrm{A}. \tag{5.3}$$

(The values of R_0 and i_0 are different from the values of 0·006 m and $1{\cdot}6 \times 10^{-8}$ A quoted on p. 96 of Jones's paper. While the discrepancies are puzzling, they do not significantly affect the general conclusions below, which refer to order of magnitude only.)

Use of the values in equations (5.2) and (5.3), and other data in Jones's paper, gives the results in Table 1. Comparison between columns 1 and 2 shows that, while the measured values of $\sigma/\bar{\rho}$ are greater than 1, they are less than predicted by the last result in equation (5.1). Similarly, comparison of columns 3 and 4 indicates that theory everywhere overestimates the value of σ.

There are at least two explanations for these observations. As will be discussed in more detail in Section 6, molecular diffusion causes $\overline{(\rho')^2}$ to decay more rapidly than is predicted by equation (5.1), but is without significant effect on $\bar{\rho}$. The other phenomenon that could explain the observations is the smoothing effect of the instruments, due principally, in this case, to the finite size of the ion collector (diameter ≈ 0·036 m). This effect is discussed in Carn & Chatwin (1985) and Mole & Chatwin (1987).

TABLE 1
Results derived from data in Jones (1983).

				$\sigma^\dagger$ (10^{-9} C m^{-3})	
x (m)	L (m)	$(L^2/A)^{\frac{1}{2}}$	$\sigma^\dagger/\bar{\rho}$ Measured	Estimated (5.1)	Measured
2	0·39	5·1	3·0	21	13
5	1·10	9·3	4·2	4·9	2·2
10	1·63	10·0	3·4	2·4	0·8
15	2·00	10·0	2·1	1·6	0·35
Column No:		1	2	3	4

† $\sigma = [\overline{(\rho')^2}]^{\frac{1}{2}}$

6. The role of molecular diffusion

A second important reason for including Section 3 of this paper is the insight it gives into the likely role of molecular diffusion. Consider first small clouds of *uncharged* passive tracer. Equations (3.12) and (3.16) show that, in the absence of molecular diffusion, the smallest dimensions of such a cloud would shrink to zero exponentially quickly with time. In reality, this shrinking to zero is accompanied by exponentially increasing gradients of the tracer concentration and the cloud surface area; thus, the neglect of molecular diffusion can eventually no longer be justified. It is well known (Batchelor, 1959; Chatwin & Sullivan, 1979a) that there is eventually a dynamic balance between the competing effects of shrinking, caused by advection, and molecular diffusion. As a result, the smallest length scales present in the spatial structure of the dispersing cloud are of order λ, where λ is the conduction cut-off length defined by (Batchelor, 1959)

$$\lambda = (2\kappa/\alpha)^{\frac{1}{2}} \sim (\nu\kappa^2/e)^{\frac{1}{4}}. \tag{6.1}$$

In (6.1), $-\alpha$ ($\alpha > 0$) is the most negative rate of strain of the velocity field, ν is the kinematic viscosity, and e is the rate of dissipation of mechanical energy per unit mass. In the atmosphere $\lambda \sim 10^{-3}$ m (Chatwin & Sullivan, 1979b).

One important effect of this dynamic balance is to cause ρ^2 to dissipate, i.e. the second term on the right-hand side of equation (4.7) is not negligible and is dominated by contributions from regions of the cloud where the spatial structure is at its finest. It is also well known that molecular diffusion has little effect on $\bar{\rho}$, and it follows that the most significant effect of molecular diffusion on statistical properties of the cloud is to cause $\overline{(\rho')^2}$ to decay with t.

Even for *uncharged* clouds of passive tracer of realistic size, it is not known how to quantify the rate of decay of $\overline{(\rho')^2}$ due to molecular diffusion. The problem is the usual one for any phenomenon connected with turbulence. In physical terms, the difficulty is the accurate assessment of how the random small-scale processes summarized above (which can be quantified – Chatwin & Sullivan, 1979a) combine in the presence of the random and relatively large-scale advection that causes, among other things, the cloud to become like the ball of wool referred to above; in mathematical terms, the difficulty is the notorious closure problem.

For the *charged* clouds of present concern, it is therefore also impossible to quantify the rate of decay of $\overline{(\rho')^2}$ with t. We shall accordingly emphasize the *changes* in the small-scale structure caused by electrostatic repulsion, and illustrated by the contrasts already noted in Section 3 between the results in equations (3.11) and (3.12), and between those in equations (3.15) and (3.16). The aim of the work that follows is therefore understanding of the basic physics.

Consider a charge distribution in the neighbourhood of any point some time after release. At this point, incompressibility requires – see equation (3.2) – that at least one rate of strain is negative. For the purposes of this discussion, it will be assumed that two rates of strain are positive (but changes to the mathematical details that follow can easily be made when there is only one positive rate of strain). In that case, the charge distribution is approximately uniform along

planes normal to the principal axis of the rate-of-strain tensor corresponding to the negative rate of strain (Chatwin, 1985). Let this axis be the z-axis, and let the negative rate of strain be $-\alpha$ ($\alpha > 0$). A good approximation to equation (2.2) for ρ when the thickness of the distribution of charge is small is (Chatwin, 1985)

$$\frac{\partial \rho}{\partial t} - \alpha z \frac{\partial \rho}{\partial z} - \mu \frac{\partial}{\partial z}\left(\rho \frac{\partial \varphi}{\partial z}\right) = \kappa \frac{\partial^2 \rho}{\partial z^2}, \tag{6.2}$$

where, to a corresponding approximation, equation (2.1) becomes

$$\frac{\partial^2 \varphi}{\partial z^2} = -\frac{\rho}{\epsilon_0}. \tag{6.3}$$

For an uncharged cloud, $\mu = 0$ in equation (6.2), and the solution for ρ is

$$\rho = \rho_1 e^{-\alpha t} \exp\left[-(z/\lambda)^2\right], \tag{6.4}$$

where λ is defined in equation (6.1) and ρ_1 is a constant which could, consistent with the approximation in equation (6.2), be a slowly varying function of x and y. Equation (6.4) shows clearly the influence of molecular diffusion in that, as predicted earlier in this section, ρ is nonzero over a distance of *constant* order of magnitude λ but that, because of diffusion, the magnitude of ρ is decreasing exponentially with t. In contrast, when there is no molecular diffusion, it is clear from the arguments in Section 3 that equation (6.4) must be replaced by

$$\rho = \frac{\rho_1 \lambda \pi^{\frac{1}{2}}}{2l} \quad \text{for } |z| \leq l e^{-\alpha t}, \tag{6.9}$$

where $2l$ is the initial thickness of the cloud. Both equations (6.4) and (6.5) hold over a region in the xy-plane whose area is proportional to $e^{\alpha t}$ (Chatwin, 1985), and both give the same value to

$$\int_{-\infty}^{\infty} \rho \, dz.$$

Hence, the total charge is conserved. For equation (6.4)

$$\int_{-\infty}^{\infty} \rho^2 \, dz = \lambda(\tfrac{1}{2}\pi)^{\frac{1}{2}} \rho_1^2 e^{-2\alpha t}, \tag{6.6}$$

whereas, with equation (6.5),

$$\int_{-\infty}^{\infty} \rho^2 \, dz = \frac{\lambda^2 \pi}{2l} \rho_1^2 e^{-\alpha t}. \tag{6.7}$$

Thus, without molecular diffusion,

$$\int \rho^2 \, dV$$

is conserved but since, combining equations (6.6) and (6.7),

$$\left[\int \rho^2 \, dV\right]_{\substack{\mu=0 \\ \kappa \neq 0}} = \left[\int \rho^2 \, dV\right]_{\substack{\mu=0 \\ \kappa=0}} \left(\frac{2}{\pi}\right)^{\frac{1}{2}} \frac{l}{\lambda} e^{-\alpha t}, \tag{6.8}$$

this quantity decays in real clouds, as a result of molecular diffusion.

In charged clouds, repulsion opposes advection in the model equations (6.2) and (6.3). Apparently, but not surprisingly, there is no simple analytic solution of these equations. However, some progress has been made.

It is clear, first, that ρ and φ are even functions of z. For an initial distribution of ρ proportional to $\exp(-kz^2)$ for some constant k, it can easily be seen, as shown schematically in Fig. 1, that the effect of the electrostatic term in equation

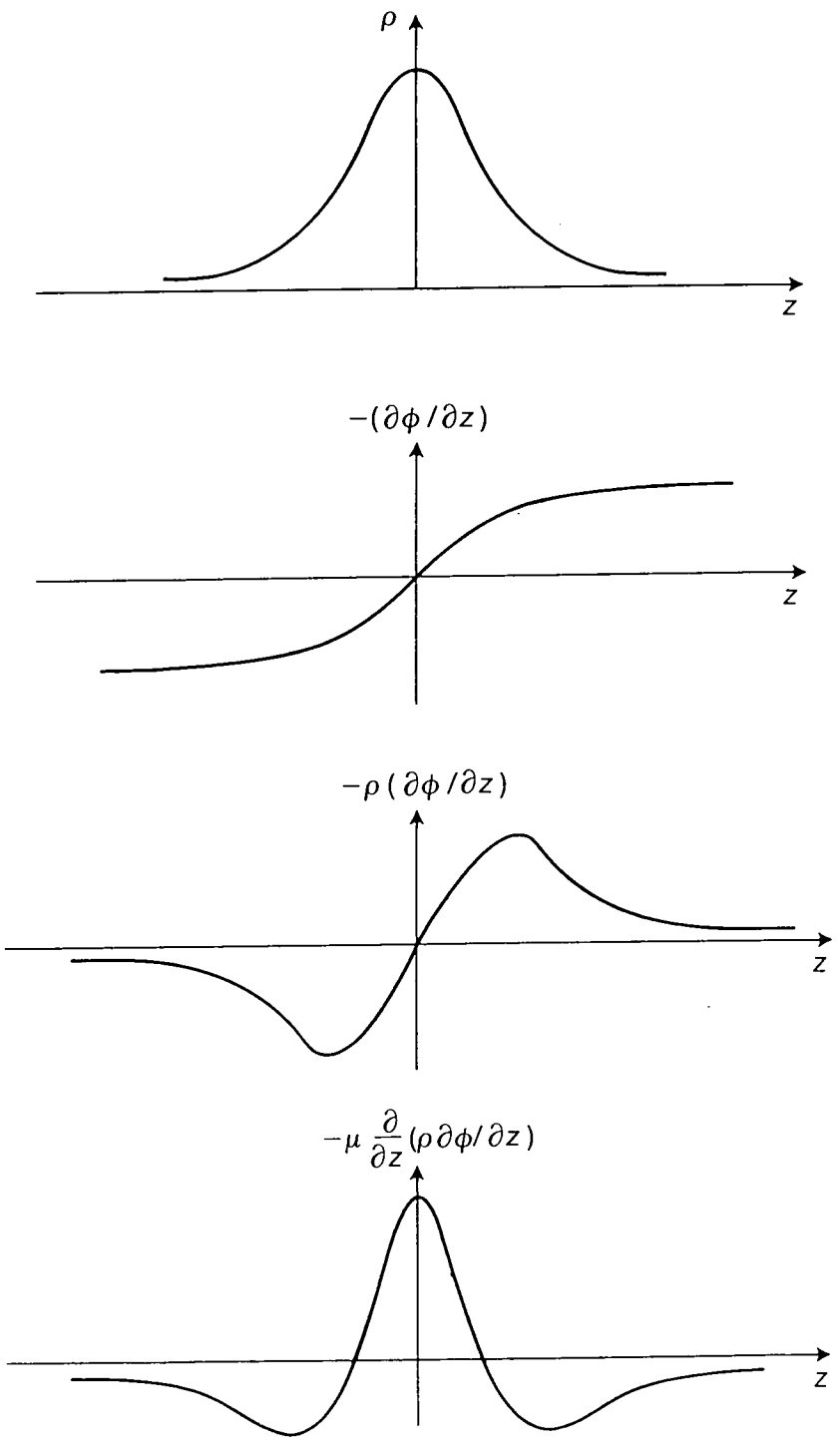

FIG. 1. Schematic diagram showing the effect of the electrostatic term in equation (6.2) for an initial charge distribution $\rho(z, 0)$ proportional to $\exp(-kz^2)$.

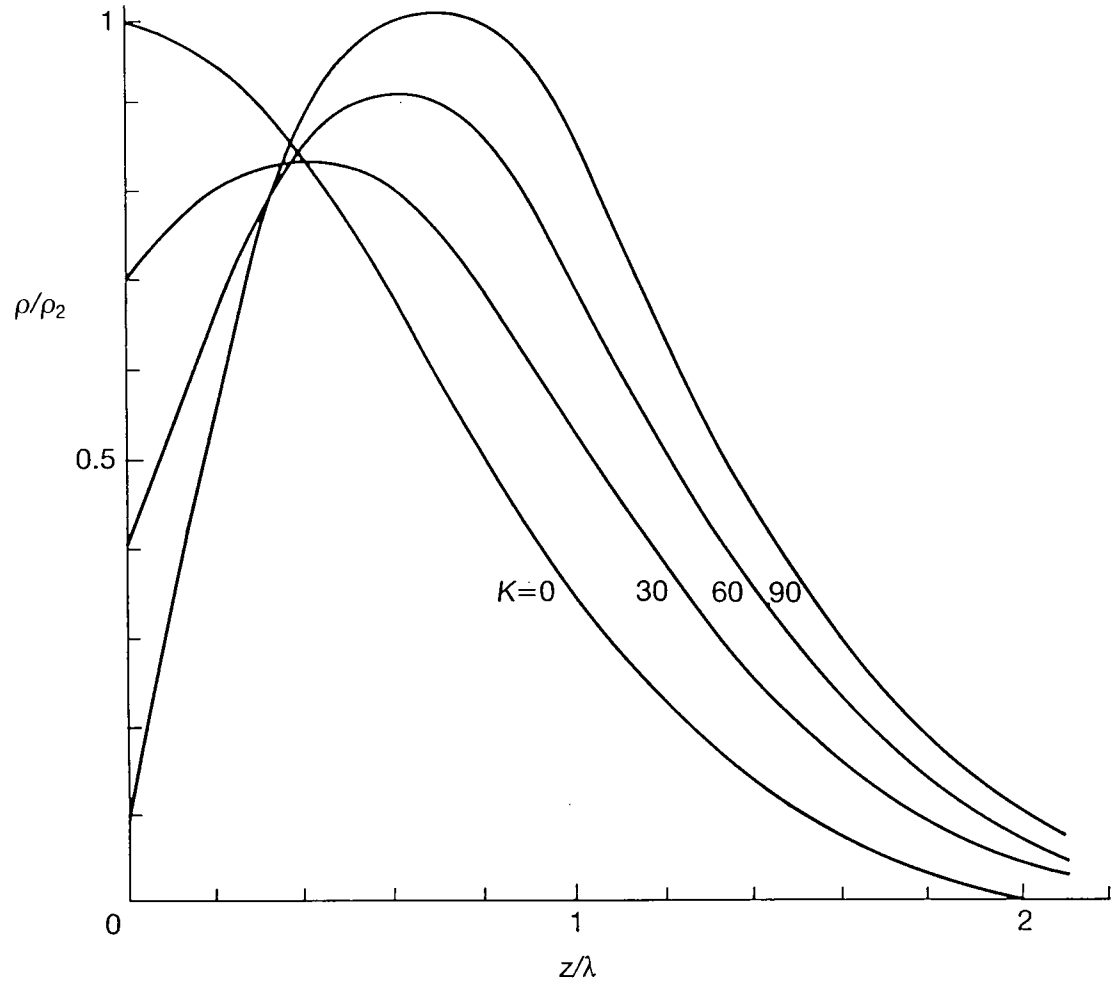

FIG. 2. Sketches showing the charge distribution for $\alpha t = 0{\cdot}01$ for various values of K defined in equation (6.13).

(6.2) is greatest at $z = 0$. As a result, the centre is depleted of charge, resulting in a distribution of charge for $t > 0$ like that sketched in Fig. 2. The same effect occurs for other (e.g. uniform) initial distributions.

The work that follows will suppose that

$$\rho(z, 0) = \rho_2 \exp[-(z/\lambda)^2], \tag{6.9}$$

for some constant ρ_2. This is a natural assumption in view of equation (6.4). Clearly

$$\int_{-\infty}^{\infty} \rho(z, t)\, dz = \rho_2 \lambda \pi^{\frac{1}{2}} e^{-\alpha t}, \tag{6.10}$$

since this quantity must be unaffected by electrostatic repulsion and must be consistent with equation (6.9). Note also, for later use, that

$$-\frac{\partial \varphi}{\partial z} = \frac{1}{\epsilon_0} \int_0^z \rho(\zeta, t)\, d\zeta. \tag{6.11}$$

Some indication of the rapidity of depletion of the charge initially in the centre can be obtained by setting $t = 0$ in equation (6.2). After a few lines of algebra, there results

$$\left[\frac{\partial \rho}{\partial t}\right]_{t=0} = -\alpha\rho_2 e^{-(z/\lambda)^2}\left[1 + K\left(e^{-(z/\lambda)^2} - \pi^{\frac{1}{2}}\frac{z}{\lambda}\operatorname{erf}\frac{z}{\lambda}\right)\right], \tag{6.12}$$

where the constant K is defined by

$$K = \frac{\mu\rho_2}{\epsilon_0\alpha} = \frac{\alpha^{-1}}{(\epsilon_0/\mu\rho_2)}. \tag{6.13}$$

Thus, from equation (6.12),

$$\left[\frac{d\rho}{dt}\right]_{\substack{t=0\\z=0}} = -\alpha\rho_2(1 + K). \tag{6.14}$$

The term involving K in equation (6.14) represents the additional effect due to repulsion. In the atmosphere $\alpha^{-1} \lesssim 10^{-1}$ s so, using equation (6.13) and referring to the discussion following equation (2.9), values of K in actual use of the sensor system have ranged from 5×10^{-3} (Jennings & Jones, 1977) to 200 (Storebø *et al.*, 1983). One interpretation of K – obvious from the way equation (6.13) is written – is as the ratio of the time scale for small-scale advection (α^{-1}) to the electrostatic time scale ($\epsilon_0/\mu\rho_2$). Alternatively, $K = (\lambda/\lambda_D)^2$, where λ is defined in equation (6.1), and

$$\lambda_D = \left(2K\frac{\epsilon_0}{\mu\rho_2}\right)^{\frac{1}{2}} \tag{6.15}$$

is the diffusion distance associated with the electrostatic time scale, i.e. λ_D can be thought of as a Debye distance (Alfvén & Fälthammar, 1963: pp. 142–3) for this model cloud.

It is clear from equation (6.14) and from Fig. 2 that the rate of depletion of charge from the cloud centre can be very rapid (unless $K \ll 1$) and it is important to determine where this charge is relocated. More particularly, it is crucial to know whether this evacuation of the charge results in an order-of-magnitude change in the cloud thickness, since such a change would alter the rate of decay of ρ^2. The work in Section 3 suggested that, in the absence of molecular diffusion, the changes would be relatively small and the arguments below suggest that molecular diffusion does not affect this conclusion significantly.

Define $m_i(t)$ $(i = 0, 1, \ldots)$ by

$$m_i(t) = \int_0^\infty z^i \rho(z, t)\, dz. \tag{6.16}$$

Since ρ is even, $m_0(t) = \frac{1}{2}\rho_2\lambda\pi^{\frac{1}{2}}e^{-\alpha t}$ from equation (6.10). A measure of the cloud thickness is $\sigma(t)$, where

$$\sigma^2(t) = m_2(t)/m_0(t). \tag{6.17}$$

In the absence of electrostatic repulsion, $\sigma(t) = \sigma_0(t)$, where, from equation (6.4),

$$\sigma_0^2(t) = \tfrac{1}{2}\lambda^2 = \kappa/\alpha. \tag{6.18}$$

For $\mu \neq 0$, multiply equation (6.2) by z^2 and integrate. Use of equation (6.16) and the fact that ρ is even gives

$$\left(\frac{\mathrm{d}}{\mathrm{d}t} + 3\alpha\right) m_2 = \kappa\rho_2\lambda\pi^{\frac{1}{2}}\mathrm{e}^{-\alpha t} - \mu\int_{-\infty}^{\infty} \rho z \frac{\partial\varphi}{\partial z}\,\mathrm{d}z. \tag{6.19}$$

But

$$-\int_{-\infty}^{\infty} \rho z \frac{\partial\varphi}{\partial z}\,\mathrm{d}z = 2\int_0^{\infty} \rho z\left(-\frac{\partial\varphi}{\partial z}\right)\mathrm{d}z \leq 2\int_{-\infty}^{\infty} \rho z\left(-\left[\frac{\partial\varphi}{\partial z}\right]_{z=\infty}\right)\mathrm{d}z,$$

so, from equations (6.10) and (6.11),

$$-\int_{-\infty}^{\infty} \rho z \frac{\partial\varphi}{\partial z}\,\mathrm{d}z \leq \frac{\rho_2\lambda\pi^{\frac{1}{2}}}{\epsilon_0}\mathrm{e}^{-\alpha t} m_1(t).$$

Hence,

$$\left(\frac{\mathrm{d}}{\mathrm{d}t} + 3\alpha\right) m_2 \leq \kappa\rho_2\lambda\pi^{\frac{1}{2}}\mathrm{e}^{-\alpha t} + \frac{\mu\rho_2\lambda\pi^{\frac{1}{2}}}{\epsilon_0}\mathrm{e}^{-\alpha t} m_1(t). \tag{6.20}$$

It is therefore necessary to estimate $m_1(t)$. It follows from equation (6.2) that

$$\left(\frac{\mathrm{d}}{\mathrm{d}t} + 2\alpha\right) m_1 = \kappa\rho(0, t) + \tfrac{1}{2}\mu\epsilon_0\left(\left[\frac{\partial\varphi}{\partial z}\right]_{z=\infty}\right)^2,$$

so that, using equation (6.11),

$$\frac{\mathrm{d}}{\mathrm{d}t}(m_1\,\mathrm{e}^{2\alpha t}) = \frac{\mu\rho_2^2\lambda^2\pi}{8\epsilon_0} + \kappa\rho(0, t)\mathrm{e}^{2\alpha t}. \tag{6.21}$$

When $\mu = 0$, $\rho(0, t) = \rho_2\mathrm{e}^{-\alpha t}$. In view of the fact that repulsion reduces $\rho(0, t)$, at least initially (see equation (6.14)), it seems reasonable to assume that $\rho(0, t) \leq \rho_2\mathrm{e}^{-\alpha t}$ for all t. Equation (6.21) then leads to

$$m_1(t) \leq \frac{\kappa\rho_2}{\alpha}(\mathrm{e}^{-\alpha t} - \mathrm{e}^{-2\alpha t}) + \frac{\mu\rho_2^2\lambda^2\pi}{8\epsilon_0} t\mathrm{e}^{-2\alpha t} + m_1(0)\mathrm{e}^{-2\alpha t}.$$

Hence, for sufficiently large αt,

$$m_1(t) \leq \frac{2\kappa\rho_2}{\alpha}\mathrm{e}^{-\alpha t}. \tag{6.22}$$

Use of equation (6.22) in equation (6.20) then gives, for sufficiently large αt,

$$m_2(t) \leq \frac{\kappa\rho_2\lambda\pi^{\frac{1}{2}}}{2\alpha}(\mathrm{e}^{-\alpha t} - \mathrm{e}^{-3\alpha t}) + \frac{2\mu\kappa\rho_2^2\lambda\pi^{\frac{1}{2}}}{\epsilon_0\alpha^2}(\mathrm{e}^{-2\alpha t} - \mathrm{e}^{-3\alpha t}) + m_2(0)\mathrm{e}^{-3\alpha t},$$

so that, for sufficiently large αt,

$$m_2(t) \leq \frac{\kappa\rho_2\lambda\pi^{\frac{1}{2}}}{\alpha}\mathrm{e}^{-\alpha t}.$$

Finally, it follows from equations (6.17) and (6.18) that

$$\sigma^2(t) \leq 2\kappa/\alpha = 2\sigma_0^2(t), \tag{6.23}$$

for sufficiently large αt. It can in fact be shown, using equations (6.20) and (6.21) and the same assumption about $\rho(0, t)$, that

$$\sigma^2(t) \leq A\sigma_0^2(t) \tag{6.24}$$

for *all* t, where the constant A satisfies

$$A = (1 + \tfrac{1}{2}K + \tfrac{1}{4}\pi\, e^{-2}K^2). \tag{6.25}$$

However, as (6.23) shows, this is far too conservative for large αt (and large K). Nevertheless, there is a possibility, to be resolved by numerical integration of (6.2) and (6.3), that $\sigma^2(t)/\sigma_0^2(t)$ could be much greater than 1 for values of t of order α^{-1}.

It has therefore been shown, based on the single and very plausible assumption that electrostatic repulsion does not *increase* $\rho(0, t)$, that the thickness of the model cloud eventually has the same order of magnitude whether or not there is repulsion. Therefore, the rate of decay of $\int \rho^2\, dV$ given by (6.8) for uncharged clouds should have the correct order of magnitude for charged clouds also.

7. Conclusions

The work in this paper has suggested that, provided condition (2.12) is satisfied, observations of charged clouds and plumes with the sensor system under investigation give many results that apply to clouds and plumes of uncharged passive tracer with the same release geometry and the same atmospheric conditions. In particular, the overall dimensions and the mean concentration are likely to be estimated closely. However, the mean-square fluctuation in the charged cloud is likely to be less than that in the uncharged cloud by a factor of about $(1 + t/T_e)^{-1}$, where T_e is the electrostatic time scale given in equation (2.8). Discussion of the likely effects of molecular diffusion suggests that electrostatic repulsion does not affect the order of magnitude of the decay of the mean-square fluctuations.

The sensor system has great potential advantages, connected with its rapid response and with its stability and robustness. It should therefore be used in more trials with the aim, particularly, of validating the conclusions of this report by comparison with the results obtained for uncharged clouds and plumes with the same geometry. Such work is in progress.

Acknowledgements

We wish to thank Dr J. T. Bartlett and Dr D. J. Ride of CDE for their support and advice. Work on this topic is now being carried out under MOD Agreement No. 2066/062(CDE).

References

Alfvén, H., & Fälthammar, C.-G. 1963 *Cosmical Electrodynamics: Fundamental Principles.* Oxford University Press.

Batchelor, G. K. 1952a The effect of homogeneous turbulence on material lines and surfaces. *Proc. R. Soc. A* **213,** 349–66.

Batchelor, G. K. 1952b Diffusion in a field of homogeneous turbulence. II. The relative motion of particles. *Proc. Camb. Phil. Soc.* **48,** 345–62.

Batchelor, G. K. 1959 Small-scale variation of convected quantities like temperature in turbulent fluid. Part 1. General discussion and the case of small conductivity. *J. Fluid Mech.* **5,** 113–33.

Bustin, W. M., Koszman, I., & Tobye, I. T. 1964 A new theory for static relaxation. *Hydrocarbon Processing* **43,** 209–16.

Carn, K. K., & Chatwin, P. C. 1985 Variability and heavy gas dispersion. *J. Haz. Mater.* **11,** 281–300.

Chatwin, P. C. 1982 The use of statistics in describing and predicting the effects of dispersing gas clouds. *J. Haz. Mater.* **6,** 213–30.

Chatwin, P. C. 1985 Interaction between turbulent and electrostatic effects in the atmospheric dispersion of electrically charged tracers. Report, Chemical Defence Establishment, Porton Down.

Chatwin, P. C., & Sullivan, P. J. 1979a The relative diffusion of a cloud of passive contaminant in incompressible turbulent flow. *J. Fluid Mech.* **91,** 337–55.

Chatwin, P. C., & Sullivan, P. J. 1979b The basic structure of clouds of diffusing contaminant. In: *Mathematical Modelling of Turbulent Diffusion in the Environment* (C. J. Harris, Ed.). London: Academic Press, pp. 3–32.

Chatwin, P. C., & Sullivan, P. J. 1979c Measurements of concentration fluctuations in relative turbulent diffusion. *J. Fluid Mech.* **94,** 83–101.

Corrsin, S. 1959 Outline of some topics in homogeneous turbulent flow. *J. Geophys. Res.* **64,** 2134–50.

Gavis, J. 1967 Relaxation of electrically charged hydrocarbon liquids. *Chem. Eng. Sci.* **22,** 633–35.

Griffiths, R. F., & Harper, A. S. 1985 A speculation on the importance of concentration fluctuations in the estimation of toxic response to irritant gases. *J. Haz. Mater.* **11,** 369–72.

Jennings, S. G., & Jones, C. D. 1977 Tracking electrically charged puffs as used in short range atmospheric diffusion investigations, by ground level electric field measurements. *J. Electrostat.* **2,** 367–73.

Jones, C. D. 1977a Ion concentration variations at short distances downwind of continuous and quasi-instantaneous point sources. *Pesticide Sci.* **8,** 84–95.

Jones, C. D. 1977b Ionised air as a wind tunnel tracer. *J. Phys. E* **10,** 1287–91.

Jones, C. D. 1979 Statistics of the concentration fluctuations in short range atmospheric diffusion. In: *Mathematical Modelling of Turbulent Diffusion in the Environment* (C. J. Harris, Ed.). London: Academic Press, pp. 277–98.

Jones, C. D. 1983 On the structure of instantaneous plumes in the atmosphere. *J. Haz. Mater.* **7,** 87–112.

Jones, C. D., & Hutchinson, W. C. A. 1976 Plumes of electric space charge in the lower atmosphere. *J. Atmos. Terr. Phys.* **38,** 485–94.

Kellogg, O. D. 1953 *Foundations of Potential Theory.* New York: Dover.

Mole, N., & Chatwin, P. C. 1987 Assessing and modelling variability in dispersing vapour clouds. *Proc. I. Chem. E/AIChE International Conference on Vapour Cloud Modelling,* Boston, MA.

Monin, A. S., & Yaglom, A. M. 1971 *Statistical Fluid Mechanics: Mechanics of Turbulence,* Vol. 1; 1975, Vol. 2 (J. L. Lumley, Ed.). Boston, MA: MIT Press.

Pasquill, F., & Smith, F. B. 1983 *Atmospheric Diffusion: The Dispersion of Windborne Material from Industrial and other Sources.* Chichester, UK: Ellis Horwood.

RIDE, D. J. 1984 An assessment of the effects of fluctuations on the severity of poisoning by toxic vapours. *J. Haz. Mater.* **9,** 235–40.

SAFFMAN, P. G. 1963 On the fine-scale structure of vector fields convected by a turbulent fluid. *J. Fluid Mech.* **16,** 545–72.

STOREBØ, P. B., BJORVATTEN, T., HØNNASHAGEN, K., LILLEGRAVEN, A., JONES, C. D., & VAN BUIJTENEN, C. J. P. 1983 Tracer experiments with turbulently dispersed air ions. *Boundary-Layer Met.* **26,** 127–39.

TOWNSEND, A. A. 1951 The diffusion of heat spots in isotropic turbulence. *Proc. R. Soc. A* **209,** 418–30.

Mole N. and Jones C. D. (1994).

Concentration fluctuation data from dispersion experiments carried out in stable and unstable conditions.

Bound. Layer Met. **67**, 41 - 74.

CONCENTRATION FLUCTUATION DATA FROM DISPERSION EXPERIMENTS CARRIED OUT IN STABLE AND UNSTABLE CONDITIONS

NILS MOLE

Department of Applied and Computational Mathematics, University of Sheffield, P.O. Box 597, Sheffield S10 2UN, U.K.

and

C. D. JONES

Chemical and Biological Defence Establishment, Porton Down, Salisbury, Wilts. SP4 0JQ, U.K.

(Received in final form 7 April, 1993)

Abstract. Experiments have been carried out to investigate the dispersion of plumes at short range in the atmospheric boundary layer during stable and unstable conditions. The experiments and measurement system are described, and the results are compared with those of previous experiments. The slow meandering under stable conditions found by Mylne (1992) is not present here (probably because of topographic effects), so the plume is present on the mean centreline more often, and timescales are shorter, under stable conditions. Associated with this, statistics during stable conditions exhibit greater stability to changes in total sampling time. Intensity is found to be greater under unstable conditions, but there do not appear to be large differences in the shape of the probability density function between stable and unstable conditions. The intermittency is calculated using several variations on the conventional definition. The values obtained vary substantially according to which definition is used (although they are always higher in the stable than in the unstable experiments), demonstrating the sensitivity to both the precise definition and to measurement system characteristics. It is shown that even at very short range the mean and variance of concentration are determined almost entirely by the fluid not emanating from the source. Thus the partition between source and non-source fluid suggested by Chatwin and Sullivan (1989), while providing a more scientifically sound definition of intermittency, does not have an obvious direct practical application.

1. Introduction

In the majority of circumstances of practical interest, atmospheric flows, at least near the surface, are turbulent in nature and thus any material released which remains airborne for an appreciable time will be transported and dispersed in a complex manner. Nevertheless, clear and simple structures (understood to be statistical structures obtained from a suitably defined ensemble of releases) do exist. These structures are determined by the relevant physics as represented through the Navier–Stokes and advection-diffusion equations. In the atmosphere, turbulent fluctuations exist on a very wide range of scales, the smallest being typically a fraction of a millimetre while the largest, in this context, would be several hundred metres in extent. The concentration of material released from a small source in such an environment will inevitably exhibit spatial structure at an

Boundary-Layer Meteorology **67**: 41–74, 1994.

increasingly wide range of scales as time proceeds, although molecular diffusion will eventually smooth out variations at the very smallest scales.

A feature of particular importance is the effect which atmospheric stability has on the distribution of concentration. This is the result of the profound changes which occur in the nature of the turbulence as the stability varies. Broadly speaking, in unstable, i.e. convective conditions, vertical motions are markedly accentuated and the turbulence scale tends to be larger. Conversely, in stable conditions, vertical motions tend to be strongly damped by the unfavourable density (i.e. temperature) gradients. In cases of extreme stability, turbulence can be almost entirely eliminated. In less extreme cases, there may be episodes of very weak turbulence with intermittent "bursts" of more highly turbulent flow. Another important aspect of stable flows is their sensitivity to topographical influences, the best example being the well-known katabatic (downhill) flow.

Much of the experimental work that has been carried out to date has been concerned with neutral or near-neutral conditions, because such conditions are the most prevalent in mid to high latitudes, and because, thermal effects being largely absent, the turbulent structure is easier to understand and to model. Releases of neutrally buoyant tracers under neutral conditions have included those of Ramsdell and Hinds (1971), Jones (1979, 1983), Sawford *et al.* (1985), Dinar *et al.* (1988), Mikkelsen *et al.* (1990) and Mylne and Mason (1991). Releases of heavy gases during neutral conditions are described by, for example, Picknett (1981), McQuaid and Roebuck (1985) and Nielsen and Jensen (1991).

Many experiments have also been carried out during daytime convective conditions. Neutrally buoyant releases include those of Jones (1979), Hanna (1984), Sawford *et al.* (1985), Lamb *et al.* (1985), Peterson *et al.* (1988), Mikkelsen *et al.* (1990) and Mylne and Mason (1991), while heavy gas releases include those of Picknett (1981), McQuaid and Roebuck (1985) and Nielsen and Jensen (1991). Willis and Deardorff (1976, 1978, 1981, 1983, 1984) have also carried out a series of laboratory studies of dispersion in a convective boundary layer.

However, in situations where damage caused by toxic contaminants is the prime concern, it is usually the value of the instantaneous concentration (probably raised to some power greater than one – see Griffiths and Megson, 1984) that is the single most important factor. The available evidence suggests that on time scales of the order of half an hour large concentrations are present immediately downwind of a source more often during stable conditions (Lamb *et al.*, 1985; Peterson *et al.* 1988; Mikkelsen *et al.*, 1990; Mylne, 1992). Clearly, since material must be conserved regardless of the dispersion conditions, the corollary of this is that the short-time mean plume is more localised during stable conditions. The trade-off between smaller extent and higher concentration in determining harmful effect is far from evident at this stage. If the toxicological effect depends non-linearly on the concentration, as suggested above, then there must be a strong possibility that the total danger will be greater during stable conditions. Unfortunately, relatively few experiments have been undertaken during stable conditions. In addition to

those quoted above, they include those of Picknett (1981), McQuaid and Roebuck (1985) and Nielsen and Jensen (1991) – all heavy gas releases – and Guenther and Lamb (1989). Even in these studies, the attention given to dispersion in stable conditions is relatively little.

The general paucity of high resolution concentration fluctuation data in stable conditions provided the impetus to conduct the series of experiments described in this paper. Indeed, several earlier attempts had been made to obtain data in the U.K., but these had been frustrated by difficulties with the dependability of suitable weather conditions. Consequently a collaborative arrangement was developed with the United States Army Atmospheric Sciences Laboratory so that experiments could be conducted at their field station in southern New Mexico. This is essentially a desert location with small cloud amounts; daytime instability alternates with nighttime stability with very predictable regularity. Whilst the acquisition of data in daytime convective conditions was not regarded as a main experimental objective, the opportunity was taken to collect such data for comparison purposes.

2. Experimental Aspects

2.1. Experimental site and conditions

The experiments were conducted during November 1989. Although the experimental area was substantially flat in all directions for several tens of kilometres, the site was located in a rift valley between two parallel mountain ranges reaching about 1000 m above the valley floor, which ran roughly north–south. These topographic features probably had little effect on the daytime convective regime, at least on local scales well away from the mountains themselves. However, there is strong evidence to suggest that nocturnal katabatic flows were generated by the mountain ranges and that these flows continued throughout the rift valley floor in a complex pattern.

Surface vegetation consisted largely of patchy scrub with maximum height not exceeding 40 cm. Several kilometres from the experimental area, one could find occasional mesquite bushes up to about 2 m in height.

The experiments reported herein were to some extent preliminary in nature and designed to verify techniques as much as to obtain data suitable for analysis. However, as a result of the excellent weather conditions prevailing at the time, of the 18 releases conducted (each of which was typically of $\frac{1}{2}$ to $1\frac{1}{2}$ hr duration) approximately half yielded high quality data. Of the experiments analysed here, those numbered 8–11 and 13 were conducted in daytime unstable conditions, while 16 and 17 took place at night in a stable regime.

2.2. Tracer technique

The underlying principles of the tracer technique employed in these experiments have been detailed elsewhere (Jones, 1977). However, some novel features have been incorporated for these experiments and it is appropriate to describe these in more detail.

The system is based on the controlled release of unipolarly ionised air which, after undergoing dispersion, is detected by a number of ion collectors (ICs) designed specially to exploit the fast time-resolution potential of the system. The ionised air source consists essentially of a tube of a few centimetres diameter through which a gentle current (at about 3 m s^{-1}) of air is established using a low power DC fan. Near the outlet end of the tube, a fine wire, typically 5–10 microns radius, is mounted radially. The device has been found empirically to work optimally when the length of the wire is such that it extends about $\frac{1}{3}$ of the distance between its central supporting electrode and the outer tube. In operation, a stabilised DC voltage of 2–4 kV is applied to the wire and this causes the electric field close to the tips of the wire to exceed the breakdown value and hence a local corona discharge occurs. The geometry of the device is such that the electric field distribution within it is highly asymmetrical; as a result, the region away from the wire is filled with ions having the same polarity as the voltage applied and moving towards the outer electrode. These ions are moving into a weaker field region and are thus slowing down. By contrast ions of opposite polarity are rapidly attracted onto the fine wire and discharged. The action of the longitudinal air current is to expel a proportion of the ions into the atmosphere where they are then transported and dispersed. (The effects of the electrostatic repulsion and image phenomena which can vitiate experimental data if the ions are released at too high a rate have been discussed in detail by Chatwin *et al.* (1989). For the parameter values in these experiments, we expect image phenomena to be negligible, and the mean concentration and mean plume width to be virtually unaffected by repulsion.)

The latest ion collectors in use are based on coaxial cylinder geometry and operate in the following manner. Ionised air is drawn into the collector at, in the present device, a speed of 3 m s^{-1}, which corresponds to a volumetric flow rate of 0.0085 $m^3 s^{-1}$. Once in the collector, the ions encounter a strong electric field which is created by a bias potential of some 600 V applied to a cylindrical electrode of 0.015 m radius surrounding the central collecting rod (0.001 m radius) which is connected to earth via the input stage of the signal amplifier. The magnitude of the applied bias in conjunction with the length of the electrode system, the air flow speed and the ionic mobility ensures that all the ions entering the device are repelled onto the central rod. The ions arriving at this rod are discharged and effectively constitute an electric current whose value is typically in the range 1–500 pA. These very small currents are then amplified to provide an output voltage suitable for recording.

As indicated above, a major feature of the ion collector is its very fast time

response which is important for examining the details of clouds dispersing in the lower atmosphere. However, the device has several other advantages. In particular it is very straightforward to install and operate in the field as it requires no calibration (once the air flow rate has been determined initially of course) and virtually no maintenance. It also possesses a fully linear response to the ion concentration and does not suffer from the saturation and hysteresis effects exhibited by some types of chemically based detectors. Its temporal response is also completely symmetrical, i.e., it responds identically to rising and falling ion concentrations. However, it should be noted that the current model does not work well in high humidity conditions owing to difficulties in maintaining the integrity of the insulators. Measures are being taken to alleviate this problem.

Specific improvements that have been incorporated in the present collector as compared with those referenced earlier include:

1. An autozeroing circuit based on a temperature controlling circuit applied to the input chip (where thermal drift proved a major problem). The system uses a Peltier heater/cooler and is very effective.
2. Precision control of the suction fan motor speed.
3. Incorporation of the entire electronics at the site of the collecting electrode system. As well as reducing microphony and sensitivity to extraneous noise, this modification has markedly improved the compactness and portability of the device.

A particular development in these experiments was that first use was made of an extensively redesigned ion source which featured a considerably enhanced output stability so as to provide an accurately known source strength. (The source concentration can be calculated from the source current given the cross-sectional area of the source and the speed with which air is expelled from the source.) This has often been a parameter difficult to specify precisely in many other tracer methods. This system includes a "floating" anode, thereby enabling the current output to be sensed directly and compared with a reference signal. If the current then deviates from the set value, an error voltage is developed which is used to control the applied EHT in such a way as to restore the output to its original value. In practice, stabilities within a few percent could be readily obtained. In the experiments discussed here the ion current was set at -30 nA.

2.3. Sampling Array Details

In this series of experiments, four ion collectors were employed throughout but the array configurations were adjusted to reflect the narrower plumes expected in stable conditions, although one unstable experiment was conducted with the array in this latter configuration. The two arrays are detailed in Figure 1. Note that the separations between the ion collectors were not designed to be the precise values shown – the dimensions merely reflect the placement constraints imposed by the mechanical arrangements used to support them. In all the experiments care was

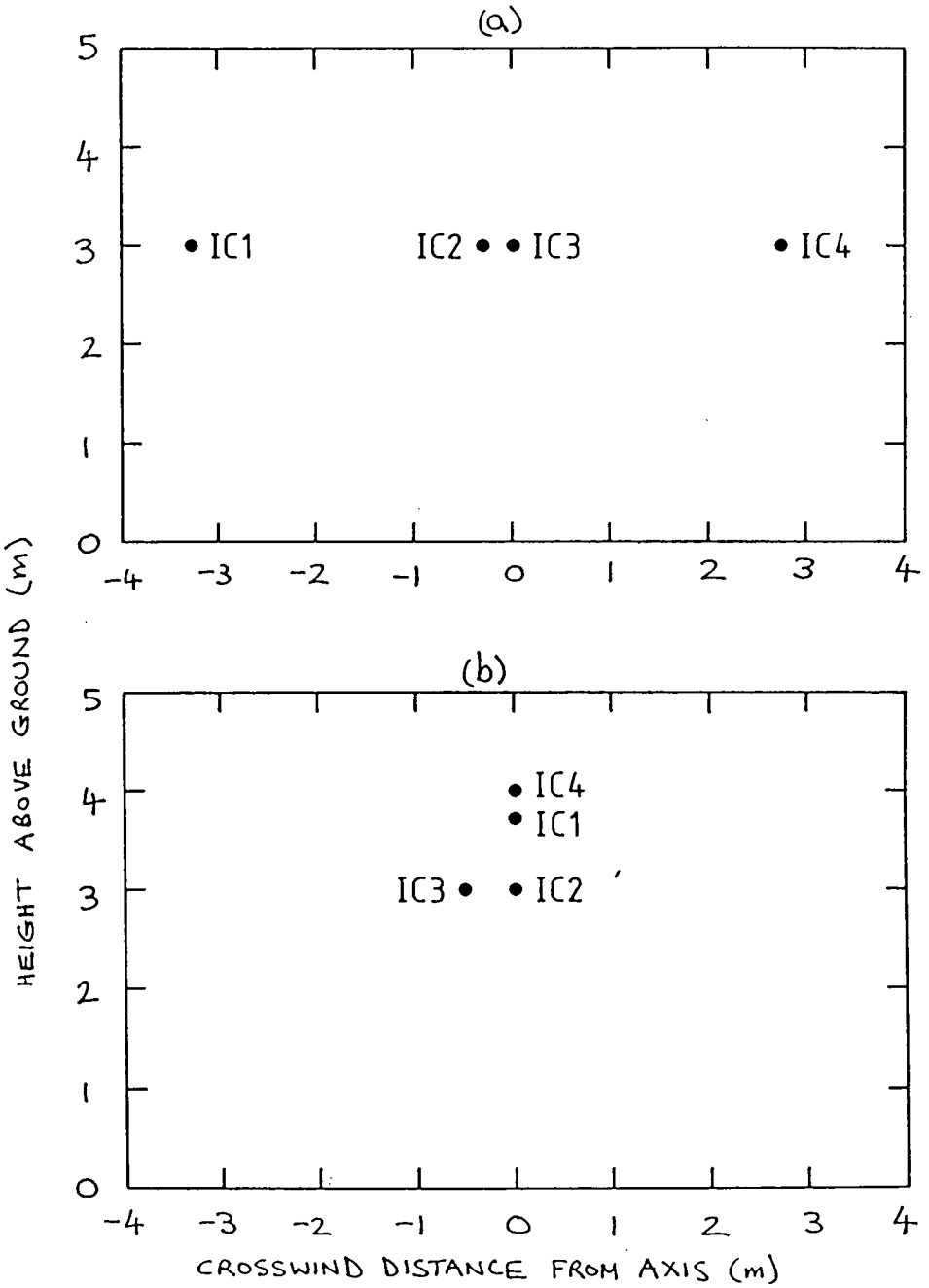

Fig. 1. The ion collector arrays, looking downwind from the source. (a) Experiments 8–11. Source height 3 m. (b) Experiments 13, 16, 17. Source height 3.5 m.

taken to orient the collector array perpendicular to the line joining the source and the array axis. Hence the plane of the array was set in the nominal crosswind plane. The downwind separations between these arrays and the ion generator are given in Table I. Experiments 8–11 were carried out consecutively in time with no break in recording. Between experiments, the ion generator was switched off and moved up- or downwind before being switched on again. Thus periods of

TABLE I

Downwind separation (m) between ion generator and array of ion collectors, the approximate duration of experiments (minutes) and whether the conditions were stable (S) or unstable (U)

Experiment	8	9	10	11	13	16	17
Downwind separation (m)	12.5	15	10	7.5	5	5	10
Duration (minutes)	42	43	43	55	78	30	25
Stable or Unstable	U	U	U	U	U	S	S

noise of length about 5 min were recorded between experiments. Experiments 16 and 17 were also recorded consecutively.

2.4. Data recording and processing

Ion concentration signals, which were in the form of analogue voltages in the range 0 to +1.5 V, were recorded on tape using an FM Instumentation tape recorder. They were then digitised at 10 Hz using a 12 bit A-D converter, having first passed the analogue signal through an analogue 5 Hz filter. Thus structures with the smallest time scales present in the flow cannot be resolved. However, the digitisation was such that each concentration value is representative of 1 μs, so the sampling rate has negligible effect on statistics like the concentration moments. The temporal resolution of the ion collectors is also sufficient to avoid significant effects on the measured variance (Mole, 1989). The effect on the higher moments will be greater, but is still probably not large for the third and fourth moments. However, there is probably a significant effect on the extreme tail of the probability density function.

The range of concentration values measured was such that about 1900 of the 4096 bins were utilised. The bin width was about 4.3×10^{-3} n Cm^{-3} in experiments 8–10, and about 1.3×10^{-2} n Cm^{-3} in the others. The largest (negative) charge density measured was about -25 n Cm^{-3} (in experiment 16), which compares with the source charge density $\theta_0 \approx -2300$ n Cm^{-3}. (Henceforth the negative sign will be dropped, so a positive concentration will imply a negative charge density.)

Figure 2 shows a typical time series of concentration, both for an unstable case (experiment 13) and for a stable case (experiment 16). The plotted values are the digitised ones, with no further analysis having been undertaken. The true zero of concentration is slightly displaced from the zero of the instrument for all 4 ion collectors, and the statistics for the recorded periods of noise before and after experiments show that there is a small drift (maximum 0.055 n Cm^{-3}) in the position of the true zero (to be referred to subsequently as the baseline). Concentration statistics were calculated after subtracting the constant value given by the mean of the period of noise immediately before the experiment (or after in the case of experiments 11 and 16). No account was taken of the drift in baseline during the experiments. The effect of this drift is unlikely to be significant for any

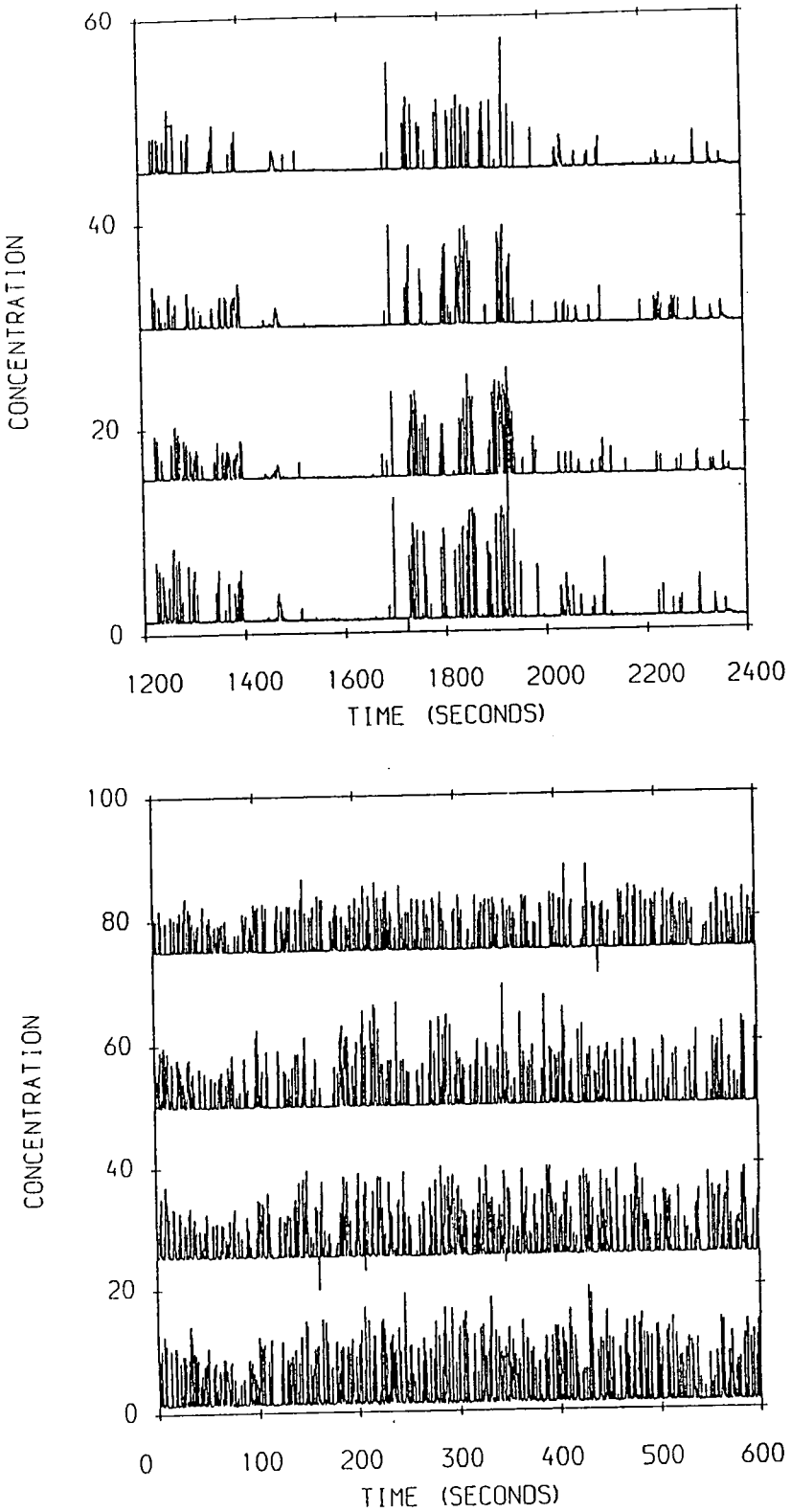

Fig. 2. Sample concentration time series, with IC1 at bottom, IC4 at top. (a) Experiment 13, each IC displaced by 15. (b) Experiment 16, each IC displaced by 25. Units are n Cm^{-3}.

of the statistics quoted below except the mean and intensity for experiments 8 and 9 (and to some extent 10) when the mean concentration was small. The intermittency could be affected for all experiments, although probably not to a very great extent. However, even in the absence of baseline drift, there are substantial problems with intermittency (see Section 5) resulting from the inevitable presence of baseline noise.

Also apparent from Figure 2 is the presence of spurious negative spikes after about 1700 of experiment 13, and after about 160 and 450 s of experiment 16. These occurred occasionally in all the experiments, and arise from instrumental malfunction. They have therefore been excluded. The number of concentration values ignored for this reason comprised less than 0.2% of the total in all cases (and nearly always much less).

3. Central Moments of Concentration

3.1. Stationarity of concentration moments

The central moments of concentration were calculated for subperiods of different lengths within each experiment to investigate any temporal variability in the moments, and whether the moments calculated for a whole experiment can be considered to be independent of the chosen total sample time. Figure 3 shows some results for the mean for experiments 13 and 16 for overlapping subperiods of length 400, 800 (experiment 16) and 1200 s (experiment 13). The calculated statistics are only plotted at 200 equally spaced times.

In experiment 16, a subperiod of 800 s was sufficient to give fairly constant statistics in most cases. In the other stable case (experiment 17, not shown), most of the statistics showed clear trends when the subperiods had length 800 s – the means of all channels decreased while the skewness, kurtosis and intensity of all channels increased. This was a result of systematic departures of the wind direction from the array axis line.

In experiment 13, subperiods of length 1200 s were clearly not long enough to give steady values of the statistics, and even at 2000 s there was considerable variation. In general the unstable cases showed greater variability than the stable cases. In experiment 13 it is clear that timescales of the order of the experimental length or greater are important, since there is much less activity towards the end of the experiment than in the earlier parts. It is also interesting to note the cyclic variation, with very regular period, of the mean and standard deviation in the earlier part of the experiment. This feature is clearly related to the structure of the convective boundary layer. There appear to have been pronounced eddies with a period of about 700 s, sweeping the plume past the collector array. This is consistent with the time scale of convectively driven turbulence being typically about 10 min (Kaimal *et al.*, 1976).

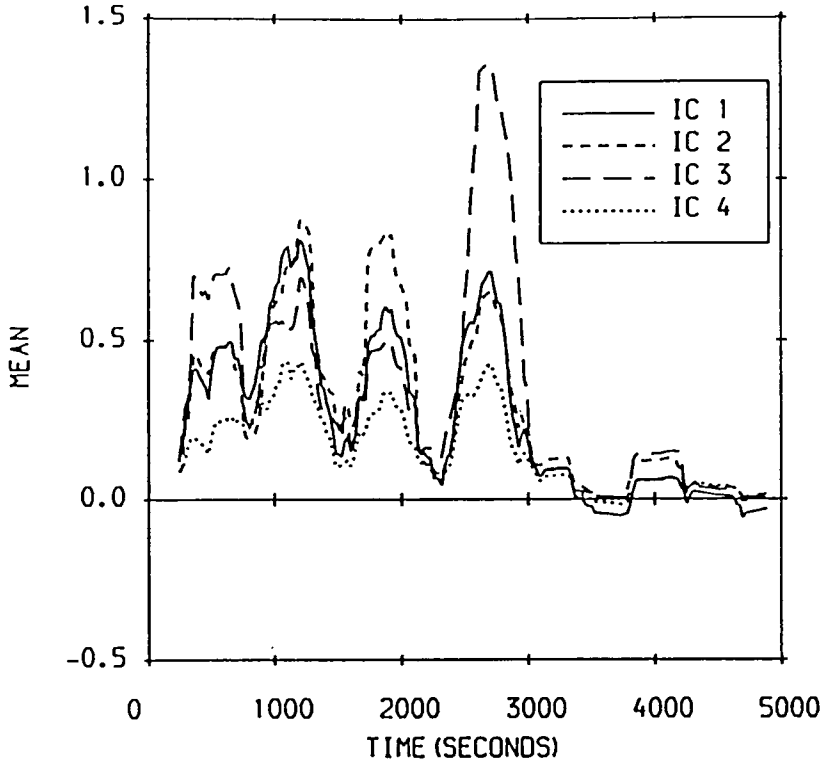
1.5
1.0
0.5
0.0
-0.5
MEAN
IC 1
IC 2
IC 3
IC 4
0
1000
2000
3000
4000
5000
TIME (SECONDS)

Fig. 3(a)

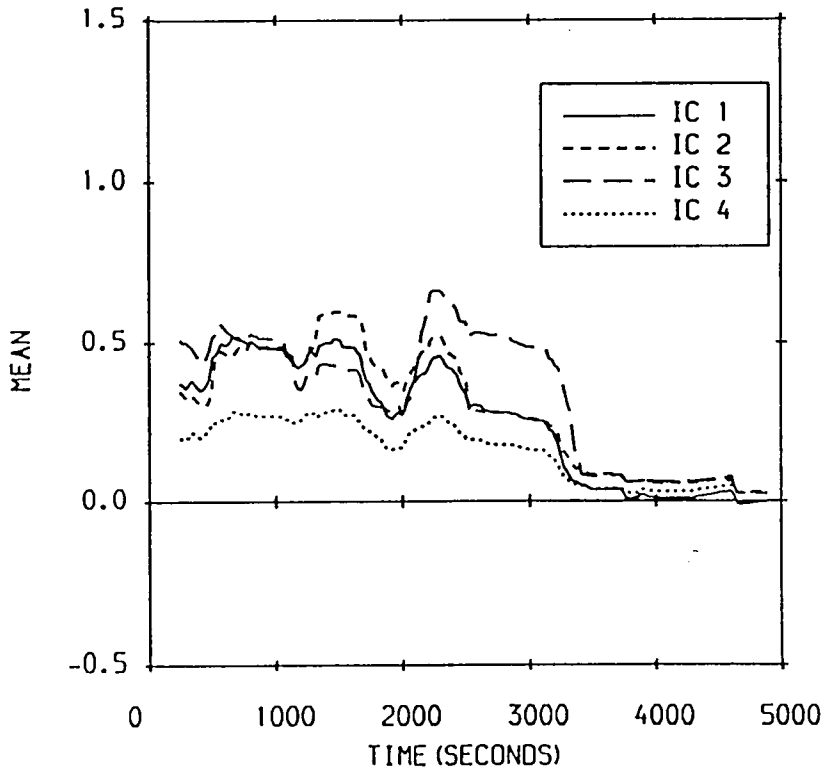
1.5
1.0
0.5
0.0
-0.5
MEAN
IC 1
IC 2
IC 3
IC 4
0
1000
2000
3000
4000
5000
TIME (SECONDS)

Fig. 3(b)

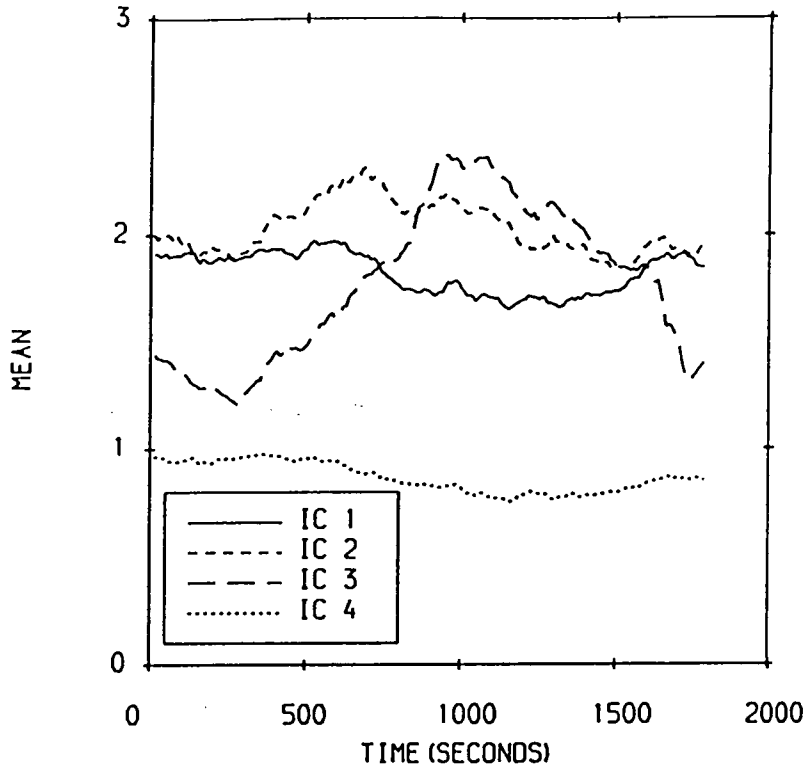

Fig. 3(d)

Fig. 3. The time variation of the mean concentration (in n Cm^{-3}). In all cases the mean has been calculated at 200 equally spaced times. (a) Experiment 13, means calculated over 400 s. (b) Experiment 13, means calculated over 1200 s. (c) Experiment 16, means calculated over 400 s. (d) Experiment 16, means calculated over 800 s.

extrapolate to the centreline if necessary, or simply to choose the ion collector with the largest mean concentration as being most representative of the mean plume centreline. Figure 4 shows the results for the latter choice, for the statistics given in Table II. Ideally the downwind distance would be normalised by the mean velocity and a Lagrangian timescale for the turbulence, as in Mylne (1992). Here the latter quantity is unavailable so the downwind distance has been normalised by the estimated mean velocity of 2 m s^{-1} in the unstable cases and 4.5 m s^{-1} in the stable cases. (The recording equipment for the wind speed failed during the experiments, so only rough estimates from visual readings are available.) Also shown, for comparison, are results from experiments carried out at Cardington in neutral conditions. Details of these experiments can be found in Chatwin and Hajian (1990). The source strength (−10 nA) was different from that in the present experiments, so only the non-dimensional quantities are compared.

The mean concentration and the variance both decrease downwind, but the dependence on stability is not clearcut. There is perhaps some sign of these statistics being larger in the stable cases, as was true for the centreline mean in Peterson *et al.* (1988) and Mikkelsen *et al.* (1990).

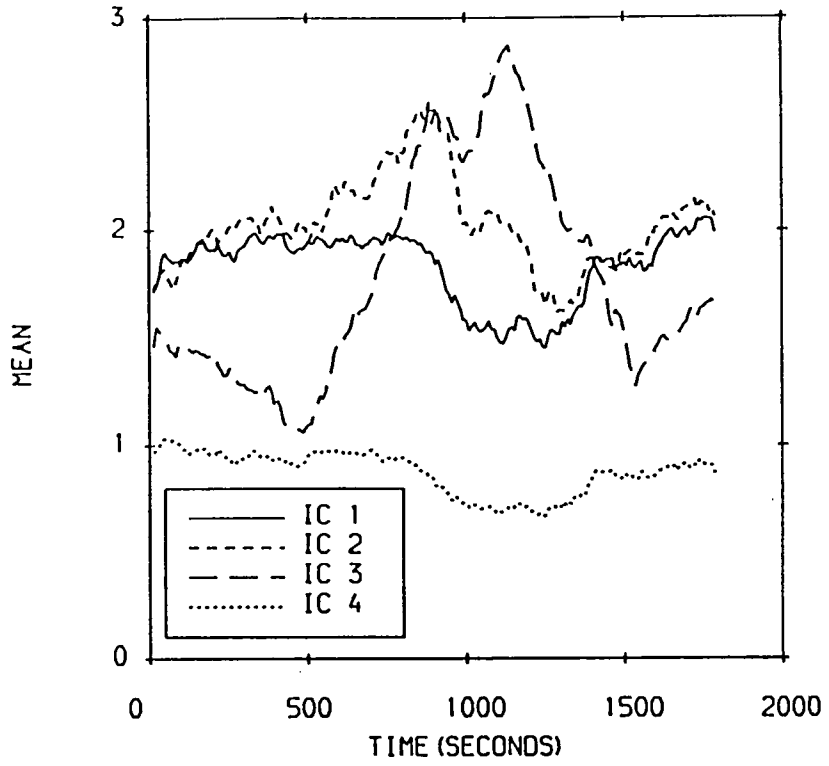

Fig. 3(c)

3.2. Results for the concentration moments

The two time series in Figure 2 show the clearly different characters of the experiments under stable and unstable conditions (and in this respect these examples are entirely representative of these experiments). During stable conditions, the probability of recording a concentration significantly greater than zero was substantially higher than under unstable conditions. Correspondingly, one would expect that at larger distances from the mean plume centreline, this probablity would have been larger during unstable conditions. However, when the mean wind speed and downwind distance are taken into account, the difference between the stable and unstable cases is less clearcut, as will be seen below.

Table II gives the mean, standard deviation, skewness, kurtosis and intensity of concentration. Because of the limited number of ion collectors in each experiment, there is only one experiment (11) in which there is clear evidence that the mean plume centreline falls within the array. Thus there is little useful analysis of cross-plume structure that can be performed. In experiment 11 the lateral spread σ_y of the mean plume is approximately 1.8 m, but the profile of mean concentration is not very well fitted by a Gaussian curve.

A further consequence of the limited cross-plume coverage is that downwind variations are less easily analysed since the mean plume centreline cannot be identified. The best that can be done is either to fit a curve like the Gaussian and

TABLE II

Mean (C), standard deviation (σ), skewness (S), kurtosis (K) and intensity (I)

Experiment	Ion collector	C	σ	S	K	I
8	1	0.0779	0.376	5.57	37.4	4.83
	2	0.0782	0.316	5.17	34.2	4.04
	3	0.0600	0.340	4.90	30.2	5.67
	4	0.0539	0.270	5.08	32.9	5.01
9	1	0.0992	0.372	6.19	51.8	3.75
	2	0.0400	0.187	7.34	73.1	4.69
	3	0.0333	0.166	7.53	74.4	4.99
	4	0.0163	0.0677	9.34	168	4.17
10	1	0.108	0.481	5.94	44.1	4.46
	2	0.139	0.544	4.98	30.9	3.91
	3	0.177	0.624	4.62	27.1	3.52
	4	0.198	0.619	4.30	24.8	3.13
11	1	0.252	0.906	5.05	32.2	3.59
	2	0.294	0.903	3.97	21.3	3.07
	3	0.266	0.831	3.94	21.5	3.13
	4	0.116	0.458	6.22	59.1	3.96
13	1	0.256	1.06	5.03	33.7	4.15
	2	0.289	0.993	4.68	28.0	3.44
	3	0.331	1.09	4.26	23.2	3.30
	4	0.157	0.669	5.67	45.5	4.25
16	1	1.83	3.11	2.05	6.88	1.70
	2	2.04	3.12	1.72	5.25	1.53
	3	1.78	3.24	2.36	8.99	1.82
	4	0.872	1.89	2.88	13.1	2.17
17	1	0.733	1.40	2.66	10.9	1.91
	2	0.773	1.46	2.60	10.6	1.89
	3	0.604	1.27	2.93	13.0	2.11
	4	0.468	0.994	2.87	12.4	2.13

The skewness (always clearly positive) and kurtosis (always greater than 3) both increase downwind, although with a hint of an initial decrease, and appear to be slightly larger in the unstable cases. Jones (1979, 1983) found an initial increase of these statistics, followed by a decrease at the farthest downwind distance, the reverse of the present findings. However, in all of these experiments there is uncertainty as to the position relative to the plume centreline, so cross-plume variations could account for some of these observed trends. In all cases, the dominant feature is the downstream increase.

The intensity is larger in the unstable cases, as found by Peterson *et al.* (1988), and shows no clear trend with downwind distance. Mylne (1992) on the other hand found no significant difference in intensity between stable and near-neutral conditions when the local turbulence was used to scale the downwind distance.

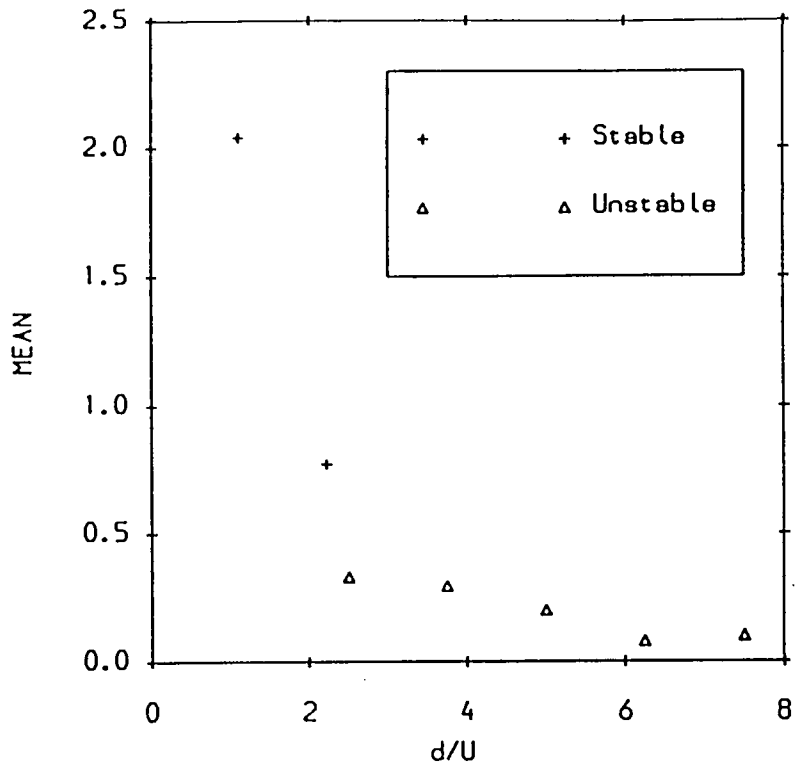
2.5
2.0
1.5
1.0
0.5
0.0
MEAN
0
2
4
6
8
d/U
Stable
Unstable

Fig. 4(a)

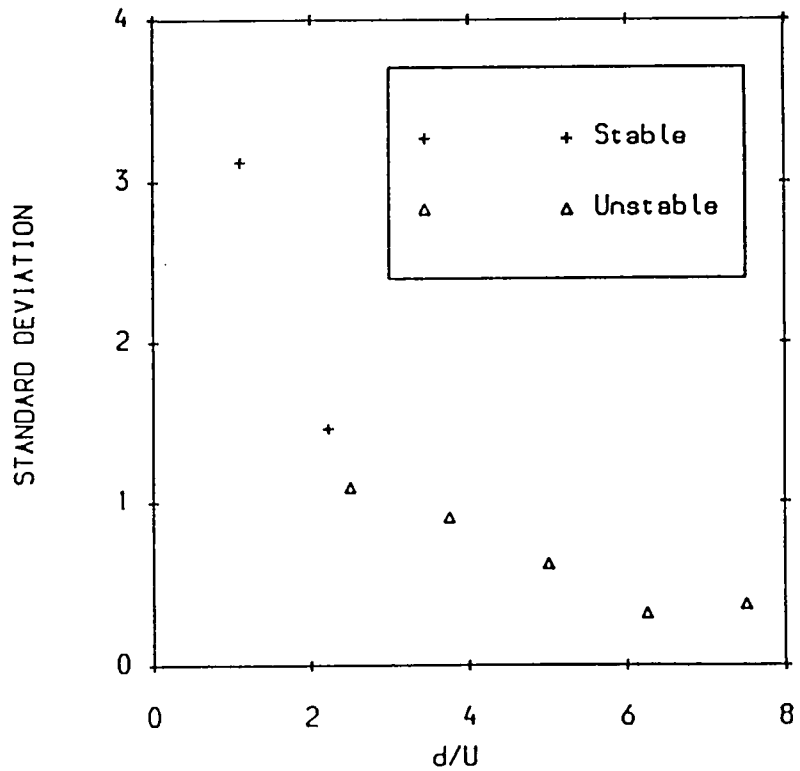
4
3
2
1
0
STANDARD DEVIATION
0
2
4
6
8
d/U
Stable
Unstable

Fig. 4(b)

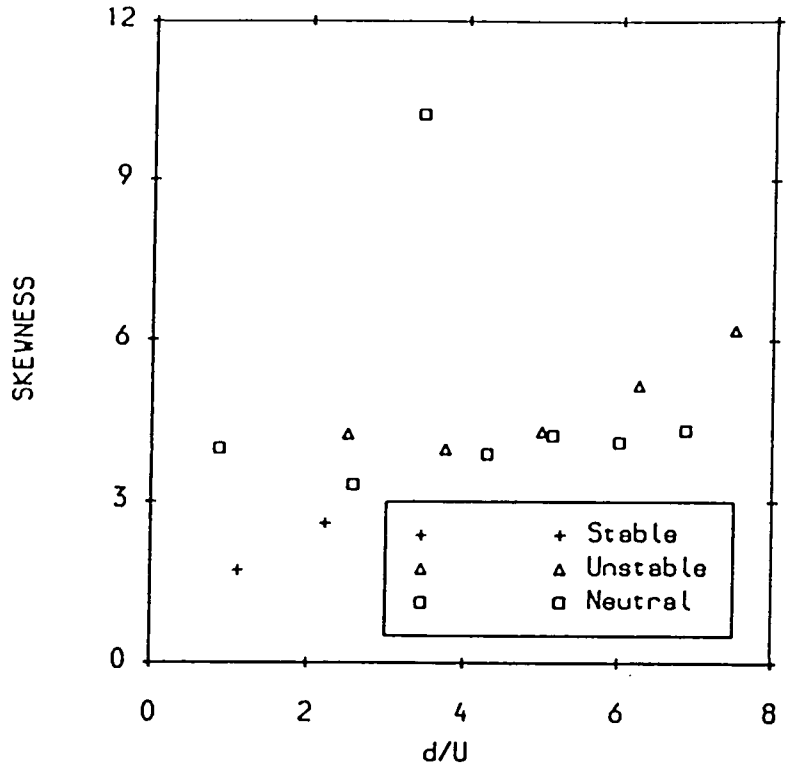
SKEWNESS
d/U
Stable
Unstable
Neutral
0
3
6
9
12
0
2
4
6
8

Fig. 4(c)

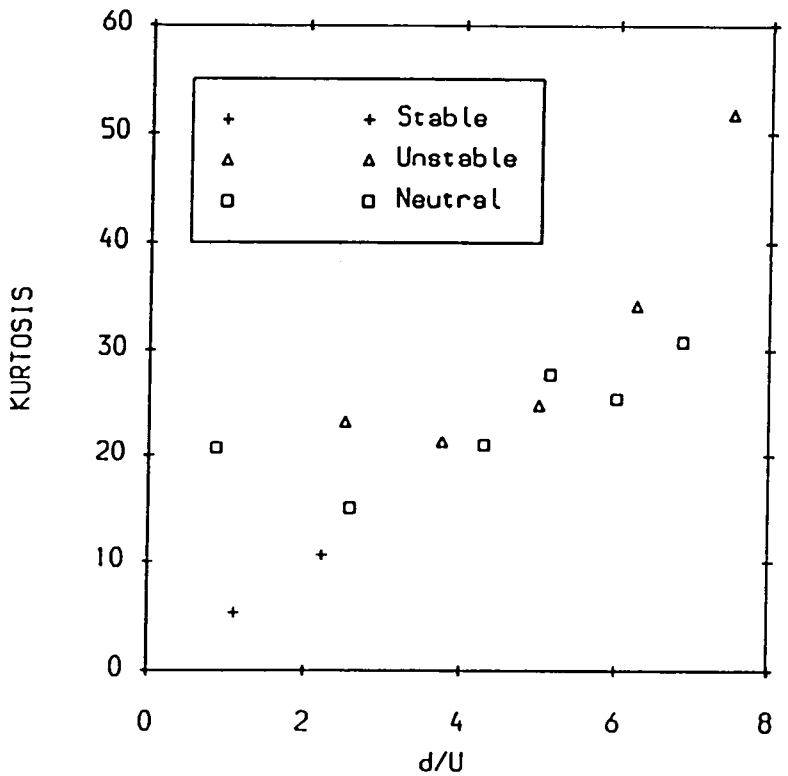
KURTOSIS
d/U
Stable
Unstable
Neutral
0
10
20
30
40
50
60
0
2
4
6
8

Fig. 4(d)

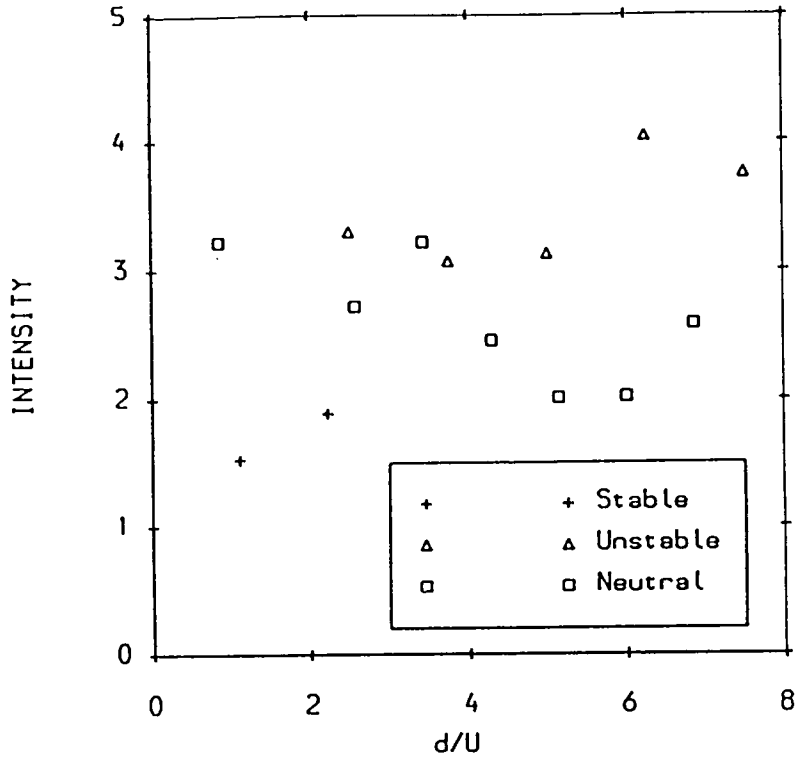

Fig. 4(e)

Fig. 4. Concentration statistics plotted against downwind distance d(m) normalised by mean wind speed U ($m\,s^{-1}$). (a) Mean. (b) Standard deviation. (c) Skewness. (d) Kurtosis. One neutral point, with $d/U = 3.43$ and kurtosis 518, has been omitted. (e) Intensity.

Among previous studies Jones (1979) and Sawford *et al.* (1985) have found a downwind increase of intensity, while in Lewellen and Sykes (1986) and Dinar *et al.* (1988), the dependence on distance was unclear (although there was possibly a slight downwind increase in the latter case). Jones (1983) obtained an initial increase followed by a decrease, while Mylne and Mason (1991) found a clear decrease followed by a long range throughout which the intensity was constant or possibly slightly decreasing. In the laboratory, Deardorff and Willis (1984) obtained a decrease in intensity with downstream distance (although their measurements were of ground-level concentration), and Fackrell and Robins (1982) found an increase followed by a decrease. All of these results seem to be consistent with a picture where the intensity close to the source increases downwind, as one would expect, reaches a maximum and then decreases at an ever-decreasing rate. The maximum seems to be reached at values of the ratio of downwind distance to mean wind speed, d/U, roughly in the range 2–20 s, the precise value depending on factors like source size and atmospheric stability. The present results would then be interpreted as falling in the transition region around the maximum. Of the studies listed here, those which considered the intensity in different stability

TABLE III

Values of the ratio of the overall standard deviation (σ) to that of the noise (σ_N)

Ion collector	Experiment						
	8	9	10	11	13	16	17
1	17.5	12.3	13.9	13.3	21.7	75.6	34.1
2	17.7	6.7	18.6	11.5	23.1	85.6	40.0
3	17.5	5.1	18.1	10.1	26.7	90.3	35.5
4	9.3	2.1	18.5	7.8	14.6	42.0	22.0

conditions found little effect of stability. In all of these other cases, the values of intensity fall within the range 0.2–5.0 (except for Mylne (1992), where values in the plume fringes were as high as 10), consistent with the present results.

4. The Probability Density Function

Figure 5 shows the probability density functions (p.d.f.s) for all ion collectors of experiment 16. The p.d.f.s were estimated non-parametrically using the Gaussian kernel method (see Silverman, 1986) with kernel width set from Silverman's equation (3.31). This experiment is the one with largest signal-to-noise ratio (see Table III), and the largest intermittency (loosely defined as the probability of positive concentration – see Section 5 for a fuller discussion). Nevertheless, the visual impression is dominated by the peaks at zero concentration associated with the noise. Plotting the p.d.f. on logarithmic scales is more revealing of behaviour in the tail, which represents genuine concentration, especially if one is looking for particular parametric distributions such as the exponential or normal. However, to this end it is simpler to work with the cumulative density function (c.d.f.) since then the data can be used directly, without having to perform any analysis such as is necessary to produce a p.d.f. or a histogram. Results for the c.d.f. are presented below.

Another class of methods of extracting information about the true concentration is possible when instrument smoothing effects are negligible (see the discussion in Mole, 1990). This relies on the fact that the measured p.d.f. is a convolution integral over the p.d.f.s of the noise and of the true concentration – see Equation (3). If the p.d.f. of the noise can be estimated, then the p.d.f. of the true concentration can be estimated. In these experiments, since periods of pure noise were recorded, the p.d.f. of the noise may be estimated. Figure 6 shows the noise c.d.f. $F_N(\theta)$ for experiment 13 plotted on a normal probability scale. Thus the abscissa X is defined by $X = \Phi^{-1}\{F_N(\theta)\}$, where θ is the concentration and $\Phi(X)$ is the standard normal c.d.f. It can be seen that the noise is very closely Gaussian except in the extreme tails of the distribution. (Note that the discontinuous form of the curves is the result of the digitisation of the data into a finite number of

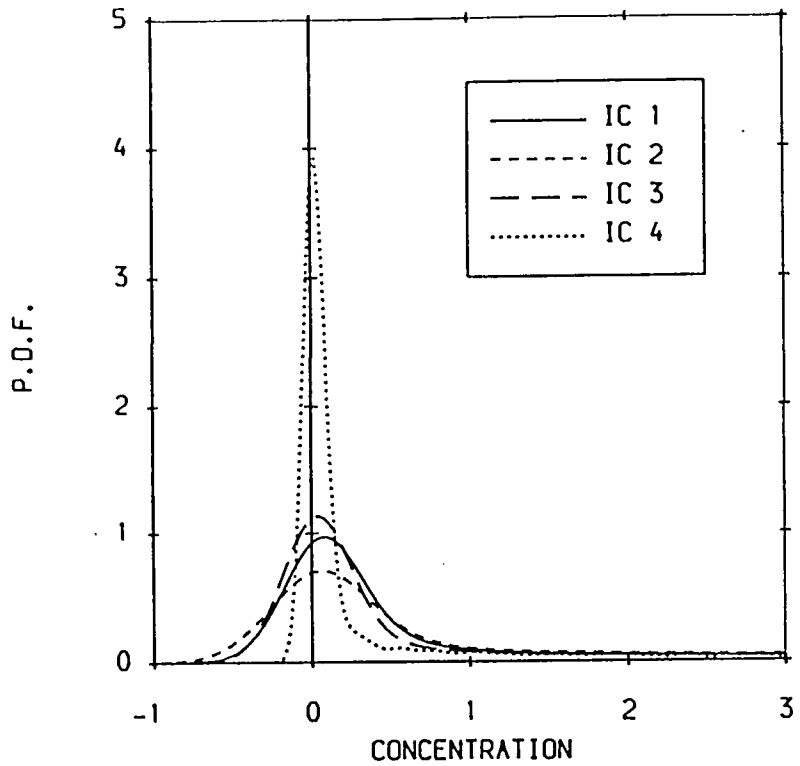

Fig. 5. P.d.f.s for experiment 16, estimated using the Gaussian kernel method, as described in the text.

bins.) The deviation from normality in the left-hand tail is largely the result of the rarely occurring negative spikes, but the deviation in the right-hand tail appears to be more systematic. The standard deviation of the fitted Gaussian p.d.f. is given by the slope of the middle portions of the c.d.f.s, which in this case is about 0.044 n Cm^{-3}, in good agreement with the calculated standard deviations.

In Figure 7, the full c.d.f.s for experiments 13 and 16 are shown. They are plotted in two different ways, in which a straight line corresponds to an exponential or to a truncated normal distribution. Visual inspection suggests that the truncated normal gives the best fit, except possibly in the experiments with lowest mean concentration. Statistical tests (see e.g., D'Agostino and Stephens, 1986) of the normality and exponentiality of the conditional distributions suggest that the normal distribution generally provides a better fit than the exponential distribution. This is particularly so for the stable cases. For example, taking a significance level (the probability of rejecting the assumed distributional form as being a poor fit to the sample, when the sample does come from such a distribution) of 10% gives the following results. In experiment 13, the concentration at all ICs could come from a normal or an exponential distribution, with the exception of IC 3 for which it could not come from an exponential distribution. In experiment 16, the concentration at ICs 1, 3 and 4 could be normally distributed, but at none could it be exponentially distributed. This form of plot also shows fairly clearly the

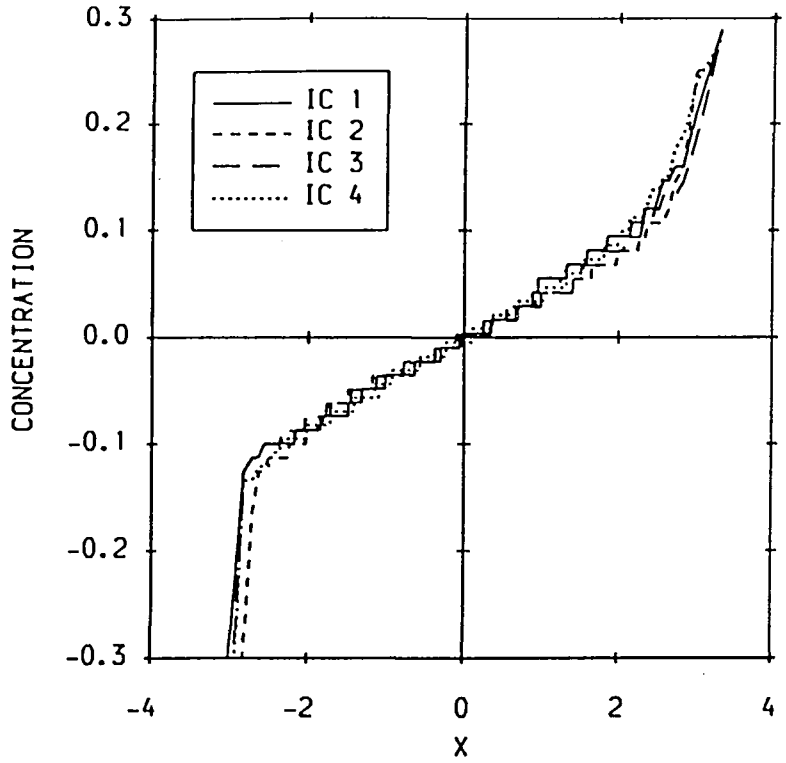

Fig. 6. C.d.f.s for the period of noise in experiment 13, plotted on a normal probability scale.

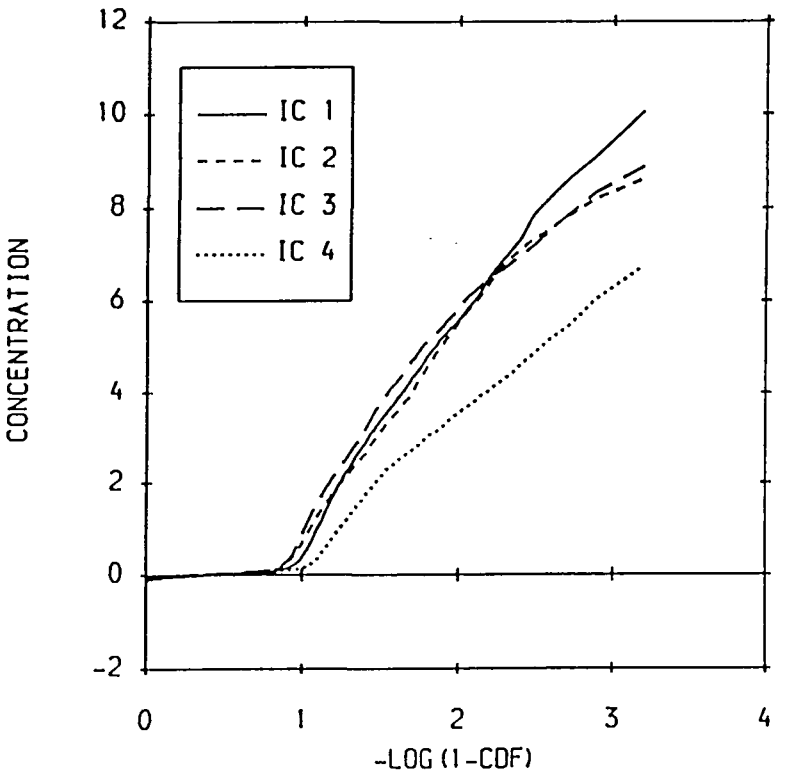

Fig. 7(a)

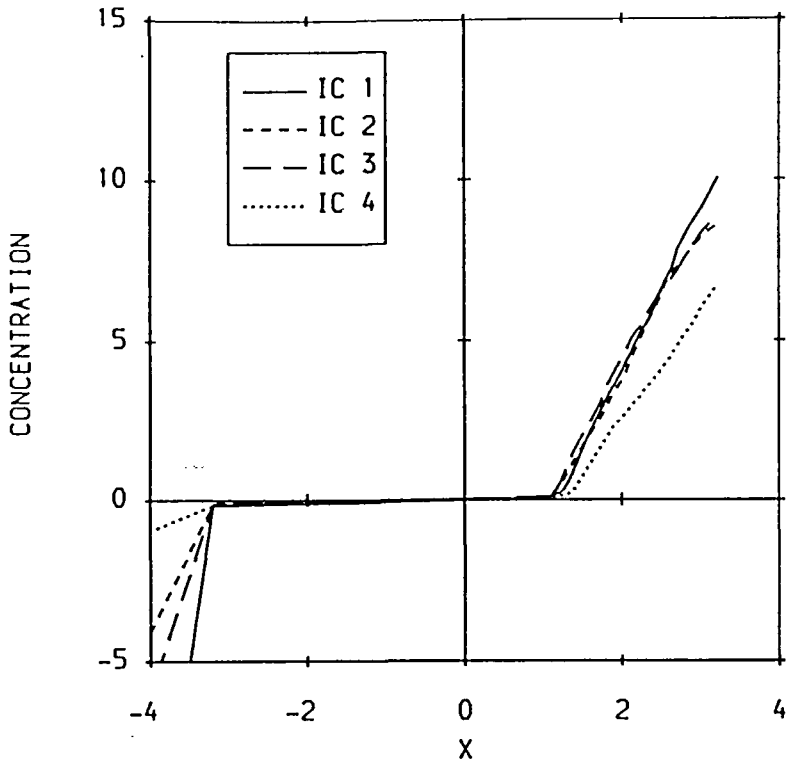
15
10
5
0
-5
-4
-2
0
2
4
X
CONCENTRATION
IC 1
IC 2
IC 3
IC 4

Fig. 7(b)

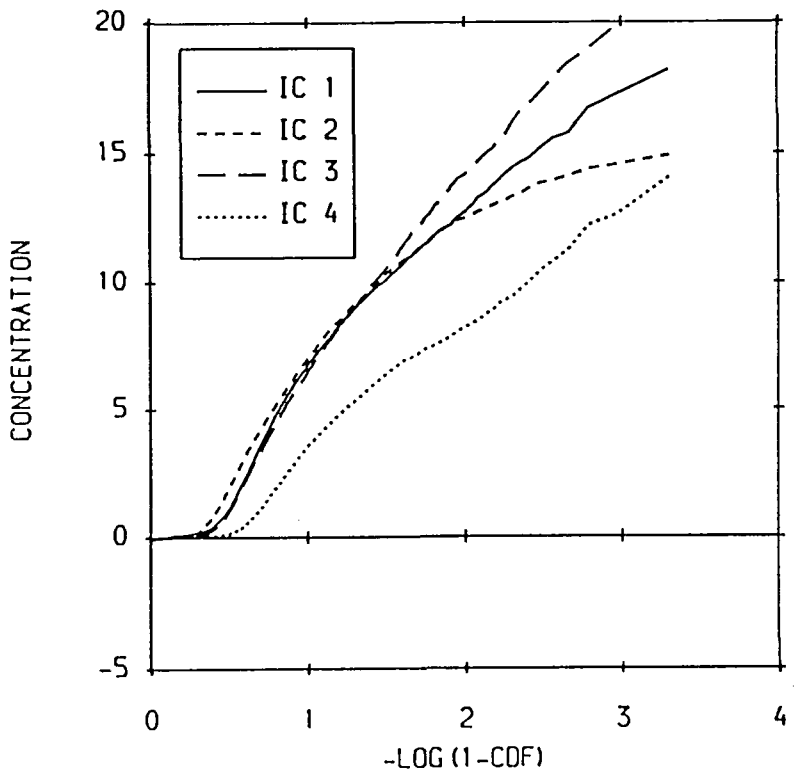
20
15
10
5
0
-5
0
1
2
3
4
-LOG (1-CDF)
CONCENTRATION
IC 1
IC 2
IC 3
IC 4

Fig. 7(c)

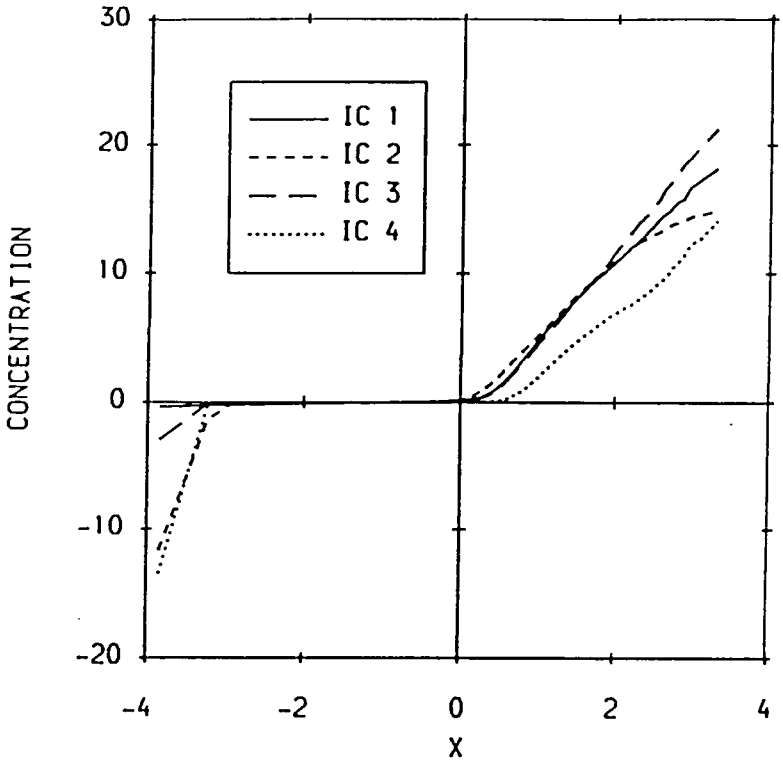

Fig. 7(d)

Fig. 7. C.d.f.s. (a) Experiment 13, exponential scale. (b) Experiment 13, normal probability scale. (c) Experiment 16, exponential scale. (d) Experiment 16, normal probability scale.

transition from true concentration to noise at $X \approx 1.2$ in experiment 13 and $X \approx 0.3$ in experiment 16. The difference in these values is consistent with the larger signal-to-noise ratio and intermittency in experiment 16. Figure 8 shows the c.d.f.s for the other experiments, plotted in truncated normal form.

5. Intermittency

5.1. Conventional definition

The intermittency γ is usually defined as the probability of a positive concentration. It is well known, however, that there are both theoretical and practical drawbacks to this definition, as discussed by Sreenivasan (1985) and Chatwin and Sullivan (1989). In practice, the problem caused by the presence of noise in the measured concentration is usually dealt with by introducing an arbitrary threshold θ_T:

$$\gamma = \Pr\{\Gamma > \theta_T\} = 1 - F(\theta_T)\,, \tag{1}$$

where Γ is the concentration and $F(\theta)$ is the c.d.f. With this definition, γ can be found from Figures 7 and 8 once θ_T has been chosen.

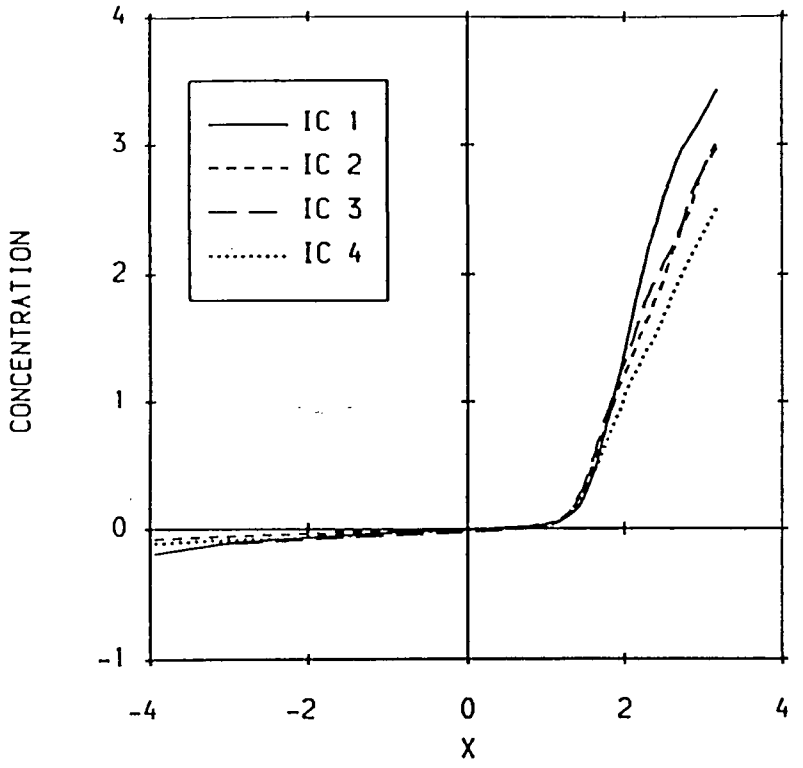
IC 1
IC 2
IC 3
IC 4
CONCENTRATION
X
4
3
2
1
0
-1
-4
-2
0
2
4

Fig. 8(a)

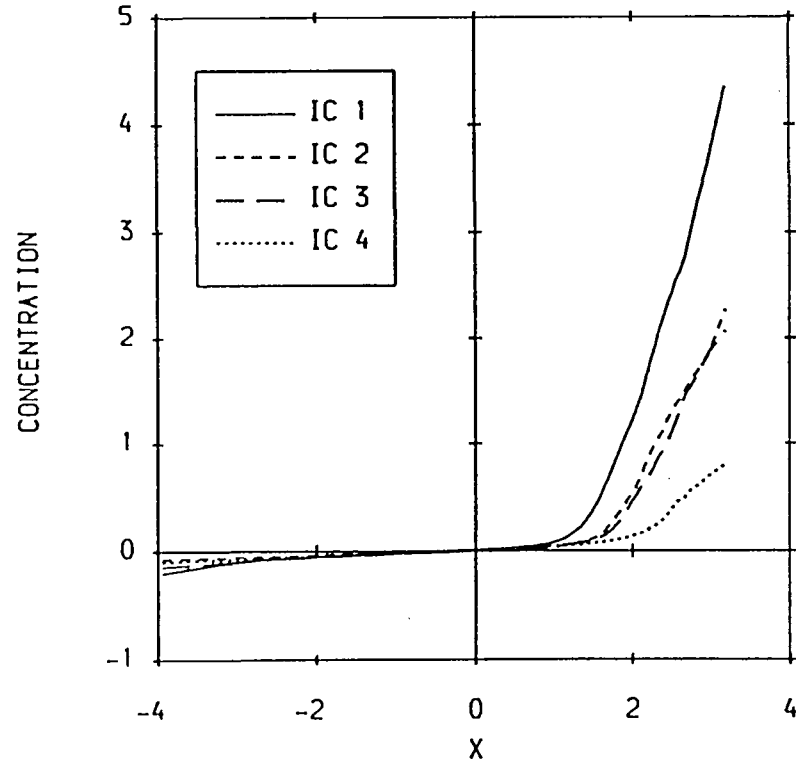
IC 1
IC 2
IC 3
IC 4
CONCENTRATION
X
5
4
3
2
1
0
-1
-4
-2
0
2
4

Fig. 8(b)

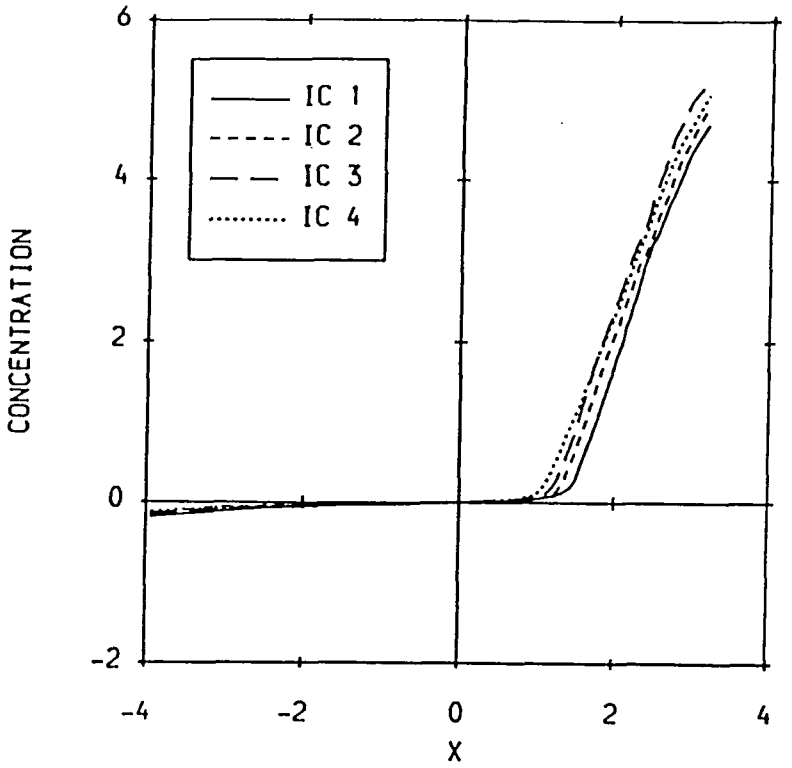
IC 1
IC 2
IC 3
IC 4
CONCENTRATION
X
6
4
2
0
-2
-4
-2
0
2
4

Fig. 8(c)

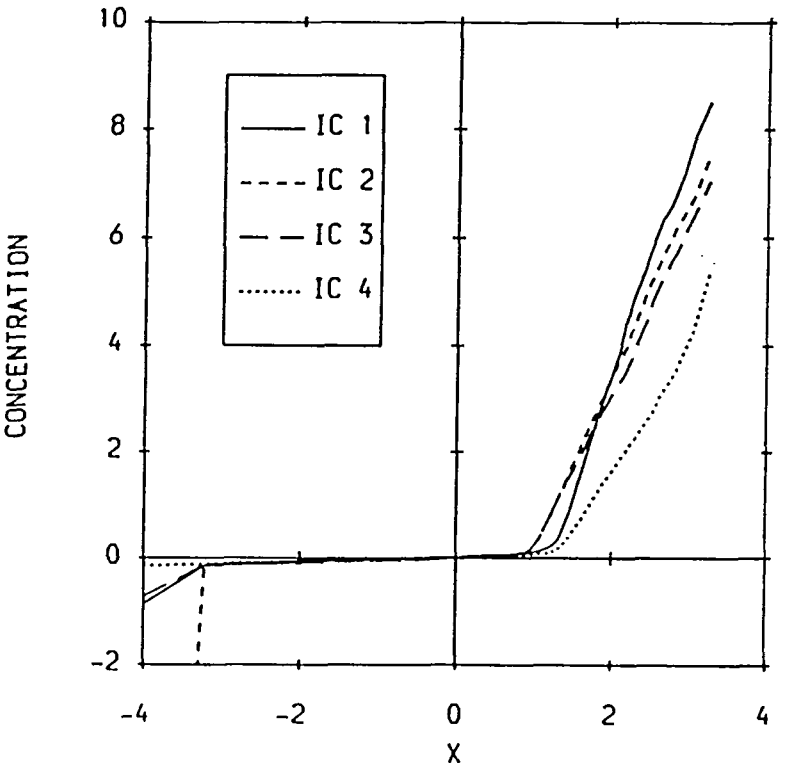
IC 1
IC 2
IC 3
IC 4
CONCENTRATION
X
10
8
6
4
2
0
-2
-4
-2
0
2
4

Fig. 8(d)

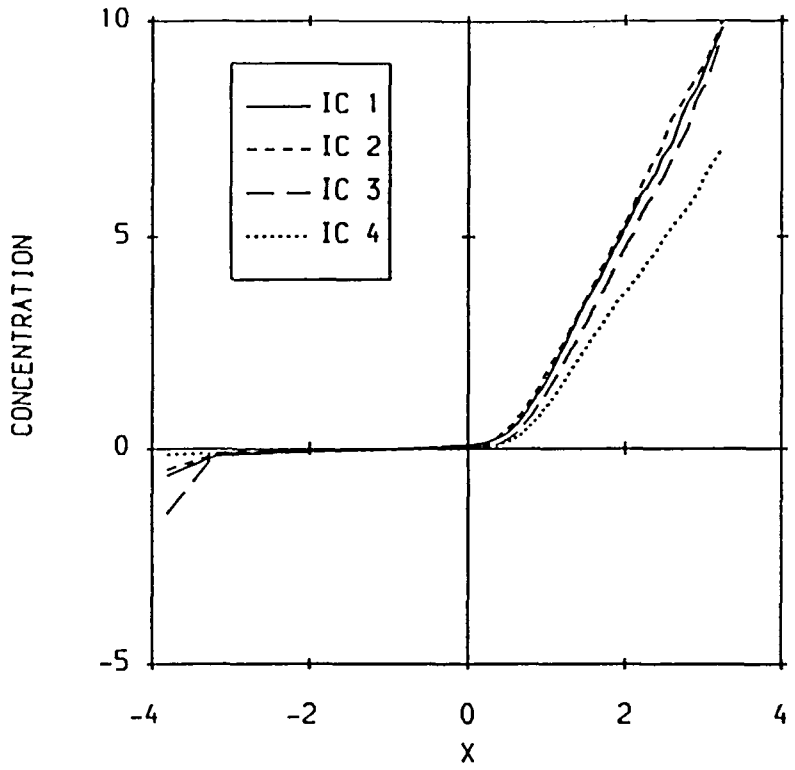

Fig. 8(e)

Fig. 8. C.d.f.s plotted on normal probability scale. Experiments (a) 8, (b) 9, (c) 10, (d) 11, (e) 17.

A fairly rational way to choose θ_T is as a fixed multiple of σ_N, the standard deviation of the measurement noise. Table III gives the values of the signal-to-noise ratio σ/σ_N (where σ is the measured standard deviation of concentration). The smaller the value of σ/σ_N, the less successful one would expect a threshold to be in distinguishing between noise and non-zero values of the true concentration. Since the noise is approximately Gaussian, a choice of $\theta_T = 2\sigma_N$ is reasonable, and the resulting downwind variation of γ is shown in Figure 9. In the stable cases, γ is relatively large (values around 0.5) and decreases downwind, while in the unstable cases, γ is relatively small (just under 0.2) and hardly varies downwind. The relative size of γ in stable and unstable conditions is probably sensitive to local effects, in particular topography. Mylne (1992) found lower values of γ in stable than in neutral conditions, because of long timescale meandering under stable conditions. In the present experiments, such meandering was not present, probably because of the katabatic winds being channelled down the valley. (Mylne (1992) found timescales based on the autocorrelation function to be an order of magnitude greater in the stable than the near-neutral cases. In the present experiments, the timescales were an order of magnitude greater in the unstable than the stable cases.)

An alternative method of choosing θ_T would be to take it as the value where

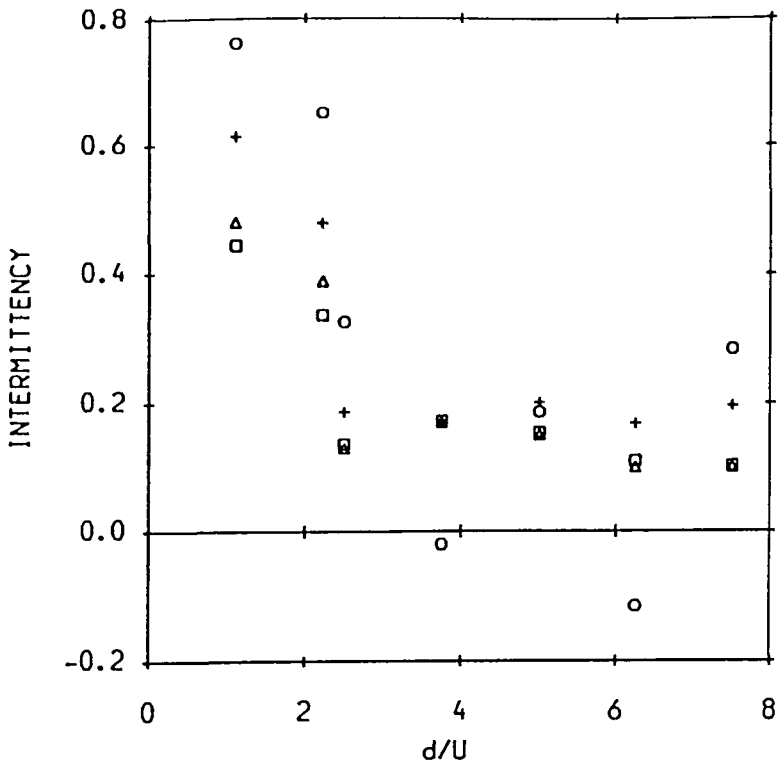

Fig. 9. Intermittency estimates plotted against downwind distance d(m) normalised by mean wind speed $U(\mathrm{m\,s^{-1}})$. + $\theta_T = 2\sigma_N$, Δ θ_T set at change in slope, □ intermittency determined by truncated normal fit, O intermittency determined from (6). The stable cases are those at the two smallest values of d/U.

the c.d.f. curves in Figure 8 show a sharp change in gradient. This also involves considerable subjectivity; the result of our attempt is shown in Figure 9. These values follow much the same pattern as with the first method, but are slightly smaller.

An intermittency can also be obtained by fitting truncated normal models for the c.d.f. to the sections of the plots in Figures 7 and 8 judged to be greater than the noise level. The results from fitting truncated normal c.d.f.s by linear regression are also shown in Figure 9. Figure 10 shows the c.d.f. fit for experiments 13 and 16. The resulting values of intermittency are much the same as those obtained by setting θ_T at the change in slope.

Finally, there is another possible method based on the formulation presented by Chatwin and Hajian (1990). This involves letting the p.d.f. $p(\theta)$ of the true concentration be given by

$$p(\theta) = (1 - \gamma)\delta(\theta) + \gamma f(\theta)\,, \tag{2}$$

where $\delta(\theta)$ is the Dirac delta-function, and using the relationship

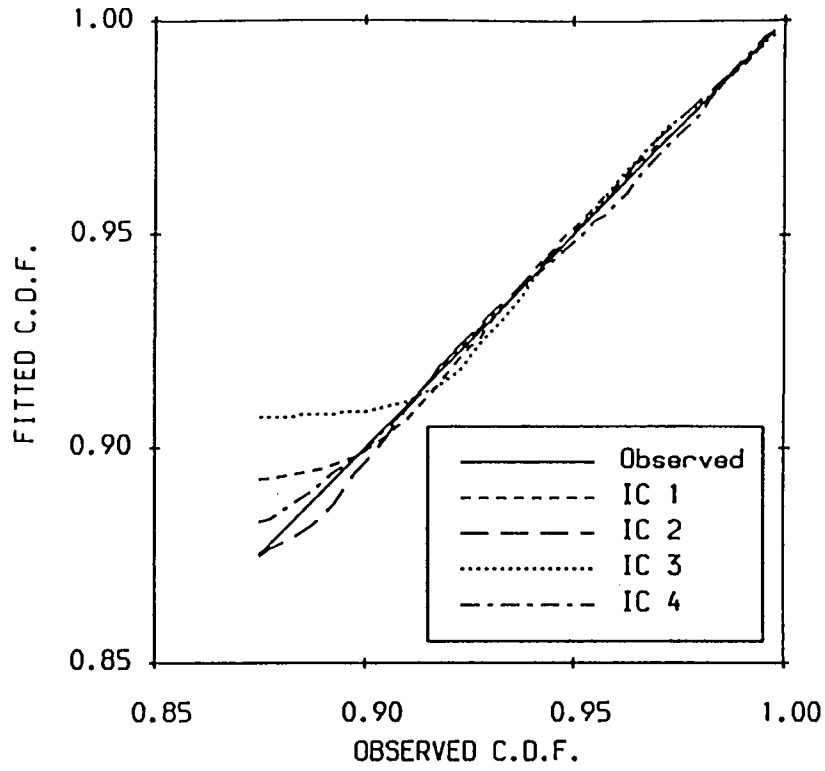

Fig. 10(a)

$$p_M(\theta) = \int_{-\infty}^{\infty} p(\phi) p_N(\theta - \phi)\, \mathrm{d}\phi\,, \tag{3}$$

where $p_M(\theta)$ is the p.d.f. of the measured concentration and $p_N(\theta)$ is the p.d.f. of the noise. Combining (2) and (3) gives

$$p_M(\theta) = (1 - \gamma) p_N(\theta) + \gamma \int_0^{\infty} f(\phi) p_N(\theta - \phi)\, \mathrm{d}\phi$$

since $f(\theta)$ is zero for negative values of θ. Let

$$P = \int_0^{\infty} p_M(\theta)\, \mathrm{d}\theta\,.$$

Then if $p_N(\theta)$ is symmetric with zero mean,

$$P = \tfrac{1}{2}(1 + \gamma) - \gamma \int_0^{\infty} \mathrm{d}\phi f(\phi) \int_{\phi}^{\infty} \mathrm{d}\theta p_N(\theta)\,.$$

Let

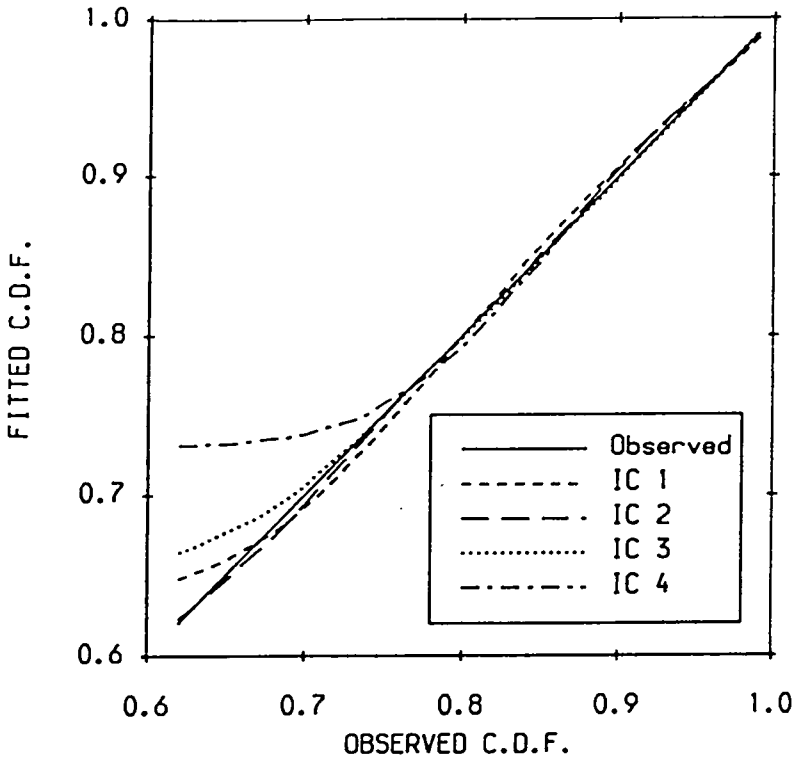

Fig. 10(b)

Fig. 10. Normal c.d.f. fit illustrated by plotting the fitted c.d.f. against the actual c.d.f. (a) Experiment 13, (b) Experiment 16.

$$F(\phi) = \int_0^{\phi} f(s)\,\mathrm{d}s\,.$$

Then, integrating by parts,

$$P = \tfrac{1}{2}(1+\gamma) + \gamma \int_{\phi}^{\infty} \mathrm{d}\phi F(\phi) p_N(\phi)\,. \tag{4}$$

Assume that $p_N(\theta)$ is Gaussian with standard deviation σ_N:

$$p_N(\theta) = \frac{1}{\sqrt{2\pi}\sigma_N} \exp\left(\frac{-\theta^2}{2\sigma_N^2}\right),$$

and that

$$F(\theta) = G\left(\frac{\theta}{\sigma_c}\right),$$

where $F(\theta) \ll 1$ for $\theta \ll \sigma_c$, and $F(\sigma_c) = O(1)$. Then (4) becomes

$$P = \tfrac{1}{2}(1+\gamma) + \gamma \int_0^\infty d\theta G\left(\frac{\sigma_N}{\sigma_c}\theta\right)\frac{1}{\sqrt{2\pi}}\exp(-\tfrac{1}{2}\theta^2)\,.$$

If $\sigma_N/\sigma_c \ll 1$, then

$$P \sim \tfrac{1}{2}(1+\gamma) + \gamma \int_0^\infty d\theta \left\{\frac{\sigma_N}{\sigma_c}\theta G'(0) + \right.$$

$$\left. + \frac{1}{2}\left(\frac{\sigma_N}{\sigma_c}\right)^2 \theta^2 G''(0) + \cdots\right\}\frac{1}{\sqrt{2\pi}}\exp(-\tfrac{1}{2}\theta^2)$$

$$\sim \tfrac{1}{2}(1+\gamma) + \frac{\gamma}{\sqrt{2\pi}}\frac{\sigma_N}{\sigma_c}\left\{G'(0) + \frac{1}{2}\sqrt{\frac{\pi}{2}}\frac{\sigma_N}{\sigma_c}G''(0) + \right.$$

$$\left. + \frac{1}{3}\left(\frac{\sigma_N}{\sigma_c}\right)^2 G'''(0) + \cdots\right\}. \tag{5}$$

To leading order

$$\gamma = 2P - 1\,. \tag{6}$$

To obtain higher order estimates, it is necessary to make an assumption about $f(\theta)$, for example that it is truncated normal:

$$f(\theta) = \frac{1}{\sqrt{2\pi}\sigma_c A}\exp\left\{-\frac{(\theta-\mu_c)^2}{2\sigma_c^2}\right\},$$

where $A = 1 - \Phi(-\mu_c/\sigma_c)$. Then

$$G'(\theta) = \sigma_c f(\sigma_c\theta) = \frac{1}{\sqrt{2\pi}A}\exp\left\{-\frac{1}{2}\left(\theta - \frac{\mu_c}{\sigma_c}\right)^2\right\}.$$

This implies that

$$P \sim \tfrac{1}{2}(1+\gamma) + \frac{\gamma}{2\pi A}\frac{\sigma_N}{\sigma_c}\exp\left(-\frac{\mu_c^2}{2\sigma_c^2}\right)\times$$

$$\times\left[1 + \frac{1}{2}\sqrt{\frac{\pi}{2}}\left(\frac{\sigma_N}{\sigma_c}\right)\left(\frac{\mu_c}{\sigma_c}\right) + \frac{1}{3}\left(\frac{\sigma_N}{\sigma_c}\right)^2\left\{\left(\frac{\mu_c}{\sigma_c}\right)^2 - 1\right\} + \cdots\right]. \tag{7}$$

This can be rearranged to give higher order corrections to (6). For the present data, $\sigma_N/\sigma_c \sim 0.01$ and these corrections only make of order 1% difference to (6).

The values of γ obtained from (6) are also plotted in Figure 9. These follow the same broad pattern as with the other methods, i.e., larger values in the stable cases, and no obvious downwind trend for the unstable cases, but are more

variable. The variability is particularly acute for the farther downwind experiments in which the mean concentrations were small, with negative values of γ in two experiments. This is indicative of baseline uncertainty, and emphasizes the sensitivity of estimates of the intermittency to both the precise definition of intermittency and to measurement system properties such as smoothing, noise and baseline drift.

5.2. Chatwin and Sullivan definition

Although the above definitions of intermittency involve a large degree of subjectivity and are sensitive to instrument properties, they do give a quantitative indication of how likely the concentration is to be "close to zero" and "far from zero". As discussed by Chatwin and Sullivan (1989), they do not, however, have a sound physical basis. By considering source and non-source fluid, to which the concept of intermittency can be applied precisely, Chatwin and Sullivan proposed another definition of intermittency:

$$\gamma_0 = C/\theta_0 ,$$

where C is the mean concentration and θ_0 is the source concentration. In turbulent flow, C can be expected to be very close to the value that would obtain for zero molecular diffusion, so γ_0 is a good approximation to the probability of being in source fluid. See Chatwin and Sullivan (1989).

Correspondingly, the p.d.f. of concentration is

$$p(\theta) = (1 - \gamma_0)g(\theta) + \gamma_0 f(\theta) ,$$

where $f(\theta)$ is the p.d.f. conditional on being in marked (source) fluid, and $g(\theta)$ is the p.d.f. conditional on being in unmarked fluid. In the present experiments, it is always true that $\gamma_0 \ll 1$, so that $p(\theta) \approx g(\theta)$ for all θ, except possibly at large values of θ, where $f(\theta)$ might be much larger than $g(\theta)$. In other words, even at these short downwind distances, marked fluid occupies a very small proportion of time (or, equivalently, of space). A question of interest is whether the marked fluid can still have a significant effect on concentration statistics.

The first two moments of concentration are given by

$$C = (1 - \gamma_0)C_g + \gamma_0 C_f ,$$

$$\sigma^2 = (1 - \gamma_0)\sigma_g^2 + \gamma_0\sigma_f^2 + \gamma_0(1 - \gamma_0)(C_f - C_g)^2 .$$

The contribution to the mean from $f(\theta)$ is negligible if $\gamma_0 C_f \ll C$, i.e., if $C_f \ll \theta_0$. Furthermore, when $\gamma_0 \ll 1$

$$\sigma^2 \approx \sigma_g^2 + \gamma_0\sigma_f^2 + \gamma_0 C_f^2(1 - C_g/C_f)^2 .$$

It is safe to assume that $C_g/C_f \leqslant 1$, so a necessary and sufficient condition to ensure that $\sigma^2 \approx \sigma_g^2$ is then

$$\sigma^2 \gg \gamma_0\sigma_f^2 \quad \text{and} \quad \sigma^2 \gg \gamma_0 C_f^2 .$$

Thus when $\gamma_0 \ll 1$, there is a negligible contribution from $f(\theta)$ to the mean and variance *iff* the following three conditions are satisfied:

$$1.\ C_f \ll \theta_0; \qquad 2.\ \gamma_0\sigma_f^2 \ll \sigma^2; \quad \text{and} \quad 3.\ \gamma_0 C_f^2 \ll \sigma^2 .$$

In practice one could estimate C_f and σ_f^2 by assuming that the top fraction γ_0 of concentration values represents $f(\theta)$. If measurements were accurate and sampling errors were negligible, this would give an upper bound for C_f. Since the only process which can change $f(\theta)$ is molecular diffusion, which acts downgradient, the largest concentrations must be found in source fluid. Therefore such a choice would almost certainly give a lower bound for σ_f (since overlapping the measurements contributing to f and g would increase the spread of those contributing to f).

In practice, instrument spatial resolution is nearly always insufficient to resolve source fluid (which will be found in strands of width comparable to the conduction cut-off – see the fine resolution experiments of Baines and Corriveau (1992)), so that measured concentrations will be less than those in source fluid. This is certainly the case with the present measurements. Since smoothing will tend to reduce the largest concentrations most, it is very likely that the measured σ_f, derived from the above choice, would be a lower bound for the true value.

Measured values of C_f would be less than the true values because of the smoothing. The most conservative estimate we can make for C_f is the maximum measured concentration $\theta_{\max}$. As long as this is an overestimate of the true value of C_f, satisfaction of conditions 1 and 3 by $\theta_{\max}$ guarantees satisfaction by C_f.

If one assumes that $p(\theta)$ is either exponential or beta (of the form $s(1-\theta)^{s-1}$ for $0 \leqslant \theta \leqslant 1$ with $s \geqslant 2$), and that $f(\theta)$ is given by the top proportion γ_0 of concentration values, then $\sigma_f = \sigma$ (in which case condition 2 would be satisfied). In fact, this is a consequence of these distributions being special cases of the generalised Pareto distribution, which has this self-similar property. In the case of an exponential distribution, the most extreme rearrangement is to assume that f is given by the lowest fraction $\gamma_0/2$ of measurements and the highest fraction $\gamma_0/2$ of measurements. In this case $\gamma_0\sigma_f^2 \to 0$ as $\gamma_0 \to 0$, providing further support to the argument that overlapping the measurements contributing to f and g will not affect the satisfaction of condition 2. So it is plausible that condition 2 might be satisfied. Thus one would still expect $\sigma^2 \approx \sigma_g^2$, provided that this were true for the non-overlapping choice of f and g. As for conditions 1 and 3, if they are satisfied when the maximum occurring concentration, $\theta_{\max}$, is used to estimate C_f, then they are also likely to be satisfied by the true value. Results based on $\theta_{\max}$ are given in Table IV. The cases omitted from the table satisfy conditions 1 and 3 more comfortably than those presented. Subject to the above reservations, it appears that the first two moments are dominated by non-source fluid statistics. One can also note that far downwind, $C_f \to 0$ and $C_g \to 0$, in which case the first two moments must be dominated by non-source fluid statistics.

This suggests that while this new definition of intermittency provides a superior

TABLE IV

Values of the ratios occurring in conditions 1 and 3

Experiment	Ion collector	$1000\gamma_0$	$100\theta_{max}/\theta_0$	$\gamma_0\theta^2_{max}/\sigma^2$
8	2	0.034	0.17	0.0050
9	1	0.043	0.22	0.0078
10	4	0.086	0.33	0.013
11	2	0.13	0.42	0.015
13	3	0.14	0.48	0.015
16	1	0.80	0.87	0.033
	2	0.89	0.67	0.022
	3	0.77	1.0	0.042
	4	0.38	1.1	0.064
17	2	0.34	0.50	0.021

theoretical framework, with a sound physical basis, its direct practical use is less obvious. One possible use would be in the investigation of extremes of concentration, which would be determined by $f(\theta)$. The conventional definition, on the other hand, has qualitative value for descriptive and modelling purposes, but is quantitatively suspect.

6. Discussion

All of the experiments described here display some lack of stationarity, rendering interpretation of results uncertain. It is particularly clear in experiment 13 that there are meander timescales of the same order as the length of the experiment. To obtain properly representative statistics, it would be necessary to carry out a number of replications of each experiment to cover the range of conditions within a suitably defined ensemble. Ideally this ensemble would be for specific conditions, e.g., fixed mean wind speed and direction and atmospheric stability. In practice this would not be possible in the field, and a less specific but more realistic ensemble could be used. For example, an ensemble could be defined by restricting to a particular time of day or year – one would then carry out a series of identical experiments within the selected time period which would encompass a variety of wind directions, speeds, etc. occurring within this ensemble. Replicated experiments have been carried out in the wind tunnel – for example Fackrell and Robins (1986, personal communication), Hall *et al.* (1991) and replicated field experiments would be extremely valuable.

In contrast to the results of Mylne (1992), there was a greater degree of stationarity in the stable experiments. This was probably a result of the channelling of katabatic winds down the valley, inhibiting the longer period meandering observed by Mylne (1992) under stable conditions. The earlier part of experiment 13 exhibited a cyclic variation with a period of just over 10 min, suggesting that the convective boundary layer possessed quite clearcut quasi-periodic motions.

As a result of the reduced meandering in the stable experiments, there was a greater chance of experiencing "non-zero" concentration near the mean plume centreline. This is manifested in the generally higher values of intermittency (for all the definitions investigated here) in the stable cases. The skewness and kurtosis appear to have been larger during unstable or neutral conditions, as was the case for the intensity (as in Peterson *et al.*, 1988). No large differences in the shape of the p.d.f. between stable and unstable cases were detected, although the exponential distribution gave a poorer fit to the stable cases than to the unstable ones.

The data were also used to illustrate the effect of the considerable subjectivity associated with conventional definitions of the intermittency. Different choices of threshold (or of analogous procedures) produce quite different values for the intermittency, even when these choices have a rational basis. The fact that one of these procedures yielded some negative values of intermittency makes clear the sensitivity of the results to instrument characteristics such as baseline drift, noise and smoothing. The definition of intermittency proposed by Chatwin and Sullivan (1989) is sounder from both a theoretical and a practical viewpoint. However, the present results show that the direct practical utility of the partitioning between source and non-source fluid is not obvious, since even 5 m downwind of the source, the source fluid made a negligible contribution to the mean and variance of concentration. Since the largest concentrations will be attained in the source fluid, further work would be worthwhile.

Acknowledgements

We would like to thank the Atmospheric Sciences Laboratory, White Sands Missile Range, New Mexico for the provision of the site, facilities and personnel which enabled these experiments to be conducted. We are also grateful to Liz Clarke for allowing us to use the results of her calculations of the autocorrelation functions and associated timescales, and to Philip Chatwin and Paul Sullivan for helpful discussions.

References

Baines, W. D. and Corriveau, A. F.: 1992, 'Mixing in Turbulent Jets as Revealed by pH Indicator', *Proc. 2nd Caribbean Conf. on Fluid Dynamics*, St. Augustine, Trinidad, pp. 142–148.

Chatwin, P. C. and Hajian, N. T.:1990, 'Concentration Fluctuations in Atmospheric Dispersion', Final Report to CDE on Agreement No. 2066/62 (CDE). (Also Brunel University Department of Mathematics and Statistics Technical Report TR/05/90.) 54 pp.

Chatwin, P. C., Hajian, N. T., Mole, N. and Jones, C. D.: 1989, 'Investigations on the Atmospheric Dispersion of Clouds Containing Charged Tracers', *IMA J. Appl. Mathematics* **42**, 97–117.

Chatwin, P. C. and Sullivan, P. J.: 1989, 'The Intermittency Factor of Scalars in Turbulence', *Phys. Fluids A* **1**, 761–763.

D'Agostino, R. B. and Stephens, M. A. (eds.): 1986, *Goodness-of-Fit Techniques*, Marcel Dekker, New York.

Deardorff, J. W. and Willis, G. E.: 1984, 'Groundlevel Concentration Fluctuations from a Buoyant

and a Non-buoyant Source within a Laboratory Convectively Mixed Layer', *Atmos. Environ.* **18**, 1297–1309.

Dinar, N., Kaplan, H. and Kleiman, M.: 1988, 'Characterization of Concentration Fluctuations of a Surface Plume in a Neutral Boundary Layer', *Boundary-Layer Meteorol.* **45**, 157–175.

Fackrell, J. E. and Robins, A. G.: 1982, 'The Effects of Source Size on Concentration Fluctuations in Plumes', *Boundary-Layer Meteorol.* **22**, 335–350.

Griffiths, R. F. and Megson, L. C.: 1984, 'The Effect of Uncertainties in Human Toxic Response on Hazard Range Estimation for Ammonia and Chlorine', *Atmos. Environ.* **18**, 1195–1206.

Guenther, A. and Lamb, B.: 1989, 'Atmospheric Dispersion in the Arctic: Wintertime Boundary Layer Measurements', *Boundary-Layer Meteorol.* **49**, 339–366.

Hall, D. J., Waters, R. A., Marsland, G. W., Upton, S. L. and Emmott, M. A.: 1991, 'Repeat Variability in Instantaneously Released Heavy Gas Clouds – Some Wind Tunnel Model Experiments', Warren Spring Laboratory Report LR804(PA).

Hanna, S. R.: 1984, 'The Exponential Probability Density Function and Concentration Fluctuations in Smoke Plumes', *Boundary-Layer Meteorol.* **29**, 361–375.

Jones, C. D.: 1977, 'Ionised Air as a Wind Tunnel Tracer', *J. Phys. E. Scientific Instruments* **10**, 1287–1291.

Jones, C. D.: 1979, 'Statistics of the Concentration Fluctuations in Short Range Atmospheric Diffusion', in C. J. Harris (ed.), *Mathematical Modelling of Turbulent Diffusion in the Environment*, Academic Press, New York, pp. 277–298.

Jones, C. D.: 1983, 'On the Structure of Instantaneous Plumes in the Atmosphere', *J. Hazardous Materials* **7**, 87–112.

Kaimal, J. C, Wyngaard, J. C., Haugen, D. A., Cote, O. R., Izumi, Y., Caughey, S. J. and Readings, C. J.: 1976, 'Turbulence Structure in the Convective Boundary Layer', *J. Atmos. Sci.* **33**, 2152–2169.

Lamb, B., Peterson, H., Campbell, M. and Stock, D.: 1985, 'Concentration Fluctuations in Dispersing Tracer Plumes', *Seventh Symposium on Turbulence and Diffusion*, AMS, Boston, pp. 331–334.

Lewellen, W. S. and Sykes, R. I.: 1986, 'Analysis of Concentration Fluctuations from Lidar Observations of Atmospheric Plumes', *J. Clim. Appl. Meteorol.* **25**, 1145– 1154.

McQuaid, J. and Roebuck, B.: 1985, 'Large Scale Field Trials on Dense Vapour Dispersion', *Final Report to Sponsors on the Heavy Gas Dispersion Trials at Thorney Island 1982–84*, HSE, Sheffield.

Mikkelsen,T., Jørgensen, H. E. and Thykier-Nielsen, S.: 1990, 'Model Validation Experiments over Short Distances', *CEC Seminar on Methods and Codes for Assessing the Consequences of Nuclear Accidents*, Athens.

Mole, N.: 1989, 'Estimating Statistics of Concentration Fluctuations from Measurements', *Proc. Seventh Symposium on Turbulent Shear Flows*, Stanford University, pp. 29.5.1–29.5.6.

Mole, N.: 1990, 'Some Intersections between Turbulent Dispersion and Statistics', *Environmetrics* **1**, 179–194.

Mylne, K. R.: 1992, 'Concentration Fluctuation Measurements in a Plume Dispersing in a Stable Surface Layer', *Boundary-Layer Meteorol.* **60**, 15–48.

Mylne, K. R. and Mason, P. J.: 1991, 'Concentration Fluctuation Measurements in a Dispersing Plume at a Range of up to 1000 m', *Q.J.R. Meteorol. Soc.* **117**, 177–206.

Nielsen, M. and Jensen, N. O.: 1991, 'Continuous Release, Dense Gas, Field Experiments with Obstacles – Final Report on Project BA.X2', *Report Risø-M-2923* of Risø National Laboratory, Roskilde, Denmark.

Peterson, H. G., Lamb, B. K. and Stock, D. E.: 1988, 'Plume Concentration and Velocity Fluctuations during Convective and Stable Conditions', *Eighth Symposium on Turbulence and Diffusion*, AMS, Boston, pp. 341–344.

Picknett, R. G.: 1981, 'Dispersion of Dense Gas Puffs Released in the Atmosphere at Ground Level', *Atmos. Environ.* **15**, 509–525.

Ramsdell, J. V. and Hinds, W. T.: 1971, 'Concentration Fluctuations and Peak-to-Mean Ratios in Plumes from a Ground-Level Continuous Point Source', *Atmos. Environ.* 5, 483–495.

Ride, D. J.: 1987, 'Modelling Fluctuations in the Concentration of Neutrally Buoyant Substances in the Atmosphere', Ph.D. Thesis, University of Liverpool.

Sawford, B. L., Frost, C. C. and Allan, T. C.: 1985, 'Atmospheric Boundary-Layer Measurements of

Concentration Statistics from Isolated and Multiple Sources', *Boundary-Layer Meteorol.* **31**, 249–268.

Silverman, B. W.: 1986, *Density Estimation for Statistics and Data Analysis*, Chapman and Hall, London.

Sreenivasan, K. R.: 1985, 'On the Fine-scale Intermittency of Turbulence', *J. Fluid Mech.* **151**, 81–103.

Willis, G. E. and Deardorff, J. W.: 1976, 'A Laboratory Model of Diffusion into the Convective Planetary Boundary Layer', *Q. J. R. Meteorol. Soc.* **102**, 427–445.

Willis, G. E. and Deardorff, J. W.: 1978, 'A Laboratory Study of Dispersion from an Elevated Source within a Modeled Convective Planetary Boundary Layer', *Atmos. Environ.* **12**, 1305–1311.

Willis, G. E. and Deardorff, J. W.: 1981, 'A Laboratory Study of Dispersion from a Source in the Middle of the Convectively Mixed Layer', *Atmos. Environ.* **15**, 109–117.

Willis, G. E. and Deardorff, J. W.: 1983, 'On Plume Rise within a Convective Boundary Layer', *Atmos. Environ.* **17**, 2435–2447.